AIX-MARSEILLE UNIVERSITÉ

UNIVERSITY OF ALEXANDRIA

ECOLE DOCTORALE DES SCIENCES DE LA VIE ET DE LA SANTE

THESE DE NEUROSCIENCES

Presented publicly,
to obtain the degree of Doctor of Aix-Marseille University and of the University of Alexandria, by:

Heba ELSEEDY

March 12, 2019

ROLE OF THE SUPRAMAMMILLARY NUCLEUS - DENTATE GYRUS PATHWAY IN PHYSIOLOGICAL CONDITIONS AND IN MESIAL TEMPORAL LOBE EPILEPSIES AN OPTOGENETIC APPROACH

Under the co-direction of

Dr Monique Esclapez
Institut de Neurosciences des Systèmes, Inserm UMR 1106, Aix Marseille Université
And
Dr Nabila El Sayed Abdelmeguid
Zoology department , Faculty of Science , Alexandria university

Jury Members of the PhD Thesis :

Pr Carolyn HOUSER, Los Angeles, USA	Rewiever
Dr Jean Christophe PONCER, Paris, France	Rewiever
Pr Nabila ABDELMEGUID, Alexandria, Egypt	Co-supervisor
Dr Monique ESCLAPEZ, Marseille, France	Supervisor
Dr Sherine ABDEL SALAM, Alexandria, Egypt	Examinator
Dr Valérie CREPEL, Marseille, France	Examinator

Abstract

Mesial temporal lobe epilepsies (MTLE) are among the most common clinical forms of drug-resistant partial epilepsies in adults and children. These epilepsies are characterized by the occurrence of spontaneous recurrent seizures associated with excessive and hypersynchronous discharges of neuronal populations generated by a multi-structural epileptogenic zone involving several regions of the limbic system within the mesial temporal lobe including the hippocampal formation (HF), the entorhinal cortex (EC) and the amygdala. Electroclinical observations as well as studies performed in animal models of MTLE provide evidence that these epilepsies are network diseases in which the emergence of spontaneous seizures requires not only hyperactivity of principal cells within the limbic cortex but also the synchronization of activities between these different limbic cortex structures of the temporal lobe. The Supramammillary nucleus (SuM) is one of the main sub-cortical structure innervating all limbic cortex. In rat, it has been shown to be involved in the control of hippocampal theta rhythms and associated functions such as REM sleep as well as emotional learning and memory. More recently, it was shown that the projections from neurons of lateral region of the SuM (SuML) that innervate the dorsal dentate gyrus (DG) display a unique GABAergic and Glutamatergic neurotransmitter phenotype and this pathway is reorganized in epileptic animals. In this thesis we first investigate the role of the SuML-dDG pathway in physiological condition with the hypothesis that this pathway is instrumental to potentiate and synchronize activities between EC and the hippocampus allowing dentate granule cells (GC) to discharge in particular during REM sleep. Then, we investigate whether the plasticity of these connections in epileptic animals could influence the emergence and strength of seizures. Using a multidisciplinary approach combining in optogenetic and electrophysiological recordings with structural connectivity and neurochemical techniques performed in VGLUT2-Cre mutant mice expressing Chanelrhodopsine (ChR2, excitatory opsin, VGLUT2-ChR2 mice) or Halorhodopsine (eNpHR3, inhibitory opsin,) within SuML neurons and their axon terminals we demonstrate that:

1) All the neurons from the SuML innervating the dDG co-express markers for both GABAergic

and glutamatergic neurotransmissions, establish asymmetric (excitatory) and symmetric (inhibitory) synapses and co-release GABA and glutamate on GCs. Activation of this pathway increases theta power and frequency as well as gamma power in particular during REM sleep and induced net firing of some GCs. These results are in keeping with a previous recent study showing that this pathway potentiates GC firing when temporally associated with perforant path inputs.

2) The population of GABA/GLU SuML neurons innervating the dDG is heterogeneous. Among these neurons 70% contain calretinin whereas 30% do not. These two populations are topographically organized, GABA/GLU SuML neurons containing calretinin being more numerous within the rostral part of this nucleus. These two populations that innervate both GCs and parvalbumin interneurons of the DG could be involved in the control of different dDG-dependent functions.

3) In epileptic mice the SuML-dDG pathway is reorganized as previously described in rat. Our preliminary results using in vivo optogenetic show that activation or inactivation of this pathway do not modify the seizure duration. However, this pathway modulates the variability of the seizure frequency content power. Further studies will have to examine whether such modulation could trigger seizures during specific vigilance states.

Key-Words: Mesial Temporal Lobe Epilepsy; Hippocampus; Dentate Gyrus, Supramammillary nucleus; transgenic mouse; vesicular glutamate transporter 2 (VGLUT-2); Vesicular GABA transporter (VGAT); Calretinin; plasticity; pilocarpine.

Résumé

Les épilepsies du lobe temporal médian (ELTM) sont parmi les formes les plus courantes d'épilepsie partielle pharmaco-résistante de l'adulte et l'enfant. Ces épilepsies sont caractérisées par la survenue de crises récurrentes spontanées associées à des décharges excessives et synchrones de populations neuronales générées par un réseau multi structural (Zone Epileptogène, ZE) incluant les cortex limbiques tels que l'hippocampe et le cortex entorhinal (EC). Les observations électrocliniques ainsi que les études effectuées sur des modèles animaux d'ELTM montrent que ces épilepsies sont des maladies de réseau dans lesquelles la survenue des crises spontanées nécessite non seulement une hyperactivité des cellules principales des cortex limbiques, mais aussi la synchronisation des activités entre ces différents cortex limbiques du lobe temporal. Le noyau supramammillaire (SuM) est l'une des principales structures sous-corticales innervant tous les cortex limbiques. Chez le rat, il a été démontré qu'il était impliqué dans le contrôle des rythmes thêta de l'hippocampe et des fonctions associées telles que le sommeil paradoxal (SP), ainsi que l'apprentissage et la mémoire émotionnelle. Plus récemment, il a été démontré que les projections des neurones de la région latérale du SuM (SuML) qui innervent le gyrus dentelé (DG) dorsal (dDG) présentent un phénotype unique à la foie GABAergique et Glutamatergique. De plus cette voie est réorganisée chez les animaux épileptiques. Dans cette thèse, nous examinons d'abord le rôle de la voie SuML-dDG en condition physiologique avec l' hypothèse que cette voie est essentielle pour potentialiser et synchroniser les activités entre la CE et l'hippocampe permettant aux cellules granulaires (GC) de décharger, en particulier pendant le SP. Ensuite, nous étudions si la plasticité de ces connexions chez les animaux épileptiques pourrait influer sur l'apparition et la force des crises. En utilisant une approche multidisciplinaire combinant les techniques d'optogénétiques et d'électrophysiologie avec celles d'anatomie fonctionnelles réalisées sur des souris mutantes VGLUT2-Cre exprimant la Chanelrhodopsine (ChR2, opsine excitatrice) ou Halorhodopsine (eNpHR3, opsine inhibitrice) dans les neurones du SuML et leur terminaisons axonales nous démontrons que:

1) Tous les neurones du SuML innervant le DG co-expriment les marqueurs pour les

neurotransmissions GABAergique et glutamatergique, établissent des synapses asymétriques (excitatrices) et symétriques (inhibitrices) et co-libèrent le GABA et le glutamate sur les CGs du DG. L'activation de cette voie augmente la puissance et la fréquence des oscillations thêta ainsi que la puissance du gamma, en particulier pendant le SP et induit la décharge des CGs. Ces résultats sont en accord avec une étude récente montrant que cette voie potentialise la décharge des GCs lorsqu'elle est associée temporellement aux entrées de la voie perforante.

2) La population de neurones GABA / GLU du SuML innervant le dDG est hétérogène. Parmi ces neurones, 70% contiennent la calrétinine, tandis que 30% n'en contiennent pas. Ces deux populations sont organisées de manière topographique, les neurones GABA / GLU du SuML contenant la calrétinine étant plus nombreux dans la partie rostrale du noyau. Ces deux populations qui innervent les GCs et les interneurones parvalbumin du DG pourraient être impliquées dans le contrôle des différentes fonctions associées au DG.

3) Chez les souris épileptiques, la voie SuML-dDG est réorganisée comme décrit précédemment chez le rat. Nos résultats préliminaires utilisant les techniques d'optogénétique in vivo montrent que l'activation ou l'inactivation de cette voie ne modifie pas la durée de la crise. Cependant, cette voie module la variabilité de la puissance du contenu fréquentiel des crises. Des études ultérieures devront examiner si une telle modulation pourrait participer à l'expression des crises pendant certains états de vigilance spécifiques.

Mots- cléfs: Epilepsies deu lobe temporal median; Hippocampe; Gyrus Dentelé; Noyeau supramammillaire; souris trangenique; transporteur vésiculaire du glutamate (VGLUT-2); Transporteur vésiculaire du GABA (VGAT); Calretinin; plasticité; pilocarpine.

Acknowledgments

First of all, Thanks GOD that helped me to finish my PhD thesis and of course I cannot write the acknowledgment of my PhD thesis without my Family. Therefore, I am so grateful to them, for their endless help and love. Sometimes you meet someone who change your way of thinking and act as a member of your family I am so thankful for *Samir*, you helped me a lot with your thought and how you trusted me that I will do the best.

Dr Monique Esclapez, my supervisor, no words can explain how much you mean to me. You were like my family in France I never feel alone or afraid that I am away from my family because of you. I learned from you a lot of things that gave to me a lot of experience and I hope that I can transfer it to my students. You were a great supervisor thanks a lot.

Dr. Nabila Abdelmeguid, you are not just my supervisor you are my mum. My Knowledge for Electron microscopy was one of the most and precious knowledge I learned during my PhD and this was because of you. I will never forget how you and *Dr Ismail Sadek* who helped me during my master.

Dr Sherine Abdelsalam, my youngest supervisor and what I really feel my old sister as I usually say to you: "you are like Asmaa". I knew you since I was undergraduate student. I don't know how I can describe our relation. I know that maybe we had some difficulties, but you are still my older sister and I always remember what your mother used to say to you about me (al3sfora bt3tk).

Dr Helen Bras and Dr Patrice Coulon; Thanks a lot for helping me in RV injections.

Pascale, Thanks for helping me in my thesis and teaching me how to analyze my data and being so supportive for me.

Jenny, Antoine, the engineers in the lab thanks a lot for all. You have been helped me tremendously during my PhD. Jenny I will never forget our confocal session and how you want to learn Arabic language (koulo kwys) , Antoine of course I will miss playing with mice with you .

Maiava, Thanks for being so friendly and supportive with me.

Kenza, my Marocaine twins; I don't know what I say to you, but I will really miss you and how you tried to teach me Marocain language and I will never forget (sekon kter ya heba).

Mayada , Osama and Ali , you were my family in france thanks a lot

In my life I was so lucky to meet some people who influence a lot in my personality, and I am so thankful to them. *Dr Safaa Zaki, Dr Mona Rageh and Dr Essam Abdallah thanks a lot to you.*

My close friends *Dr Salma Shwemi, Roro, Salmaz , Dodo* I wrote it with you nick names you are my life I hope that we will continue our life together our calls that take at least one hour a day were like a magic drugs for me. I love you all. *Moataz*, my young brother I really have been missing you when you left Marseille I miss (elmaghara) I hope you can survive in (kwkb elyaban).

I would like also to thanks Prof. Carolyn Houser and Dr. Jean-Christophe for accepting to review my PhD thesis. Many thanks to them and also to Dr. Valerie Crepel for accepting to be part of the jury of my PhD thesis defend

Thank you all again!

Synopsis

Table of contents

List of Figures……I
List of Abbreviations …… III
Foreword…… .1
1. The Hippocampal Formation (HF) in Rodents…… 5
1.1 Description…… …… .5
1.2 Cytoarchitectonic Organization…… ……...6
1.2.1 The subiculum…… .6
1.2.2 The hippocampus proper…… 6
1.2.3 The dentate gyrus…….... 6
1.2.4 Hippocampal cells…….... .7
1.3 Hippocampal connections…… .7
1.3.1 Intra-hippocampal connections…… …..7
1.3.2 Commissural connections……8
1.3.3 Extrinsic connections……9
2. Supramammillary Nucleus (Sum)……..…12
2.1 Sum position and structure……...12
2.2 Neuronal population in supramamillary region…….....14
2.3 Sum connections…….....15
2.3.1 Afferents to SuM……16
2.3.2 Efferents from SuM…….....18
2.4 The Sum-hippocampus network…….....19
2.5 The role of supramammillary nucleus ……21
3. Epilepsy…….....24
3.1 General Classification……..……... 24
3.2 Temporal lobe epilepsy (TLE) ……..... 25
3.3 The Pilocarpine model of MLTE……..... .26
3.4 Neural alteration in pilocarpine model induced in rodents……..…… 27
3.4.1 Neuronal loss…… ..……..29
3.4.2 Axonal plasticity of glutamatergic networks…… 31
3.4.3 Plasticity of GABAergic networks…… .33
3.4.4 Granular cell dispersion…… .34
3.4.5 Neurogenesis…… .34
3.4.6 Functional alteration…… ..35
3.5 Reorganization of the Sum-hippocampus unique network in TLE…… …35
4. Optogenatics…… ..37
4.1 Opsins…… .37
4.1.1 Activation…….. 38
4.1.2 Inhibition…… 38
4.2 Viral vectors…… 39
4.3 Cre inducible system…… .41
5. Objectives…… 43

6. First study: ……..……..44
Francesca Billwiller, Laura Castillo, Heba Elseedy, Anton Ivanov, Jennyfer Scapula, Antoine Ghestem, , Julien Carponcy, Paul Antoine Libourel, Hélène Bras ,Nabila El Sayed Abdelmeguid, Esther Krook-Magnuson, Ivan Soltesz, Christophe Bernard, Pierre-Hervé Luppi, Monique Esclapez.
The GABA-Glutamate supramammillary–dorsal Dentate Gyrus pathway controls theta and gamma oscillations in the DG during paradoxical sleep, Submitted..

7. Second study:……91
Heba Elseedy, Jennyfer Scapula, Antoine. Ghestem, Hélène Bras, Sherine AbdelSalam, Nabila El Sayed Abdelmeguid, Monique Esclapez.
Two populations of neurons from the lateral supramammillary nucleus innervate the dorsal dentate gyrus: both display a dual glutamatergic and GABAergic neurotransmittion phenotype but differ by their Calretinin content and rostro-caudal distribution; Comparative neurology, Submitted.

8. Third study: Supramammillary lateral- dorsal dentate gyrus pathway modulates seizure dynamics in mouse pilocarpine model of mesial temporal lobe epilepsy…… …….120

9. Conclusion and prespective……..……148

10. References ……..……150

List of Figures

Figure1: Schematic representations of hippocampal formation in rat.

Figure2: Cytoarchitectonic organization of the mouse dorsal hippocampus.

Figure 3: Organization of the DG.

Figure 4: The neural circuitry in the rodent hippocampus.

Figure 5: Dissociation of hippocampal functions in rats.

Figure 6: Coronal view of the mouse brain showing the location of the SuM .

Figure 7: Connections of the SuM regardless of its divisions into parts.

Figure 8: Afferent projections to the SuM.

Figure 9: Efferents originating from the SuM.

Figure10: Schematic representation of the structural organization of the rat hippocampus and changes occurs during the TLE.

Figure 11: Comparisons of somatostatin (SOM)- and parvalbumin (PV)-labeled neurons in the rostral dentate gyrus of control and pilocarpine mice.

Figure 12: Axonal sprouting of mossy fibers in the pilocarpine model in mice.

Figure 13: Schematic representation of aberrant connectivity in the hippocampus of chronic pilocarpine-treated rats.

Figure 14: Types of opsins.

Figure 15: Viral vectors for introducing microbial opsin genes into the brain.

Figure 16: Diagram shows the experimental timeline.

Figure 17 : Identification of bregma and lambda locations in mice on stereotaxic apparatus for virus injection.

Figure 18: Identification of electrode and virus injection coordinates stereotaxic apparatus for Sham group.

Figure 19: Optrode preparation.

Figure 20: Identification of optrode and virus injection coordinates on stereotaxic apparatus in Epileptic control and ChR mice.

Figure 21: Identification of electrode and virus injection coordinates on stereotaxic apparatus in HR mice.

Figure 22: Diagram shows the real-time optogenetics intervention system.

Figure 23: Field potential recording by EEG system for epileptic animals.

Figure 24: Epileptic seizures time course over 8 weeks.

Figure 25: The distributions of seizure around the median number of seizure duration.

Figure 26: Spectral analysis of the seizure content for both control and optogenetic manipulation of the SuM in.

Figure 27: Hippocampal changes in pilocarpine induced animals.

Figure 28: Cell loss in pilocarpine induced mice in Hilus.

Figure 29: Co-expression of vesicular GABA transporter (VGAT) and glutamate (VGLUT2) mRNA in the supramammilary lateral nucleus (SuML).

Figure 30: Reorganization of SuML fibers projecting to the dorsal DG in epileptic mice and co-expression of VGLUT2 and VGAT proteins at these projections in epileptic and non-epileptic mice.

List of abbreviations

3V	Third Ventricle
4V	Fourth Ventricle
5HT	5-hydroxytryptamine (Seretonin)
ABC	Avidin-Biotine Complex
AD	Alzheimer's Disease
AH	Anterior Hypothalamic area
AM	Anteromedial thalamic nucleus
AMYG	Amygdala
ATN	Anterior Thalamic Nuclei
AV	Anteroventral thalamic nucleus
CA	Corne d'Ammon (Ammon's Horn)
CA1, 2, 3	area 1,2,3 of the Ammon's Horn
CC	Corpus Callosum
CCK	Cholecytokinine
CE	Cerebellar nuclei
CG	Central Gray region
ChR	channelrhodopsin
CLAU	Claustrum
CM	Central Medial thalamic nucleus
CR	Calretinine
CSN	Compact Subnucleus of the Central Superior Nuclei
D3V	Dorsal Third Ventricle
DA	Dopamine
DAB	Diaminobenzidine tetrahydrochloride
DBB	Diagonal Band of Broca
DG	Dentate Gyrus
DH	Dorsal Hypothalamic area
DP	Dorsal Peduncular cortex
DR	Dorsal Raphe nucleus
EC	Entorhinal Cortex

EEG	Electroencephalographe
ENK	Enkephaline
EYFP	Enhanced Yellow Fluorescence Protein
EZ	epileptogenic zone
FC	Frontal Cortex
G / GCL	Granular layer of DG
GABA	Gamma-Aminobutyric Acid
GAD 65	Glutamic Acid Decarboxylase 65
GFP	Green Fluorescence Protein
GLU	Glutamate
HF	hippocampal formation
Hippo/HP	Hippocampus
HR	Halorhodopsin
HS	hippocampal sclerosis
HZ	Hertz
i.p.	intraperitoneal
IL	Infralimbic cortex
IP	Interpeduncular nucleus
KPBS	Potassium Phosphate Buffer Saline
L6	Lamina 6 of the spinal cord
LC	Locus Coeruleus
LD	Laterodorsal thalamic nucleus
LDTG	Laterodorsal Tegmental Nucleus
LH	Lateral Hypothalamus
LHB	Lateral Habenula
LM	Lateral Mammillary bodies
LP	Lateroposterior thalamic nucleus
LS	Lateral Septum
LV	Lateral Ventricle
MB	Mammillary Bodies
MCX	Motor Cortex

MD	Mediodorsal thalamic nucleus
MFB	Medial Forebrain Bundle
ML	Molecular Layer
MM	Median mammillary bodies
MR	Median Raphe nucleus
mRNA	Messager RNA
MS	Medial Septum
MT	Mammillary Tract
MTLE	Mesial temporal lobe epilepsy
MTT	Mammiliothalamic Tract
NT	Neurotensine
OLF BULB	Olfactory Bulb
PBS	Phosphate Buffer Saline
PFC	Prefrontal Cortex
PH	Posterior Hypothalamic area
PM	Premammillary nucleus
PO	Preoptic nuclei
RE	Nucleus Reuniens
REM	Rapid Eye Movement
RN	Raphe Nucleus
RNA	ribonucleic acid
SC	Sensory Cortical regions
SE	status epilepticus
SGL	Supragranular Layer
SI	Substantia Innominata
SM/nBD	complexe septum médian-noyaux de la bande diagonale de Broca
SP	Substance P
SRIF	Somatotropin Release–Inhibiting Factor (Somatostatine)
SST	somatostatine
SUB	Subicular Complex
SuM	Supramammillary nucleus
SuML	Lateral Supramammillary nucleus
SuMM	Medial supramammillary nucleus

TLE	Temporal lob epilepsy
VC	Visual Cortex
VGAT	Vesicular GABA Transporter
VGLUT1	Vesicular Glutamate Transporter 1
VGLUT2	Vesicular Glutamate Transporter 2
VIP	Vasointestinal Peptide
VMH	Ventromedial Hypothalamus
VTG	Ventral Tegmental nucleus

Foreword

Epilepsy is a central nervous system disease that affects nearly 1% of the world population. It is characterized by the occurrence of spontaneous and recurrent seizures, epileptic seizures, which are due to the excessive and synchronous discharge of neuron populations. There are two major families of epilepsies: generalized epilepsies and partial epilepsies. In partial epilepsies, seizures result from the activity of a neural network involving one or more brain regions, called the epileptogenic zone. The epileptogenic zone (or epileptogenic network) designates a set of neurons necessary and sufficient for the organization of an abnormal discharge (Talairach & Bancaud, 1966; Kahane & Landré, 2008). If partial epilepsies are network diseases, the mechanisms involved in the construction of these abnormal neural networks (mechanisms of epileptogenesis) and the emergence of seizures (ictogenesis) are still poorly understood.

The team in which I conducted my research has been working for many years on mesial temporal lobe epilepsies (MTLE) that are among the most common clinical forms of drug-resistant partial epilepsies in adults and children (Engel, 1996). These epilepsies are characterized by the occurrence of spontaneous recurrent seizures associated with excessive and hypersynchronous discharges of neuronal populations generated by a multi-structural epileptogenic zone involving several regions of the limbic system within the mesial temporal lobe including the hippocampal formation (HF), the entorhinal cortex and the amygdala (Kahane & Bartolomei, 2010). If certain factors such as febrile seizures, status epilepticus (status epilepticus), head trauma, meningitis are known to favor the development of these MTLEs; the basic mechanisms responsible for these epilepsies and their drug resistance are still poorly characterized. To understand these mechanisms, it is essential not only to determine how the epileptogenic zone is organized (anatomical and functional organization) but also how it built up. These mechanisms are difficult to study in humans because epilepsy is a progressive disease and epileptogenesis a dynamic process that can take several years between the initial insult and the onset of the first spontaneous seizure. The use of animal models is therefore essential

to understand the mechanisms that lead to the expression of the disease from those resulting from it and so may at longer term orient us towards new therapeutic strategies.

Hippocampal sclerosis (HS) is frequently observed in patients with temporal lobe epilepsies(Wieser & ILAE Commission on Neurosurgery of Epilepsy, 2004), This may explain that many studies carried out in humans and animals have focused on this structure with the assumption that this focal lesion may be the cause of the seizures. However, this concept of "epileptogenic focus" in MTLE is clearly challenged. Indeed, electro-clinical studies as well as several studies carried out in animal models of MTLE provide evidence that in these epilepsies the abnormal network responsible for the generation of seizures, the EZ, cannot be restricted to the HF. Studies in animal models of MTLE including in the chronic model of limbic seizures induced by pilocarpine in rodents (rats and mice) demonstrate that an initial cerebral aggression such as a status epilepticus (SE) leads to a gradual reorganization of the intrinsic GABAergic (Obenaus *et al.*, 1993; Houser & Esclapez, 1996; Esclapez *et al.*, 1997; Esclapez & Houser, 1999; Cossart *et al.*, 2001; Dinocourt *et al.*, 2003; Kobayashi & Buckmaster, 2003; Sloviter *et al.*, 2003) and glutamatergics (Mello *et al.*, 1993; Okazaki *et al.*, 1995; Esclapez *et al.*, 1997; Lehmann *et al.*, 2001; Okazaki & Nadler, 2001; Buckmaster *et al.*, 2002; Boulland *et al.*, 2007; Jiao & Nadler, 2007; Ribak *et al.*, 2012) neural networks of the HF. These reorganizations lead to a clear hyperactivity of the hippocampal principal cells (Cossart *et al.*, 2001; El-Hassar *et al.*, 2007), however this not sufficient by itself to generate seizures (El-Hassar *et al.*, 2007). Thus, in experimental MTLEs, the epileptogenic zone cannot be reduced to the hippocampus. Electro-clinical studies in patients with MTLE show that the emergence of spontaneous seizures requires the synchronization of activities (co-activation) between the different limbic cortex of the temporal lobe: hippocampus, amygdala and entorhinal cortex (Kahane & Bartolomei, 2010).

These conclusions led Dr. Esclapez to develop a research program on the structural and functional properties of neural networks, which may be involved in limbic cortex synchronization in these MTLEs. With her team, they first focused on the connectivity between the hypothalamus and the hippocampal formation, and more specifically on the projections from the supramammillary nucleus (SuM), the main region of the hypothalamus innervating the limbic

cortex including the hippocampal formation. Indeed, the SuM is involved in the regulation of hippocampal theta rhythms (Kocsis & Vertes, 1994; Vertes & Kocsis, 1997; Kocsis & Kaminski, 2006) and could play a crucial role in the control of several Hippocampal-dependent functions such as working memory, emotional behavior including stress and anxiety (Pasquier & Reinoso-Suarez, 1976; Richmond *et al.*, 1999; Pan & McNaughton, 2002, 2004a; Santín *et al.*, 2003; Shahidi, Motamedi, Bakeshloo, *et al.*, 2004; Shahidi, Motamedi, & Naghdi, 2004)but also, some vigilance states like REM sleep (Renouard *et al.*, 2015). Interestingly it has been shown that all these functions are altered in MTLE in animals (Chauvière *et al.*, 2009; Marcelin *et al.*, 2009) and in humans (Bettus *et al.*, 2008) and that in these epilepsies, the occurrence of seizure is particularly sensitive to stress (Zeitlin *et al.*, 1995; Lanteaume *et al.*, 2009) and vigilance states (Renouard *et al.*, 2015).

The anatomic-functional substrate supporting these functions and their modifications in MTLEs is still poorly understood despite numerous studies carried out in several species on supramammillary-hippocampal connections(Haglund *et al.*, 1984a; Maglóczky *et al.*, 1994; Vertes & Kocsis, 1997; Leranth & Hajszan, 2007).

The work of Dr. Esclapez and her colleagues first established the neurotransmitter phenotypes that characterize the two main pathways between the SuM and the hippocampus in rats(Soussi *et al.*, 2010). They demonstrate that the first pathway originates from neurons of the SuM lateral region (SuML) innervating the supragranular layer of the dorsal dentate gyrus (DG) and, to a lesser extent, the ventral DG has a unique neurotransmitter phenotype being both glutamatergic and GABAergic. The second pathway, originating from the neurons of the most posterior and medial region of SuM (SuMM) and innervating the internal molecular layer of the ventral DG as well as layer of pyramidal cells of CA2 is only glutamatergic.

M. Esclapez's team further reported a surprising structural plasticity of the SuML-DG pathway in the pilocarpine model of MTLE induced in rat (Soussi *et al.*, 2015). Such plasticity, characterized by an increased number of axon terminals from neurons of the SuML, invading the entire inner molecular layer of the DG, reflects an axon terminal sprouting from SuML neurons making aberrant synaptic contact on DG granule cells.

These data led us to propose that the structural plasticity of the SuML-DG pathways could contributes to the epileptogenic network in MLTE by triggering spontaneous seizures within an altered hippocampal intrinsic circuit according to the emotional, cognitive and/or vigilance states of the subject.

The main objective of my PhD research project has been to test this hypothesis by studying the functional consequences of the reorganization of these projections on the expression, intensity and frequency of seizures. For this purpose, I used a multidisciplinary approach combining in vivo optogenetic and electrophysiological recordings with structural connectivity techniques using neurotropic viral vectors (rabies virus, AAV), neurochemical anatomy (immunohistochemistry, in situ hybridization) and imaging (light, electron and confocal microscopy). This approach was performed first in naïve transgenic VGLUT-2 mouse in order to characterize the anatomo-functionnal properties of the SuML-DG pathways in this transgenic mouse strain then in the pilocarpine model of MTLE induced in these mice.

Before presenting the results that we obtained, I will present in a first chapter the hippocampal formation of the rodent (rat and mouse): its anatomy, its main connections and functions focusing in the DG. In a second chapter, I will summarize our knowledge on the supramammillary-hippocampal projection pathway when I started this thesis work. In the third chapter, I will introduce mesial temporal lobe epilepsies and the pilocarpine model I used for my work. In the fourth part, I describe the main anatomo-functional changes that have been reported mainly in the pilocarpine model of MTLE induce in the rat and/or mouse. Chapters Five and Six present the studies that I made in the naive VGLUT-2 transgenic mouse and Chapter seven the study performed in the epileptic mouse. Finally, in the last part, we discuss the results and research perspectives that arise from these studies.

1 – The Hippocampal Formation (HF) in Rodents

1.1 Description

In rodents (rat or mouse), the hippocampal formation is a bilateral and symmetric structure of the telencephalum. This cortical structure extends from the septal nuclei, rostro-dorsally to the basal forebrain, above and behind the diencephalon, bypassing the latter to end ventrally (Fig. 1). The longitudinal axis of the hippocampal formation is the dorso-ventral axis (or "septotemporal") with two poles, a septal / dorsal pole and a temporal / ventral pole. There is also an orthogonal axis of the hippocampal formation, the transverse axis and an axis perpendicular to it, the radial axis.

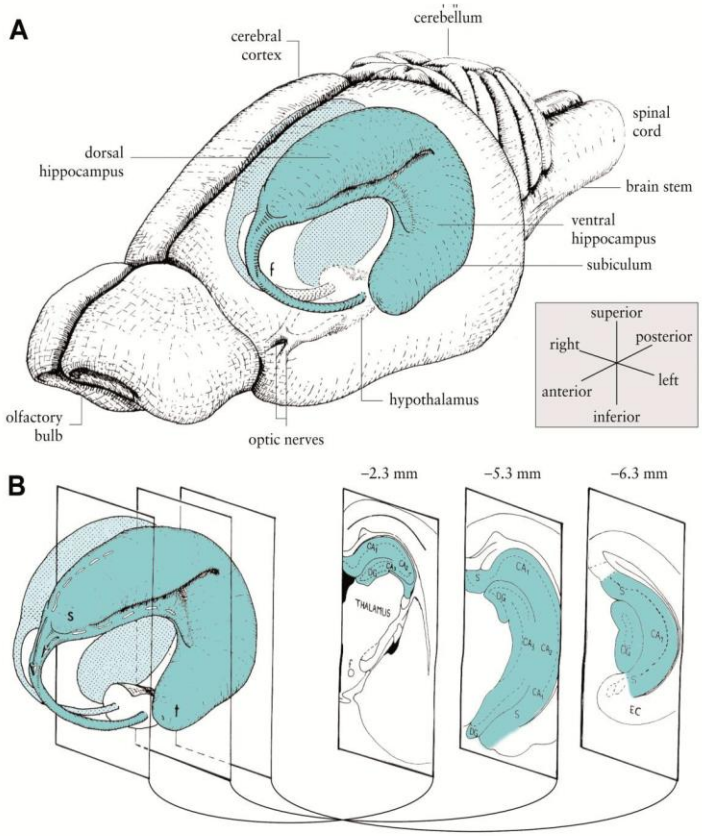

Figure 1: Schematic representations of hippocampal formation in rat.
A. Location of hippocampal formation in the rat brain. B. Coronal sections of the hippocampal formation along the anteroposterior axis. Antero-posterior coordinates with respect to the bregma are indicated above each section plane. CA1, 2, 3: ammon's horn fields 1-3; DG: dentate gyrus, EC: entorhinal cortex, f: fornix; s: septal pole of the hippocampal formation, t: pole"Temporal" of the hippocampal formation, S: subiculum. (Cheung & Cardinal, 2005), modified figure

According to Amaral and Witter (2004), the hippocampal region includes two sets of structures: The HF and the para-hippocampal region.

Three regions define the HF: the subiculum, the hippocampus proper (or Ammon's Horn) and the dentate gyrus (DG). In this manuscript, we will use the term hippocampus to refer to the region including the DG and the hippocampus proper.

1.2. Cytoarchitectonic Organization

In transverse (or coronal) view, the hippocampal formation is formed of two inverted U which constitute the principal cell layers of 2 regions: the Ammon Horn (subdivided into three fields named CA1, CA2 and CA3) and the dentate gyrus (Fig. 2). Each region of the hippocampal formation is organized in allocortical layers.

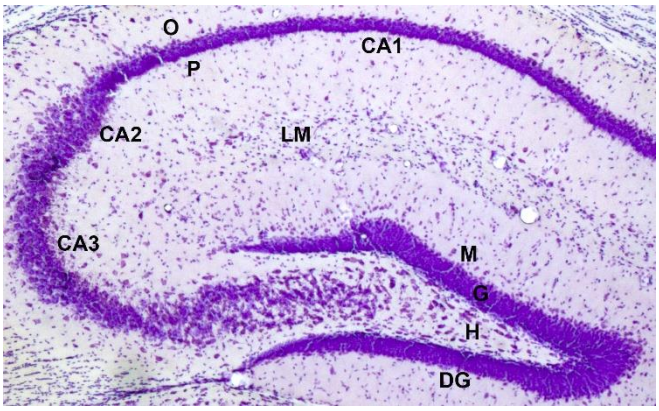

Figure 2: Cytoarchitectonic organization of the mouse dorsal hippocampus

Coronal section of the dorsal hippocampal stained with a cresyl violet coloration illustrating the different cell layers. CA1, CA2, CA3: CA1-3 fields of the Ammon Horn; O: stratum oriens; P: pyramidal stratum; R: stratum radiatum; LM: stratum lacunosum moleculare; DG: dentate gyrus; M: molecular layer; G: layer of granular cells; H: hilus.

1.2.1 The subiculum

The subiculum corresponds to the transition zone between the hippocampus and the regions of the parahippocampal cortex. It represents with CA1 the output regions of the hippocampal formation. The main histological feature of this region is a wider and less dense pyramidal cell layer than that of CA1.

1.2.2 The hippocampus proper

In the dorsal hippocampus, the CA1 field constitutes the upper part of the Ammon's Horn and the CA2 and CA3 regions, the lower regions (Fig. 2). In the rat and mouse, the region CA2 of the hippocampus is difficult to identify because it is not very large. It is often ignored or confused with the distal part of CA3: CA3a and in the literature, the CA2-CA3a terminology is usually used to refer to this region. At the level of the CA1-3 fields, the different layers can be distinguished: the alveus, a fiber layer enclosing the afferent and efferent fibers of the hippocampus; the stratum oriens; the pyramidal cell layer composed essentially of the cell bodies of the pyramidal cells; strata radiatum and lacunosum moleculare. At the level of the

CA3 field, there is an additional layer located between the stratum pyramidale and the stratum radiatum: the stratum lucidum which contains the axons of the granule cells called mossy fibers and their axon terminals innervating the distal dendrites of the CA3 pyramidal cells.

1.2.3 The dentate gyrus

The dendate gyrus (DG) is composed of three layers: the molecular layer (ML; subdivided into three layers: internal, middle and outer), the granule cell layer (GCL) that contains the cell bodies of the principal cells, and the hilus. It is the main entrance of the information in the hippocampus.

Two DG regions are distinguished: the suprapyramidal and infrapyramidal regions (Claiborne *et al.*, 1990) that differ by the level of proliferation and survival of adult newly born cells (Snyder et al., 2009) and the density of their inputs (Wyss, Swanson, & Cowan, 1979; Tamamaki, 1997).

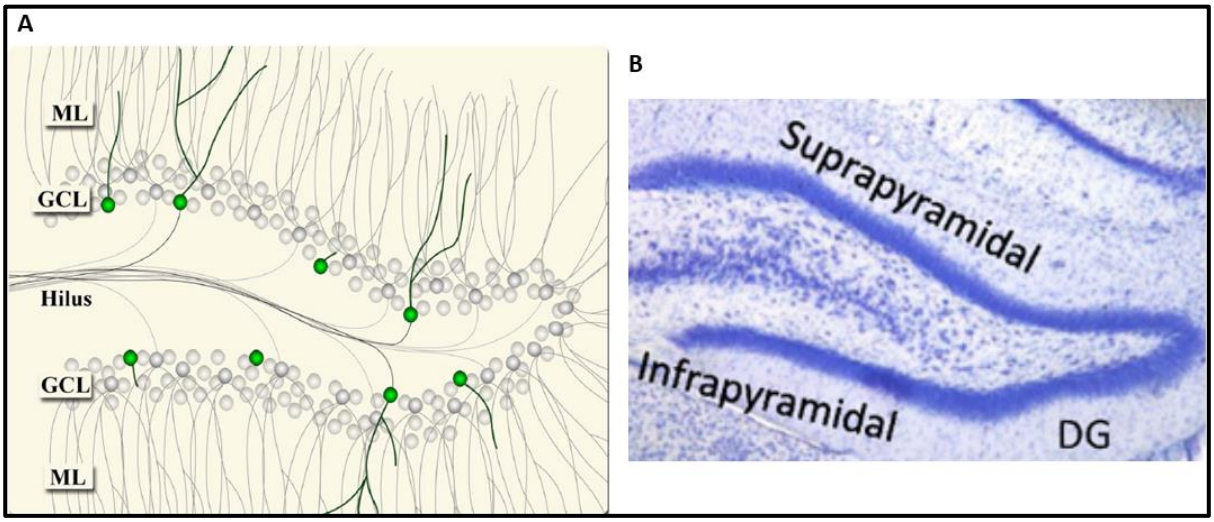

Figure 3: organization of the DG
(A)The main layers of the dentate gyrus (DG). The DG is mainly composed of a granular cell layer (GCL) , a molecular layer (ML) and the hilus.(Rosenzweig & Wojtowicz, 2011). (B) coronal section of DG stained with cresyl violet. Showing granular cell layers divided into two suprapyramydal and infrapyramidal (Schmidt, Marrone, & Markus, 2012)

1.2.4 Hippocampal cells

Many cell types are present in the hippocampal formation, they can be classified in three large families:

- excitatory Glutamatergic neurons including the pyramidal cells of the CA1, CA2 and CA3 regions, the granule cells (GC) of the DG ; the "giant cells" located in the stratum radiatum layers of CA1 (Gulyás et al., 1998) and CA3 (Savić & Sciancalepore, 2001), and hilar mossy cells (Ribak et al., 1985, Scharfman et al., 1990, Frotscher et al., 1991).
- The inhibitory GABAergic neurons are distributed in all layers of the HF. It is a very heterogenous population of neurons including many cell types that differ by their morphology, projection sites, and neurochemical content (Freund & Buzsaki, 1996, Sik et al., 1997, Cossart et al., 2006; Houser, 2007);
- Finally, non-neuronal glial cells, mainly include astrocytes, distributed in all layers of the HF and oligodendrocytes whose cell bodies are mainly located in the white matter including the alveus.

1.3 Hippocampal connections

1.3.1 Intra-hippocampal connections.

The connections between the different regions of the hippocampus are essentially unidirectional. The granule cells (GC) of the DG project on the CA3 pyramidal cells via the mossy fibers; the information then passes via the axonal fibers of the CA3 pyramidal cells, the Schaeffer collaterals, in CA1 and the information then leaves the hippocampus. The dentate gyrus is the main entrance of the information provided mainly by the entorhinal cortex through the perforant path. In addition to this main "tri-synaptic" glutamatergic network (Fig. 4), CA3 pyramidal cells send collaterals to CA2, and CA1 to the subiculum (Witter & Amaral, 2004).

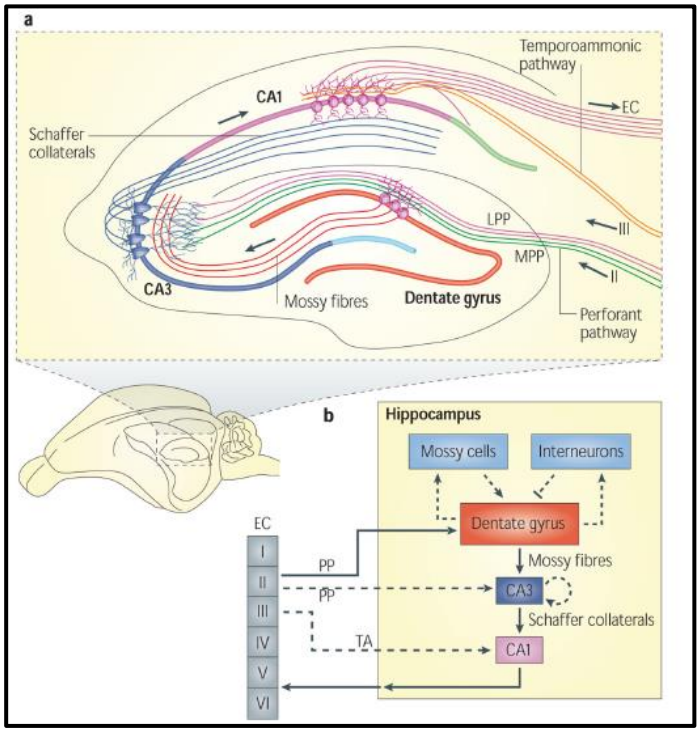

Figure 4. The neural circuitry in the rodent hippocampus
(a) An illustration of the hippocampal circuitry. **(b)** Diagram of the hippocampal neural network. The traditional excitatory trisynaptic pathway (solid arrows). The axons of layer II neurons in the entorhinal cortex project to the dentate gyrus through the perforant pathway (PP), including the lateral performant pathway (LPP) and medial perforant pathway (MPP). The dentate gyrus sends projections to the pyramidal cells in CA3 through the mossy fibers. CA3 pyramidal neurons relay the information to CA1 pyramidal neurons through Schaffer collaterals. CA1 pyramidal neurons send back projections into deep-layer neurons of the EC. CA3 also receives direct projections from EC layer II neurons through the PP. CA1 receives direct input from EC layer III neurons through the temporoammonic pathway (TA). The dentate granule cells also project to the mossy cells in the hilus and hilar interneurons, which send excitatory and inhibitory projections, respectively, back to the granule cells.(Deng, Aimone, & Gage, 2010).

Along the septo-temporal axis, there is a complex intrinsic connectivity between the principal cells and the interneurons in each region. Interneurons that are present in all regions of the hippocampus contact both glutamatergic cells and other interneurons (Freund & Buzsáki, 1996; Houser, 2007). Their projections are either transverse, meaning that these cells project at the same hippocampal level such as the granule cells of the DG, or longitudinal. It is the case of DG "basket cells" whose axons can extend transversely but also longitudinally along the septo-temporal axis up to 1.5 mm distance (Sik *et al.*, 1997; Houser, 2007).

The glutamatergic mossy cells in the hilus of dentate gyrus that innervate the proximal dendrites of the granule cells at the level of the inner molecular layer (Fig.4), also project longitudinally (Frotscher *et al.*, 1991). They constitute the main system of projection allowing interaction between the dorsal and ventral regions of DG.

The principal cells can also be interconnected with each other. It is the case of the CA3 pyramidal cells that form a recurrent glutamatergic local circuit. The principal cells of CA1 and CA2 have no or very few recurrent collaterals.

1.3.2 Commissural connections

In rodent rat as mouse, both hippocampal formations are highly interconnected. These connections are called commissural. They are made by certain GABAergic neurons, the hilar mossy cells and the pyramidal cells of CA3 and CA1. These commissural connections do not existent in monkeys and humans (Amaral & Witter, 2004).

1.3.3. Extrinsic connections

- *Efferents*

The principal cells of the subiculum and CA1 are the main output neurons of the hippocampal formation They innervate the neocortex and all limbic structures including the prefrontal and entorhinal cortex, the amygdala, mammillary body and lateral septum (Yoshida & Oka, 1995; Pitkänen *et al.*, 2000; Ishizuka, 2001).

In addition, pyramidal cells of the CA3 region project to the lateral septum (Swanson & Cowan, 1977), whereas some GABAergic cells of CA1, CA3 and the hilus of DG project to the median septum ((Toth & Freund, 1992; Freund & Buzsaki, 1996, Houser, 2007)C. R. Houser, 2007)*.*

- *Afferents*

The hippocampus is highly interconnected with two cortical structures, the amygdala and the entorhinal cortex. The perforant pathway axon bundle originating from the neurons of the superficial layers (II-III) of the entorhinal cortex is the main cortical pathway to the hippocampus (Steward & Scoville, 1976, Amaral & Witter, 2004). The neurons of layer II innervate the outer two thirds of the molecular layer of DG and, the neurons of layer III, the stratum lacunosum moleculare of the CA1 and CA3 regions. Another pathway originating from the neurons of the deeper layers of the entorhinal cortex was also highlighted. These neurons within the layers IV-VI innervate the molecular layer of the ventral DG only (Deller et al., 1996, 1998). The amygdala nuclei that project to the hippocampus innervate the ventral CA1-CA3 regions, especially CA1 but not the DG (Pitkänen *et al.*, 2000).

The hippocampus is also connected with subcortical structures in particular the septum nuclei (Nyakas *et al.*, 1987; Gaykema *et al.*, 1990; Yoshida & Oka, 1995; Lübke *et al.*, 1997). It receives GABAergic and cholinergic afferents mainly from the median septum and nuclei of the Broca Diagonal Band (complex SM / BDB). The cholinergic fibers innervate mainly the supragranular layer and the middle part of the molecular layer of the DG, the Stratum radiatum and lacunosum moleculare of CA1 as well as the stratum oriens and radiatum layers of CA3. The GABAergic fibers end in the same layers of CA1 and CA3 as well as in the hilus of DG but exclusively on GABAergic neurons(Freund & Antal, 1988). This septo-hippocampal projection is topographically organized so that the cells located in the most medial parts of the median septum project towards the dorsal regions of the hippocampus and the cells that are located laterally innervate the ventral regions of the hippocampus.(Nyakas *et al.*, 1987; Gaykema *et al.*, 1990). More recently it has been suggested that medial septal glutamatergic neurons innervate CA1, CA3 and DG regions(Colom *et al.*, 2005) but the distribution profile of these fibers in these regions, their postsynaptic targets as well as the topography of these projections have not yet been well characterized.

The hippocampus also receives afferents from other subcortical structures, including the thalamus, brainstem, and hypothalamus. The neurons of the thalamus innervating the hippocampus are essentially neurons located in the nucleus reuniens. They project into the molecular layers of CA1 and subiculum. These glutamatergic afferences are topographically organized: the neurons located in the dorsal part of the nucleus project into the dorsal hippocampus and those located in the ventral part of the nucleus innervate the ventral hippocampus(Amaral & Witter, 1989; Dolleman-Van der Weel & Witter, 2000; Halasy *et al.*, 2004).

Brain stem nuclei that project into the hippocampus are locus coeruleus and nuclei of the median and dorsal raphe (Amaral & Witter, 2004). The raphe nuclei project to the hilus of DG, CA3 and CA1 and only on interneurons (Halasy *et al.*, 1992); some of these afferents are serotoninergic. Most of the neurons of the locus coeruleus innervating the DG and CA1-CA3 regions are noradrenergic.

The afferents from the hypothalamus originate mainly from the supramammillary region but also from the tuberomammillary nucleus. The neurons of the tuberomammillary nucleus provide innervation to the hippocampus (Köhler *et al.*, 1985) and these afferences are histaminergic (Panula *et al.*, 1989). Supramammillaro-hippocampal projections will be described in Chapter II.

Thus, the connections of the hippocampal formation can be considered at three levels: intrinsic, local connections present in the dorsal and ventral regions of the hippocampus; connections connecting these two regions that involve essentially the mossy cells of the DG hile and extrinsic connectivity very varied but nevertheless organized with extrinsic afferences that innervate neuronal populations and very specific cell layers. Since the dorsal (septal) and ventral (temporal) regions of the hippocampal formation are involved in different and have different connectivities, this selective and specific connectivity along the septotemporal axis can be related to different functional properties of the hippocampus (Fig.5).

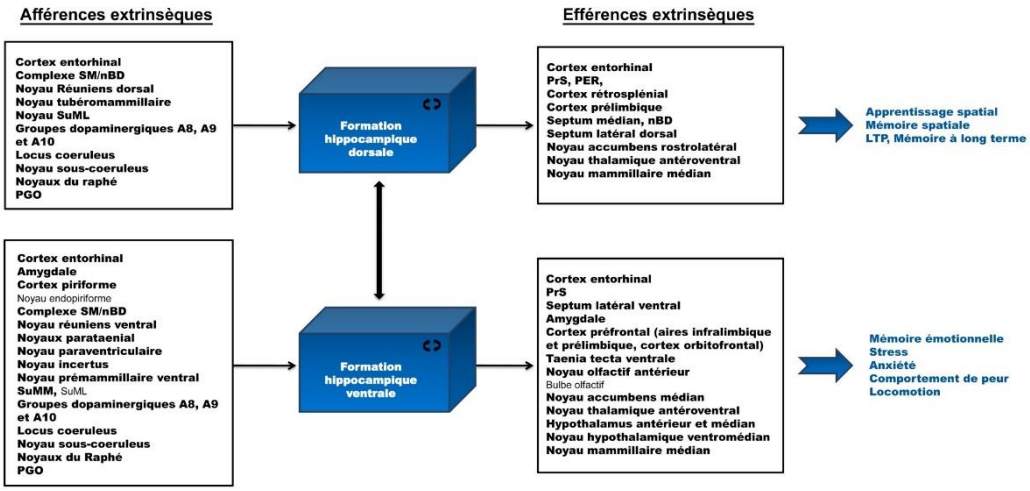

Figure 5 : Dissociation of hippocampal functions in rats
local intra-hippocampal longitudinal connections. Extrinsic afferences and efferences of the hippocampal formation related to the different functions of the hippocampal formation. Abbreviations : SM / BDB: septum complex of the Broca diagonal band; SuML: supramammillary lateral nucleus; SuMM: medial supramammillary nucleus; A8: dopaminergic region of the retrorbral field; A9: dopaminergic region of the substantia nigra; A10: dopaminergic regions in the ventral tegmental area; PGO: onto-geniculo-occipital; PrS: presubiculum; PER: perirhinal cortex.

2. Supramammillary Nucleus (SuM).

2.1. SuM position and Structure.

The boundary delineation of the SuM and its dissection into parts mainly described in rat display some differences according to different authors. According to the rat brain atlas of (Paxinos & Watson, 1998) or of the mouse brain Atlas (Paxinos & Franklin, 2004), SuM is a small nucleus or set of nuclei, lying above the mammillary bodies and below the posterior hypothalamic area.

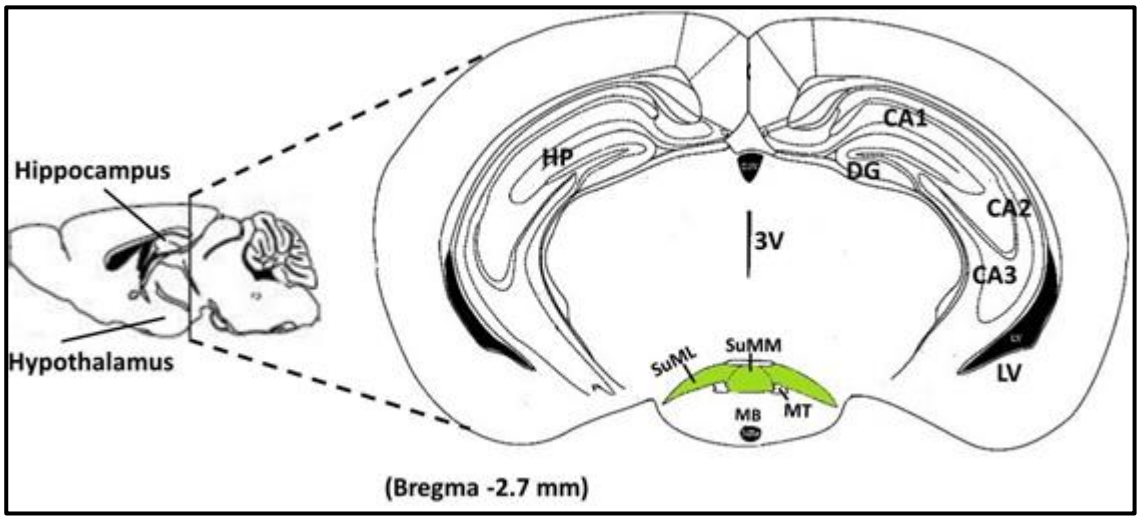

Figure 6: Coronal view of the mouse brain showing the location of the SuM (green fills).
It illustrates the lateral part of the SuM (SuML) and the median part (SuMM) as well.
Abbreviations: 3V: third ventricle; **CA**: Corn of Ammon CA (1-3); **DG**: dentate gyrus; **HP**: hippocampus **LV**: lateral ventricle; **MB**: mammillary bodies; **MT**: mammillary tract; **RSC**: retrosplenial cortex; **SuML**: lateral supramammillary nucleus **SuMM**: median supramammillary nucleus (Paxinos & Franklin 2004)

.

The lateral area of the hypothalamus borders it dorsolaterally. The caudal lateral part of the area is named, by them, the lateral SuM (abbreviated by them, SuML), and the caudal medial part is named medial SuM (SuMM), but the rostral part is simply called SuM and is not explicitly divided into medial and lateral parts (Fig.6).

Swanson (1998) divided SuM into a medial part (SuMm) and a lateral part (SuMl). The medial part contains smaller cells and the lateral part contain the larger ones (Swanson, 1982; Risold & Swanson, 1997). This definition is based on the cellular content: SuMm includes dopaminergic cells, which project to the lateral septal nucleus (LS), but not to the hippocampus (Swanson, 1982); while SuMl contains large cells that project directly to the hippocampus (Haglund *et al.*,

1984b; Maglóczky *et al.*, 1994) and the entorhinal area (Swanson, 1982). The SuM area in Swanson' s atlas is larger. Swanson' s SuMl includes parts of the lateral hypothalamus (LH) of Paxinos and Watson and at its most rostral, includes their submammillothalamic nucleus.

Pan and McNaughton (2004) propose a new, nomenclature derived from the superficial appearance of the cells in the different areas. They name the most central area the parvicellular SuM (SuMp). This is characterized most easily by having small cells (10– 15 mm, (Borhegyi & Leranth, 1997) and being centrally located without making contact with the mammillary tract (MT). It contains cells that label for substance P or. It corresponds to the most medial part of medial SuM (SuMM) in most other classifications. It is largely the same as Swanson' s and Paxinos's SuMm except that its border remains clear of MT. The next area, moving laterally, is termed the grandicellular SuM (SuMg). It is characterized most easily by its content in large cells (30 mm, (Borhegyi & Leranth, 1997) that are clustered around, or located above and to either side of MT. These large cells are scattered among smaller cells and so the boundary of the nucleus does not correspond to the location of the large cells themselves. The nucleus corresponds, caudally, in its lateral boundary to Paxinos and Watson' s SuML and rostrally to their SMT. It is a medial portion of Swanson' s SuMl. the SuMg contains calretinin but not subtance P containing neurons. The most lateral area is named the supramammillary shell (SuMs). This corresponds to the lateral part of the SuMl of Swanson and to the ventromedial part of the LH of Paxinos and Watson. It is characterized by smaller cells that are less tightly packed than those of SuMp. It contains cells labeled for calretinin (Borhegyi & Leranth, 1997) or cholecystokinin (CCK) (Lantos *et al.*, 1995).

2.2. Neuronal populations in supramammillary region.

The SuM is composed of a heterogenous population of neurons that differ by their neurochemical content and the specificity of their connections (see below).

All these neuronal populations in the SuM project to several brain regions in a topographic pattern as well as within the different SuM regions. For example, dopaminergic neurons which are located in SuMM innervate the Mammillary Bodies (MB) ((Gonzalo-Ruiz *et al.*, 1992a,

1992b) as well as LS (Shepard *et al.*, 1988) (Fig.8). SuMM also contains Substance P-expressing cells projecting to CA2 pyramidal cells of the hippocampus (HP) (Borhegyi & Leranth, 1997). SuMM gutamatergic neurons innervate the medial PO (Kocsis *et al.*, 2003), CA2 region of HP (Soussi *et al.*, 2010) and the ventral dentate gyrus (DG). VIP-immunoreactive cells (Haglund *et al.*, 1984b) and CCK- expressing cells in the most lateral part of the SuML(SuMs) innervate the HP and the entorhinal cortex (Greenwood *et al.*, 1981). A population of CCK- expressing cells also projects to the brain stem (Kiyama, Shiosaka, Takami, *et al.*, 1984; Kiyama, Shiosaka, Tateishi, *et al.*, 1984) especially to ventral tegmental area (VTG) (Fig. 9). Calretinin-containing neurons are distributed troughout all region of the SuM (Borhegyi & Leranth, 1997). Some CR-containing neurons mainly located within the SuML has been described to innervate the MS and LS (Leranth & Kiss, 1996a) , the CA2 region of the HP as well as the DG (Kiss *et al.*, 2000). Whereas all these calretinin neurons belong to an homogenous population of neurons targeting these different brain structures is still unclear. In our second studying which investigate the neurochemical properties of the neurons from the SuML innervating the dorsal DG we address and discuss this issue.

2.3. SuM connections.

The SuM as a whole structure, interacts with many structures located in different regions of the central nervous system (Fig. 7): the brainstem, the hypothalamus, the thalamus, the septum nuclei, the substance innominata and several neocortical and cortical regions. In a general way the SuM is connected to the different structures of the limbic system including the hippocampus.

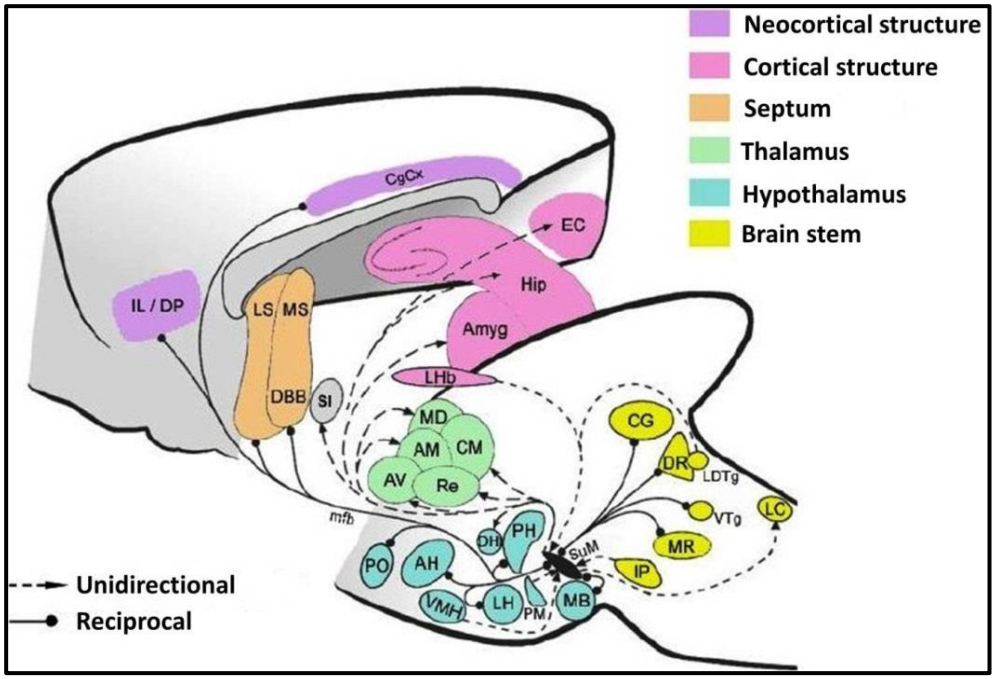

Figure 7: Connections of the SuM regardless of its divisions into parts.
This figure illustrates the several unidirectional (efferent or afferent) and reciprocal connections between the SuM (black fill at the bottom) and most of the brain regions. Each brain region is differentiated with a defined color. **Abbreviations**: see list of abbreviations (W.X. Pan & McNaughton, 2004)**.**

2.3.1. *Afferents to SuM*.

SuM receives many inputs from different regions of the brain (Fig. 7 and Fig. 8). These inputs are divided into descending afferents which are coming from the anterior parts of the brain and ascending afferents which are coming from the posterior parts of the brain (Fig. 7) (for review see W.-X. Pan & McNaughton, 2004).

The main ascending inputs to the SuM are principally from the brain stem including; latero-dorsal tegmental nucleus (LDTg), populations of Raphe Nucleus (RN) and central gray region (CG) (Gonzalo-Ruiz *et al.*, 1999; Vertes *et al.*, 1999).

The main descending inputs to the SuM (Fig. 8) originate from neocortical structures such as the infralimbic cortex (IL) and the dorsal peduncular cortex (DP). The septum, in particular the medial (MS) and lateral (LS) nuclei, also innervates the SuM massively, as well as the DBB. Moreover, the SuM receives axon fibers from the lateral habenula (LHB) which is a caudal thalamus nucleus. The pre-mammillary nucleus (PM) also projects to the SuM (Kiss *et al.*,

2002). In addition, the anterior hypothalamus (AH) innervates the SuM through its medial and lateral preoptic area (PO) (Kiss *et al.*, 2002)

The inputs are not only direct inputs, but also, there are some indirect inputs such as the entorhinal-septo-supramammillary nucleus network. The EC innervates the SuM indirectly through a neuronal population located on the border between the MS and LS (Leranth *et al.*, 1999).

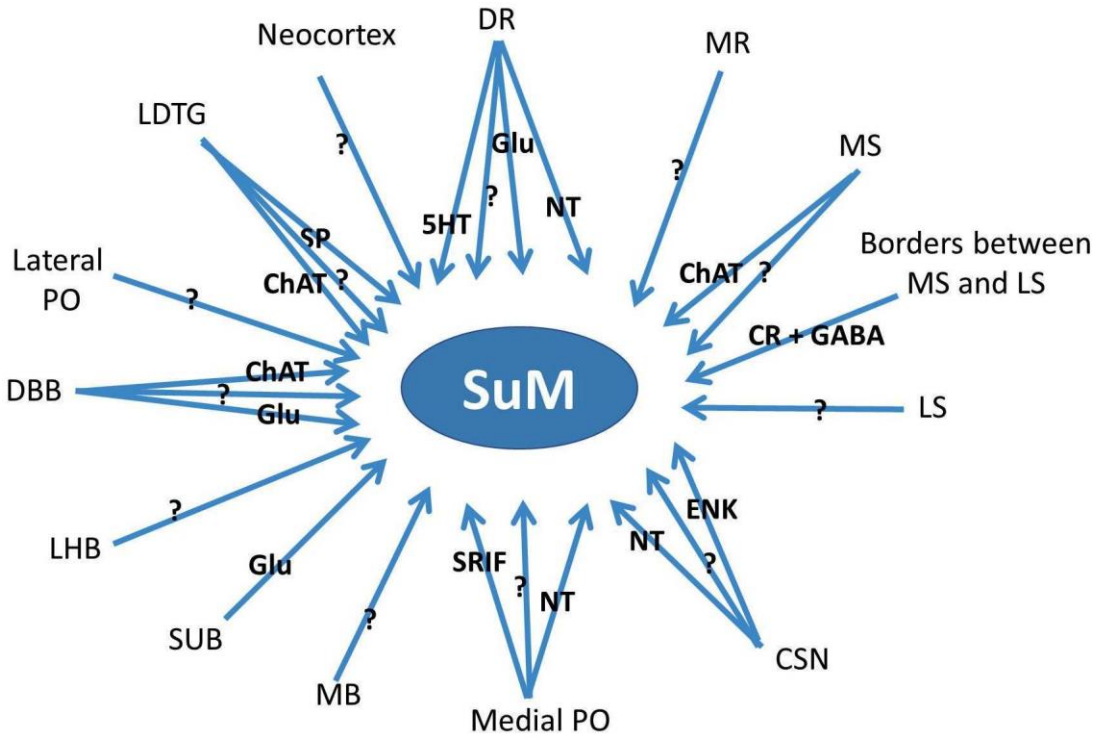

Figure 8: Afferent projections to the SuM. This diagram represents the projections from the different brain regions innervating the SuM. The neuronal types of some of these projections have been identified while the rest of them remain to be known. **Abbreviations**: see list of abbreviations.

Abbreviations:

5HT : 5-hydroxytryptamine (Seretonin)
ChAT : Choline acetyltransferase
SRIF : Somatotropin release–inhibiting factor (Somatostatin)
GABA: Gamma-Aminobutyric acid
ENK : Enkephaline
Glu : Glutamate
SP : Substance P
NT : Neurotensine
CR : Calretinine
? : Unknown

2.3.2. Efferents from SuM.

The SuM itself projects to several brain regions. Like the afferents, the efferents from the SuM are also divided into ascending and descending projections. The ascending projections include the projections from the SuM to the diencephalon (thalamus and hypothalamus) and telencephalon (cerebral cortices). The descending projections from the SuM innervate the brain stem (Shibata *et al.*, 1986; Grove, 1988).

The descending outputs from the SuM to the brain stem (Fig. 9) are principally to Central Gray (CG), median and dorsal RN. In addition, it innervates the Locus Coeruleus (LC) which is a nucleus in the posterior part of the brain stem.

The ascending efferents from the SuM (Fig. 9) are reciprocal with the MS LS, and MB as well as the DBB. In addition, SuM provided unidirectional projections to the frontal cortex (FC), Entorhinal cortex (EC), amygdala (AMYG) and massively the HP. In the thalamus, the SuM projects to most of the medial nuclei (Vertes, 1992).

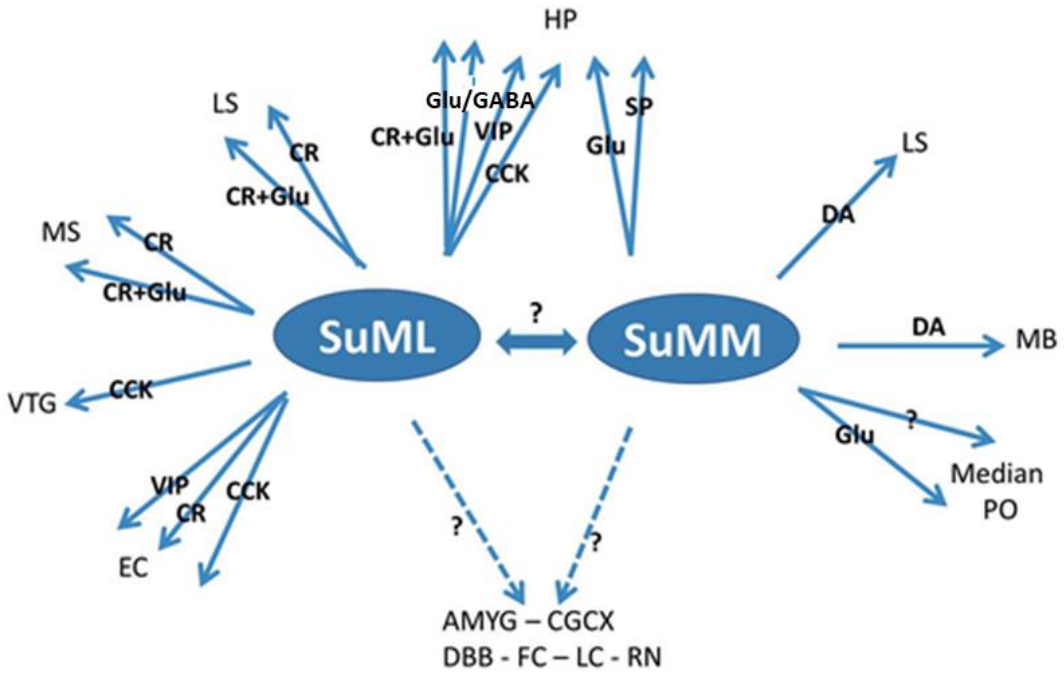

Figure 9: Efferents originating from the SuM. Some brain regions receive inputs from the SuM without knowing from which part exactly (dashed arrow). The neuronal types of some of these projections have been identified while the rest of them are still unknown. **Abbreviations**: see list of abbreviations.
Abbreviations:

Glu : Glutamate
DA : Dopamine
? : Unknown
SP : Substance P
CCK : Cholecytokinine
CR : Calretinine
VIP : Vasointestinal peptide

2.4. The Sum-hippocampus network.

The SuM provides substantial unidirectional and monosynaptic projections to the hippocampal formation (Segal & Landis, 1974; Pasquier & Reinoso-Suarez, 1976, 1978; Wyss *et al.*, 1979a; Haglund *et al.*, 1984a; Vertes, 1992; Maglóczky *et al.*, 1994; Vertes & McKenna, 2000). Extensive investigations have been performed in several species on the supramammillary–hippocampal pathway (for review see Vertes & Kocsis, 1997; Leranth & Hajszan, 2007). In the rat, hippocampal formation afferents from the SuM mainly originate from the lateral two-thirds of the SuM (SuML) (Wyss *et al.*, 1979a; Saper, 1984; Maglóczky *et al.*, 1994; Vertes & McKenna, 2000) that predominantly innervate the DG throughout the dorsal and

ventral hippocampus and the CA2／CA3a region of the dorsal hippocampus(Wyss *et al.*, 1979b; Haglund *et al.*, 1984a; Saper, 1984; Vertes, 1992; Maglóczky *et al.*, 1994) . Neurons of the medial part of the SuM (SuMM) project almost exclusively to the ventral DG (Vertes, 1992; Maglóczky *et al.*, 1994). The majority of the SuM projections target the proximal dendrites and somata of principal neurons (granule and pyramidal cells) (Maglóczky *et al.*, 1994) . However, some specific populations of GABAergic interneurons are also innervated by SuM fibers(Nitsch & Leranth, 1996a) .

For many years the neurotransmitter identity of these SuM-Hippocampal pathways was source of debates. Several authors considered these pathways likely to be glutamatergic (excitatory). This was based on studies showing that: (i) some afferents from the SuM form asymmetric synapses(Dent *et al.*, 1983; Stanfield & Maxwell Cowan, 1984; Maglóczky *et al.*, 1994), considered to be a feature of excitatory synapses, and (ii) supramammillary neurons and associated axon terminals that innervate the inner molecular layer of the DG and the CA2 pyramidal layer contain calretinin but lack GABA immunoreactivity(Maglóczky *et al.*, 1994; Leranth *et al.*, 1999; Kiss *et al.*, 2000). Such an excitatory glutamatergic phenotype for SuM–hippocampal direct projections was difficult to reconcile with electrophysiological studies reporting that neurons from the SuM inhibit dentate neurons (Segal, 1979; Mizumori *et al.*, 1989) and facilitate perforant path elicited population spikes in the dentate gyrus (Mizumori *et al.*, 1989; Carre & Harley, 1991; Nakanishi *et al.*, 2001) via disinhibition of DG interneurones (Mizumori *et al.*, 1989; Nakanishi *et al.*, 2001).

Few years ago, Soussi and colleagues (2010) revealed two distinct neurochemical SuM-Hippocampal pathways in rat, resolving a long-lasting dispute. They demonstrated that SuM neurons from the most medial part of the SuM (SuMM, referred also as SuMp by Pan and McNaughton, 2004) innervating the inner molecular layer of the ventral DG and CA2 pyramidal cells are glutamatergic. Whereas SuM neurons located in the lateral two-third region of the SuM (SuML, also referred as SuMg by Pan and McNaughton, 2004) that innervate the supragranular layer of the dorsal DG and to a lesser extend the ventral DG, display a unique dual neurotransmitter phenotype being both glutamatergic and GABAergic. Indeed, these neurons

and their axon terminals contain markers of GABAergic neurotransmission, including the synthesizing enzyme of GABA, glutamate decarboxylase 65, and the vesicular GABA transporter as well as a marker of glutamatergic neurotransmission, the vesicular glutamate transporter 2. (Boulland *et al.*, 2009; Soussi *et al.*, 2010). These axon terminals from SuML neurons establish asymmetric (excitatory) and symmetric synapses (inhibitory) on DG cells (Soussi *et al.*, 2010) suggesting that SuML neurons innervating DG could co-release of GABA and Glutamate on granule cells. One of the goal of our first study was to test this hypothesis combining structural connectivity techniques using neurotropic viral vectors (rabies virus, AAV), neurochemical anatomy (immunohistochemistry, in situ hybridization) with optogenetic and in vitro (patch clamp) electrophysiological recordings performed in the dorsal DG of transgenic VGLUT2-cre mice expressing specifically the excitatory opsin Channel Rhodopsine 2 (ChR2) in the SuM-DG pathway (see first study).

2.5. The role of supramammillary nucleus.

The SuM has been shown to be involved in the regulation of hippocampal theta rhythm(Kirk & McNaughton, 1991, 1993; Kocsis & Vertes, 1994; Pan & McNaughton, 2004a; Kocsis & Kaminski, 2006) and therefore could play a role in the control of several hippocampal-dependent cognitive functions such as emotional learning and memory(Pasquier & Reinoso-Suarez, 1976; Richmond *et al.*, 1999; Pan & McNaughton, 2002; Santín *et al.*, 2003; Pan & McNaughton, 2004a; Shahidi, Motamedi, & Naghdi, 2004) as well as sleep-waking cycle (Renouard *et al.*, 2015; Pedersen *et al.*, 2017) including REM sleep (Renouard *et al.*, 2015). Many of these studies have used, as experimental approaches, reversible or non-reversible, chemical or electrolytic lesions of the SuM, and the analysis of the expression of the c-Fos protein. The increased immunoreactivity of the c-Fos protein in a given region accounts for an increase in cellular activity in this region (Dragunow & Faull, 1989) and the study of the expression of this protein is often used as a marker of neuronal activity to visualize the brain regions that are active in given situations. These techniques have been combined with behavioral and / or memory tasks.

It has been shown that when the animal is placed under stress or anxiety, a strong increase of the c-Fos protein is observed in the supramammillary nucleus suggesting a role of the SuM in the treatment of these emotional responses (Silveira *et al.*, 1993; Kiyohara *et al.*, 1995; Cullinan *et al.*, 1996; Wirtshafter *et al.*, 1998; Vann *et al.*, 2000). The SuM is also associated with other emotional behaviors: passive avoidance behavior, emotional defense behavior (Shahidi, Motamedi, Bakeshloo, *et al.*, 2004; Aranda *et al.*, 2006) and fear behaviour (Pan & McNaughton, 2002, 2004c). As a result of these studies, the medial supramammillary nucleus is always the region of the SuM implicated in these emotional behaviors.

SuM lesions impair the memory performance of rats when tested in the Morris Pool, a test that studies learning and spatial memory. These studies have shown that the supramammillary nucleus plays a minimal role in spatial working memory and is not involved in the task acquisition phase (Shahidi, Motamedi, & Naghdi, 2004; Aranda *et al.*, 2006). Learning and spatial memory involve the dorsal hippocampus (Moser & Moser, 1998; Bannerman *et al.*, 1999; Richmond *et al.*, 1999), which is mainly innervated by SuML. However, these lesion studies have targeted predominantly SuMM (Pan & McNaughton, 1997, 2004c).

Several recent studies suggest that the SuML-DG pathway could be instrumental for REM sleep functions. Indeed it has been shown that granule cells of the DG play a key role in the formation of the contextual component of fear memories (Denny *et al.*, 2014). In parallel, it has recently been demonstrated that consolidation of contextual fear conditioning (Boyce *et al.*, 2016; Ravassard *et al.*, 2016) is impairs by REM sleep deprivation or theta inactivation specifically during REM. Interestingly the DG is the only cortical region that display more activated neurons during PS hypersomnia than waking (Renouard *et al.*, 2015). In contrast, the other main hippocampal structures CA1 and CA3 did contain activated neurons only during waking. Combining retrograde tracing, neurotoxic lesion and FOS immunostaining, it was therefore suggested that neurons from the SuML were responsible for the activation of DG granule cells during REM sleep (Renouard *et al.*, 2015). Such activation might play a key role in the previously reported beneficial effect of REM sleep on learning and memory (Maquet *et al.*, 2000). The second goal of our first study was to determine if and how the SuML-DG pathway

control DG neurons activity during REM and other vigilance states. For this purpose we combined innovative structural connectivity techniques using neurotropic viral vectors (rabies virus, AAV), neurochemical anatomy (immunohistochemistry, in situ hybridization) with in vivo (LFP, EEG) optogenetic and electrophysiological recordings performed in the dorsal DG of transgenic VGLUT2-cre mice expressing specifically the excitatory opsin Channel Rhodopsine 2 (ChR2) or inhibitory opsin Halorhodopsin (NpHR3) in the SuM-DG pathway (see first study).

3. Epilepsies.

3.1. General classification

Epilepsy is one the most common chronic neurological disorder. Approximately 1% of the world population is affected and up to 5% suffering from single seizure during their life. The International League Against Epilepsy (ILAE) identified seizure and epilepsy as following (Fisher *et al.*, 2014):

An epileptic seizure: is a transient occurrence of signs and/or symptoms due to abnormal excessive or/and synchronous neuronal activity in the brain.

Epilepsy: is a disorder of the brain characterized by an enduring predisposition to generate epileptic seizures, and by the neurobiological, cognitive, psychological, and social consequences of this condition. The definition of epilepsy requires the recurrence of spontaneous seizure.

The classification of seizures is summarized in the ILAE 2017 seizure classification (Fisher, Cross, D'Souza, *et al.*, 2017; Fisher, Cross, French, *et al.*, 2017). Seizures were classified into: focal (partial), generalized and unknown onset. (Table 1).

Focal Onset	Generalized Onset	Unknown Onset
Aware/impaired awarenes	Motor (Tonic- clonic/other motors	Motor (Tonic- clonic/other motors
Motor & non-motor onset	Non-motor (Absence)	Non-motor (Absence)
Focal to bilateral tonic-clonic		Un classified

Table 1 The basic ILAE 2017 operational classification of seizure types (Fisher, Cross, D'Souza, *et al.*, 2017; Fisher, Cross, French, *et al.*, 2017)

3.2. Temporal lobe Epilepsies (TLE).

Temporal lobe epilepsy (TLE) is the most common form of focal onset (partial) epilepsy in humans. It is the most common form of drug-resistant epilepsy. ILAE in 1985 defined TLE as a condition characterized by recurrent seizures originated from the temporal lobe of one hemisphere.

TLE classified into two main categories according to the structure involved during seizures: The lateral temporal lobe epilepsy (LTLE) where seizures originate from the neocortex of the outer surface of temporal lobe and the Mesial temporal lobe epilepsy (MTLE) where seizures arise from the limbic structure in the medial temporal lobe including the hippocampal formation the entorhinal cotex and the amygdala (Bartolomei *et al.*, 2001).

MTLE seizures, in terms of semiology, are characterized by:

- A dream state, epigastric, olfactory or taste subjective sensations ("auras") associated with emotional sensations (eg fear, anxiety). These auras usually occur at the onset of seizures and typically last for a few seconds (Maillard *et al.*, 2004; Dupont *et al.*, 2015)
- Oro-alimentary automatisms (chewing), abnormal uncontrolled movements of the upper limbs and vocalizations. These symptoms are more common during the second phase of seizures and usually last for one to two minutes (Maillard *et al.*, 2004; Dupont *et al.*, 2015), After seizures, patients often experience disorientation, short-term memory deficit, amnesia of the seizure and dysphasia (language disorder). This phase lasts a few minutes (Maillard *et al.*, 2004; Dupont *et al.*, 2015).

MLTEs are frequently associated with hippocampal sclerosis (HS). In the case of hippocampal atrophy, magnetic resonance imaging (MRI) scanners reveal a marked decrease in the volume of the hippocampus by 15 to 35% (Berg, 2008).The histopathological analysis of the surgical specimen confirms these results and shows significant cell loss in the (CA1) region and in the hilus of the DG (Thom, 2004) associated with gliosis. Dispersion of DG granule cells is also reported in some cases (Houser, 1990)as well as Spouting of mossy fibers, the axon of granule cells that invade the inner molecular layer of the DG (Houser *et al.*, 1990).

The clinical history of patients with MTLE and HS is often related to an initial trauma (prolonged

febrile seizures, for example) that occurred shortly after birth or in infancy, the first spontaneous seizure occurring in adolescence or adulthood (Engel, 1996; Berg, 2008). Some patients with MTLE also suffer from cognitive deficits and sometimes mood disorders, anxiety or depression that are the most frequent comorbidities in these epilepsies. They occur during the intercritical phase (between seizures) and have a significant impact on the quality of life of patients(Hermann *et al.*, 1997).

Several studiez suggests that some emotional factors such as stress and anxiety may induce seizures in some patients (Zeitlin *et al.*, 1995; Fisher, 2000; Lanteaume *et al.*, 2009). The cognitive deficits associated to these epilepsies are mostly episodic memory and spatial memory disorders(Abrahams *et al.*, 1999; Helmstaedter & Kurthen, 2001).

3.3. The Pilocarpine model of MTLE

The animal model of MTLE we used in our study is induced by intraperitoneal injection of pilocarpine, a muscarinic cholinergic agonist. This model has been first developed in rat (Turski, Cavalheiro, Schwarz, *et al.*, 1983; Turski *et al.*, 1986; Cavalheiro *et al.*, 1987) and adapted to mouse (see last study). It is a model of epilepsy (spontaneous recurrent seizures) induced by a status epilepticus (SE) triggered by the injection of the drug. In this model, spontaneous recurrent seizures are of limbic origin (Leite *et al.*, 1990).

Three phases in the evolution of this epilepsy can be distinguished:

-A period following the injection of pilocarpine during which the animal display electrographic seizure associated with several behavioal changes including staring spells, limbic gustatory automatisms, and motor limbic seizures that progressively developed into limbic SE. This SE corresponds to a continuous seizure activity that can last up to 24 hours without pharmacological intervention. During this phase, electroclinic seizure activity of limbic origin is (Turski, Cavalheiro, Schwarz, *et al.*, 1983; Turski *et al.*, 1986; Cavalheiro *et al.*, 1987).

- A latent period whose duration varies according to species (around two weeks in rats; 3days in mouse) and during which the animals display a relatively normal behavior and no seizure;

- A chronic stage, characterized by recurrent spontaneous seizure of limbic origin, the animals are epileptic. The seizures persist for the rest of the animal's life (Mello *et al.*, 1993; Cavalheiro *et al.*, 1994).

This model reproduces some electrographic and neuropathological aspects of humans MTLE (Turski, Cavalheiro, Schwarz, *et al.*, 1983; Turski *et al.*, 1984). The epileptogenic network involves the limbic system, some brain alteration are similar to those described in patients with ELTM (brain damage, cell loss that can progress to hippocampal sclerosis, reactive axon plasticity, cognitive impairment, ...). These alterations are discussed in the next chapter.

3.4. Neuronal alterations in the pilocarpine model induced in rodents

Status epilepticus (SE) induced by the injection of pilocarpine induce complex alterations and reorganization of neuronal networks. Most of the initial lesions have been reported in the hippocampus and the entorhinal cortex. At the chronic stage when the animals display spontaneous seizure additional lesions are observed in several other brain structures including the amygdala, the piriform cortex, the claustrum and thalamus (Turski, Cavalheiro, Turski, *et al.*, 1983; Scorza *et al.*, 2009). The majority of studies have been performed in the hippocampus with the hypothesis that MTLE results from an aberrant hippocampal network triggered by the initial brain insult (SE). In several animal models of MTLE induced easier by kainic acid or pilocarpine I.P. injection many studies have demonstrated that the initial brain insult caused by status epilepticus leads to a complex time-dependent reorganization of the intrinsic gammaaminobutyric acid (GABA)-ergic (Obenaus *et al.*, 1993; Houser & Esclapez, 1996; Esclapez & Houser, 1999; Cossart *et al.*, 2001; Dinocourt *et al.*, 2003; Kobayashi & Buckmaster, 2003; Sloviter *et al.*, 2003; Peng *et al.*, 2013) and glutamatergic(Nadler *et al.*, 1980; Ben-Ari *et al.*, 1981; Tauck & Nadler, 1985; Mello *et al.*, 1993; Represa *et al.*, 1993; Okazaki *et al.*, 1995; Esclapez *et al.*, 1999; Lehmann *et al.*, 2001; Okazaki & Nadler, 2001; Buckmaster *et al.*, 2002; Sloviter *et al.*, 2003; Boulland *et al.*, 2007; Jiao & Nadler, 2007; Ribak *et al.*, 2012) hippocampal networks. It includes: 1) A neuronal loss that is dose- (Turski *et al.*,

1989; Liu *et al.*, 1994) and age-dependent (Cavalheiro *et al.*, 1987) and is associated with significant reactive gliosis (Mello *et al.*, 1993; Obenaus *et al.*, 1993). It leads to a deformation of the hippocampal tissue including shrinkage (Obenaus *et al.*, 1993; Liu *et al.*, 1994); 2) A reorganization of the surviving cells including reactive axon plasticity and modification of their membrane properties(Houser & Esclapez, 2003; Epsztein *et al.*, 2005; Ben-Ari *et al.*, 2008; Marcelin *et al.*, 2009; Peret *et al.*, 2014; Artinian *et al.*, 2015; Crépel & Mulle, 2015; Ouedraogo *et al.*, 2016). Most of these alterations are illustrated in Fig 10 and we will describe in the following sections those reported in both the rat and mouse pilocarpine model of MTLE.

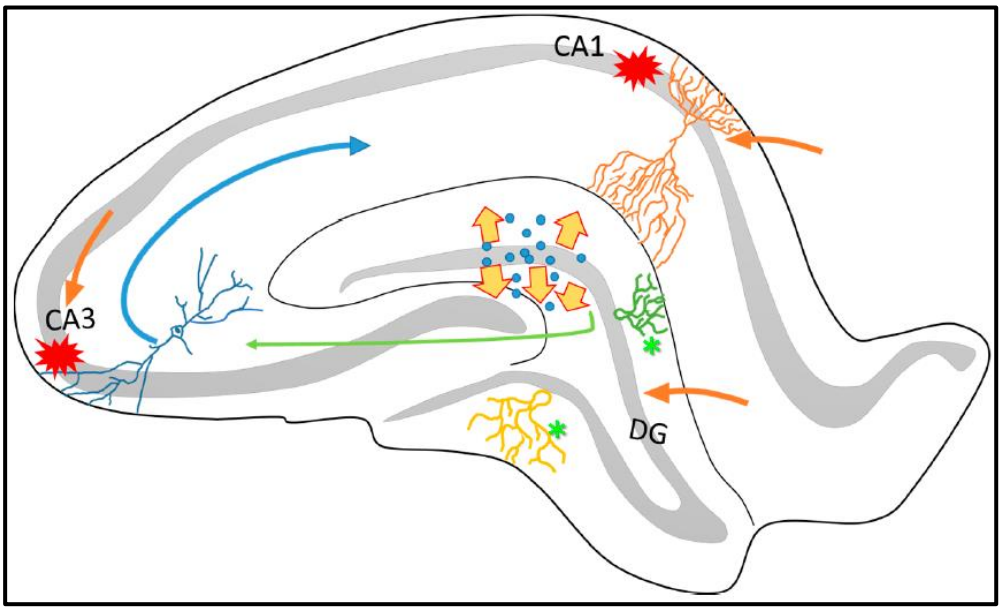

Figure 10. Schematic representation of the structural organization of the rat hippocampus and changes occurs during the TLE. The perforant pathway projects from the DG and the CA3 to the CA1 (green and blue arrows). The DG, CA3 and the apical layers of CA1 (orange arrows) project mainly via the superficial layers of the entorhinal cortex (II and III). On the other hand, many pieces of evidence have reported that the hippocampus is highly vulnerable to cell loss via seizure activity, particularly in the CA1 and CA3 subfields (red marks). The dispersion of dentate granule cells (yellow arrows) and intense axonal sprouting (asterisks) are common in epileptogenesis process. These structural changes affect the organization and function of hippocampal circuitry and contribute to the establishment of the TLE (Jarero-Basulto *et al.*, 2018).

3.4.1. Neuronal loss.

The loss of GABAergic interneurons in the hilus of the DG is now well established (Obenaus *et al.*, 1993; Esclapez *et al.*, 1996; Dinocourt *et al.*, 2003) it is observed few hours after SE (André *et al.*, 2001; Ferhat *et al.*, 2003; Boulland *et al.*, 2007). One of the clearest findings of that this loss of DG GABA neurons, corresponds to the loss of somatostatin (SOM)-containing neurons. It is observed in all models of acquired epilepsy, including kindling, status epilepticus and traumatic brain injury models (Sloviter, 1987; Lowenstein *et al.*, 1992; Schwarzer *et al.*, 1995; Buckmaster & Dudek, 1997; Gorter *et al.*, 2001) including in the pilocarpine model induced in mouse (Houser 2014, Fig. 11). A loss of PARV-containing neurons has also been described in the DG in several MTLE models in rat (André *et al.*, 2001; Gorter *et al.*, 2001; Kobayashi & Buckmaster, 2003). When described, this loss is generally less severe than that of SOM-interneurons (Buckmaster & Dudek, 1997). In the pilocarpine model induce in mouse PAR-containing neurons seems to be preserved (Houser, 2014) (Fig. 11). A loss of GABAergic interneurones was also reported in the CA1 region of pilocarpine rat. It corresponds to the loss of two types of interneurones in stratum oriens: 1- O-LM cells (Oriens lacunosum-moleculare) that contain SOM and innervates the distal dendrites of pyramidal cells (Cossart *et al.*, 2001; Dinocourt *et al.*, 2003), and 2- Axo-axonic cells that contain PARV (Dinocourt *et al.*, 2003).

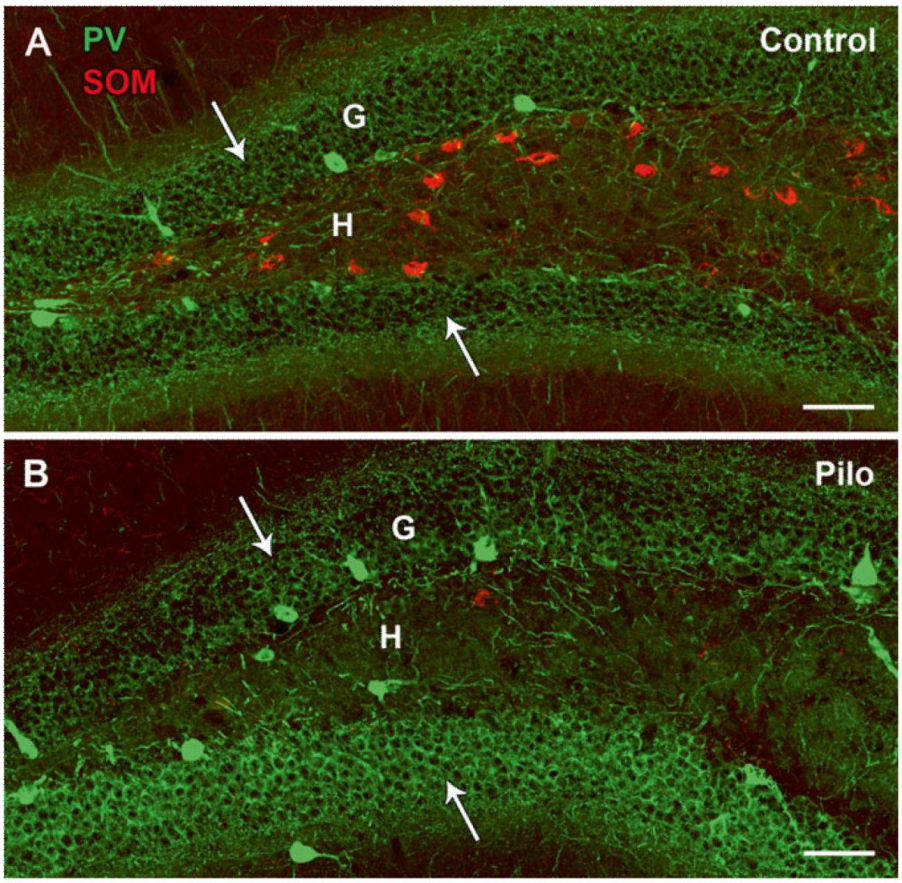

Fig. 11. Comparisons of somatostatin (SOM)- and parvalbumin (PV)-labeled neurons in the rostral dentate gyrus of control and pilocarpine mice. (**A**) In the control dentate gyrus, cell bodies of SOM neurons are located primarily within the hilus (H) whereas those of PV neurons are positioned predominantly along the base of the granule cell layer (G). PV-labeled axon terminals are concentrated in perisomatic locations within the granule cell layer (*arrows*) while SOM terminal fields are located in dendritic regions in the outer molecular layer (not shown). (**B**) In the pilocarpine-treated mouse at 2 months after status epilepticus, a severe loss of SOM neurons is evident in the hilus whereas many PV neurons and their axon terminals (*arrows*) in the granule cell layer are preserved. Scale bars, 100 µm (Houser, 2014).

A Loss of mossy cells, glutamergic neurons within the hilus of theDG has been also reported in the dorsal DG in rats (Sloviter *et al.*, 2003; Boulland *et al.*, 2007). Mossy cells loss is characterized by the loss of cell bodies and their axon terminals in the inner molecular layer of DG (Boulland *et al.*, 2007).

A loss of principal cells has been also described. In humans, when hippocampal sclerosis is present, pyramidal cells, mainly in the CA1 region, are no more observed. Some patients can also display a loss of granule cells (de Lanerolle *et al.*, 1989; Blümcke *et al.*, 1999). In animal models of MTLE, the profile of this loss varies from one model to another. The death of CA1 and CA3 pyramidal cells has been reported in kainate models in mice

(Bouilleret *et al.*, 1999) and lithium-pilocarpine in rats (Dubé *et al.*, 2001). In the rat kainate model, it is essentially the pyramidal cells of the CA3 region that degenerate(Nadler *et al.*, 1980). In the pilocarpine model induced in rat(Houser & Esclapez, 2003; Boulland *et al.*, 2007) as in the mouse (Houser 2014) there is a good preservation of all the pyramidal cells even if pyramidal cell loss in the CA1 regions and CA3 have been reported in this model by other authors(Mello *et al.*, 1993; Covolan & Mello, 2000). All of these damages were described mainly in the dorsal region of the hippocampus in animals in which SE was induced in adulthood.

In a more recent study, Ekstrand et al., (2011) have shown hippocampal sclerosis, greater in the ventral hippocampus than in the dorsal region when lithium- pilocarpine was injected in 20-day-old young rats (Ekstrand *et al.*, 2011). Thus, hippocampal sclerosis observed in animal models is a function of the model considered, of age, duration of the chronic stage and may display significant regional differences in hippocampal formation. However, in human MTLE as well as in associated animal models, CA2 pyramidal cells are preserved and this region is considered as a resistant region(Margerison & Corsellis, 1966).

3.4.2. Axonal plasticity of gulatamergic networks.

In the pilocarpine model (Mello et al., 1993; Okazaki et al., 1995; Buckmaster et al., 2002) as in most animal models (Tauck & Nadler, 1985; Cavazos *et al.*, 1991; Ben-Ari & Cossart, 2000) and human MTLE (Sutula *et al.*, 1989; Houser *et al.*, 1990; Babb *et al.*, 1991), the glutamatergic networks within the DG is strongly reorganized. It is characterized by the growth or “sprouting” of mossy fibers, the axon of granule cells (mossy fiber sprouting). The newly formed axon collaterals innervate the inner molecular layer and form synaptic contacts on the proximal apical dendrites (Okazaki *et al.*, 1995; Cavalheiro *et al.*, 1996) (Fig. 12). Mossy fibers sprouting occurs transversally but also along the septotemporal axis of the hippocampus in mice (Buckmaster *et al.*, 2002). A correlation has been reported between mossy fiber sprouting and the loss of mossy cells along the septotemporal axis (Jiao & Nadler, 2007). Mossy fiber sprouting will be a reactive plasticity process taking place after the degeneration of mossy cells

in the hilus and of their axon terminals making contact on the dendrite of granule cells in inner molecular layer.

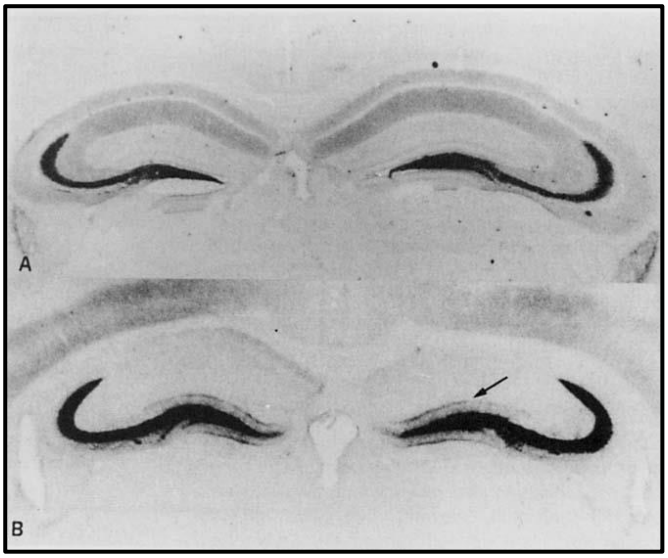

FIG. 12 Axonal sprouting of mossy fibers in the pilocarpine model in mice
Neo-Timm staining of the supragranular region of the hippocampal formation. **A:** Pattern in a control animal.**B:** Experimental animal with neo-Timmpositive granules in dentate gyrus (arrow)(Cavalheiro *et al.*, 1996).

Axonal plasticity is not specific to granule cells. It also concerns all principal cells of the hippocampus. Thus, In epileptic rat CA1 pyramidal cells form new axons collaterals that invade the stratum radiatum that make aberrant and functional synapses with their own dendrites and with other pyramidal CA1 cells (Esclapez *et al.*, 1999). This axonal plasticity has also been described in kainate (Perez *et al.*, 1996) but have to be shown in epileptic mice. This plasticity leads to different aberrant excitatory feedback loops between different regions of the hippocampus (Fig. 13): 1) from the CA1 pyramidal cells on the pyramidal of the CA3 region; 2) between pyramidal cells of subiculum and CA1; 3) projections of the hilus towards the pyramidal cells of the subiculum (Figure 13, dotted line). These projections were only described in the pilocarpine model and were observed during the chronic phase (Lehmann *et al.*, 2001)

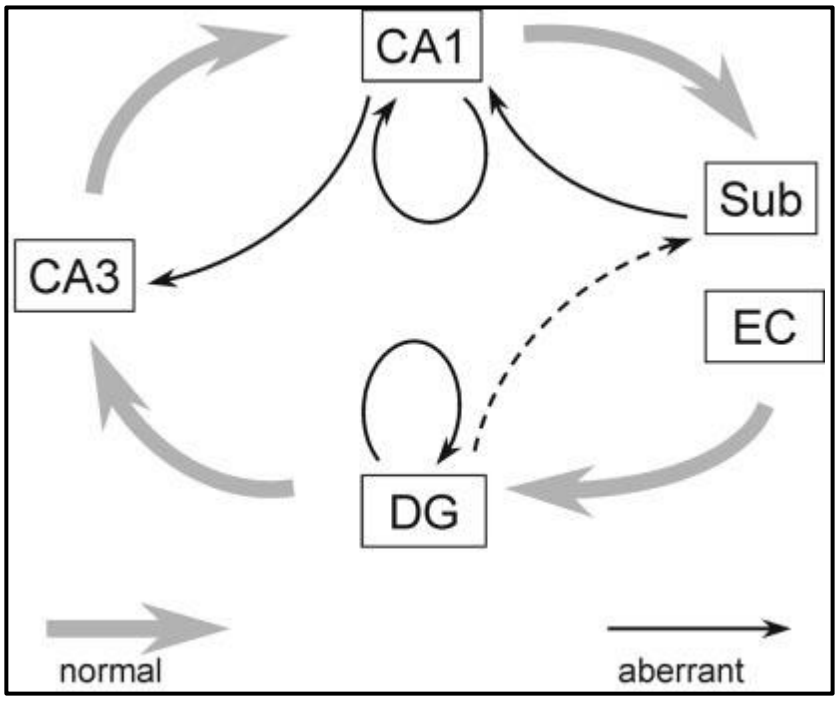

Fig.13. Schematic representation of aberrant connectivity in the hippocampus of chronic pilocarpine-treated rats. Abreviations: CA1, CA3: regions CA1 et CA3 of hippocampus; Sub: subiculum ; DG : dentate gyrus ; EC : Entorinal cortex. (Lehmann *et al.*, 2001)

3.4.3. Plasticity of GABAergic networks.

There is a plasticity of resistant GABAergic neurons in MTLE that essentially corresponds to a functional plasticity illustrated by an increase in most of the molecules involved in presynaptic GABAergic neurotransmission (Esclapez & Houser, 1999; Boulland *et al.*, 2007). Thus, in pilocarpine rat at the chronic stage an increased expression of the two isoforms of the GABA synthesis enzyme, GAD65 (glutamic acid decarboxylase, 65 kDa) and GAD67, and of the vesicular GABA transporter (VGAT) at the level of messenger RNA as well as proteins level has been in all GABAergic neurons of the hippocampus (Esclapez & Houser, 1999; Houser & Esclapez, 2003). These changes take place during the latent period (Boulland *et al.*, 2007). This plasticity has also been described in the kainate model (Feldblum *et al.*, 1990) and in humans, where an increase in GAD65 and the GABA transporter, GAT1, is reported in the inner molecular layer of DG (Mathern *et al.*, 1995).

Axonal sprouting of resistant GABAergic neurons has been also described in the in rat (Long *et al.*, 2011) and mice(Peng *et al.*, 2013) pilocarpine models.

3.4.4. Granule cell dispersion.

In human MTLE, morphological alterations of the granule cell layer including cell loss, dispersion or bilamination of granule cells are often observed(Houser, 1990; Houser *et al.*, 1990; Mathern *et al.*, 1995; Blümcke *et al.*, 1999). A dispersion of granule cells is also described in some studies performed in the rat pilocarpine model (Mello *et al.*, 1993). In a healthy hippocampal tissue, the soma of the granule cells forms a very compact layer. In epileptic tissue, the granule cell layer expends and dispersed granule cell bodies invade the inner molecular layer. The dispersion of granule cells has been suggested to be correlated with the loss of DG hilar cells and the sprouting of mossy fibers (Mello *et al.*, 1993). The authors suggest that gliosis, tissue shrinkage or neoformed cell migration may be the cause of this morphological abnormality. The dispersion of granule cells has also been observed in the model induced by intra-hippocampal injection of kainate in mice (Suzuki *et al.*, 2005).

3.4.5. Neurogenesis.

In the adult hippocampus, neurogenesis persists and leads to the formation of new granule cells in the granule cell layer. It has been shown in the rat pilocarpine model that hippocampal neurogenesis can be stimulated by epileptic seizures and can lead to abnormal migration of newly formed granule cells into the hilus and into the inner molecular layer (Parent *et al.*, 1997, 2006; Parent, 2007). This aberrant neurogenesis takes place within five days of status epilepticus and the newly formed cells are integrated in the neural circuitry. Hilar ectopic cells establish many aberrant contacts with remaining mossy cells and also contribute to the sprouting of mossy fibers in the inner molecular layer (Parent, 2007; Shapiro *et al.*, 2007; Pierce *et al.*, 2011).

3.4.6. Functional alteration.

These extremely complex morpho-functional reorganizations described in animal models leads to a clear imbalance between excitation and inhibition in favor of excitation on the principal cells of the DG, the main entrance of the information in the HP(Kobayashi & Buckmaster, 2003) as well as of CA1, the main output region (Cossart *et al.*, 2001) and hyperactivity of the hippocampal network during the chronic stage. Such hyperactivity could participate to the emergence of recurrent spontaneous seizures. However, many morphological alterations are already present during the latent period in the rat pilocarpine model, such as the loss of interneurons (Obenaus *et al.*, 1993; Dinocourt *et al.*, 2003; Kobayashi & Buckmaster, 2003) . In addition, hyperexcitability of the pyramidal cells of the CA1 region has been demonstrated during the latent phase that persists during the chronic stage (El-Hassar *et al.*, 2007). In this study, the glutamatergic and GABAergic conductances received by the pyramidal cells of the CA1 region were measured during the latent period and the chronic stage. The results reveal an increase in the excitation / inhibition ratio received by the soma and dendrites of pyramidal cell present already during the latent period and surprisingly this ratio was not further modified during the chronic stage (El-Hassar *et al.*, 2007). Therefore if this complex reorganizations of the intrinsic hippocampal networks lead to a clear hyperactivity of the hippocampal principal cells (Cossart *et al.*, 2001; El-Hassar *et al.*, 2007) such hyperactivity is not sufficient by itself to generate seizures (El-Hassar *et al.*, 2007).

3.5. Reorganization of the SuM-hippocampus unique network in TLE.

A Recent study (Soussi *et al.*, 2015) has investigated the anatomical organization (reorganization) of the SUM-Hippocampal pathways in the rat pilocapine model of chronic limbic seizures with the hypothesis that this pathway could contribute to trigger spontaneous seizures within an altered hyperexcitable hippocampal intrinsic circuitry. Indeed as previously described in the previous chapter the SuM provides substantial projections to the HP

including the DG.This hypothalamic nucleus is involved in the regulation of hippocampal theta rhythms (Kocsis & Vertes, 1994; Vertes & Kocsis, 1997; Kocsis & Kaminski, 2006) and could play a crucial role in the control of several Hippocampal-dependent functions such as working memory, emotional behavior including stress and anxiety (Pasquier & Reinoso-Suarez, 1976; Richmond *et al.*, 1999; Pan & McNaughton, 2002; Santín *et al.*, 2003; Pan & McNaughton, 2004a; Shahidi, Motamedi, Bakeshloo, *et al.*, 2004; Shahidi, Motamedi, & Naghdi, 2004) and some vigilance states like REM sleep (Renouard *et al.*, 2015). Interestingly it has been shown that all these functions are altered in MTLE in animals (Chauvière *et al.*, 2009; Marcelin *et al.*, 2009) and in humans (Bettus *et al.*, 2008) and that in these epilepsies, the occurrence of seizure is particularly sensitive to stress (Zeitlin *et al.*, 1995; Lanteaume *et al.*, 2009) and vigilance states (Renouard *et al.*, 2015).

The authors demonstrate a marked reorganization of DG afferents originating from the SuM in pilocarpine treated rats. This reorganization, starts during the latent period, is massive when animals become epileptic and continue to evolve during epilepsy. It is characterized by an aberrant distribution and an increased number of axon terminals from neurons of both the SuML and SuMM, invading the entire inner molecular layer of the DG. This reorganization reflects an axon terminal sprouting in particular from SuML which express makers from both GABAergic and glutamatergic neurotransmission.

This study leads us to investigate the role of this SuML-DG network in the control of epileptic seizure combining optogenetic with in vivo electrophysiological recording (LFP) within the DG in the pilocarpine model of MTLE induced in VGLUT2-EYFP-ChR2 mice. The preliminary results of this study are described in the third paper.

4. Optogenetics.

Optogenetics refers to the combination of optical techniques with genetics to manage gain or loss of specific function in specific cells in living tissue.

The application of the optogenetic technique in neuroscience creates without any doubt a revolutionary advance that will allow us to reach an understanding of neural circuits functions in animal behavior. This Technology was chosen as the Method of the Year by Nature Methods in 2010, as it allows the control of spatial and temporal activity of specific types of neurons in the living brain.

Neurons are first genetically modified to express light-sensitive proteins (opsins). When these neurons are then illuminated with the light of the correct frequency, they are transiently inhibited or activated or their signaling pathways are modulated according to the specific type of opsin they express. Expression of opsin in a specific cell type is usually achieved with the use of transgenic animals, viral vectors, or a combination of both, and the exact application of light modulates the activity of specific regions in the brain. The optogenetic method, first used a decade ago (Boyden *et al.*, 2005), has been largely developed in recent years and continues to progress with the introduction of increasingly advanced and functional opsins.

4.1. Opsins.

Opsins are seven-transmembrane ion channels or G-protein-coupled receptors; they require retinal as a cofactor, a molecule closely related to vitamin A, which absorbs a photon and undergoes isomerization. When retinal is bound to an opsin, forms a mixed molecule called rhodopsin. Activation of retinal by light induces conformational changes of opsins which causes a modification of the potential of membrane and activation or inhibition of neuronal activity.

4.1.1. Activation.

Channelrhodopsins (ChRS) are light-dependent ion channels discovered in unicellular green algae (Nagel *et al.*, 2003, 2005). The most used of CHRS is Channelrhodopsin-2 (ChR2), a non-selective cation channel naturally expressed by the algae Chlamydomonas reinhardtii, was the first depolarizing opsin successfully expressed in mammalian neurons (Boyden *et al.*, 2005). Upon exposure to blue light (maximum absorption peak at 470 nm) ChR2 allows passive movement of Na+, H+, Ca+2 and K+ (Figure 14A) (Nagel *et al.*, 2003). These movements of ions cause depolarization of the cell membrane and generation of action potentials. ChR2 has a very rapid activation kinetic following exposure to light, and closes quickly when light is switched off, allowing generation of single action potentials by brief (1-2 ms) light pulse exposure, making it a very attractive tool for the precise and selective stimulation of particular neuronal populations.

4.1.2. Inhibition.

The most commonly used inhibitory opsins are Halorhodopsin (NpHR) and Archeorhodopsin (Arch). NpHR, found in the halobacterium Natronomonas pharaonic, (Han & Boyden, 2007; Zhang *et al.*, 2007) is a pump that cause the influx of chloride ions into the cell when activated by light, resulting in hyperpolarization. eNpHR3.0 is a form evolved NpHR with better membrane conductance, higher levels more robust expression and photocurrents (Gradinaru *et al.*, 2008; Zhao *et al.*, 2008). With maximum excitation at 590 nm, eNpHR3.0 can be activated by green, yellow, red wave (Fig.14B). However, the accumulation of chlorine ions in the intracellular medium can lead to an increase in the inversion potential of the chlorine (and thus the channel becomes less and less hyperpolarized) and on the other hand, the formation of GABA-A excitatory currents when the photostimulation stops: the GABA A receptors are permeable to Cl-, so the massive entry of these ions into the cell can cause a drop in the Cl- gradient which induces the formation of excitatory GABA currents. Indeed, it has been shown that after stimulation with yellow light, the cells expressing NpHR increase their probability of

discharge(Tsunematsu *et al.*, 2011; Raimondo *et al.*, 2012). Moreover, the hyperpolarization induced by eNpHR3.0 is not constant through time: if there is inhibition of the neuronal discharge is observed at the beginning of the stimulation, after about 1 min action potentials begin to reappear(Tsunematsu *et al.*, 2011).

For that reason, Arch is used for the specific inhibition of neurons. This opsin, derived from Halorubrum sodomense, is a proton pump. The activation of this opsin causes a current H + ions efflux, thus a decrease of the intracellular pH and an increase in extracellular pH in the vicinity of the stimulated cell(Chow *et al.*, 2010; Gradinaru *et al.*, 2010; Han *et al.*, 2011). Arch has a maximum of excitation between 520 and 550 nm (Fig. 14B).

During this thesis, we used ChR2 and eNpHR3.0.

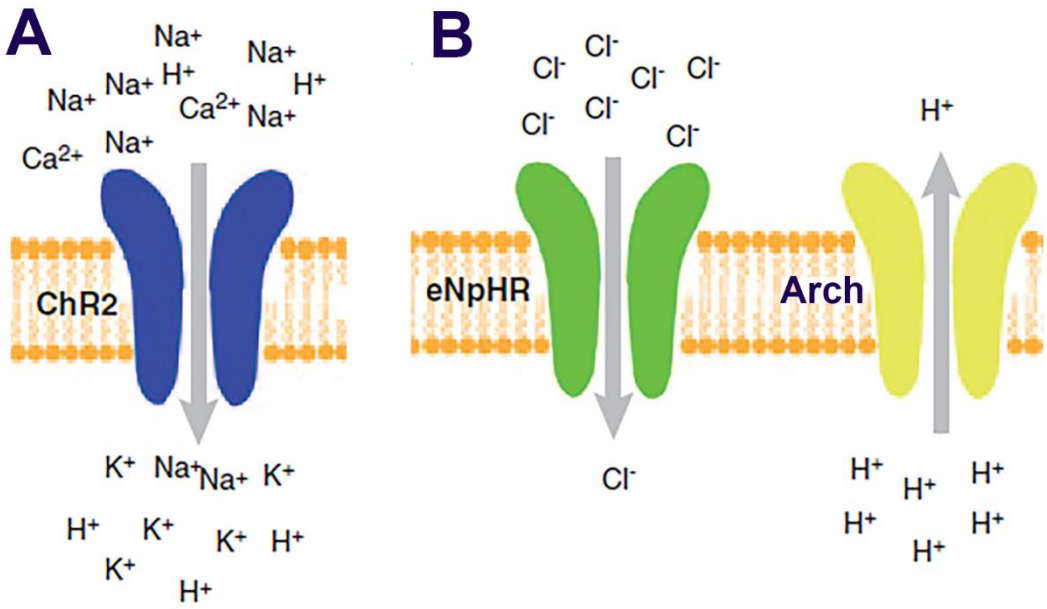

Figure 14. Types pf Opsins. (A) Opsins are membrane-bound proteins that are activated with light, which results in cell activation (depolarization), inhibition (hyperpolarization), or modulation of intracellular signaling cascades. A wide variety of opsins are now available. Illustrated here are ChR2 (a cation channel used to stimulate neural activity), (B) eNpHR3.0 (a chloride pump used to inhibit neural activity), Arch (a proton pump used to inhibit neural activity)(Guru *et al.*, 2015).

4.2. Viral vectors.

The specific expression of opsins in the neurons of interest is obtained with the aid of viral vectors. Using this approach, a modified virus containing an opsin gene with a specific promoter is injected into the region of interest then opsin is expressed in the target neurons. Various viral vectors such as lentiviruses, the adenoassociated viral vectors and the rabies virus can be used to induce the specific expression of opsins in mice, rats, zebrafish, and primate models (Zhu *et al.*, 2009; Zhang *et al.*, 2010). The viral vector that we used during this thesis is an adeno-associated viral vector modified (AAV).

AAVs are small viruses (about 25 nm in diameter) with DNA single strand that are naturally found in the tissues. They are unable to replicate themselves without the help of a "helper virus". In the absence of helper virus, AAVs establish a latent infection within the cell, either by site-specific integration into the host genome or by persisting in episomal forms. In our case, AAVs are modified (recombinant) so that they have a preferential tropism for the neurons, they are non-replicative and do not cause the degeneration of neurons. The AAV DNA is 4.7 kb long and consists of two open reading phases "open reading frame ", ORF). The left ORF (rep) encodes the rep proteins needed for the replication of the AAV; the right ORF (cap) codes for the capsid proteins. OFRs are flanked by inverted terminal repeats (ITRs), sequences of about 145 bp that make it possible to form the hairpin structure necessary for the integration of DNA of AAV in the genome of the host cell. The capsid of AAV consists of 60 copies of 3 proteins called VP1, VP2 and VP3, in a ratio of 1: 1: 18 (Wu *et al.*, 2006). There are several serotypes of AAV, which differ essentially in the composition of the capsid. The different serotypes do not interact in the same way with the cells and differ also in the effectiveness of their infection and therefore the transduction depends on the type of serotype used. For example, AAV5 and 9 have a better CNS transfection compared to other AAVs (Wu *et al.*, 2006; McCown, 2011; Aschauer *et al.*, 2013). Once the AAV is injected into the brain, its capsid interacts with the plasma membrane glycosaminoglycans and act as receptors. Then, the capsid interacts with coreceptors, which regulate successive stages of intracellular signaling. AAV2 interacts with proteoglycans from

heparan sulfate, whereas AAV5 requires sialic acid to adhere to the cell and can be transduced. AAV then undergoes endocytosis in the presence of clathrin and dynamin. AAV5 after endocytosis is transported mainly to trans-Golgi, which suggests that this serotype uses a different type of endocytosis compared to other serotypes (Bantel-Schaal *et al.*, 2002). The mechanisms that regulate the disassembly of AAV and its transport in the nucleus are not known. Probably the disassembly of the capsid takes place following the interaction of AAV with proteins of the nuclear membrane, and these interactions could be different depending on the serotype. For example, Thomas et al. (Thomas *et al.*, 2004) proposed that rapid disassembly of AAV8 could contribute the higher and faster transduction of this serotype in the liver compared with AAV2.

4.3. Cre inducible system.

Some promoters have rather low transcriptional activity and are therefore ineffective to induce a level of expression of the opsin gene sufficient to obtain activation or inhibition of neuronal activity; Moreover, the length of the genetic material of a viral vector is modest, which limits the promotor size and thus reduces the diversity of cell types that can be specifically transfected. So, the current strategy used to target genetically defined cell types and amplification of the transcriptional activity lead to the use of Cre-recombinase-based mouse lines in combination with viral vectors. Cre-recombinase is an enzyme that catalyzes the recombination between two loxP sites (34 bp sequences) flanking a gene of interest. Depending on the orientation of these sites, the genetic material between them will be reversed when the Cre-recombinase enzyme is present. Typically, a viral vector containing a gene inverted and "floxed" (flanked by loxP) is injected locally into the region of the brain of interest in transgenic or knock-in mice expressing Cre-recombinase in a specific cell type. Although the viral vector can infect all cells, opsin will be returned to the correct orientation and will therefore be functional only in the cell type which contains Cre-recombinase. With this method, a mouse Cre line can be used for many types of experiments with many different type of opsins by only changing the viral vector (Zhang *et al.*, 2010).

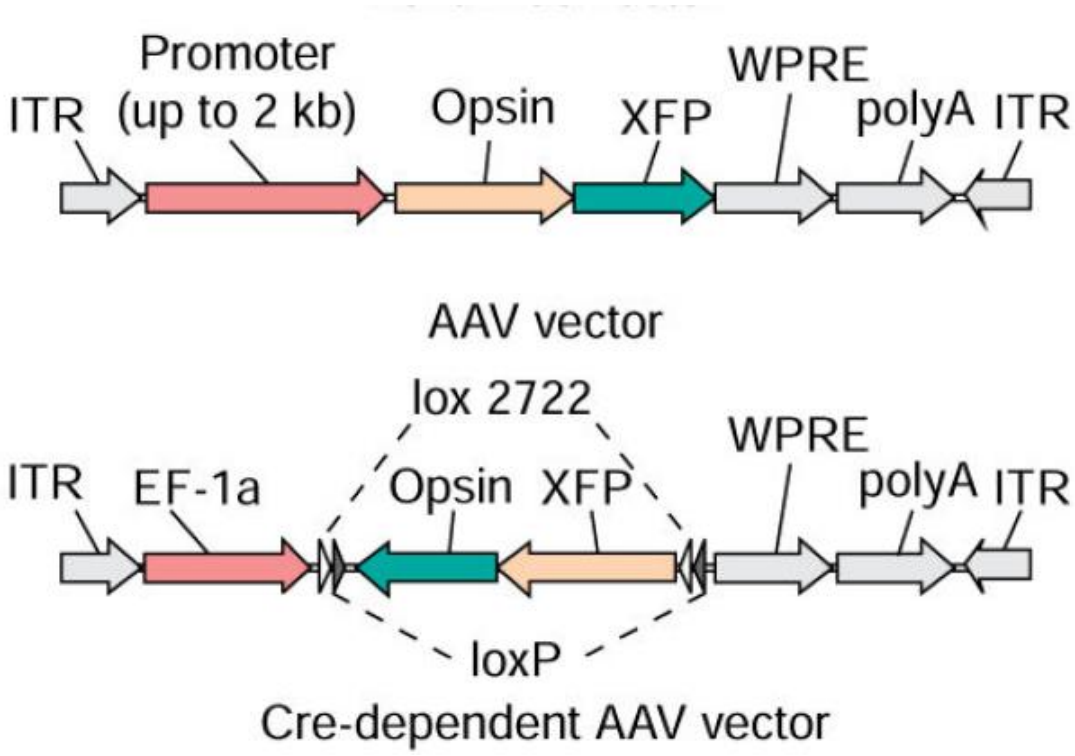

Figure 15. Viral vectors for introducing microbial opsin genes into the brain. *Top*: AAV vectors can be used to deliver a cell-specific promoter along with the opsin gene and its fluorescent marker. *Bottom*: Cre-dependent adeno-associated virus (AAV) vector carries a doubly floxed inverted opsin (DIO) fusion gene. Upon transduction into Cre recombinase-expressing cells, the opsin fusion gene will be irreversibly inverted and enable cell-specific gene expression.(Zhang *et al.*, 2010)

OBJECTIVES

The main objective of my thesis is to determine the role of the SuML projections to DG in physiological and pathological conditions. For this purpose, we performed three studies.

First Study: Characterization of the anatomo-functionnal properties of the SuML-DG pathways in this transgenic mouse strain (naïve transgenic VGLUT-2 cre mouse)

Second Study: Characterization of the heterogeneity of the SuML (GABA /GLU population) in the SuML-DG pathways.

Third Study: Determination of the functional consequences of the reorganization of the projections from SuML-DG in Pilocarpine VGLUT-2 cre mouse model by using invivo optogenetics.

FIRST STUDY

The GABA-Glutamate supramammillary–dorsal Dentate Gyrus pathway controls theta and gamma oscillations in the DG during paradoxical sleep

In this study I was responsible for the anatomical part

Title: The GABA-Glutamate supramammillary–dorsal Dentate Gyrus pathway controls theta and gamma oscillations in the DG during paradoxical sleep

Abbreviated title:

SuML-dDG increases θ and γ powers during REM

Francesca Billwiller[1]*, Laura Castillo[2]*, Heba Elseedy[2,4]*, Anton Ivanovich Ivanov[2], Jennyfer Scapula[2], Antoine Ghestem[2], Julien Carponcy[1], Paul Antoine Libourel[1], Hélène Bras[3], Nabila ElSayed Abdelmeguid[4], Esther Krook-Magnuson[5], Ivan Soltesz[6], Christophe Bernard[2], Pierre-Hervé Luppi[1$], Monique Esclapez[2$@]

* equal contributing first authors; [$] equal contributing senior authors

[1]UMR 5292 CNRS/U1028 INSERM, Centre de Recherche en Neurosciences de Lyon (CRNL), Université Claude Bernard Lyon I, LYON Cedex 08, France

[2]Aix Marseille Univ, INSERM, INS, Institut de Neurosciences de Systèmes, Marseille, France

[3] Aix Marseille Univ, CNRS, INT, Institut de Neurosciences Timone, Marseille, France

[4] Zoology Department, Faculty of Science, Alexandria University, Alexandria, Egypt

[5]Department of Neuroscience, University of Minnesota, Minneapolis, MN 55455, USA

[6]Department of Neurosurgery, Stanford University, USA

Corresponding author: Dr. Monique Esclapez
Institut de Neurosciences des Systèmes - INS
UMR 1106 INSERM - Aix-Marseille Université,
Faculté de Médecine Timone,
27 Boulevard Jean Moulin
13385 Marseille Cedex 05, France
@ monique.esclapez@univ-amu.fr

Acknowledgements
We thank the animal facility (CEFOS, AMU, Marseille), the imaging facility (INPHIM, AMU, Marseille) and the electron microscope facility (IBDM, Marseille).
This work was supported by INSERM and Aix-Marseille University (M. E, H. E., C. B., L. C., AI. I, A. G., J. S.,); Partenariats Hubert Curien (PHC) IMHOTEP (M.E., H.E., NE. A.); Agence Universitaire de la francophonie (H.E); CNRS, Fondation pour la recherche médicale (FRM), Societé Francaise de Recherche et Médecine du Sommeil (SFRMS), University Claude Bernard of Lyon (F.B., P-H. L., P-A. L., S. A.) and NS104590 (I. S., E. K-M).

Abstract

Several studies suggest that neurons from the lateral region of the SuM (SuML) innervating the dorsal dentate gyrus (DG) display a dual GABAergic and glutamatergic transmission and are specifically activated during paradoxical (REM) sleep (PS). The objective of the present study is to fully characterize the anatomical, neurochemical and electrophysiological properties of the SuML-DG projection neurons and to determine how they control DG oscillations and neuronal activation during PS and other vigilance states. For this purpose, we combine structural connectivity techniques using neurotropic viral vectors (rabies virus, AAV), neurochemical anatomy (immunohistochemistry, in situ hybridization) and imaging (light, electron and confocal microscopy) with *in vitro* (patch clamp) and *in vivo* (LFP, EEG) optogenetic and electrophysiological recordings performed in transgenic VGLUT2-cre mice. At the cellular level, we show that the SuML-DG neurons co-release GABA and glutamate on dentate granule cells and increase the activity of a subset of DG granule cells. At the network level, we show that the activation of the SuML-DG pathway increases theta power and frequency during PS and increases gamma power during PS and waking in the DG. At the behavioral level, we show that the activation of this pathway does not change animal behavior during PS, induces awakening during slow wave sleep and increases motor and exploratory activity during waking. These results suggest that the SuML-DG pathway is capable of supporting the increase of theta and gamma power in the DG observed during PS and plays an important modulatory role of DG network activity during this state.

Introduction

The supramammillary nucleus (SuM) is a thin structure overlying the mammillary bodies in the hypothalamus that provides substantial projections to many regions of the limbic system including the hippocampal formation (for review see Pan and McNaughton 2004, Vertes 2015). The SuM is composed of several populations of neurons that differ in their neurochemical content and the specificity of their connections (Swanson et al., 1982; Gonzalo-Ruiz et al., 1992; Leranth and Kiss, 1996; Kocsis et al., 2003; Borhegyi and Leranth, 1997; Haglund et al., 1984). In rats, many studies have described the projections from SuM neurons to the hippocampus (Segal & Landis, 1974; Pasquier & Reinoso-Suarez, 1976, 1978; Wyss et al., 1979; Haglund et al., 1984; Saper et al., 1985; Vertes, 1992; Magloczky et al., 1994; Nitsch and Leranth 1996; Vertes & McKenna, 2000). We (Soussi et al., 2010) and others (Boulland et al., 2009) demonstrated in rats that SuM neurons from the most medial part of the SuM (SuMM; Paxinos and Watson, 1998), referred as SuMm by Swanson (1998), or SuMp by Pan and McNaughton (2004) innervating the inner molecular layer of the ventral dentate gyrus (DG) and CA2 pyramidal cells are glutamatergic (Soussi et al., 2010). In contrast, SuM neurons located in the lateral two-third region of the SuM (SuML), referred as SuMg by Pan and McNaughton (2004), innervate the supragranular layer of the dorsal DG (dDG) and to a lesser extend the ventral DG (vDG) and display a unique dual glutamatergic and GABAergic neurotransmitter phenotype (Boulland et al., 2009; Soussi et al., 2010). Indeed, these SuML neurons and their projections to the dDG co-express markers for both glutamatergic (vesicular glutamate transporter 2; VGLUT2) and GABAergic (glutamate decarboxylase 65, GAD65 and vesicular GABA transporter, VGAT) neurotransmission and establish asymmetric and symmetric synapses on DG cells (Soussi et al., 2010). The connectivity and neurochemical properties of these different SuM-hippocampal pathways suggest that they may contribute differently to hippocampal dependent functions. Indeed, it has been shown that the SuM controls hippocampal theta rhythm (Kocsis and Vertes 1994, Vertes and Kocsis 1997, Kocsis and Kaminski 2006) and is involved in emotional learning and memory (Pasquier and Reinoso-Suarez 1976, Richmond et

al 1999, Pan and McNaughton 2002, Santin et al 2003, Pan and McNaughton 2004, Shahidi et al. al., 2004). By combining retrograde tracing, neurotoxic lesion and FOS immunostaining, it was recently shown that SuML GABA/Glutamate neurons are responsible for the activation of dDG granule cells during paradoxical sleep (PS) (Renouard et al., 2015 ; Billwiller et al., 2016). Such activation may play a key role in the previously reported beneficial effect of PS on learning and memory (Maquet et al., 2000). In addition, Pedersen and colleagues (2017), by using a chemogenetic approach in transgenic mice, showed that SuM neurons containing only VGLUT2 but not those containing VGAT and VGLUT2 play a crucial role in waking. Altogether these results suggest that glutamatergic neurons from the SuM known to innervate several limbic regions including the CA2/CA3a hippocampal region and the vDG are involved in normal wakefulness whereas the GABA/Glutamate SuML neurons projecting to the dDG could be instrumental for PS function.

In this study we investigate how the SuML-dDG pathway control dDG neurons activity during PS and other vigilance states. For this purpose we combine innovative structural connectivity techniques using neurotropic viral vectors (rabies virus, AAV), neurochemical anatomy (immunohistochemistry, *in situ* hybridization) and imaging (light, electron and confocal microscopy) with *in vitro* (patch clamp) and *in vivo* (LFP, EEG) optogenetic and electrophysiological recordings performed in transgenic VGLUT2-cre mice in order: 1) to fully characterize the anatomical, neurochemical and electrophysiological properties of the SuML-dDG projection neurons in our mice trangenic model and 2) to determine the influences of this specific pathway on behaviors and associated oscillatory activities characterizing the different vigilance states as well as DG neuron activity.

Materials and methods

Animals

For this study, we used 30 transgenic “VGLUT2-cre” adult mice (25-30 g; aged 10-11 weeks) obtained by mating male and female homozygote Vglut2-ires-Cre mice from Jackson Laboratories (Strain name Slc17a6$^{tm2(cre)Lowl}$/J, stock #016963). All mice were bred in-house and maintained in standard cages, with food and water *ad libitum*, in a temperature- and humidity-controlled room under a 12 hr light/12 hr dark cycle. All the surgical and experimental procedures were performed according to the National Institutes of Health guidelines and the European communities Council Directive of 86/609/EEC and were approved by the University of Aix-Marseille and Lyon University Chancellor's Animal Research Committees.

Vectors

Rabies virus

Four VGLUT2-cre mice underwent stereotaxic injection of rabies virus (RV) within the inner molecular layer of the dDG in order to obtain golgi-like retrograde-labeling of SuM neurons projecting to this region. The strain of RV used was the Challenge Virus Standard (CVS, 4.10^7 plaque-forming units/mL) (Bras et al. 2008; Ugolini 2010; Coulon et al. 2011). Only vaccinated personnels conducted these experiments at the appropriate biosafety containment level until the sacrifice of the animals as described below.

These animals were used to determine the neurotransmiter phenotype of SuM neurons projecting to dDG at the mRNA level, combining immunohistofluorescent detection of RV with fluorescent *in situ* hybridization detection of VGAT and VGLUT2 mRNAs.

Adeno-Associated Virus (AAV) Double floxed Inverted ORF (DIO) vectors

Sixteen VGLUT2-cre mice underwent stereotaxic injection of the cre-dependent viral vectors: AAV5-EF1a-DIO-EYFP (3.5 10^{12} virus molecules / ml; UNC Gene Therapy Center Vector Core; Dr Deisseroth) into the SuML. These VGLUT2-EYFP mice expressing the Yellow Fluorescent Protein (YFP) in VGLUT2 SuM neurons and their axon terminals were used 1) to determine the neurotransmitter phenotype of SuM neurons innervating the dDG at the protein level, by simultaneous immunohistofluorescent detection of EYFP labeled axon fibers and terminals, VGAT and VGLUT2 in dDG (n=3); 2) to determine the synaptic profile of these EYFP labeled axon terminals at the electron microscopy level (n=3); 3) as control animals (n=3) for *in vitro* optogenetic stimulation and patch clamp electrophysiological recordings; 4) as control animals (n=7) for *in vivo* optogenetic stimulation and electrophysiological recordings.

Nine VGLUT2-cre mice underwent stereotaxic injection of the cre-dependent viral vectors: AAV5-EF1a-DIO-hChR2(H134R)-EYFP (3.2 10^{12} virus molecules / ml; UNC Gene Therapy Center Vector Core; Dr. Deisseroth) into the SuML. These VGLUT2-ChR2 mice expressing the excitatory opsin, channelrhodopsine 2 (ChR2) and the reporter protein EYFP in VGLUT2 SuM neurons and their axon terminals were used for 1) *in vitro* optogenetic stimulation and patch clamp electrophysiological recordings experiments (n=5); 2) *in vivo* optogenetic stimulation and electrophysiological recordings (n=4).

Four VGLUT2-cre mice underwent stereotaxic injection of the cre-dependent viral vectors: AAV5-EF1a-DIO-eNpHR 3.0-EYFP (3.2 10^{12} virus molecules / ml; UNC Gene Therapy Center Vector Core; Deisseroth's lab) into the SuML. These VGLUT2-NpHR3

mice expressing the inhibitory opsin Halorhodopsin (NpHR3) were used for *in vivo* optogenetic inhibition and electrophysiological recordings.

Surgery

Mice were anesthetized by an intraperitoneal injection (i.p.) of Ketamin (50mg/kg) / Xylazine (5mg/kg) solution. If necessary, this anesthesia was repeated during the surgery. Animals were then secured in a stereotaxic frame (David Kopf instruments). The body temperature of mice was monitored and maintained at about 37°C during the entire procedure by means of an anal probe and heating blanket respectively. The head was shaved and sanitized with Betadine and 0.9% NaCl. Local anesthesia was performed by infiltration of the scalp with xylocaine (lidocaine hydrochloride 0,5%), and an ophthalmic gel was placed on the eyes to avoid drying. After scalp incision, holes were drilled in the skull, with antero-posterior (AP), medio-lateral (ML) and dorso-ventral (DV) coordinates based on Paxinos & Franklin's atlas (2005).

RV and AAV viral vector injections

The RV (200nl) was pressure-injected unilaterally (n=2) or bilaterally (n=2) within the dDG inner molecular layer of VGLUT2-cre mice according to the following coordinates: AP = -2; ML = +/-1.5; DV = -1.7. Injections were performed by using a 33-gauge Hamilton syringe connected to a Micro4 injection pump system (World Precision Instruments). After completion of the injection procedures, the syringe was removed and the skin was sutured. Animals were treated with local anesthetic, returned to their cages kept at the appropriate biosafety containment level for a survival period of 38h to observe an optimal RV retrograde labeling for the dendritic arbor of SuM neurons. AAV5-EF1a-DIO viral vectors (500nl) were injected bilaterally within the SuML of

VGLUT2-cre mice at the following coordinates: AP = -2.7; LM = +/-1.25; DV = -4.8 using an 11°angle to avoid the high vascularization at the midline.

Optrode and electrode implantation

After AAV injections, 15 VGLUT2-mice were implanted with an optrode in the left dDG (AP = -2; ML = -1.1; DV = -1.7) for optic stimulation of axon terminals originating from transfected SuML neurons and local field potential (LFP) recordings from the DG. The optrode consisted of an optic fiber (250 μm ∅, 0.39 NA; Thorlabs SAS) and the LFP electrode. The LFP electrodes consisted of two 45 μm diameter tungsten wires (California Fire Wire Company), twisted and glued together to form a rigid and solid structure, with the 2 ends of the wires separated by 100 μm from each other. Two small screws (1 mm in diameter, Plastics One) each soldered to a wire were fixed on the skull. The first screw was fixed in the parietal part of the skull for EEG recording; the second screw, at the level of cerebellum as reference electrode. Two wire electrodes were inserted into the neck muscles for bipolar EMG recordings. All leads were connected to a miniature plug (Plastics One) that was cemented on the skull.

After completion of the surgery the skin was sutured. Mice were treated with local anesthetic, and an intramuscular injection of antibiotic (Baytril, 5mg/kg) to prevent any risk of infection. Mice were monitored until waking and replaced in their home cages for a survival period of 3 weeks.

Histology

Tissue preparation for light microscopy

Animals were deeply anesthetized with ketamine and xylazine and transcardially perfused with 4% paraformaldehyde (PFA) in 0.12 M sodium phosphate buffer, pH 7.4 (PB). After perfusion, the brains were removed from the skull, post-fixed in the same fixative for 1 h at room temperature (RT), rinsed in PB, cryoprotected in 20% sucrose

overnight, frozen on dry ice and sectioned coronally at 40 µm with a cryostat (Microm). The sections were rinsed in PB, collected sequentially in tubes containing an ethylene glycol-based cryoprotective solution and stored at -20°C until histological processing. One of every ten sections was stained with cresyl violet to determine the general histological characteristics of the tissue throughout the rostro-caudal extent of the brain. Selected sections were processed for 1) simultaneous detection of VGLUT2 mRNA, VGAT mRNA and RV; 2) simultaneous immunohistofluorescent detection of EYFP, VGLUT2 and GAD65 or VGAT and / or 3) immunohistochemical detection of cFos.

Simultaneous detection of VGLUT2 mRNA, VGAT mRNA and RV combining fluorescent in situ hybridization (RNAscope technology) and immonhistofluorescent methods performed in VGLUT2-cre mice injected with RV

Selected sections at the level of the SuM were first treated with 1% H2O2 rinsed in PB mounted on SuperFrost Plus slides (Fisher Scientific) and air dried at RT. They were then processed for fluorescent RNAscope *in situ* hybridization according to the manufacter's protocol (Advanced Cell Diagnostics). Briefly sections were treated with 100% ethanol and protease III for 30 min at 40°C. They were incubated in a solution containing both RNAscope® Probe - Mm-S1c17a6 for detection of VGLUT2 mRNA and Mm-S1c32a1-C3 for detection of VGAT mRNA. After hybridization, sections were then processed for visualization using the RNA-scope Multiplex Fluorescent reagent Kit v2 (Advanced Cell Diagnostics) and the Tyramide Signal Amplification (TSA™) Plus Cyanine 3 and TSA Plus Cyanine 5 systems (Perkin Elmer).

After the RNAscope assay, sections were rinsed in 0.02 M potassium phosphate-buffered saline (KPBS, pH 7.2-7.4) and processed for immnohistofluorescent detection of the RV using a Mouse On Mouse kit (MOM, Vector Laboratory) to eliminate non specific labeling due to use of mouse monoclonal antibody on mouse tissue. Sections were incubated for 1 h at RT in MOM mouse IgG blocking reagent diluted in KPBS

containing 0.3% Triton X-100. Sections were rinsed twice with KPBS for 5 min and pre-incubated in MOM diluent for 15 min. Sections were then incubated overnight at RT in a solution containing the mouse monoclonal antibody directed against RV (1:3000; Raux et al., 1997 Kindling provided By Dr. Patrice Coulon), diluted in MOM diluent. After several rinses in KPBS, they were incubated for 2h in Alexa488-conjugated donkey anti-mouse (1:200; Invitrogen) diluted in MOM diluent. After several rinses in KPBS, all sections were coverslipped with Fluoromount (Electron Microscopy Sciences). The specimens were analyzed with a Zeiss laser-scanning confocal microscope.

Quantification of co-localizing RV, VGLUT2 and VGAT mRNAs

Quantitative analysis was conducted to evaluate the extent of SuM neurons with direct projections to the dDG that co-express VGLUT2 and VGAT mRNAs. For this purpose, the number of triple neurons was determined for each animal (n=4), from 3 sections (120 µm apart from each other) across the antero-posterior extent of the SuM. For each section, an image of the entire SuM region was obtained from a single confocal slice using the Tile Scan function with a 20x objective and sequential acquisition of the different wavelength channels to avoid fluorescent talk with ZEN software (Zeiss). The analysis was then performed with Neurolucida software (version 7, mbfBioscience) as follows: for each confocal image, all RV- labeled neurons were identified on the green channels and examined for colocalization of VGLUT2 mRNA in the blue channel and/or VGAT mRNA in the red one. Triple- double- and single-labeled neurons were tagged differently and counted by the software. A total of 380 RV-labeled neurons were analyzed.

Simultaneous immunohistofluorescent detection of EYFP, VGLUT2 and GAD65 or VGAT performed in VGLUT2-EYFP mice

Selected sections at the level of the dDG were processed using the MOM kit as described above. Sections were incubated overnight at RT in a solution containing rabbit anti-GFP (1:2000, Invitrogen), guinea pig anti-VGLUT2 (1:5000, Millipore) and mouse anti-GAD65 (1:100, Millipore) or mouse anti-GFP (1:100, Invitrogen), guinea pig anti-VGLUT2 (1:5000, Millipore) and rabbit anti-VGAT (1:1000, Synaptic System) diluted in MOM diluent. After several rinses in KPBS, they were incubated for 2h in Alexa488-conjugated donkey anti-rabbit IgG (1:200; Invitrogen), Cy5-conjugated donkey anti-guinea pig (1:100; Jackson ImmunoResearch Laboratories, Inc.), and Cy3-conjugated donkey anti-mouse (1:100; Jackson ImmunoResearch Laboratories, Inc.) or Alexa488-conjugated donkey anti-mouse IgG (1:200; Invitrogen), Cy5-conjugated donkey anti-guinea pig (1:100; Jackson ImmunoResearch Laboratories, Inc.), and Cy3-conjugated donkey anti-rabbit (1:100; Jackson ImmunoResearch Laboratories, Inc.) diluted in MOM diluent. After several rinses in KPBS, all sections were then mounted on superfrost-coated slides, dried overnight at RT and coverslipped with Fluoromount. The specimens were analyzed with confocal microscope (Zeiss).

Quantification of co-localizing GFP, VGLUT2 and VGAT

Two quantification protocols were used in order to evaluate the extent of the different neurochemical phenotypes of axon terminals from the SuM innervating the dDG. In the first protocol previously described (Soussi et al., 2015), the densities of VGLUT2/VGAT and VGLUT2 only labeled terminals were assessed by the quantification of immunolabeling for VGLUT2/VGAT and VGLUT2 only, respectively. These analyses were performed on 4 sections for each mouse. Single optical confocal images were acquired with Zeiss LSM 510 laser-scanning microscope and analyzed with the software provided by the microscope manufacturer (LSM 510 Zen, Zeiss). All images were acquired from the suprapyramidal and infrapyramidal

blades of the dDG, using identical parameters. The percentages of VGLUT2 labeled terminals containing VGAT were estimated by the the Manders' coefficient (proportion of pixels for VGLUT2 also positive for VGAT) obtained with the JACoP co-localization Plugin for Image J, in the region of interest (ROI) which included granule cell layer (GCL) and the narrow zone superficial to the granule cells defined as the supragranular layer (SGL) following recommendations from Bolte & Cordelières (2006). For each channel, an identical bottom threshold was applied throughout the analyses, and only the pixels with a value above this threshold were counted. When a pixel had a value above the threshold in both channels, it was counted as double positive. The size and the shape of the ROI was the same for each confocal image. The average % of co-localization was calculated for each blade of the DG for each mouse.

In the second quantification protocol, we determined for each mouse (n=4), the relative percentages of triple- and double-labeled boutons for the GFP anterograde tracer and VGAT and/or VGLUT2 in the SGL and infragranular blade of the dDG from several z-stacks of 10 confocal slices, acquired with the 100X objective and a numerical zoom 8, in three different sections. The analysis was performed as previously described (Persson et al., 2006; Soussi et al., 2010) and following recommendations from Bolte & Cordelières (2006). For each z-stack, the confocal images obtained from separate wavelength channels (green, red and blue) were displayed side by side on the computer screen together with the images corresponding to colocalized pixels within each optical slice of the z-stack obtained with the colocalization highlighter plugin in ImageJ. The GFP-labeled boutons were identified in the green channel within a probe volume defined by the size of the confocal slice (19.38 μm · 19.38 μm) and the height of the z-stack (2 μm). Each bouton was examined for colocalization through the individual optical slices of the z-stack. Single-, double- and triple-labeled boutons were counted using the Cell Counter plugin in Image J. The total number of GFP-labeled terminals

analyzed in the two regions of interest was 400.

Immunohistochemical detection of cFos performed in VGLUT2-EYFP (n=6), VGLUT2-ChR2 (n=4) and VGLUT2-NpHR3 (n=4) mice

Selected sections at the level of the DG were processed for immunohistochemistry according to previously described protocol (Esclapez et al. 1994). Sections were pre-treated for 30 min in 1 % H2O2, rinsed in PB and KPBS, preincubated for 1 h in 3 % normal goat serum (NGS, Vector Laboratories) diluted in KPBS containing 0.3 % Triton X-100 and incubated overnight at RT in cFos rabbit polyclonal antiserum (1:20,000; Calbiochem) diluted in KPBS containing 1 % NGS and 0.3 % Triton X-100. After several rinses in KPBS, sections were incubated for 1 h at RT in biotinylated goat anti-rabbit immunoglobulin G (IgG; Vector Laboratories) diluted 1:200 in KPBS containing 3 % NGS and then for 1 h at RT in an avidin-biotin-peroxidase complex solution prepared in KPBS according to the manufacturer's recommendations (Vectastain ABC kit, Vector Laboratories). Sections from VGLUT2-EYFP, VGLUT2-ChR2 and VGLUT2-NpHR3 mice were processed In parallel and for the same period of time (15 min) in 3.3'-diaminobenzidine tetrahydrochloride (DAB, Sigma fast tablets; Sigma), rinsed in KPBS, mounted onto Superfrost Plus slides, dehydrated and coverslipped with Permount.

Quantification of cFos immunolabeled neurons

The number of cFos labeled neurons was calculated in the DG GCL of the right and left (ipsilateral to the optic stimulation) hemispheres in VGLUT2-EYFP control (n=7), VGLUT2-ChR2 (n=4) and VGLUT2-NpHR3 (n=4) mice. These analyses were performed using a computer-assisted system connected to a Nikon 90i microscope and the Neurolucida software (MicroBrightField). A total of 4 sections (400 µm apart from each other) surrounding the optrode site were analyzed for each animal. In each section the GCL was delineated and all neurons labeled for cFos were plotted. The software calculated the total number of labeled neurons in each hemisphere for each animal. The average total number of labeled neurons per hemisphere ± SEM was calculated for

each group of control VGLUT2-EYFP, VGLUT2-ChR2, and VGLUT2-NpHR3 mice. Statistical analysis was performed by Statview software using Wilcoxon Rank Sum Test.

Tissue preparation for electron microscopy

Three VGLUT2-EYFP mice were perfused intracardially with a fixative solution containing 4% PFA and 0.1% glutaraldehyde in 0.12 m PB. After perfusion, the brain was removed from the skull, post-fixed in the same fixative overnight at 4°C and rinsed in PB for 1.5 h. Blocks of the forebrain were sectioned coronally at 60 µm with a vibratome. Pre-embedding immunolabeling for GFP sections at the level of dDG were pre-treated for 15 min in 1% sodium borohydride prepared in PB and rinsed for 30 min in PB and 3 x 30 min in KPBS. Sections were incubated for 1h in normal goat serum diluted in 0.02M KPBS, then incubated overnight in primary antibody rabbit anti-GFP (1:2000) diluted in KPBS containing normal goat serum at RT. On the following day sections were rinsed for 1.5 h in 0.02M KPBS then incubated for 1 h in the secondary antibody goat anti-rabbit (1:200) diluted in KPBS containing normal goat serum. After rinsing in KPBS for 1.5 h, sections were incubated for 1h in an avidin-biotinylated-peroxidase complex (ABC Elite; Vector Laboratories) prepared in KPBS. After 3 x 30 min rinses in KPBS, sections were incubated for 12 min in 3.3'-diaminobenzidine tetrahydrochloride and 0.01% H2O2, rinses in KPBS, post-fixed in 2% PFA and 2.5% Glutaraldahyde diluted in PB for 3 h, then washed for 1.5 h in PB. After all these steps, sections were treated with 1% osmium tetroxide in PB for 45 min, dehydrated in ethanol, flat embedded in Durcupan resin and polymerized at 56°C for 24h (Zhang & Houser, 1999). Labeled regions of the DG that contained the molecular and granule cell layers were trimmed from the sections, re-embedded on capsules filled with polymerized Durcupan and further polymerized at 56°C for an additional 24 h. Ultrathin sections from the most superficial face of the blocks were cut on an ultramicrotome. Serial sections were picked up on nickel mesh grids and stained with uranyl acetate and lead citrate. Sections were examined and photographed with a JEOL electron microscope.

In vitro electrophysiology: optic stimulation and patch clamp recordings

Hippocampal slice preparation

VGLUT2-ChR2-EYFP mice (n=5) and VGLUT2-EYFP mice (n=3) were decapitated under isofluorane anesthesia. Brains were quickly removed and placed into an ice-cold (4°C) cutting solution containing (in mM): 140 potassium gluconate, 10 HEPES, 15 sodium gluconate, 0.2 EGTA, 4 NaCl (pH 7.2). Coronal slices were cut (350 µm) using a vibratome (Leica Microsystem). In order to increase cell survival over time in slices from 10 to 11 week-old adult, slices were incubated first in a solution containing (in mM): 110 choline chloride; 2.5 KCl; 1.25 NaH_2PO_4; 10 $MgCl_2$, 0.5 $CaCl_2$; 25 $NaHCO_3$; 10 glucose, 5 sodium pyruvate, for 15 min at 20-23°C. Then, they were transferred to a holding chamber containing an artificial cerebrospinal fluid (ACSF) composed of (in mM) 126 NaCl, 3.5 KCl, 1.2 NaH_2PO_4, 1.3 $MgCl_2$, 2 $CaCl_2$, 25 $NaHCO_3$, 10 D-glucose (pH = 7.3-7.4) at RT for at least 1 h before recording. The two last solutions were saturated with 95% O_2 and 5% CO_2.

Whole-cell voltage-clamp recordings

Slices were submerged in a low-volume recording chamber and continuously superfused with 32-34°C ACSF at 5 ml/min perfusion rate. For each mouse, four slices containing the dDG were selected for patch clamp recordings. DG neurons were visualized by infrared video microscopy using an upright microscope (SliceScope, Scentifica Ltd). Patch pipettes were pulled from borosilicate glass tubing (1.5 mm outer diameter, 0.5 mm wall thickness) and filled with an intracellular solution containing (in mM) 20 CsCl, 115 CsGlu, 10 HEPES, 1.1 EGTA, 4 MgATP, 10 Na phosphocreatine and 0.4 Na_2GTP as well as 0.2% biocytin for *post-hoc* morphological identification of the recorded neuron (see below). The pipette resistance was 4–6 MΩ. Recordings were performed in the Apex, upper and lower blades of the dDG. Signals were fed to a

Multiclamp 700A (Molecular Devices), digitized (10 kHz) with a DigiData 1550 (Molecular Devices) interface to a personal computer and analysed with ClampFit software (Molecular Devices). Optical stimulation of ChR2-expressing axon terminals was performed by pulses of 470 nm blue light delivered by a LED (pE-2, CoolLED) through a 40X objective attached to microscope (SliceScope, Scientifika Ltd). Stimulations consisted of paired 5 ms pulses (500 ms between pulses, every 30 s). For VGLUT2-ChR2 mice, the light intensity corresponded to 20-30% (1.6-2.5 mW) of the LED maximum power (7.5 mW) and for the VGLUT2-EYFP control mice, it varied between 20 to 90% (6.9 mW) of LED maximum power. Postsynaptic current (PSC) responses to optic stimulations were recorded at different holding potentials ranging from -70 mV (close to reversal potential of GABA-A currents but far below the reversal potential of glutamate receptor-mediated currents) to +10mV (close to reversal potential of glutamate receptor-mediated currents but far above the reversal potential of GABA-A-mediated currents). Pharmacological characterization of inhibitory PSCs (IPSCs) and excitatory PSCs (EPSCs) was achieved using antagonists of GABA-A, AMPA and NMDA receptors. We used Gabazine or bicuculline (antagonist of GABA-A receptors, 10 µM), D-AP5 (antagonist of NMDA receptors, 40 µM) and NBQX (antagonist of AMPA and Kaïnate receptors, 10 µM). The co-release of glutamate and GABA was further demonstrated in several DG granule cells (n=5), by recording first light stimulated PSC at -70 mV (Figure 4K). At this holding potential the recorded currents were essentially generated by glutamate receptors. Then the glutamate component was abolished by NBQX and D-AP5, and the GABA component was revealed at +10 mV holding potential. This PSC was completely inhibited by bicuculline application that confirmed the GABA receptor origin of these remaining currents (see also Figure 4J).

Double immunohistofluorescent labeling for Biocytin and GFP

After recordings slices were processed for simultaneous detection of the biocytin-filled neurons and GFP-labeled axon fibers and terminals in order to identify the recorded cells and evaluate the efficiency of the transfection, respectively. Slices were fixed overnight at 4°C in a solution containing 4% PFA in PB. Then they were rinsed in PB, cryoprotected in 20% sucrose and quickly frozen on dry ice. After several rinses in KPBS, slices were incubated in a solution containing normal donkey serum (NDS, 1:30; Vector Laboratory) diluted in KPBS with 0.3% Triton- X100, for 2 h at RT. They were incubated in a solution containing goat anti-biotin (1:200) and rabbit anti-GFP (1:2000), diluted in KPBS containing 0.3% Triton-X100 and NDS (1:100), overnight at RT. After several rinses in KPBS, slices were incubated for 2 h in Alexa488-conjugated donkey anti-goat IgG (1:200); Invitrogen), and Cy3-donkey anti-rabbit IgG (1:100) diluted in KPBS with 0.3% Triton-X100. After rinses in KPBS, slices were mounted on slides and coverslipped with Fluoromount. The specimens were analyzed with a fluorescence microscope (Nikon 50i) or confocal microscope (Zeiss).

***In vivo* electrophysiology: optic stimulation, LFP and EEG recordings**

All mice were placed for 7 days in a recording box in order to get them used to the recording conditions. The recording box was ventilated, as well as electrically and sound isolated. The temperature was regulated at 21°C, and a 12 h light/12 h dark cycle imposed. Mice were accustomed to the cable connecting them to the recording device. The recording cable connected the micro-connector implanted on the head of the animal to a collector, which ensured the continuity of the recorded signals without hindering the movements of the mouse. At the end of this habituation, the control recordings begun. EEG and EMG recordings were digitized at 1 kHz, amplified 5000 times with a 16 channels amplifier (A-M System) and collected on a computer via a

CED interface using Spike 2 software (Cambridge Electronic Design). The signal was band-pass filtered online between 1 and 300 Hz for EEG, and between 10 and 100 Hz for EMG. The 50 Hz signal was removed with a notch filter. The EEG and LFP signals were acquired by monopolar derivation (differential between the recording electrode and the reference electrode located above the cerebellum). The EMG bipolar signals were calculated by measuring the differential between the two EMG electrodes. Mice were recorded for 24 h of baseline followed by optogenetic manipulation.

In vivo optogenetic stimulation

Optical stimulations were delivered via a patch cable connected to either a 100 mW 473 or 532 nm laser diode (Laserglow). Stimulations were performed during 4 days: in the first 3 days, mice were stimulated during one specific vigilance state par day: waking (WK), slow wave sleep (SWS) or PS. Each day, stimulations were delivered during the same circadian period (10 AM–2 PM). Stimulations were applied 10 s after the occurrence of a stable WK, SWS or PS event as detected by real time observation by the experimenter. For WK and SWS, stimulations were spaced apart by at least 1 min; for PS, by at least 15 s.

Blue exciting stimulations consisted of 10-s trains of 10-ms pulses at 20 Hz. For green inactivating stimulations, continuous light was delivered during 10 s. Light power at the fiber tip was 10 mW.

The 4th day of experiments, 4 VGLUT2-EYFP and 4 VGLUT2-ChR2 animals were stimulated for 15 min at 20 Hz (10-ms pulses). 3 VGLUT2-EYFP and 4 VGLUT2-eNpHR3.0 animals were stimulated for 15 min with pulsed light consisting of 10 s continuous light on-10 s light off. All mice were euthanized 90 min after the beginning of the stimulation by transcardiac perfusion of 4% PFA. Brain tissues were processed for immunohistochemical detection of cFos expression (see above).

Analysis of the sleep wake states

Polysomnographic recordings were visually scored by 5 s epochs for WK, SWS and PS as previously described (Sapin et al. 2009). Hypnograms were obtained by using a custom Matlab script. For each animal, the number of awakenings during SWS and PS optogenetic stimulations was counted and expressed as percentage of the total number of stimulations.

LFP and EEG analysis

LFP and EEG signals were analyzed using a custom Matlab script using the Chronux toolbox. The time-frequency spectrograms were computed with the same toolbox and expressed in arbitrary units. The mean power spectral density in the 10 s before the stimulation was compared to that in the 10 s during the stimulation (sliding window: 1 s), in order to obtain a mean spectral power ratio (PR) ± SEM. The frequency spectra were grouped into frequency bands commonly used Delta: 1-4 Hz, Theta: 6-12 Hz, Sigma: 12-14 Hz, Beta: 15-30 Hz, Gamma: 30-100 Hz. In VGLUT2-EYFP and VGLUT2-ChR2 animals power spectral values at 20 Hz and its harmonics were excluded from the analysis.

To analyze the evolution of LFP and EEG theta and gamma bands during optogenetic stimulation, the mean PR of these spectral bands and the respective 95% confidence intervals were calculated for VGLUT2-EYFP and VGLUT2-ChR2 animals from 10 s before to 10 s after the photostimulation. In order to compute these intervals, we used a bootstrap procedure, which allows creating artificial groups from the original data, with replacement. The mean of each artificial group derived from the original data was then computed. This operation was repeated 10000 times and the 95% confidence interval was the 5^{th} and the 95^{th} percentile of the means of the randomly constructed samples.

Finally, during WK and PS the peak of theta frequency (6-12 Hz) in the 10 s before and during the optogenetic stimulation was identified in VGLUT2-EYFP and VGLUT2-ChR2 animals.

Analysis of variance (Mann-Whitney test) was performed on the percentage of awakenings, the mean spectral power ratios, and the theta frequency peaks. These statistics were performed using the Statview software.

EMG analysis

In VGLUT2-EYFP and VGLUT2-ChR2 mice EMG signals during WK were analyzed using a custom Matlab script. The mean EMG value in the 10 s before the stimulation was compared to that in the 10 s during the stimulation, in order to obtain a mean EMG ratio ± SEM. In the 2 groups of animals we performed a sequential analysis per 0.5 s on the mean of the absolute EMG values from 20 seconds before to 10 seconds after the photostimulation. The respective bootstrap 95% interval (computed as described above) was calculated for each sequential value.

Further, analysis of variance (Mann-Whitney test) was performed on the EMG mean by using the Statview software.

Results

Distribution of VGAT and/or VGLUT2 mRNA-containing neurons in the SuM of VGLUT2-Cre transgenic mice

Three populations of VGAT and/or VGLUT2 mRNA-containing neurons were observed at all antero-posterior levels of the SuM. These included a population of large neurons co-expressing VGAT and VGLUT2 mRNA (Figure 1 A, D, arrows); and two populations of smaller neurons containing either VGAT mRNA (Figure 1 A, D, arrowheads) or VGLUT2 mRNA (Figure 1 A, D, blue). The distribution as well as the density of these populations differed significantly within the SuM. Almost all VGAT/VGLUT2 mRNAs –containing neurons were clustered around and above the mammillary tract (mt) (Figure 1 A, D) in a region similar to that described in rats as the grandicellular SuM (SuMg) by Pan and Mc Naughton (2004) and that is included in the lateral SuM (SuML) region of Paxinos and Franklin's mouse Atlas. The numerous singly labeled VGLUT2 mRNA -expressing cells were small and mostly located in the most central area (Figure 1 A) termed the parvicellular SuM (SuMp) by Pan & Mc Naughton (2004) corresponding to the SuMm in Paxinos and Franklin's mouse Atlas. Some were also intermingled with the larger VGAT/VGLUT2 mRNAs-containing cells in the SuMg. Few neurons expressed VGAT mRNA only. These neurons were scattered within the SuML and SuMM.

In summary, our results indicate that in mice like in rats a large number of neurons co-expressing markers of GABAergic and glutamatergic transmission are located in the SuML region.

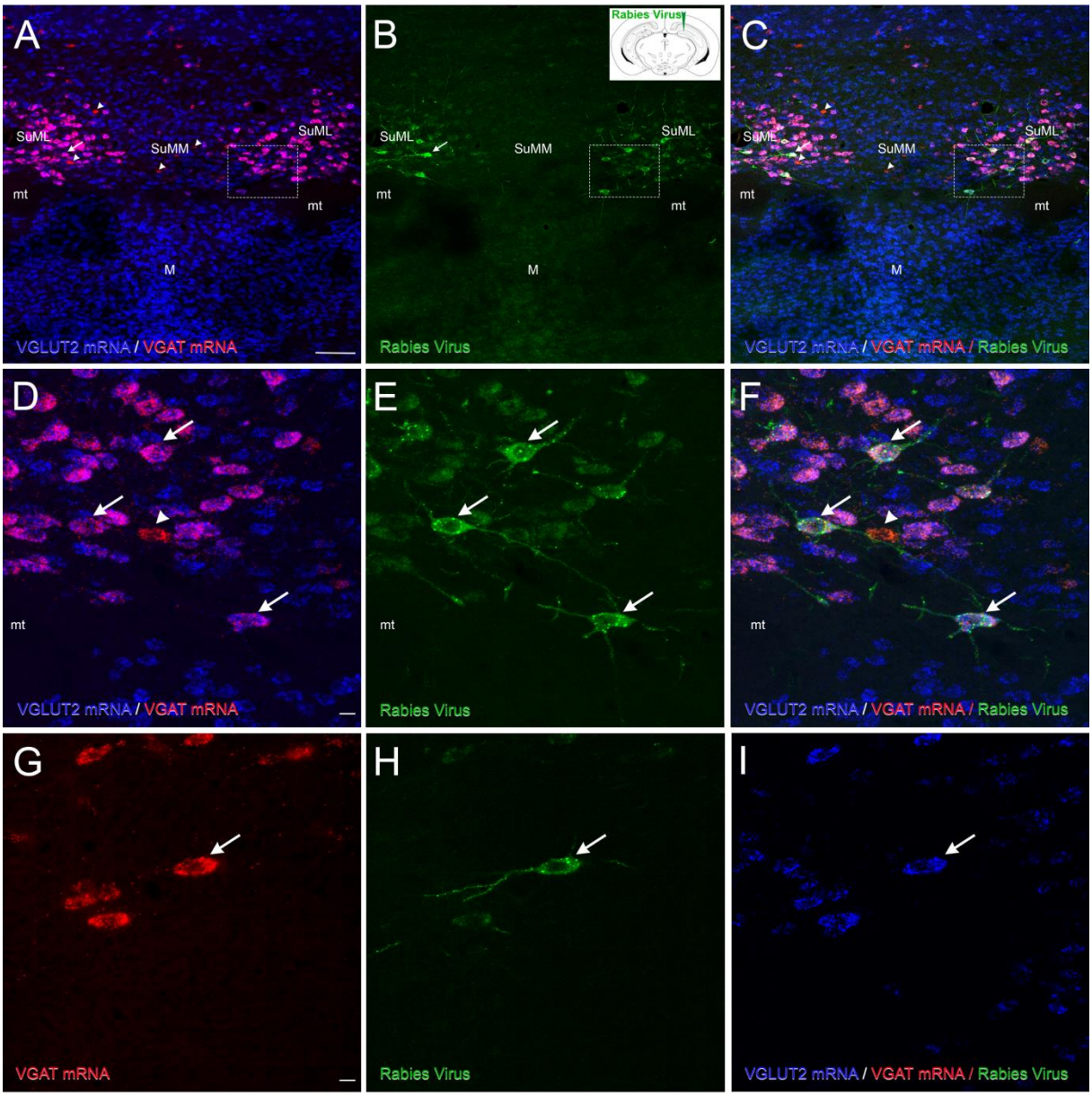

Fig.1. Neurochemical features of SuML neurons innervating the dorsal dentate gyrus (DG) characterized by simultaneous labeling for the rabies virus (RV) retrograde tracer (green), VGAT mRNA (red) and VGLUT2 mRNA (blue) in a coronal section.

(A-I) All confocal images were obtained from sequential acquisition of separate wavelength channels, corresponding to the different fluorophores used for the triple labeling, from a single optical slice. This optical slice was acquired in the supramammillary region of the hypothalamus from a coronal section of a VGLUT2-cre mouse that received an injection of RV in supragranular layer of the DG (B, insert). A) Image obtained from the merge of the two confocal images corresponding respectively to the labeling of VGLUT2 (blue) and VGAT (red) mRNAs. Many neurons expressing both VGLUT2 and VGAT mRNAs (arrow) were observed in the lateral region of the supramammillary nucleus (SuML). They were located almost exclusively above and around the mammillary tract (mt). Neurons expressing VGLUT2 mRNA only (blue) were observed mainly in the most medial part of the SuM (SuMM) and were numerous in the mammillary nucleus (M). Few neurons containing VGAT mRNA only (red, arrowheads) were distributed in the SuML and SUMM. B) Confocal image corresponding to the immunohistochemical labeling of the RV (green) showing that all RV containing neurons in the SuM were located in the region of the SuML surrounded the mt. C) Merge of A-B. (D-F) Higher magnification of region outlined in A-C showing that all these SuML neurons projecting to the DG, labeled for the RV (E, arrows), co-expressed VGLUT2 and VGAT mRNAs (D, F, arrows). (G-I) RV labeled neuron (H, arrow) co-expressed VGAT mRNA (G, arrow) and VGLUT2 mRNA (I, arrow) Scale bars: A-C, 100µm; D-I, 10µm.

Distribution of SuM neurons with dorsal dentate gyrus (dDG) projections

Unilateral or bilateral injections of rabies-virus (RV) were performed into the DG of the dorsal hippocampal formation (Figure 1 B, insert) to evaluate the distribution and proportion of SuM neurons that project to this structure. In all these mice, the RV tracer injection was located either in the granule cell layer or inner molecular region of the dorsal blade of the DG. Within the SuM, all these animals displayed retrogradely labeled neurons exclusively in the region of SuML (SuMg) immediately dorsal to the mt (Figure 1 B, E, H). Virtually none were found in the SuMM (Figure 1 B). Many of these neurons displayed a large soma with several labeled proximal dendrites (Figure 1 E). Therefore in mice, SuM neurons innervating the dDG are located in the SuML as in rats (Soussi et al., 2010).

Neurotransmitter phenotype of SuM neurons projecting to the dDG revealed by simultaneous detection of rabies-virus retrograde tracer, VGAT mRNA, and VGLUT2 mRNA

We next investigated whether the SuML neurons projecting to the dDG express markers of GABAergic and glutamatergic transmissions. Sections processed for simultaneous detection of VGAT mRNA, VGLUT2 mRNA and RV (Figure 1 A-I) showed that almost all RV retrogradely-labeled neurons co-express VGAT and VGLUT2 mRNAs (Figure 1 A-I, arrows). These data were confirmed by quantitative analysis performed on twelve sections (4 mice; 3 sections per mouse) showing that 99% (n= 378 out of 380 neurons) of the RV-labeled neurons co-expressed VGAT and VGLUT2 mRNAs. The percentages of these triple-labeled cells were the same (99%) for the three antero-posterior levels of the SuM analyzed (range 98%-100%).

Distribution and neurotransmitter phenotype of fibers and axon terminals originating from SuM neurons innervating the dorsal dentate gyrus

To further characterize the neurochemical properties of SuML neurons innervating the dDG, AAV-5-DIO-EYFP was injected bilaterally in the SuML (Figure 2 A) allowing specific EYFP labeling of VGLUT2 neurons and of their axon fibers innervating the hippocampus including the dDG (Figure 2 A). Sections of these VGLUT2-EYFP mice were processed for simultaneous

immunohistofluorescent detection of EYFP, VGLUT2 and VGAT or GAD65. All mice injected in the SuML displayed numerous anterograde EYFP-labeled fibers and axon terminals in the dDG (Figure 2 B, arrowheads) on both sides of the hippocampal formation. Labeled fibers and axon terminals were also present in the CA2／CA3a region of the hippocampus in particular when the injection sites involved more posterior levels of the SuML (Figure 2 B, arrowheads).

In the dDG, EYFP axonal fibers and terminals were mainly located in the supragranular layer of the dorsal and ventral blades of the DG (Figure 2 B-D) although some were localized in the granule cell layers. In all triple labeled sections either for EYFP, GAD65 and VGLUT2 or EYFP, VGAT and VGLUT2, the vast majority if not all EYFP-containing axon terminals present in the supragranular and granule cell layers were labeled for both GAD65 and VGLUT2 (Figure 2 C, E-H) or VGAT and VGLUT2 (Figure 2 D, I-L). Quantitative analysis of double labeling for VGLUT2 and VGAT showed that 90% (range 82% to 99%) of VGLUT2 labeled terminals were labeled for VGAT with no major differences between the infragranular blade (89%; range 82% to 99%) and the supragranular blade (91%; range 83% to 99%). Further quantification of EYFP labeling revealed that 98 % (range 96% and 100%) of the axon terminals contained both VGAT and VGLUT2 confirming that all EYFP-containing axon terminals originating from SuML neurons contained both makers of GABA and glutamate neurotransmissions.

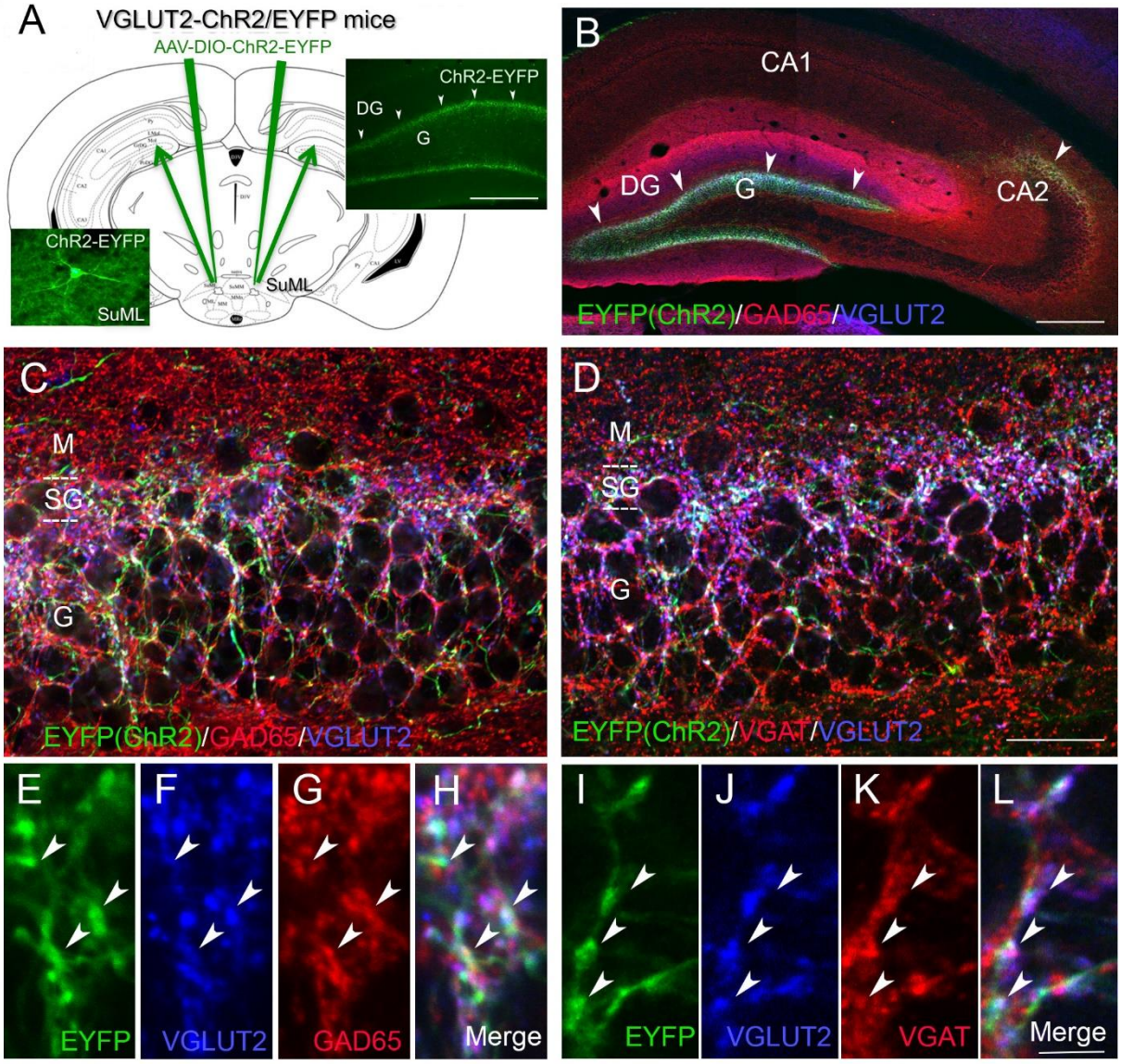

Fig. 2. Neurochemical features of axon terminals from SuML neurons innervating the dorsal DG characterized by simultaneous immunohistochemical labeling for the AAV-EYFP anterograde tracer (green), GAD65 or VGAT (red) and VGLUT2 (blue) in coronal sections.
(A) Diagram illustrating the bilateral injections of the viral vector AAV-DIO-ChR2-EYFP within the lateral region of the SuM. Images from a coronal section showing endogenous fluorescence of EYFP observed in the cell body and proximal dendrites of a transfected neuron located within the SuML as well as fibers and axon terminals within the supragranular (arrowheads) and granule layer (G) of the DG. (B) Image obtained from a single optical slice showing labeling for EYFP (green), GAD65 (red) and VGLUT2 (blue) in the hippocampus. Fibers labeled with the anterograde tracer AAV-DIO-ChR2-EYFP injected within the SUM as illustrate in (A) were exclusively located in the supragranular (arrowheads) and granule cell (G) layers as well as the CA2 region of the hippocampus. (C, D) Images corresponding to a maximum intensity z-projection of a stack of 8 optical slices spaced at 370 nm, showing labeling for EYFP (green), VGLUT2 (blue) and GAD65 (C, red) or VGAT (D, red) in the dorsal DG. Axon terminals and fibers, from neurons in the SuML, labeled for the EYFP anterograde tracer (green) were located mainly in the supragranular layer but also in the granule cell layer. Numerous GAD65- (C) or VGAT- (D) containing terminals were present in the molecular layer (M) and granule cell layer (G) of the dorsal DG. VGLUT2-containing terminals were mainly located in the supragranular layer (SG) but were also observed in G. (E–L) Images of the three different fluorophores used for the triple labeling, obtained by sequential acquisition of separate wavelength channels from a single optical slice, in the SG of the DG demonstrated that many if not all axon terminals labeled for EYFP (B, I, green, arrowheads) contained GAD65 (G, red arrowheads), VGAT (K, red, arrowheads) but also VGLUT2 (F, J blue, arrowheads). (H) Merge of E-G. (L) Merge of I-K. Scale bars: A-B, 200µm; C-D, 25µm and E-L, 3µm.

Electron microscopy analysis of synaptic contacts established by EYFP-containing axon terminals originating from SuML neurons

In the supragranular region of the dDG, axon terminals from SuML neurons labeled for EYFP displayed diffuse electron-dense labeling that contrasted with adjacent unlabeled cellular compartments. These labeled axon terminals formed synaptic contacts on the soma (Figure 3 A, B, D, E, F, I) and dendritic profiles (Figure 3 C, G, H) of presumed granule cells (GCs). These axon terminals were often very large boutons that displayed one (Figure 3 A, B, D, E) or more (Figure 3 F) synaptic zones with relatively thin post-synaptic densities (arrowheads) characteristic of symmetric synapses. Other synaptic contacts formed by these labeled terminals displayed thicker post-synaptic densities characteristic of asymmetric synapses (Figure 3 A, B, C; arrow). We also observed large labeled “en passant” boutons establishing symmetric synapses on the dendrites of a presumed granule cell (Figure 3 G, H). Finally, some axon terminals from SuML neurons formed both symmetric (arrowhead) and asymmetric (arrow) synapses on the soma or the proximal dendrite of two different neighboring GCs (Figure 3, A, B).

Together these data demonstrate that in mice all SuM neurons innervating the dDG belong to a single population of large neurons located in the SuMg region of the SuML. These cells display a dual neurochemical phenotype for GABA and glutamate neurotransmissions and establish symmetric (presumably inhibitory) and asymmetric (presumably excitatory) synapses on the GCs of the dDG.

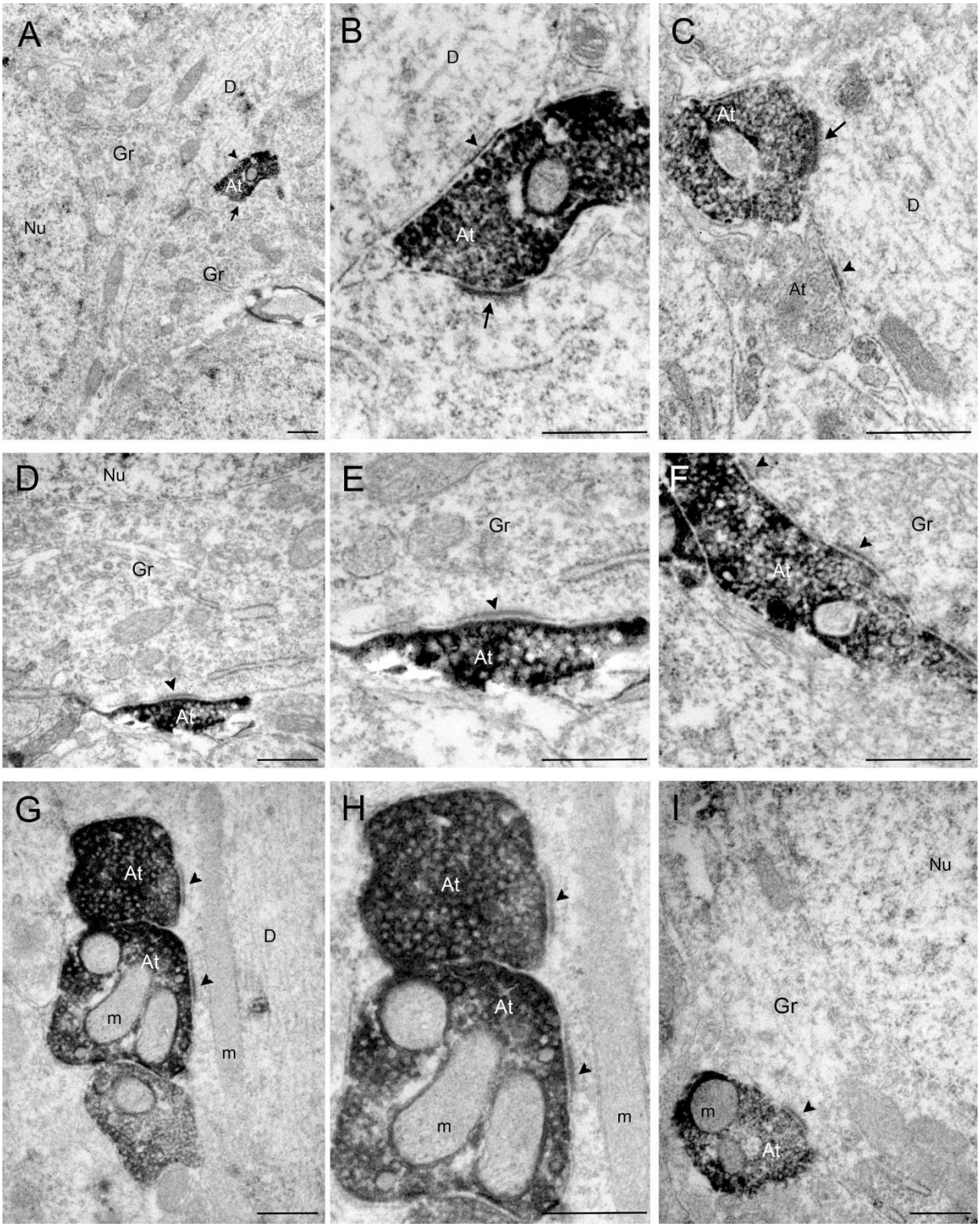

Fig. 3. Pre-embedding immunolabeling for EYFP anterograde tracer in ultrathin coronal sections of the dorsal DG.

(A–I) In the dorsal DG, numerous axon terminals were labeled for EYFP, revealed by electron-dense peroxidase 3.3'-diaminobenzidine tetrahydrochloride product. (A) A labeled axon terminal (At) making two synaptic contacts (arrow and arrowhead) on unlabeled somata of 2 presumed granule cells (Gr). (B) Higher magnification of the At illustrated in (A) showing that these two synaptic contacts were different: one displayed a relatively thin post-synaptic densities (arrowhead) characteristic of symmetric synapses on the soma of one Gr; the other one displayed a thick post-synaptic densities (arrow) characteristic of asymmetric synapses on the soma of another Gr. (C) Labeled axon terminals established synaptic contacts displaying a thick synaptic densities on unlabeled dendritic processes (D) that differed from the synaptic contact formed by the unlabeled At (arrow). The synaptic contacts illustrated in D-I displayed

relatively thin post-synaptic densities (arrowheads) on the soma (D-F, I) or dendrites (G, H) of unlabeled Gr. m, mitochondria; Nu, nucleus. Scale bar: A-I, 0.5 µm.

Co-release of glutamate and GABA at the SuML-dentate granule cells synapses

The neurochemical profile of SuML neurons projecting to the dDG strongly suggested that they co-release GABA and glutamate at the SuML-dentate granule cells synapses. To test this hypothesis, we performed patch clamp recordings of dDG granule cells layer using optogenetic stimulation in hippocampal slices obtained from VGLUT2-ChR2 mice (5 mice, 3 sections per mouse, 16 neurons) and VGLUT2-EYFP control mice (3 mice, 3 sections per mouse, 10 neurons) (Figure 4). The light stimulation of SuML-DG fibers and axonal terminals expressing ChR2 (Figure 4 A) evoked a fast inward and a slower outward synaptic current in fourteen out of sixteen neurons recorded at a holding potential of -30 mV (Figure 4 D, F, H). Post-hoc immunodetection of biocytin-filled neurons showed that all these recorded neurons correspond to GCs (Figure 4 C, E, G, I). They were equally distributed in the apex and the upper and lower blades of dDG granule cell layer (Figure 4 B). These GCs were additionally recorded at different holding potentials. At -10 mV and +10 mV (close to the reversal potential of the glutamatergic receptor-mediated currents), only the outward (positive going) synaptic current was observed (Figure 4 D, see also F, H). From -70 mV to -50mV (close to the reversal potential of GABA-A receptor-mediated currents) only the inward (negative going) synaptic current was observed (Figure 4 D, see also 4F,4H). At intermediate holdings, from -30 to -20mV, the light-evoked synaptic currents displayed both inward and outward components (Figure 4 D, F, H). Using a pharmacological approach, we confirmed the nature of these currents. Bath application of a mixture of AMPA/Kainate and NMDA receptor antagonists (NBQX 10 µM and D-AP5 40 µM) abolished the inward component (Figure 4 F, K, L, red trace) while GABA-A receptor blockers inhibited the outward component (Figure 4 H, J- gabazine; K, L– bicuculline, green trace). Quantitative analysis performed in 5 DG neurons (Fig. 4 K) further illustrated that in regular ACSF the repetitive light pulses (5 ms, 0.05 Hz) evoked PCS of relatively stable amplitude (1.00 ± 0.26 normalized, Figure 4 K, L, left hand side red trace is an example of an averaged response of one neuron). The application of glutamate receptor blockers (10 µM NBQX + 40

µM D-AP5) reduced the peak amplitude by 84% (0.16 ± 0.15, p<0.01, n= 5, paired Wilcoxon test). The remaining response seen in 4 from 5 neurons was probably due to GABA A mediated current because at -70 mV the driving force for chloride driven currents is close to but not zero (Figure 4 K, L, red trance in the middle). Therefore in case of GABA massive release some inward current is still possible. Indeed a switch to Vh= 10 mV revealed a large PSC response to light stimulation (Figure 4 L, green trace in the middle) which had a stable amplitude (1.00 ± 0.20 normalized), and was subsquently reduced to 12% (0.12 ± 0.16, p<0.01, n= 5, paired Wilcoxon test) by the addition of 10 µM bicuculline to the ACSF already containing GluR blockers (Figure 4 L, green trace at left). In 3 out of 5 neurons, bicuculline completely abolished the synaptic response to light pulses after 6 min of drug perfusion. In two neurons the small remaining current was probably due to the fact that bicuculline is a competitive antagonist and can be displaced when large quantities of GABA are released. All these results indicate that the inward synaptic current component is mediated by glutamate and the outward component by GABA. Importantly, the disappearance of the inward (glutamatergic) component induced by the light stimulation in the presence of NBQX and D-AP5 antagonists (red trace) did not affect the outgoing (GABAergic) currents (Figure 4 F). In two GCs (Figure 4 I), the disappearance of the glutamate response (incoming current recorded at -30 mV) in the presence of NBQX and AP5 (red trace) unmasked the GABAergic component (outgoing current) abolished after addition of gabazine (green trace) (Figure 4 J). The very short latency of the glutamatergic inward and GABAergic outward currents recorded in a GC after light stimulation of ChR2 containing axon terminals, and the persistence of GABAergic outflow current in the presence of NBQX and AP5 indicates that the GABAergic current results from direct light stimulated GABA release and not from the excitation of DG GABAergic neurons by light stimulated glutamate release. Together, these results suggest that activation of SuML axon terminals produce monosynaptic glutamatergic and GABAergic currents on their targets.

Finally, we verified that light stimulation (5 ms, 10%, 50% 90% max power LED) of fibers and axon terminals expressing EYFP on slices of control VGLUT2-EYFP mice (n= 3) did not evoke any response in the recorded GCs (n= 10) (Figure 4 M, N).

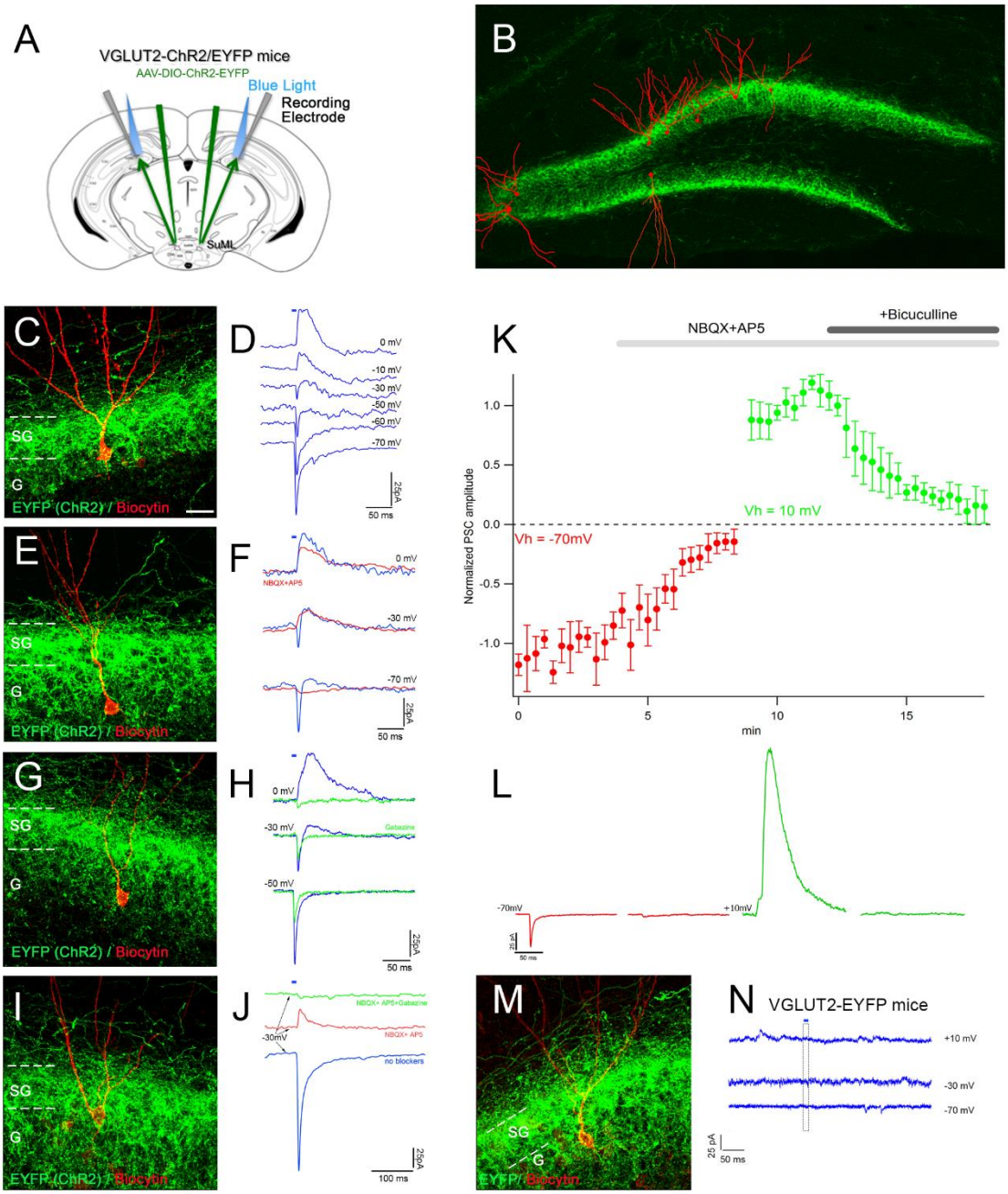

Fig. 4. Selective stimulation of axonal terminals from SuML neurons innervating the dorsal DG, performed in hippocampal slices of VGLUT2-ChR2-EYFP mice, induced co-release of GABA and glutamate on DG granule cells.

(A) Diagram illustrating the site of the bilateral injections of AAV-DIO-ChR2-EYFP in VGLUT2-cre mice, of light stimulations and of the recorded patch clamp electrode in the DG of the VGLUT2-ChR2-EYFP mice. (B) Montage illustrating the position within the dentate granule cell layer of the biocytin-filled cells reconstructed after patch clamp recordings and EYFP-labeled terminals originating from SuML neurons.

(D, F, H, J, N) Examples of light induced PSCs recorded in DG cells illustrated in (C, E, G, I, M). (D) Light induced post-synaptic currents (PSCs) recorded at different holding potentials in DG neuron; short black bar above the upper trace shows the time moment and duration of light stimulus. Note at -70 mV to -50 mV holdings the PSCs had negative-going direction (inward) currents. They were positive-going (outward) at -10 mV and 0 mV but displayed both negative- and positive-going phases when the neuron membrane was clamped at -30 mV. This suggests that light stimulation induces two types of postsynaptic currents. Indeed, the application of glutamate receptor blockers NBQX and AP5 (F, red traces) inhibited

inward (F, negative going) component of PSCs recorded at negative holding potentials (Vh), but had only small effect on outward component (positive going) recorded at positive Vh. Inversely, the outward component of light induced PSCs was sensitive to GABA A receptor inhibitor gabazine (H, green vs blue traces). This suggests that these PSCs are generated by simultaneous activation of glutamate and GABA post-synaptic receptors. Interestingly at -50 mV holding, PSC was larger without gabazine (H, blue versus green trace), probably because GABA-mediated current hyperpolarizes the membrane potential increasing thus the driving force for the glutamatergic current. In voltage-clamp condition such an interaction is possible if the pool of postsynaptic GABA Rs is close to the postsynaptic Glu R pool. (K, L) Effect of glutamate and GABA A receptors blockers on the peak amplitude of light pulse evoked PSC recorded at -70 mV (red circles) and 10 mV (green circles) holding potentials. For each Vh the peak amplitudes of first 10 PSCs were averaged and used then as a normalization factor for all peak amplitude recorded at given potential. Each point and error bars corresponds the mean ± SD of PSC normalized amplitude recorded in 5 DG neurons. In regular ACSF the repetitive light pulses (5 ms, 0.05 Hz) evoked PCS of relatively stable amplitude (1.00 ± 0.26, L left hand side red trace-an example of averaged response of one neuron). The application of glutamate receptor blockers (10 µM NBQX + 40 µM D-AP5) reduced the peak amplitude by 84% (0.16 ± 0.15, $p<0.01$, n= 5, paired Wilcoxon test). The remaining response was seen in 4 from 5 neurons and is probably due to GABA A mediated current because at -70 mV the driving force for chloride driven currents is close to but not zero (L, red trance in the middle) therefore in case of GABA massive release some inward current is still possible. Indeed a switch to Vh= 10 mV revealed a huge PSC response to light stimulation (L, green trace in the middle) which amplitude was stable (1.00 ± 0.20) but progressively reduced to 12% (0.12 ± 0.16, $p<0.01$, n= 5, paired Wilcoxon test) by the addition of 10 µM bicuculline to the ACSF already containing GluR blockers (L, green trace at left). In 3 from 5 neurons, 6 min lasting bicuculline application completely abolished response to light pulses. In two neurons the remaining current is probably due to the competitive character of bicuculline induced inhibition i.e in case of high GABA release 10 µM of bicuculline may be not sufficient to all receptors inhibition. (M, N) The identical light stimulation (5 ms, 10%, 50% 90% max power LED) of fibers and axon terminals expressing EYFP on slices of control VGLUT2-EYFP mice (n= 3) did not evoke any response in the recorded granule cells (n= 5) confirming that ChR2 activation is required to obtain the PSCs. Scale Bar: C, E, G, I, M, 20µm.

Effect of optogenetic stimulation of SuML axon terminals innervating the dDG on behavior, LFP and EEG spectral content

We analysed the effects of light stimulation of SuML axon terminals innervating the dDG on behavioral states, spectral content of the LFP recorded in dDG and cortical EEG in VGLUT2-ChR2 (n= 4) and control VGLUT2-EYFP mice (n= 4).

Light activation of SuML axon terminals in VGLUT2-ChR2 mice during waking (WK), induced a strong and significant increase in EMG value as compared to control mice (mean EMG ratio, VGLUT2-EYFP= 0.9 ± 0.03, VGLUT2-ChR2= 2.0 ± 0.31, p= 0.0209). The increase in EMG was due to an increase in animal movements (Figure 5 A, D). It was associated with a slight but not significant increase in theta power in the dDG LFP (Figure 5 B, 6 A) and the EEG (Figure 7 A) compared to control VGLUT2-EYFP mice. Theta/delta ratio was significantly increased both in the dDG LFP (Figure 6 A, B) and the EEG (Figure 7 C, D) during the stimulation compared to control mice (LFP: VGLUT2-ChR2= 1.3 ± 0.11, VGLUT2-EYFP= 0.9 ± 0.02, p=0.0209, EEG: VGLUT2-ChR2= 2.2 ± 0.31, VGLUT2-EYFP= 0.9 ± 0.05, p=0.0209). Further, the frequency at

the theta peak was not significantly increased during stimulation as compared to control VGLUT2-EYFP animals (LFP: VGLUT2-ChR2: 8.43 ± 0.43 Hz, VGLUT2-EYFP: 6.96 ± 0.23 Hz, p= 0.0833) (Figures 5 B; 6 D). Gamma power (30-100 Hz) was significantly increased during the stimulation in VGLUT2-ChR2 mice as compared to control mice in the dDG LFP (VGLUT2-ChR2= 1.6 ± 0.13, VGLUT2-EYFP= 1.0 ± 0.02, p=0.0209) (Figures 5 C, 6 A, C) and in the EEG (VGLUT2-ChR2: 1.68 ± 0.05, VGLUT2-EYFP: 0.98 ± 0.02, p=0.0209 (Figure 7 B, C, E). The increase occurred immediately after the beginning of the stimulation and lasted until the end of it (Figures 6 C, 7 E).

Stimulations during SWS induced significantly more often an awakening in VGLUT2-ChR2 than in control VGLUT2-EYFP mice (p=0.0209, VGLUT2-ChR2: 80 % of the cases, range 40%-100%; VGLUT2-EYFP: 15 % of the cases, range: 0%-30%; Figure 5 E, H). The induced waking state lasted at least the duration of the stimulation and was characterized by a significant increase in theta/delta ratio (LFP: VGLUT2-ChR2= 1.3 ± 0.14, VGLUT2-EYFP= 1.0 ± 0.02, p=0.0433; EEG: VGLUT2-ChR2= 1.5 ± 0.27, VGLUT2-EYFP= 1.0 ± 0.03, p=0.0209) (Figures 6 A, B, 7 C, D) and a decrease of delta power both in the dDG LFP (VGLUT2-ChR2= 0.6 ± 0.11, VGLUT2-EYFP= 0.9 ± 0.01, p=0.0209) and the EEG (VGLUT2-ChR2= 0.5 ± 0.13, VGLUT2-EYFP= 0.9 ± 0.02, p=0.0209) in VGLUT2-ChR2 compared to control VGLUT2-EYFP mice (Figures 5 E, F, 6 A, 7 A, C). This induced waking state was also associated to an increase in gamma power in the dDG LFP (Figures 5 E, G, 6 A, C) and in the EEG (VGLUT2-ChR2= 1.36 ± 0.16, VGLUT2-EYFP 0.99 ± 0.03, p=0.0433) (Figure 7 B, C, E).

In contrast to SWS, light stimulation of SuML axon terminals in the dDG of VGLUT2-ChR2 mice during PS did not induce significantly more awakening of VGLUT2-ChR2 mice compared to control VGLUT2-EYFP animals (p= 0.3865; Figure 5 L).

Light activation of SuML axon terminals during PS in VGLUT2-ChR2 induced a significant increase in theta power compared to VGLUT2-EYFP mice in the dDG LFP (Figures 5 I, J, 6 A, B, VGLUT2-ChR2= 1.3 ± 0.04, VGLUT2-EYFP= 0.9 ± 0.02, p= 0.209) but not in the EEG (Figure 7 C, D, p= 0.773). The frequency at the theta peak was also significantly increased in the dDG LFP compared to control EYFP-VGLUT2 animals (VGLUT2-ChR2: 8.3 ± 0.13 Hz,

VGLUT2-EYFP: 7.7 ± 0.15 Hz, p= 0.0209) (Figure 6 E). In addition, gamma was significantly increased both in the dDG LFP and the EEG during the stimulation in VGLUT2-ChR2 mice compared to control VGLUT2-EYFP mice (LFP: VGLUT2-ChR2= 1.1 ± 0.02, VGLUT2-EYFP= 1.0 ± 0.01, p= 0.0209; EEG: VGLUT2-ChR2: 1.68 ± 0.05, VGLUT2-EYFP: 0.98 ± 0.02, p= 0.0209, Figures 5 K, 6 A, C, 7 B, C, E).

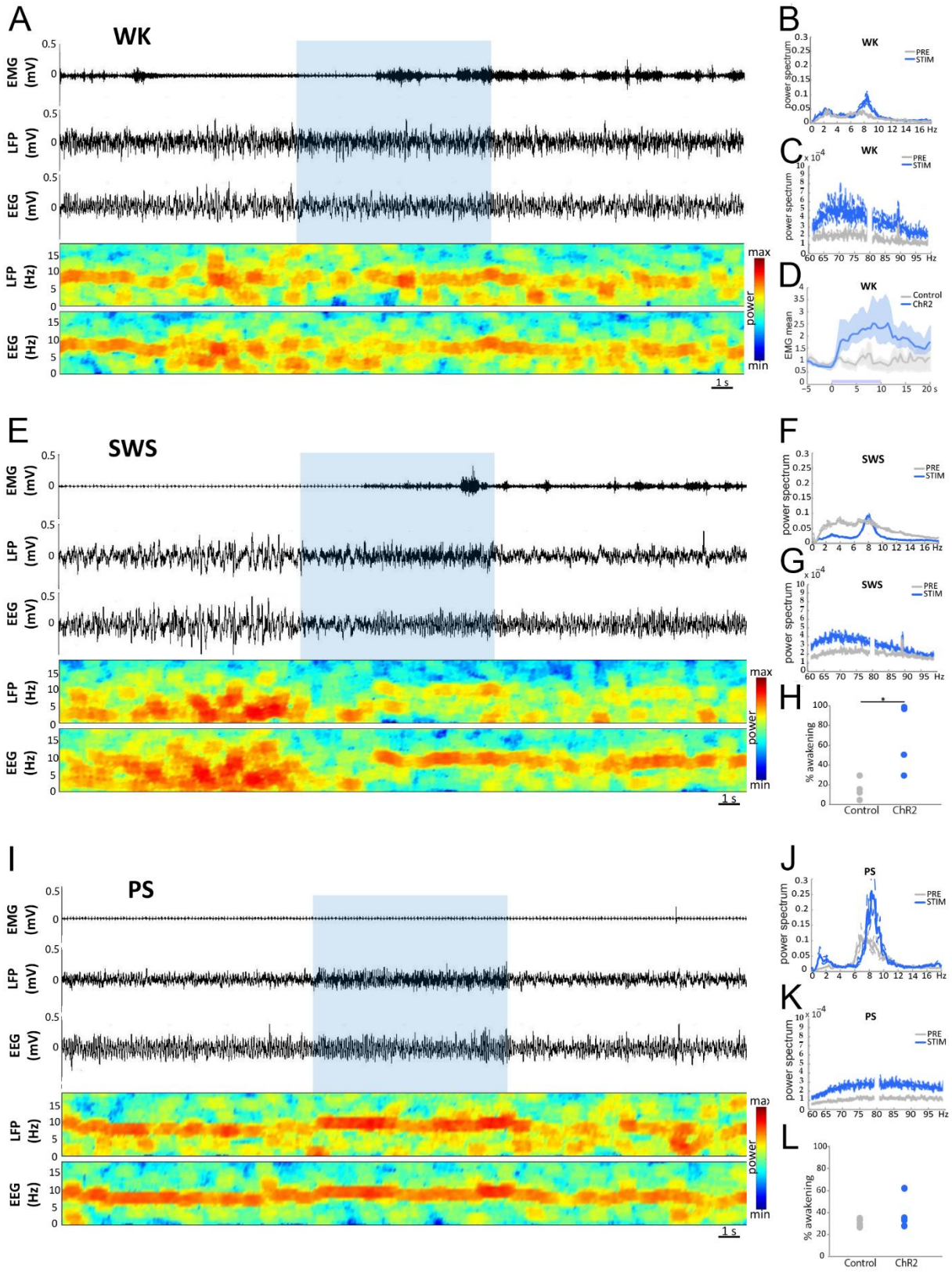
A
WK
EMG (mV)
LFP (mV)
EEG (mV)
LFP (Hz)
EEG (Hz)
max
power
min
1 s
B
WK
PRE
STIM
power spectrum
C
WK
PRE
STIM
power spectrum
D
WK
Control
ChR2
EMG mean
E
SWS
F
SWS
G
SWS
H
% awakening
Control
ChR2
I
PS
J
PS
K
PS
L
% awakening
Control
ChR2

Fig. 5. Effects of light stimulation of axonal terminals from SuML neurons innervating the dorsal DG on DG local field potential (LFP), cortical electroencephalographic (EEG) recordings and behavior of vigil VGLUT2-ChR2-EYFP mice during waking (WK), Non-REM Sleep (SWS) and REM sleep (PS).

(A, E, I) Examples of raw recording for electromyogram (EMG), LFP recorded in the DG and parietal cortex EEG as well as associated time-frequency analysis of LFP and EEG in a VGLUT2-ChR2-EYFP mouse during WK (A), SWS (E) and PS (I). The blue bar represents the optogenetic stimulation period at 20 Hz with pulses of 10 ms for 10 s. (B, C, F, G, J, K) LFP power spectra between 0-18 Hz and 60-100 Hz in VGLUT2-ChR2-EYFP mouse before and during light stimulation (20 Hz 10 s, pulses of 10 ms, during 4 h) during WK (B, C), SWS (F, G) and PS (J, K). An effect was clearly visible on the LFP in all vigilance states. The stimulation induced a slight increase in the theta power during WK (A, B) and a major increase in theta power and frequency during PS (I, J) as well as a clear reduction of slow waves oscillation during SWS (E, F). The stimulation during WK and PS also increased the power of the gamma (C, K). Light stimulation during WK increased locomotor activity reflected by an increase of EMG signal in VGLUT2-ChR2-EYFP mice (A, D, blue trace) as compared to control VGLUT2-EYFP mice (D, grey trace). (H) Light stimulation during SWS induced awakening reflected by a significant increase of the awakening percentage after stimulation in most VGLUT2-ChR2-EYFP mice (range 30% to 100%) as compared to that observed in control VGLUT2-EYFP mice (range: 0% to 30 %). (L) In contrast no significant difference in the percentage of awakening was observed between VGLUT2-CHR2-EYFP and control VGLUT2-EYFP mice when stimulation was performed during PS.

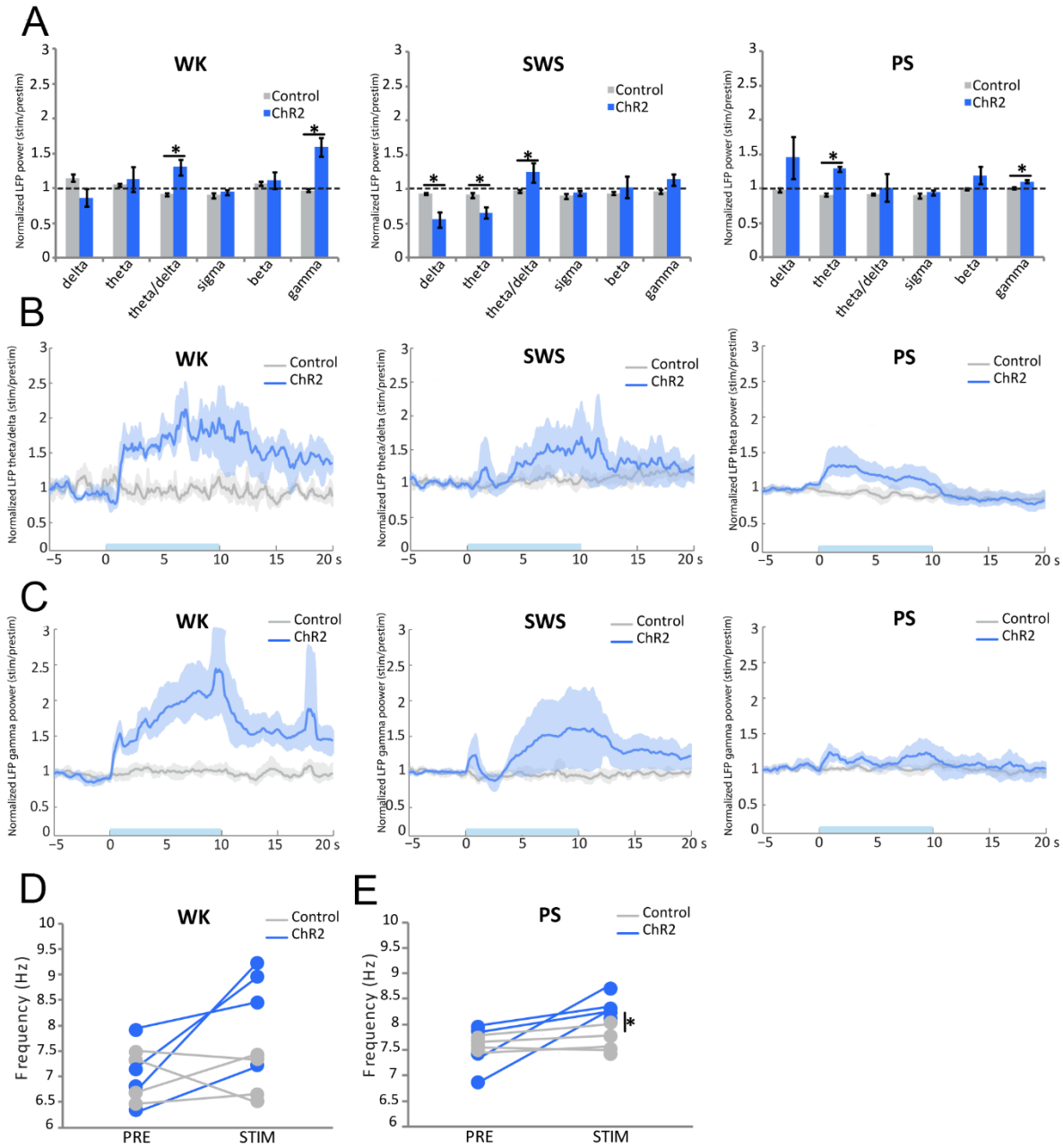

Fig. 6: Comparison of the effects of light stimulation of axonal terminals from SuML neurons innervating the dorsal DG on DG local field potential (LFP) performed during waking (WK), Non-REM Sleep (SWS) and REM sleep (PS) between VGLUT2-ChR2-EYFP and control VGLUT2-ChR2-EYFP mice.

(A) Ratio of power recorded during light stimulation to that recorded before the stimulation (20 Hz, 10 s for 4 h with pulses 10 ms) for the different frequency bands (delta, theta, gamma) of LFP in VGLUT2-ChR2-EYFP (n= 4) and control VGLUT2-EYFP (n= 4) mouse groups during WK, SWS and PS. These ratios illustrate: an increased power in the theta frequency band during stimulations performed in PS; an increase of theta/delta power during the stimulation when performed in WK and SWS and an increased power in the gamma frequency band when stimulations were performed during WK and PS in the VGLUT2-ChR2-EYFP group. Increased power observed during stimulations observed in the ChR2 group differed significantly from random variation observed before and after the stimulation in the control group. Significance: Mann Whitney: * p <0.05. (B, C) Theta/delta (B) and gamma (C) power ratios as a function of time after light stimulation during the different vigilance states. The blue bar on the x axis represents the stimulation period. Shaded regions show 95% confidence intervals. During WK a significant increase of theta/delta (B) and gamma (C) powers occurred in VGLUT2-ChR2-EYFP group immediately after the light stimulation and this increase was prolonged during all the 20 s-period analyzed including the 10 s duration of the stimulation and 10 s after the stimulation. In this animal group the increase of theta/delta

during SWS was variable and was taking place two to three s after the stimulation. The increase of theta (B) and gamma (C) powers during PS occurred immediately after the stimulation and stayed during the 10 s period of stimulation. No differences induced by the stimulation were observed in the control group. (D, E) Peak frequency analysis of theta before and during optogenetic stimulation (20 Hz, 10 s for 4 h with pulses of 10 ms) in the control group (n= 4) and the ChR2 group (n= 4). Significance: Mann Whitney, * p <0.05 compared to the control group.

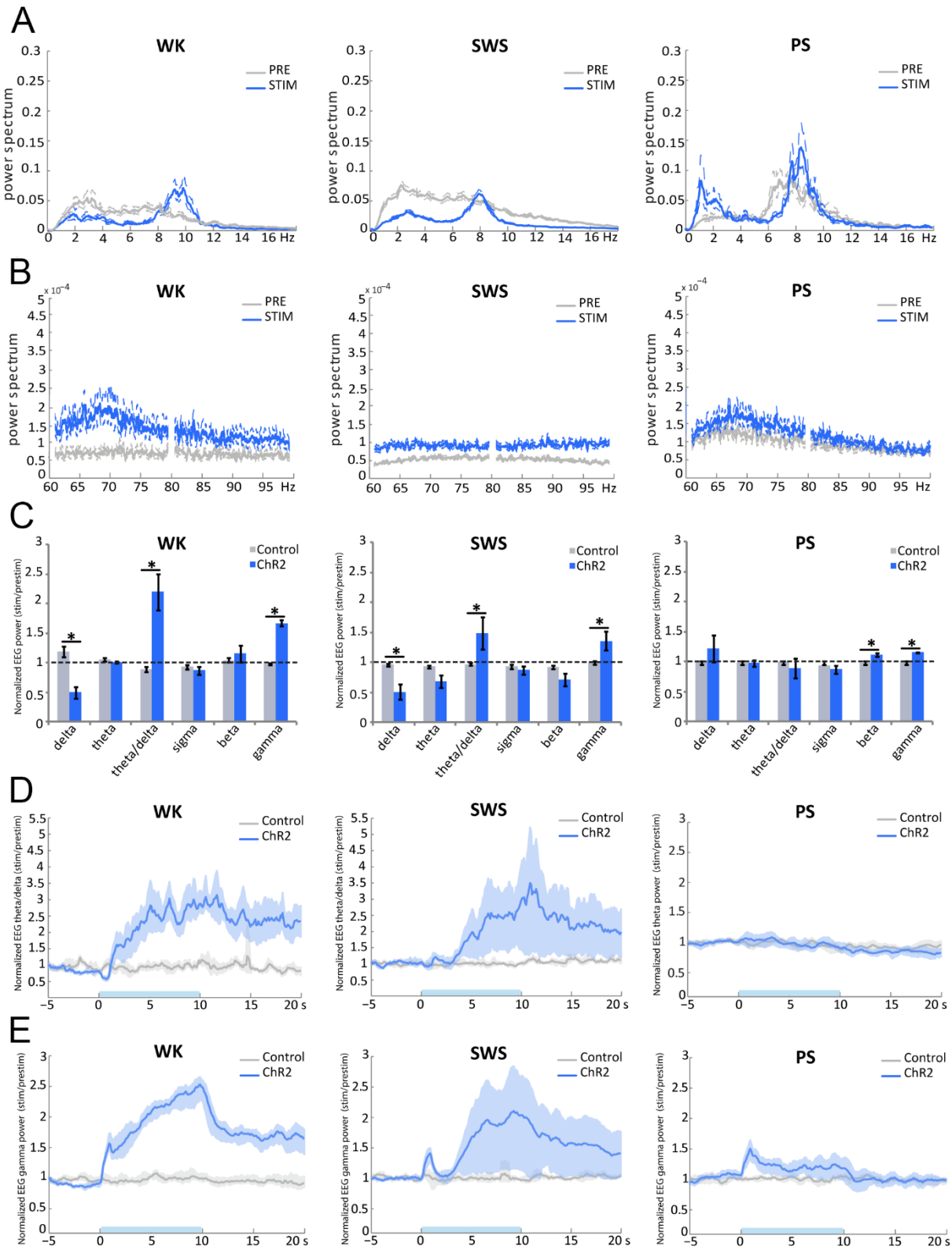

Fig. 7: Comparison of the effects of light stimulation of axonal terminals from SuML neurons innervating the dorsal DG on EEG performed during waking (WK), Non-REM Sleep (SWS) and REM sleep (PS) between VGLUT2-ChR2-EYFP and control VGLUT2-EYFP mice.
(A, B) EEG power spectra between 0-18 Hz and 60-100 Hz in a VGLUT2-ChR2-EYFP mouse before and during light stimulation (20 Hz 10 sec, pulses of 10 msec, during 4 h) during WK, SWS and PS. An effect was clearly visible on the EEG in all vigilance states. The stimulation induces an increase in the power and frequency of theta, both during WK and PS and a clear reduction of slow waves oscillation during SWS. The stimulation increased the power of the gamma in particular during WK but also during PS (B). (C) Ratio of power recorded during light stimulation to that recorded before the stimulation (20 Hz, 10 sec for 4 h with pulses 10 msec) for the different frequency bands (delta, theta, gamma) of EEG in VGLUT2-ChR2-EYFP (n = 4) and control VGLUT2 -EYFP (n = 4). These ratios illustrate an increase of theta/delta power during the stimulation when performed in WK and SWS and an increased power in the gamma frequency band when stimulations were performed during all vigilance states in the VGLUT2-ChR2-EYFP group. These increased powers during stimulations observed in ChR2 group differed significantly from random variation observed before and after the stimulation in the control group. Significance: Mann Whitney: * $p < 0.05$. (D, E) Theta/delta (D) and gamma (E) power ratios as a function of time after light stimulation during the different vigilance states. During WK a significant increase of theta/delta (B) and gamma (C) powers occurred in VGLUT2-ChR2-EYFP group immediately after the light stimulation and this increase was prolonged during all the 20 sec-period analyzed including the 10 sec duration of the stimulation and 10 sec after the stimulation similarly to what observed in the LFP (Fig.6 B, C). In this animal group the increase of theta/delta during SWS was variable and was taking place two to three sec after the stimulation. The increase of gamma (C) powers during PS occurred immediately after the stimulation and stayed during the 10sec period of stimulation. No differences induced by the stimulation were observed in the control group. An no increase in theta was observed during PS (C, D) in the EEG in contrast to LFP (Fig. 6 A, B).

Effect of light inactivation of SuML axon terminals innervating the dDG on behavior, LFP and EEG spectral content

The effects of light stimulation of SuML axon terminals innervating the dDG on the spectral features of LFP recorded in dDG, cortical EEG and associated behaviors during WK, SWS and SP were assessed in VGLUT2-NpHR3 mice (n=4) as illustrated in Figure 8 and in control VGLUT2-EYFP mice (n=3). No statistical difference of the spectral content of the LFP and EEG was observed during light inactivation of SuML axon terminals in the dDG of VGLUT2-NpHR3 mice compared to control mice. The only exception was that VGLUT2-NpHR3 mice compared to control VGLUT2-EYFP mice displayed a significant increase of the LFP sigma power ratio (VGLUT2-NpPH3: 1.11 ± 0.02, VGLUT2-EYFP: 1.03 ± 0.00, p= 0.0339; Figure 8).

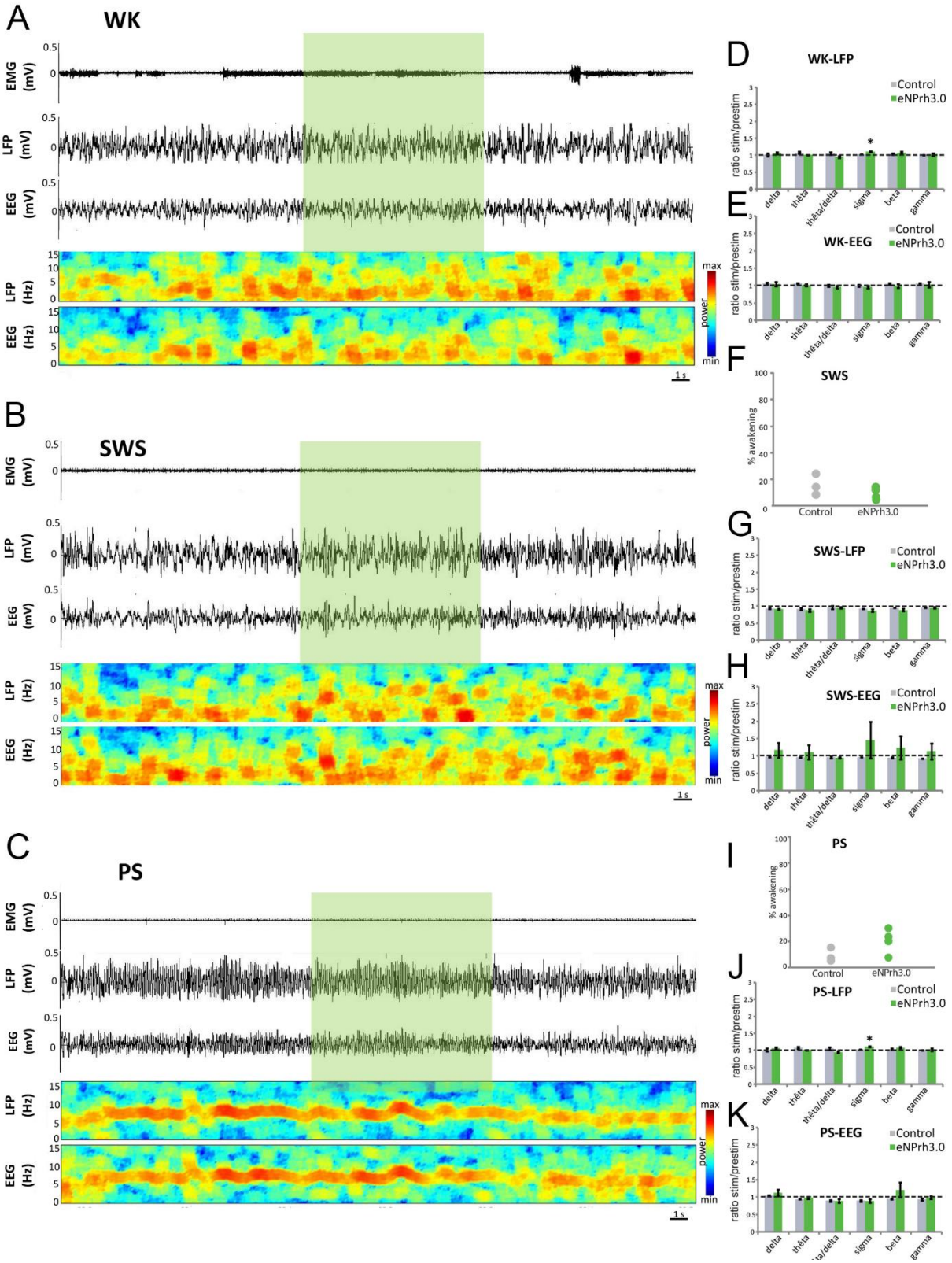
A
WK
EMG (mV)
LFP (mV)
EEG (mV)
LFP (Hz)
EEG (Hz)
max
power
min
1 s
B
SWS
C
PS
D
WK-LFP
Control
eNPrh3.0
ratio stim/prestim
delta
theta
theta/delta
sigma
beta
gamma
E
WK-EEG
F
SWS
% awakening
G
SWS-LFP
H
SWS-EEG
I
PS
J
PS-LFP
K
PS-EEG

Fig. 8 Effects of light stimulation of axonal terminals from SuML neurons innervating the dorsal DG on DG local field potential (LFP), cortical electroencephalographic (EEG) recordings and behavior of vigil VGLUT2- NpHR3 -EYFP mice during waking (WK), Non-REM Sleep (SWS) and REM sleep (PS).
(A, B, C) Examples of raw recording for electromyogram (EMG), LFP recorded in the DG and parietal cortex EEG as well as associated time-frequency analysis of LFP and EEG in a VGLUT2- NpHR3 -EYFP mouse during WK (A), SWS (E) and PS (I). The blue bar represents the light stimulation period at 20 Hz with pulses of 10 msec for 10 sec. (D, E, G, H, J, K) Ratio of power recorded during light stimulation to that recorded before the stimulation (20 Hz, 10 sec for 4 h with pulses 10 msec) for the different frequency bands (delta, theta, gamma) of LFP (D,G,J) and EEG (E,H,K) in VGLUT2- NpHR3 -EYFP (n = 4) and control VGLUT2 -EYFP (n = 4) mouse groups during WK, SWS and PS. No effect of the stimulation was observed on the LFP and EEG in all vigilance states as well as on the animal behavior. In particular, light stimulation during SWS (F) and PS (I) did not induce significant awakening in most VGLUT2- NpHR3 -EYFP mice as compared to that observed in control VGLUT2-EYFP mice.

Effect of optogenetic activation of SumL axon terminals innervating dDG on cFos expression

Mouse brains were processed for immunohistochemical detection of cFos in order to assess the effect of SuML axon terminal activation on DG cell activity. Whereas only a few neurons were labeled for cFos in the GCL of the DG in control VGLUT2-EYFP mice (n= 4) (Figure 9 A, B), numerous neurons strongly labeled for cFos were observed in the granule cell layer of the dDG in VGLUT2-ChR2 mice (n= 4) (Figure 9 C, D). Quantitative analysis showed a 241% increase in the number of labeled cFos neurons in the dDG ipsilateral to the stimulation site (270 $\pm$ 33) as compared to control mice (ipsi: 79 $\pm$ 23; p= 0.026; Figure 9 E) whereas no significant difference was observed in the contralateral dDG (VGLUT2-ChR2: 178 $\pm$ 21; VGLUT2-EYFP contra: 90 $\pm$ 33; p=0.2; Figure 9 E).

Light stimulation of SuML axon terminals innervating the dDG was also performed in VGLUT2-NpHR3 (n=4) and VGLUT2-EYFP control (n=3) mice. No significant difference in number of cFos labeled neurons was observed between VGLUT2-NpHR3 (ipsi: 47 $\pm$ 11; contra: 52 $\pm$ 12) and VGLUT2-EYFP control mice (ipsi: 53 $\pm$ 16; contra: 42 $\pm$ 12; p= 0.5; Figure 9 H-K).

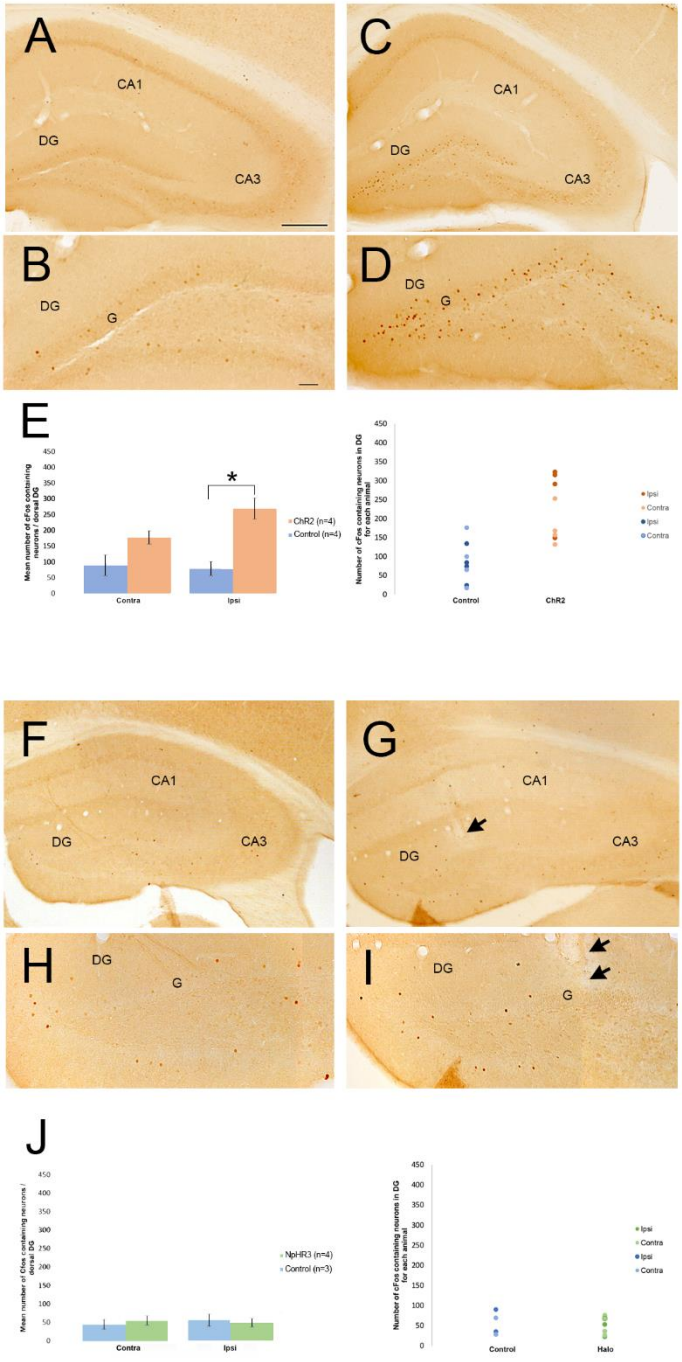

Fig. 9. Activity of DG cells after light stimulation of axon terminals from SuML neurons innervating the DG in VGLUT2-ChR2-EYFP, VGLUT2-EYFP and VGLUT2-NpHR3-EYFP as reflected by cFos immunohistochemical labeling.

(A, B, C, D, F, G, H, I) Immunohistochemical labeling for cFos on sections of control VGLUT-EYFP (A, B, F, H), VGLUT2-ChR2-EYFP (C, D) and VGLUT2- NpHR3-EYFP (G, I) mice. In control mice (A, B, F, H) only very few neurons labeled for cFos were observed in the hippocampus. There were scattered in all layers of the hippocampus including CA1, CA3 and the DG. In addition, these neurons were lightly labeled for cFos including in the granule cell layer (G) of the DG. In contrast, in VGLUT2-ChR2-EYFP mice, many c-Fos containing neurons were located in the granule cells layer (G) of the DG whereas only a few were observed within the CA3 and CA1 regions of the hippocampus. In the granule cell layer these neurons were highly labeled for cFos (D) as compared to those observed in control mice (B, H). (E) quantitative analysis confirmed a clear increase number of cFos-containing neurons in the granule cell layer of the DG stimulated (ipsi) as well as in the contralateral DG (contra) in VGLUT2-ChR2-EYFP mice (n=4) as compared to control mice (n=4). Mann Whitney test, * P< 0.05%; **P < 0.001%. (G, I) the pattern of cFos labeling neurons in VGLUT2- NpHR3-EYFP was similar to that in control VGLUT2-EYFP mice (F, H) with only very few labeled neurons observed throughout the entire hippocampus including in the granule cell layer below the optrode (arrows in G and I indicate the trace of the optrode). (J) Quantitative analysis confirmed no significant difference in the number of cFos containing neurons within the granule cell layer of the DG between VGLUT2-NpHR3-EYFP (n=3) and control mice (n=3).

Discussion

Neuroanatomical and "in vitro" experiments showing the dual glutamate-GABA feature of the SuML-DG pathway

Our results first establish at the neuroanatomical level that in mice as in rats (Soussi et al., 2010), all SuM neurons innervating the dDG display a dual GABAergic and glutamatergic neurotransmitter phenotype. We further demonstrate that these neurons correspond to a population of SuM cells located just dorsal to the mammillary tract that likely correspond to grandicellular neurons described in rat within the SuML region (Paxinos and Watson 1998) or SuMg (Pan and McNaughton 2004). In addition, our EM data show that SuML terminals form asymmetric (presumed excitatory) synapses onto some GCs and symmetric (presumed inhibitory) synapses onto others as previously described in rat (Boulland et al., 2009; Soussi et al., 2010). We further found in this study that one axon bouton from a SuML neuron can form an asymmetric (glutamate-preferring) synapse on a GC and a symmetric (GABA-preferring) synapse on another GC. In agreement with these neuroanatomical results, our *in vitro* electrophysiological experiments show that optical stimulation of SuM axon terminals innervating the dDG induce co-release of GABA and glutamate on almost all dentate GCs in line with two recent studies (Pedersen et al 2017; Hashimotodani et al., 2018). Hashimotodani et al. (2018) further showed that such co-transmission of GABA and glutamate induce net excitatory effects on GCs and potentiate GC firing when temporally associated with perforant path inputs. In line with such hypothesis, after *in vivo* optic stimulation of SuML axon terminals innervating the dDG in VGLUT2-ChR2 mice, we found that a significant number but not all GCs neurons below the optic fiber were labeled with cFos. Therefore, these cFos labeled GCs could constitute a population of GCs that are simultaneously activated by the optic stimulation of SuML axon terminals and perforant path inputs.

Effect of optogenetic stimulation of SuML-DG fibers on vigilance states

Activation of SuML axon terminals projecting to the DG induces an awakening effect in mice when performed during SWS but not during PS. It has been shown by Renouard et al. (2015)

that the SuML-DG pathway is active during PS and therefore its stimulation during PS might not induce WK because this pathway is already engaged and its overactivation might therefore not to be sufficient to awaken the animal. In contrast, when the stimulation occurs during SWS, an awakening is induced likely because the path is normally inactive during this state. It can be proposed that the stimulation of the DG granule cells by the SuML induces the reactivation of memories and subsequently of structures involved in the exploration leading to an awakening of the animal during SWS. It might be due also to the fact that there is no muscle atonia during this state compared to PS. In line with such hypothesis, stimulation during WK induces increased motor and exploratory activity. Such result is in line with the literature since an increase in exploratory activity was reported when stimulating with blue light dDG neurons expressing ChR2 (Kheirbek et al., 2013).

Optogenetic stimulation of SuML-DG fibers increases gamma and theta

Our study further demonstrates that activation of SuML axon terminals innervating the DG during PS increases theta power and frequency as well as gamma power in the DG LFP and to a minor extent in the EEG. Activation of the SuML fibers during WK also induces an increase of gamma power in the DG LFP and EEG associated with an increased locomotion. During SWS, the activation of the SuML-dDG pathway induced awakening and a switch from delta to theta activity and an increase in gamma power both in DG LFP and EEG.

It has been previously shown that the SuM can exert significant modulatory control of the theta rhythm (Vertes and Kocsis, 1997). A large percentage of SuM neurons discharge rhythmically, in phase with theta (Kirk and McNaughton, 1991, Kocsis and Vertes, 1994) and this activity is independent of that occurring in the hippocampus. Indeed, neurons in the SuM continue to fire bursts in the theta range frequency after lesion or pharmacological inactivation of the medial septum (Kirk and McNaughton, 1991) known to abolish theta rhythmic activity in the hippocampus. Further, electrical stimulation or carbachol injections in the SuM synchronously drive theta phase-locked cells in both septum (Bland et al., 1994) and hippocampus (Colom et al., 1987). In addition, the SuM controls the frequency and amplitude of theta (Kirk and

McNaughton, 1993). These results indicated that the SuM plays a role in theta occurrence but experiments were performed in anesthetized animals and did not specifically study the SuML-DG pathway like in the present study. Indeed, SuM neurons also project directly to the medial septum (Vertes and McKenna, 2000) and can influence theta through the latter structure as well.

Our results also show that the frequency at the peak of theta is higher during PS than in WK in basal conditions. Further, we found out that optical stimulation of SuML-DG fibers during PS and WK induced a similar increase of the frequency at the peak of theta. However, no effect on theta was observed after inactivation of the fibers by halorhodopsin. It is likely that it is due to the fact that the inactivation was restricted to a small portion of the fibers located beneath the optic fiber. Indeed, lesion of the SuM induced a decreased of theta power specifically during PS (Renouard et al., 2015). On the other hand, lesion of all neurons or specific inactivation of the GABAergic neurons of the medial septum strongly decreases theta during PS and WK (Mitchell et al., 1982, Green and Arduini, 1954, Boyce et al., 2016). Our data also show that stimulation of the SuML-DG fibers induces an increase in gamma power in the dDG and also in the EEG both during PS and WK. Interestingly, Montgomery et al. (2008) found by coherence analysis that dentate/CA3 theta and gamma power and synchrony was significantly higher during PS compared with active WK and that, in contrast, gamma power in CA1 and CA3-CA1 gamma coherence showed significant decreases during PS. These and our results strongly suggest that the medial septum GABAergic neurons induces theta both during WK and PS whereas the increase of theta and gamma power and theta frequency occurring in the DG during PS compared to WK is induced by the projection from the SumL.

Functional role of the SumL-DG pathway

It has been previously shown that GCs of the DG are instrumental for spatial discrimination (McHugh et al., 2007). In particular, it has been shown that small populations of GCs (2-4%) representing memory engrams are specifically activated when the animals are exposed to a specific context. These cells are reactivated each time the animal is re-exposed to the same

context (Schmidt et al., 2012). Optogenetic activation in a different context of a DG engram activated during contextual fear conditioning induces freezing (Liu et al., 2012). Conversely, inactivation during contextual fear memory recall of the DG GCs activated during encoding decreases freezing (Denny et al., 2014). These results indicate that activation of memory engrams composed of DG GCs cells is necessary for spatial learning. Interestingly, in these studies, the mean number of neurons labeled with cFos or Arc in one section (35 µm) of the DG after contextual fear conditioning was in the 30-60 range. During stimulation of the SuML fibers in the DG, a mean of 67 DG cells were expressing cFos in the DG per section (40 µm). Finally, Renouard et al. (2015) counted a mean of 68 Arc- and 66 cFos- labeled neurons in one DG section after PS hypersomnia in rats. Therefore, approximatively the same number of DG GCs cells is activated during encoding of a contextual fear memory, stimulation of the SuML fibers in the DG and PS hypersomnia. First, the fact that a similar number of cells are activated when stimulating SuML terminals as during PS hypersomnia suggests that the activation seen during PS is likely due to activation of the SuML-DG pathway. Second, the fact that the a similar number of cells are activated during a memory task as during PS hypersomnia and stimulation of the SuML fibers suggest that memory engrams could be activated in these two conditions. Therefore, the induction of an active behavior when the stimulation is made during WK could be due to the activation of memory engrams. Since only a limited number of GCs cells are activated during PS and SuML terminals stimulation despite the fact that a large number of GCs neurons seems to be innervated by SuML axon terminals, it also suggests that activation of these cells is due to a conjunction of the SuML input with another excitatory input. It can be proposed that the medial entorhinal input is involved since it is the main excitatory afferent to the DG involved in its activation during memory encoding (Sasaki et al., 2015). Such hypothesis remains to be tested using optogenetic manipulation of the activated neurons during PS.

References

Billwiller F, Renouard L, Clement O, Fort P, Luppi PH (2017) Differential origin of the activation of dorsal and ventral dentate gyrus granule cells during paradoxical (REM) sleep in the rat. Brain Struct Funct 222:1495-1507.

Bland BH, Oddie SD, Colom LV, Vertes RP (1994) Extrinsic modulation of medial septal cell discharges by the ascending brainstem hippocampal synchronizing pathway. Hippocampus 4:649-60.

Bolte S, Cordelières FP (2006) A guided tour into subcellular colocalization analysis in light microscopy. J Microsc 224:213-232.

Borhegyi Z, Leranth C (1997) Distinct substance P- and calretinin-containing projections from the supramammillary area to the hippocampus in rats; a species difference between rats and monkeys. Exp Brain Res 115:369-374.

Boulland JL, Jenstad M, Boekel AJ, Wouterlood FG, Edwards RH, Storm-Mathisen J, Chaudhry FA (2009) Vesicular Glutamate and GABA Transporters Sort to Distinct Sets of Vesicles in a Population of Presynaptic Terminals. Cereb Cortex 19:241-248.

Boyce R, Glasgow SD, Williams S, Adamantidis A (2016) Causal evidence for the role of REM sleep theta rhythm in contextual memory consolidation. Science 352:812-816.

Bras H, Gaytán SP, Portalier P, Zanella S, Pásaro R, Coulon P, Hilaire G (2008) Prenatal activation of 5-HT 2A receptor induces expression of 5-HT 1B receptor in phrenic motoneurons and alters the organization of their premotor network in newborn mice. Eur J Neurosci 28:1097-1107.

Colom LV, Ford RD, Bland BH (1987) Hippocampal formation neurons code the level of activation of the cholinergic septohippocampal pathway. Brain Res 410:12-20.

Coulon P, Bras H, Vinay L (2011) Characterization of last-order premotor interneurons by transneuronal tracing with rabies virus in the neonatal mouse spinal cord. J Comp Neurol 519:3470-3487.

Denny CA, Kheirbek MA, Alba EL, Tanaka KF, Brachman RA, Laughman KB, Tomm NK, Turi GF, Losonczy A, Hen R (2014) Hippocampal memory traces are differentially modulated by experience, time, and adult neurogenesis. Neuron 83: 189-201.

Gonzalo-Ruiz A, Alonso A, Sanz JM, Llinás RR (1992) Afferent projections to the mammillary complex of the rat, with special reference to those from surrounding hypothalamic regions. J Comp Neurol 321:277-299.

Green JD, Arduini AA (1954) Hippocampal electrical activity in arousal. J Neurophysiol 17:533-57.

Haglund L, Swanson LW, Köhler C (1984) The projection of the supramammillary nucleus to the hippocampal formation: An immunohistochemical and anterograde transport study with the lectin PHA-L in the rat. J Comp Neurol 229:171-185.

Hashimotodani Y, Karube F, Yanagawa Y, Fujiyama F, Kano M (2018) Supramammillary Nucleus Afferents to the Dentate Gyrus Co-release Glutamate and GABA and Potentiate Granule Cell Output. Cell Rep 25:2704-2715

Kheirbek MA, Drew LJ, Burghardt NS, Costantini DO, Tannenholz L, Ahmari SE, Zeng H,

Fenton AA, Hen R (2013) Differential control of learning and anxiety along the dorsoventral axis of the dentate gyrus. Neuron 77:955-968.

Kirk IJ, McNaughton N (1991) Supramammillary cell firing and hippocampal rhythmical slow activity. Neuroreport 2:723-5.

Kirk IJ, McNaughton N (1993) Mapping the differential effects of procaine on frequency and amplitude of reticularly elicited hippocampal rhythmical slow activity. Hippocampus 3:517-25.

Kocsis B, Kaminski M (2006) Dynamic changes in the direction of the theta rhythmic drive between supramammillary nucleus and the septohippocampal system. Hippocampus 16:531-540.

Kocsis B, Vertes RP (1994) Characterization of neurons of the supramammillary nucleus and mammillary body that discharge rhythmically with the hippocampal theta rhythm in the rat. J Neurosci 14:7040-7052.

Kocsis K, Kiss J, Csáki A, Halász B (2003) Location of putative glutamatergic neurons projecting to the medial preoptic area of the rat hypothalamus. Brain Res Bull 61:459-468.

Leranth C, Kiss J (1996) A population of supramammillary area calretinin neurons terminating on medial septal area cholinergic and lateral septal area calbindin-containing cells are aspartate/glutamatergic. J Neurosci 16:7699-7710.

Liu X, Ramirez S, Pang PT, Puryear CB, Govindarajan A, Deisseroth K, Tonegawa S (2012) Optogenetic stimulation of a hippocampal engram activates fear memory recall. Nature 484:381-385.

Maglóczky Z, Acsády L, Freund TF (1994) Principal cells are the postsynaptic targets of supramammillary afferents in the hippocampus of the rat. Hippocampus 4:322-334.

Maquet P, Laureys S, Peigneux P, Fuchs S, Petiau C, Phillips C, Aerts J, Del Fiore G, Degueldre C, Meulemans T, Luxen A, Franck G, Van Der Linden M, Smith C, Cleeremans A (2000) Experience-dependent changes in cerebral activation during human REM sleep. Nat Neurosci 3:831-836.

McHugh TJ, Jones MW, Quinn JJ, Balthasar N, Coppari R, Elmquist JK, Lowell BB, Fanselow MS, Wilson MA, Tonegawa S (2007) Dentate gyrus NMDA receptors mediate rapid pattern separation in the hippocampal network. Science 317:94-99.

Mitchell SJ, Rawlins JN, Steward O, Olton DS.(1982) Medial septal area lesions disrupt theta rhythm and cholinergic staining in medial entorhinal cortex and produce impaired radial arm maze behavior in rats. J Neurosci 2:292-302

Montgomery SM, Sirota A, Buzsáki G (2008) Theta and gamma coordination of hippocampal networks during waking and rapid eye movement sleep. J Neurosci 28:6731-41.

Nitsch R, Leranth C (1996) GABAergic neurons in the rat dentate gyrus are innervated by subcortical calretinin-containing afferents. J Comp Neurol 364:425-438.

Pan WX, McNaughton N (2002) The role of the medial supramammillary nucleus in the control of hippocampal theta activity and behaviour in rats. Eur J Neurosci 16:1797-1809.

Pan WX, McNaughton N (2004) The supramammillary area: its organization, functions and

relationship to the hippocampus. Prog Neurobiol 74:127-166.

Pasquier DA, Reinoso-Suarez F (1976) Direct projections from hypothalamus to hippocampus in the rat demonstrated by retrograde transport of horseradish peroxidase. Brain Res 108:165-169.

Pasquier DA, Reinoso-Suarez F (1978) The topographic organization of hypothalamic and brain stem projections to the hippocampus. Brain Res Bull 3:373-389.

Paxinos G, Franklin KB (2005) The Mouse Brain in Stereotaxic Coordinates - 5th Edition. Academic Press, San Diego.

Paxinos G, Watson, C (1998) The Rat Brain in Stereotaxic Coordinates, Academic Press, Sydney.

Pedersen NP, Ferrari L, Venner A, Wang JL, Abbott SBG, Vujovic N, Arrigoni E, Saper CB, Fuller PM (2017) Supramammillary glutamate neurons are a key node of the arousal system. Nat Commun 8:1405.

Persson S, Boulland JL, Aspling M, Larsson M, Fremeau RT Jr, Edwards RH, Storm-Mathisen J, Chaudhry FA, Broman J (2006) Distribution of vesicular glutamate transporters 1 and 2 in the rat spinal cord, with a note on the spinocervical tract. J Comp Neurol 497:683-701.

Raux H, Iseni F, Lafay F, Blondel D (1997) Mapping of monoclonal antibody epitopes of the rabies virus P protein. J Gen Virol 78:119-124.

Renouard L, Billwiller F, Ogawa K, Clément O, Camargo N, Abdelkarim M, Gay N, Scoté-Blachon C, Touré R, Libourel PA, Ravassard P, Salvert D, Peyron C, Claustrat B, Léger L, Salin P, Malleret G, Fort P, Luppi PH (2015) The supramammillary nucleus and the claustrum activate the cortex during REM sleep Sci Adv 1: *e1400177*.

Richmond MA, Yee BK, Pouzet B, Veenman L, Rawlins JN, Feldon J, Bannerman DM (1999) Dissociating context and space within the hippocampus: effects of complete, dorsal, and ventral excitotoxic hippocampal lesions on conditioned freezing and spatial learning. Behav Neurosci 113:1189-1203.

Santín LJ, Aguirre JA, Rubio S, Begega A, Miranda R, Arias JL (2003) c-Fos expression in supramammillary and medial mammillary nuclei following spatial reference and working memory tasks. Physiol Behav 78:733-739.

Saper CB (1985) Organization of cerebral cortical afferent systems in the rat. II. Hypothalamocortical projections. J Comp Neurol 237:21-46.

Sapin E, Lapray D, Bérod A, Goutagny R, Léger L, Ravassard P, Clément O, Hanriot L, Fort P, Luppi PH (2009) Localization of the brainstem GABAergic neurons controlling paradoxical (REM) sleep. PLoS One 4:e4272

Sasaki T, Leutgeb S, Leutgeb JK (2015) Spatial and memory circuits in the medial entorhinal cortex. Curr Opin Neurobiol 32:16-23

Schmidt B, Marrone DF, Markus EJ (2012) Disambiguating the similar: the dentate gyrus and pattern separation. Behav Brain Res 226:56-65.

Segal M, Landis S (1974) Afferents to the hippocampus of the rat studied with the method of retrograde transport of horseradish peroxidase. *Brain Res* 78:1-15.

Shahidi S, Motamedi F, Naghdi N (2004) Effect of reversible inactivation of the supramammillary nucleus on spatial learning and memory in rats. Brain Res 1026: 267-274.

Soussi R, Boulland JL, Bassot E, Bras H, Coulon P, Chaudhry FA, Storm-Mathisen J, Ferhat L, Esclapez M (2015) Reorganization of supramammillary–hippocampal pathways in the rat pilocarpine model of temporal lobe epilepsy: evidence for axon terminal sprouting. Brain Struct Funct 220: 2449-2468.

Soussi R, Zhang N, Tahtakran S, Houser CR, Esclapez M (2010) Heterogeneity of the supramammillary-hippocampal pathways: evidence for a unique GABAergic neurotransmitter phenotype and regional differences: GABAergic and glutamatergic supramammillary-hippocampal pathways. Eur J Neurosci 32:771-785.

.Swanson LW (1982) The projections of the ventral tegmental area and adjacent regions: a combined fluorescent retrograde tracer and immunofluorescence study in the rat. Brain Res Bull 9:321-353.

Swanson LW (1998) Brain Maps: Structure of the Rat Brain. Elsevier, Amsterdam

Ugolini G (2010) Advances in viral transneuronal tracing. J Neurosc Methods 194:2-20.

Vertes RP (1992) PHA-L analysis of projections from the supramammillary nucleus in the rat. *J Comp Neurol* 326:595-622.

Vertes RP (2015) Major diencephalic inputs to the hippocampus. *Prog Brain Res* 121:144.

Vertes RP, Kocsis B (1997) Brainstem-diencephalo-septohippocampal systems controlling the theta rhythm of the hippocampus. Neuroscience 81:893-926.

Vertes RP, McKenna JT (2000) Collateral projections from the supramammillary nucleus to the medial septum and hippocampus. Synapse 38:281-293.

Wyss JM, Swanson LW, Cowan WM (1979) A study of subcortical afferents to the hippocampal formation in the rat. Neuroscience 4:463-476.

Zhang N, Houser CR (1999) Ultrastructural localization of dynorphin in the dentate gyrus in human temporal lobe epilepsy: a study of reorganized mossy fiber synapses. J Comp Neurol 405:472-490.

SECOND STUDY

Two populations of neurons from the lateral supramammillary nucleus innervate the dorsal dentate gyrus: both display a dual glutamatergic and GABAergic neurotransmittion phenotype but differ by their Calretinin content and rostro-caudal distribution.

Title:

Two populations of neurons from the lateral supramammillary nucleus innervate the dorsal dentate gyrus: both display a dual glutamatergic and GABAergic neurotransmittion phenotype but differ by their Calretinin content and rostro-caudal distribution.

Abbreviated title:

Heba Elseedy [1,2], Jennyfer Scapula[1], Antoine. Ghestem[1], Hélène. Bras[3], Sherine Abdel. Salam[2], Nabila El Sayed Abdelmeguid[2], Monique Esclapez[1@]

1-Aix Marseille Univ, INSERM, INS, Institut de Neurosciences des Système, Marseille, France
2-Alexandria University, Faculty of Science, Zoology Department, Alexandria Egypt
3-Aix Marseille Univ, CNRS, INT, Inst Neurosci Timone, Marseille, France

Corresponding author: Dr. Monique Esclapez
Institut de Neurosciences des Systèmes - INS
UMR 1106 INSERM - Aix-Marseille Université,
Faculté de Médecine Timone,
27 Boulevard Jean Moulin
13385 Marseille Cedex 05, France
@ monique.esclapez@univ-amu.fr

Abstract

The lateral supramammillary nucleus (SuML) is the main sub-cortical region sending substantial projections to the dentate gyrus (DG). Several studies have provided evidence that this hypothalamic nucleus could play a crucial in the control of several hippocampal-dependent activities and associated functions, including theta rhythms, REM sleep as well as emotional learning and memory. However, the anatomical and physiological substrate by which such control occurs is not clearly understood.

Previous studies have demonstrated in rat (Soussi et al., 2010) and mouse (Billwiller et al., 2019) that the neurons from the lateral region of the SuM (SuML) innervating the dorsal DG display a unique dual phenotype. Their axon terminals co-express markers for both glutamatergic (vesicular glutamate transporter 2; VGLUT2) and GABAergic (glutamate decarboxylase 65, GAD65 and the vesicular GABA transporter, VGAT) neurotransmission and establish asymmetric (excitatory) and symmetric (inhibitory) synapses on DG cells. We further demonstrated using in vitro optogenetic experimental approach performed in transgenic mouse that these SuML axon terminals indeed co-release monosynaptically Glutamate (Glu) and GABA in granule cells and Paralbumin-containing interneurones of the DG. However, it is still unclear whether or not these neurons form a heterogeneous population.

In this study, we examined the potential heterogeneity of the SuML neuronal population innervating the dorsal DG by coupling tracing methods with rabies virus, RNAscope fluorescent in situ hybridization technology for detection of VGLUT2 and VGAT mRNAs and immunohistofluorescence for detection of calretinin, VGLUT2 and VGAT in mouse. We demonstrate that the population of SuML neurons expressing both VGLUT2 and VGAT is heterogeneous. Among these GABA/GLU SuML neurons projecting to the dorsal DG, 64% contain calretinin whereas 36% do not. This subpopulation of

GABA/GLU SuML neurons containing calretinin is more numerous in the anterior region than in the posterior region of the SUML, representing respectively 92% and 28% of the GABA/GLU SUML neurons. Both subpopulations of GABA/GLU SuML (GABA/GLU/CR+ and GABA/GLU/CR) innervate the cell body and dendrites of granule cells as well as Parvalbumin interneurones of the DG. These two populations of SUML neurons innervating the DG could display different electrophysiological properties and play different roles in the control of DG activity and functions.

Introduction

The supramammillary nucleus (SuM) is a hypothalamus area that provides projections to many regions of the limbic system including the hippocampal formation (Pan & McNaughton, 2004a; Vertes, 2015). This region is composed of a heterogeneous population of neurons that differ by their neurochemical content and the specificity of their connections (Swanson, 1982; Haglund *et al.*, 1984a; Carnes *et al.*, 1990; Gonzalo-Ruiz *et al.*, 1992b; Leranth & Nitsch, 1994; Leranth & Kiss, 1996b; Borhegyi & Leranth, 1997; Kocsis *et al.*, 2003). Among this heterogenous population of neurons several studies have described the distribution and projections of SuM calretinin neurons (Leranth & Kiss, 1996a; Kocsis *et al.*, 2003). In rat, it was shown that these calretinin containing neurons that are mainly located in the lateral two-thirds of the SUM (SuML,(Paxinos and Watson, 1998)) also referred as grandicellular SuM region (SuMg) by Pan and McNaughton (2004) innervate the medial and lateral part of the septum (Leranth & Kiss, 1996b) as well as the inner molecular layer of the dentate gyrus (DG) (Maglóczky et al., 1994; Kiss et al., 2000). Several authors consider these SuM calretinin neurons innervating the DG as glutamatergic (excitatory) neurons. This is based on studies showing that: (i) some afferents from the SuM form asymmetric synapses (Dent et al., 1983; Stanfield and Maxwell Cowan, 1984; Maglóczky et al., 1994),considered to be a feature of excitatory synapses, and (ii) SuM neurons and associated axon terminals that innervate the inner molecular layer of the DG and the CA2 pyramidal layer containing calretinin lack the synthesizing enzyme of GABA, the glutamic acid decarboxylase (GAD).

However it has been shown more recently, that almost all SuML neurons, known to innervate the supragranular layer of the DG throughout the dorsal and ventral hippocampus(Wyss *et al.*, 1979b; Haglund *et al.*, 1984a; Saper, 1984; Vertes, 1992; Vertes & McKenna, 2000; Soussi *et al.*, 2010), display a unique dual neurotransmitter phenotype being both glutamatergic and GABAergic (Boulland *et al.*, 2009; Soussi *et al.*, 2010). Indeed, almost all these SuML neurons and their axon terminals innervating the DG co-express markers for both glutamatergic (vesicular glutamate transporter 2; VGLUT2) and GABAergic (glutamatic acid decarboxylase 65, GAD65 one of the synthesizing of GABA and the vesicular GABA transporter, VGAT)

neurotransmission and establish asymmetric and symmetric synapses on DG cells (Soussi *et al.*, 2010). Furthermore recent studies confirmed these results in transgenic in mice at the neuroanatomical (Billwiller et al., 2019) and physiological(Pedersen et al., 2017; Hashimotodani et al., 2018; Billwiller et al., 2019) levels. They demonstrate that these neurons can indeed co-release GABA and Glutamate on DG granule cells(Pedersen et al., 2017; Hashimotodani et al., 2018; Billwiller et al., 2019) as well as on a subpopulation of DG GABAergic interneurons (Hashimotodani et al., 2018) likely corresponding to Parvalbumin (PV)-containing interneurons as previously suggested in rat(Nitsch & Leranth, 1996b).

Therefore, one of the question that still have to be determine is whether SuML calretinin-containing neurons represent a distinct or a subpopulation of these GABA/GLU SUML neurons innervating the DG. Do these GABA/GLU SuML neurons projecting to the dorsal DG form a heterogenous population of neurons? Such information is crucial knowing that the SuML-DG pathway has been suggested to contribute to several functions such as exploration of a novel environment and spatial learning(Wirtshafter et al., 1998; Santín et al., 2003; Ito et al., 2009) as well as REM sleep (Renouard et al., 2015; Billwiller et al., 2019) through regulation of several DG activity such as theta and gamma rhythms(Renouard et al., 2015; Billwiller et al., 2019). Do all these functions involve a unique and homogenous population or different populations of SuML-DG neurons is still unclear.

The aims of this study was to determine whether 1) calretinin-containing neurons and GABA/GLU-containing neurons innervating the dorsal DG forms or not distinct populations of SuML-DG neurons. 2) the GABA/GLU SuML neurons projecting to the dorsal DG form a heterogenous population of neurons regarding their content or not in calretinin. 3) These different populations of SuML-DG neurons target specific neurons in the DG including granule cells and PV interneurons. For this purpose we combined structural connectivity techniques using neurotropic viral vectors (rabies virus, AAV-EYFP) with neurochemical anatomy (immunohistochemistry, RNAscope in situ hybridization) and imaging at light and confocal microscopy levels.

Materials and Methods

Animals

In this study, we used 10 transgenic “VGLUT2-cre” adult mice (25-30 g ; aged 12-14 weeks) obtained by mating male and female homozygote Vglut2-ires-Cre mice (Strain name Slc17a6$^{tm2(cre)Lowl}$/J, stock #016963, from Jackson Laboratories). All mice were bred in-house and maintained in standard cages, with food and water ad libitum, in a temperature- and humidity-controlled room under a 12 hr light dark cycle. All the surgical and experimental procedures were performed according to the European communities Council Directive of 86/609/EEC and were approved by the University of Aix-Marseille Chancellor's Animal Research Committees.

Surgery for neuronal viral vector tracer injection

Mice were anesthetized by an intraperitoneal (i.p) injection of Ketamin (50mg/kg) / Xylazine (5mg/kg) solution. They were then secured in the stereotaxic frame (David Kopf instruments, Tujunga, CA). When necessary, ketamine injection was repeated during the surgery. The body temperature of the animal was controlled and maintained at 37 °C during the entire surgical procedure by means of an anal probe and a homoeothermic blanket. The head was shaved, sanitized with a 4% Betadine solution following by a 0.9% sodium chloride and 10% betadine solutions. Local anesthesia was performed by infiltration of the scalp with xylocaine (10 mg／kg). An ophthalmic gel was placed on the eyes to avoid dehydration. After scalp incision, holes were drilled in the skull at the antero-posterior and medio-lateral coordinates of the DG (for retrograde tracer injection) or the SuML (for anterograde tracer injection based on (Paxinos and Franklin, 2004)

Rabies virus (RV) retrograde tracer injection in the DG

Seven mice were injected unilaterally with 200 nl of RV (strain Challenge Virus Standard, 4.10^7 plaque-forming units/ml; (Bras *et al.*, 2008b; Coulon *et al.*, 2011b) in the molecular layer of the DG according to the following coordinates (AP = -2; LM = + 1.25; DV = -1.8). After surgery, animals were returned to their home cages for a survival period of 28, 30, or 42 hrs in order to

obtain golgi like retrograde-labeling of SuM neurons projecting to the DG. Only vaccinated persons conducted these experiments at the appropriate biosafety containment level until the sacrifice of the animals.

Anterograde viral vector injection in SuML (Associated AdenoVirus (AAV) Double floxed Inverted ORF (DIO))

Three mice were injected bilaterally with 1µl of cre-dependent viral vectors: AAV5-EF1a-DIO-EYFP (8.4 10^{12} copies / ml; UNC Gene Therapy Center Vector Core; Dr Deisseroth) into the SuML region, at the following coordinates (AP = -2.7; LM = + / - 1.25; DV = -4.8 with an 11°angle). The viral vector injections were performed using a micro-pump associated with an Hamilton syringe at a rate of 200 nl / minute. The animals were returned to their home cages for a survival period of 3 weeks to allow optimal anterograde labelling of axon fibers and terminals from SuML neurons. These mice will be referred as VGLUT2-EYFP mice.

Tissue preparation for In situ hybridization and immunohistochemical experiments

Animals were deeply anesthetized with ketamine/ xylazine solution and transcardially perfused with 100 ml of 4% paraformaldehyde (PFA) prepared in 0.12 M sodium phosphate buffer, pH 7.2 - 7.4 (PB). After perfusion, the brains were removed from the skull, post-fixed in the same fixative for 1 h at room temperature (RT) and rinsed in PB cryoprotected in a solution of 20% sucrose in PB overnight at 4°C, quickly frozen on dry ice and sectioned coronally at 40µm with a cryostat. The sections were rinsed in PB, collected sequentially in tubes containing an ethylene glycol-based cryoprotective solution and stored at -20°C until histological processing. To determine the general histological characteristics of the tissue along the rostro-caudal axis of the brain every 10 sections was stained with cresyl violet. Selected sections were processed for 1) detection of the RV; 2) Simultaneous detection of VGLUT2 mRNA, VGAT mRNA and RV or CR; 3) Simultaneous detection of VGAT mRNA, CR and RV; 4) Simultaneous detection for EYFP, CR and PARV

Detection of rabies virus retrograde tracer.

Free floating sections at the level of the DG were processed for immunohistochemistry using the Mouse On Mouse detection kit (MOM, Vector Laboratory) to eliminate nonspecific labelling due to use of mouse monoclonal antibody on mouse tissue according to the manufactory 's recommendations. Sections were first pre-treated for 30 min in 1 % H2O2, rinsed in PB and 0.02 M potassium phosphate-buffered saline (KPBS, pH 7.2-7.4). They were then incubated for 1 h at RT in MOM mouse IgG blocking reagent diluted in KPBS containing 0.3% Triton X-100. They were rinsed twice with KPBS for 5 min and pre-incubated in MOM diluent for 15 min. Sections were then incubated overnight at RT in a solution containing the mouse monoclonal antibody directed against RV (1: 5000; (Iseni et al., 1997) Kindling provided By Dr. Patrice Coulon, INT, Marseille), diluted in MOM diluent. After several rinses in KPBS, sections were incubated for 1 h at RT with biotinylated anti-mouse IgG M.O.M reagent secondary antibody (1:200) diluted in M.O.M diluent solution and then for 1 h at RT in Vectastain Elite ABC diluted 1:100 in KPBS. Sections were processed for 10 min in 3.3'-diaminobenzidine tetrahydrochloride (DAB), rinsed in KPBS, mounted onto Superfrost Plus slides, dehydrated and coverslipped with Permount.

***Simultaneous detection of VGLUT2 mRNA, VGAT mRNA and RV or CR combining fluorescent in situ hybridization (RNAscope technology) and immonhistofluorescent methods*.**

Free floating sections at the level of the SuM were first treated with 1% H2O2 rinsed in PB for 10 min, mounted on SuperFrost Plus slides (Fisher Scientific) and air dried at RT. They were then process for fluorescent RNAscope in situ hybridization (ISH) according to the manufactory's protocol (Advanced Cell Diagnostics). Briefly sections were treated with 100% ethanol and protease III for 30 min at 40°C. They were incubated in a solution containing both RNAscope® Probe - Mm-S1c17a6 (catalog #319171) for detection of VGLUT2 mRNA and Mm-S1c32a1-C3 (catalog #319191-C3) for detection of VGAT mRNA. After hybridization, sections were then processed for visualization using the RNA-scope Multiplex Fluorescent reagent Kit v2

(Advanced Cell Diagnostics) and the Tyramide Signal Amplification (TSA™) Plus Cyanine 3 and TSA Plus Cyanine 5 systems (Perkin Elmer).

After the RNAscope assay, all sections were rinsed in KPBS. Some sections were then processed for immunohistofluorescent detection of the RV using the M.O.M detection kit as described above. After several rinses in KPBS, sections were incubated in MOM mouse IgG blocking reagent pre-incubated in MOM diluent for 15 min, incubated overnight at RT in the mouse monoclonal antibody directed against RV (1: 3000). After several rinses in KPBS, they were incubated for 2h in Alexa488-conjugated donkey anti-mouse (1:200; Invitrogen) diluted in MOM diluent.

Another set of sections was processed for immunohistofluorescent detection of CR. These sections were incubated overnight in rabbit polyclonal antiserum directed against CR (1:3000; Swant) diluted in KPBS containing 1% normal donkey serum (NDS). After several rinses in KPBS sections were incubated for 1h at RT in Alexa488-conjugated donkey anti-rabbit (1:200; Invitrogen) diluted in KPBS containing 3% NDS.

All sections were then rinsed in KPBS and coverslipped with the Fluoromount mounting medium (Electron Microscopy Sciences, Hatfiled, PA, USA).

Simultaneous detection of VGAT mRNA, RV and CR

Sections at the level of the SuM were first processed for detection of VGAT mRNA using fluorescent RNAscope in situ hybridization (ISH) as described above. Briefly, after being treated with 1% H2O2 rinsed in PB, mounted on SuperFrost Plus slides (Fisher Scientific) and air dried, sections were treated with 100% ethanol and protease III for 30 min at 40°C. They were incubated in a solution containing the RNAscope® Probe Mm-S1c32a1-C3 (catalog #319191-C3) for detection of VGAT mRNA. After hybridization, sections were then processed for visualization using the RNA-scope Multiplex Fluorescent reagent Kit v2 (Advanced Cell Diagnostics) and the Tyramide Signal Amplification (TSA™) Plus Cyanine 3 systems (Perkin Elmer).

After the RNAscope assay, sections were rinsed in KPBS and processed for simultaneous

detection of RV and CR using M.OM detection kit. Sections were incubated for 1 h at RT in MOM mouse IgG blocking reagent diluted in KPBS containing 0.3% Triton X-100. They were rinsed twice in KPBS and pre-incubated in MOM diluent for 15 min. Sections were then incubated overnight at RT in a solution containing the mouse monoclonal antibody directed against RV (1 : 3000) and the rabbit polyclonal antiserum directed against CR (1: 3000) diluted in MOM diluent. After several rinses in KPBS, they were incubated for 2h in a solution containing Alexa488-conjugated donkey anti-rabbit (1: 200; Invitrogen) and CY5-conjugated donkey anti-mouse (1:100; Jackson ImmunoReseach) diluted in MOM diluent. Sections sections were coverslipped with Fluoromount.

Simultaneous immunofluorescent labelling for EYFP, PARV, and CR.

Selected free-floating sections at the level of the dorsal DG were processed using the M.OM kit as described above. After the different pre-treatment the sections were incubated overnight at RT in a solution containing a mouse monoclonal anti-GFP (1:100; Molecular Probes), rabbit polyclonal anti-CR (1:3000; Swant) and guinea pig polyclonal anti-PARV (1:3000; Swant) diluted in MOM diluent. After several rinses in KPBS, they were incubated for 2h in a solution containing Alexa488-conjugated donkey anti-mouse (1:200; Invitrogen), CY3 donkey anti-rabbit (1:100; Jackson ImmunoReseach) and, CY5 donkey anti-guinea pig (1:100; Jackson ImmunoReseach) diluted in MOM diluent. After several rinses in KPBS, all sections were then mounted on superfrost-coated slides, dried overnight at RT and coverslipped with Fluoromount.

Microscope imaging

All fluorescent-labelled sections were analyzed with a confocal microscope (Zeiss LSM 510, Institute des Neurosciences de la Timone (INT), Aix-Marseille University, France). Confocal images were obtained from either single optical slices or z-stack using the sequential acquisition of separate wavelength channels to avoid fluorescence cross-talk with objective lenses 20x, 40x or 63x at a digital resolution 2048 pixels X 2048 pixels. Montages were performed using NIH ImageJ and Adobe Photoshop CC 2015 softwares.

Quantitative analyses

Quantitative analysis was conducted to evaluate the extent of the co-localization between calretinin- and VGAT/VGLUT2 mRNAs containing-neurons in the SuM as previously described(Billwiller et al., 2019).This analysis was performed in VGLUT2-cre mice previously injected with RV. The numbers of single double and triple neurons were determined for each animal (n=3), from 3 sections (120 µm apart from each other) within the antero-posterior extent of the SuM. For each section, an image of the entire SuM region was obtained from a single confocal slice with 20x objective and sequential acquisition of the different wavelength channels using the Tile Scan function provided by the confocal microscope acquisition software (LSM 510 Zen, Zeiss). The analysis was then performed with Neurolucida software (version 7, mbfBioscience) as follow: In each confocal image all CR- labelled neurons were identified on the green channels and examined for colocalization for VGLUT2 mRNA in the blue channels and/or VGAT mRNA in the red one. Triple- double- and single labelled neurons were tagged differently and counted by the software for each section. all single, double or triple labelled cell bodies were marked by switching between the three different wavelength channels (Blue, Red and Green). Then, the relative percentages of triple-labeled neurons for Calretinin, VGAT mRNA and VGLUT-2 mRNA (CR +ve) and of double-labeled neurons for VGAT mRNA and VGLUT-2 mRNA (CR -ve) were determined at each of the three antero-posterior level of the SuM for each animal.

Results

Distribution and neurotransmitter phenotype of SuM neurons projecting to the dorsal dentate gyrus

Unilateral injection of rabies virus (RV) was performed into the molecular layer of dorsal dentate gyrus (DG) to evaluate the distribution of the neurons that project to this structure. Only mice with RV tracer successfully injected within the inner molecular layer of the DG as illustrate by the injection trace (Fig. 1A) were selected and sections at the level of SuM region processed for the simultaneous detection of VGLUT2 mRNA, VGAT mRNA and RV. All these mice displayed retrograde-labeled neurons (green) exclusively located in the region above and around the mt of SuML (Fig. 1B, green). These RV labeled neurons were more numerous in the SuML region ipsilateral to the injected DG. Few were also observed in the contralateral SuML. Virtually none were found in the SuMM (Fig. 1B). This distribution of RV-labelled neurons paralleled the distribution of large neurons expressing both VGAT and VGLUT2 mRNAs. Almost all these VGAT/VGLUT2mRNAs neurons were clustered around and above the mammillary tract (mt) (Fig. B) as previously described in mice (Billwiller et al., 2019) and rat (Soussi et al., 2010). Furthermore, all RV retrogradely-labelled neurons (Fig 1. C, D; green, arrows) examined in the SuML expressed both VGLUT2 mRNA (Fig 1. C, E; blue, arrows) and VGAT mRNA (Fig 1. C, F; red, arrows). Many of these triple-labelled neurons displayed a large soma with several labeled proximal dendrites (Fig. 1 C-F). These results confirmed that all SuM neurons projecting to the dorsal DG are located in the SuML region and express markers of both GABAergic (VGAT mRNA) and glutamatergic (VGLUT2 mRNA) neurotransmission as previously demonstrated (Billwiller et al., 2019).

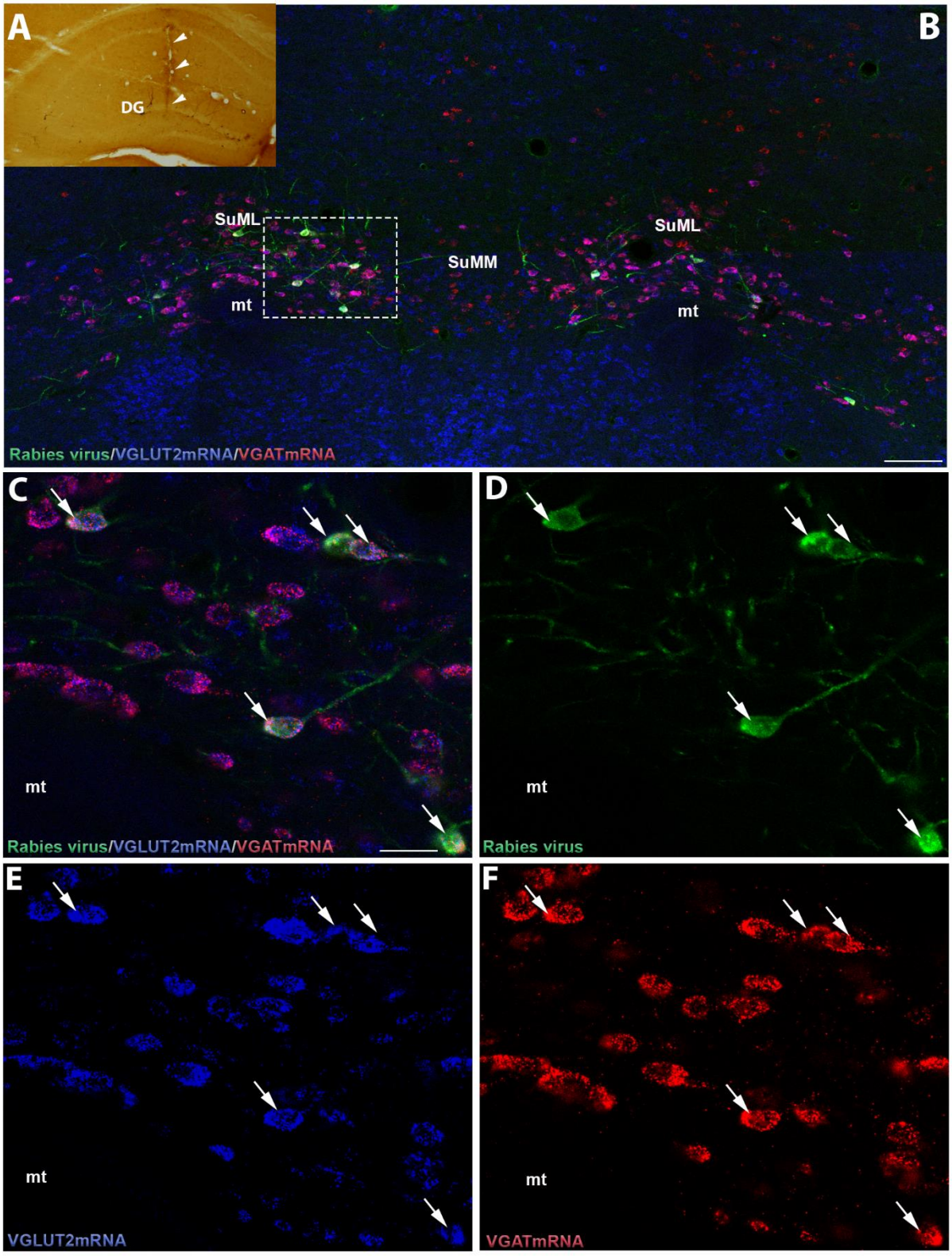

Figure1: Neurochemical features of SuML neurons innervating the dorsal dentate gyrus (DG) characterized by simultaneous labeling for the rabies virus (RV) retrograde tracer (green), VGAT mRNA (red) and VGLUT2 mRNA (blue) in coronal sections

(A) Immunohistochemical detection of RV showing the trace of the syringe (arrowheads) used for RV injection and the site of injection in the molecular layer of dentate gyrus (DG). (B-F) Confocal images of supramammillary (SuM) region obtained from a single optical slice and sequential acquisition of separate wavelength channels, corresponding to the different fluorophores used for the triple labeling performed in an adjacent coronal section to that illustrate in A. (B) Image obtained from the merge of the three confocal

images corresponding respectively to the labeling of VGLUT2 mRNA (blue) and VGAT mRNA(red) and RV (green). Many RV labelled neurons (green) were distributed in the lateral region (SuML) but not in the most medial part (SuMM) of the SuM. These RV-labelled neurons were distributed among numerous neurons expressing both VGLUT2 and VGAT mRNAs (purple) located almost exclusively above and around the mammillary tract (mt). (C-F) At higher magnification of the region outlined in B, all neurons labelled for the retrograde tracer RV (D, green arrows) contained both VGAT mRNA (F, red, arrows) and VGLUT2 mRNA (E, blue arrows). (C) Merge of D-F. Scale bars: A, 250µm; B, 100µm; C-F, 25 µm.

Neurotransmitter phenotype of CR-containing neurons projecting to the dorsal dente gyrus.

Sections along the anterio-posterior axis of the SuM were processed for simultaneous detection of CR RV and VGAT mRNA in order to determine the distribution of the population of CR neurons projecting to the dorsal DG and their neurotransmitter phenotype. Many CR-containing neurons were distributed in all region of the SuM including the SuML (Fig. 2 A, green) where RV retrogradely-labeled neurons were observed (Fig. 2, blue) as well as many large VGAT mRNA-containing neurons (Fig.2 , red) known to co-express VGUT2 mRNA (see above). Among the population of RV-labelled neurons (Fig.2 B, blue), some were labelled for CR (RV/CR+) (Fig. 2 D, F arrows) showing that in mice like in rat (Maglóczky et al., 1994) a subpopulation of CR neurons located in the SuML innervates the dorsal DG. However, not all RV-labelled neurons contained CR (RV/CR-). Therefore, these results revealed two populations of SuML neurons projecting to the inner molecular layer dorsal DG that differ by their content or not in CR. Furthermore, our data illustrated that all RV/CR+ and RV/CR- expressed the VGAT mRNA (Fig. 2, C, E, G) and therefore likely belong to the population of large neurons within the SuML that co-express VGAT and VGLUT2 mRNAs.

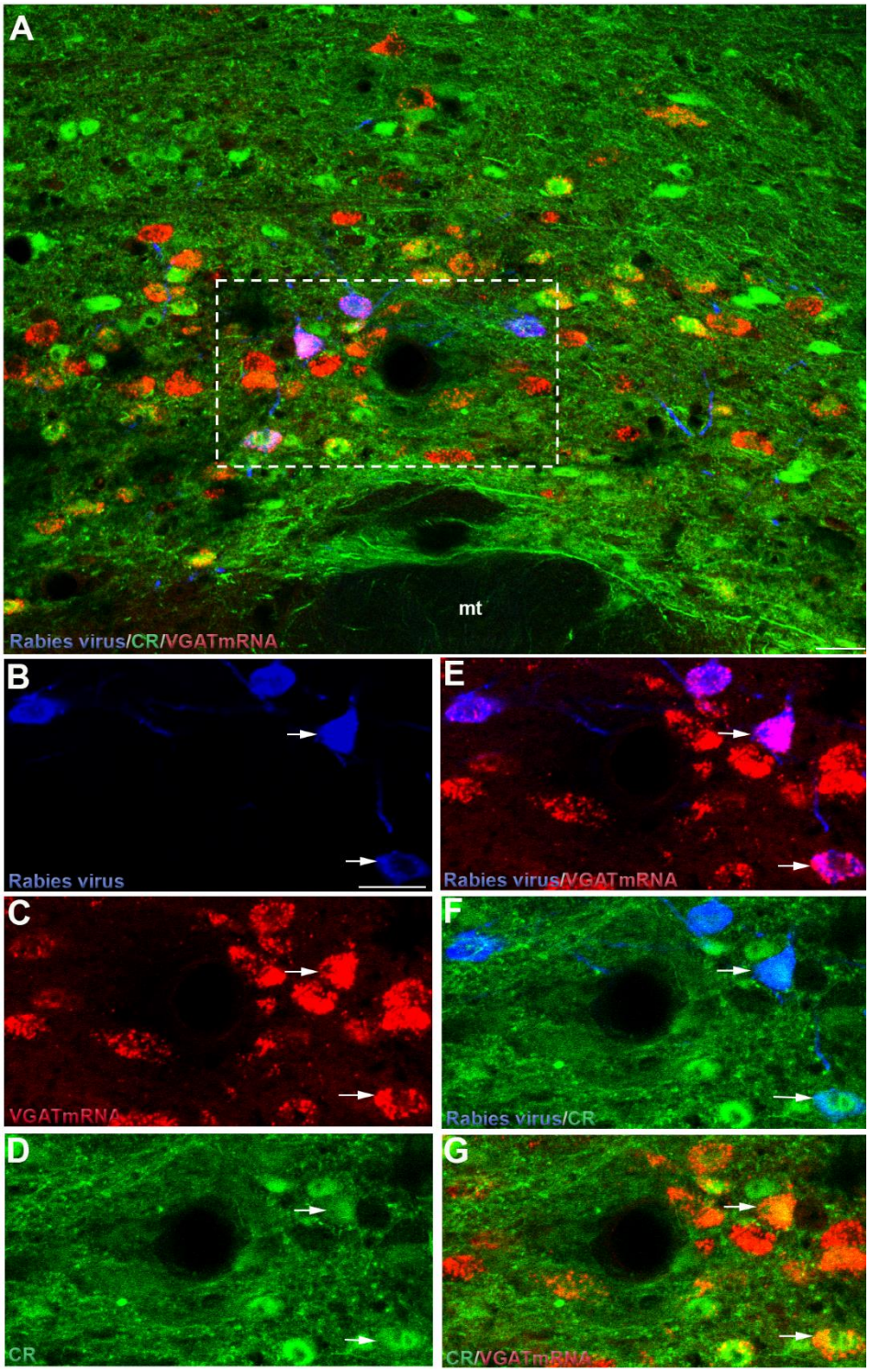

Figure 2: Distribution and neurotransmitter phenotype of Calretinin (CR)-containing neurons within the SUM innervating the dorsal DG.

(A-G) Confocal images of supramammillary (SuM) region obtained from a single optical slice and sequential acquisition of separate wavelength channels, corresponding to the different fluorophores used for simultaneous detection of CR, RV, and VGAT mRNA in a coronal section. (A) Image obtained from the merge of the three confocal images corresponding respectively to the labeling of CR (green), RV (blue) and VGAT mRNA (red). Many CR-containing neurons (green) were present in the SuML region above the mammillary tract (mt). Several RV-retrograde labelled neurons (blue) as well as many large neurons containing VGAT mRNA (red) were distributed in the SuML. (B-G) High magnification of the region outline in A. Among RV-labelled neurons (B, blue) several contained CR (D, green, arrows) but other not (B, D, F). All RV-labelled neurons containing or not CR co-expressed VGAT mRNA (C, E, G) (E) Merge of B and C. (F) Merge of B and D. (G) Merge of C and D. Scale bar: A-G 50µm.

Neurotransmitter phenotypes of the different populations of CR-containing neurons within the SuML

We further examine the neurotransmitter phenotype for GABAergic and/or glutamatergic transmission of CR neurons located within the SuML on sections processed for simultaneous detection of CR, VGAT mRNA and VGLUT2 mRNA. Within the SuML many CR-containing neurons were labelled for both VGAT and VGLUT2 mRNAs (Fig. 3 A-G) these neurons correspond at least partly to the population of CR neurons innervating the dorsal DG described above. In this SUML region, several CR-neurons containing VGLUT2 mRNA only were also present as well as neurons co-expressing VGAT and VGLUT2 mRNAs but not CR (Fig. 3 A-G). No CR-containing neurons labelled for VGAT mRNA only were observed. Therefore, these results identified two populations of CR-containing neurons within the SuM, one that coexpress both VGAT and VGLUT2 mRNAs and one that co-express VGLUT2 mRNA only.

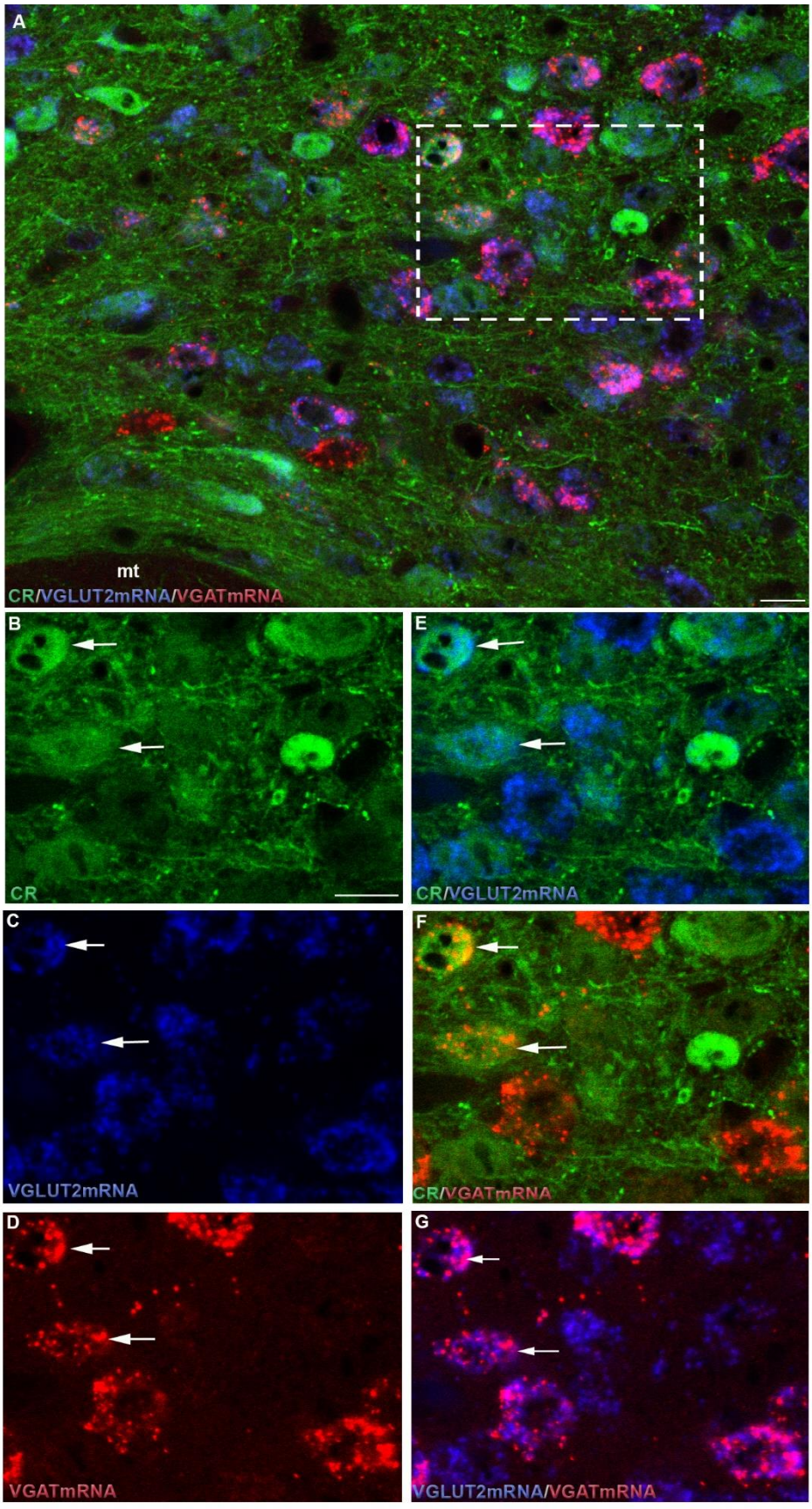
A
mt
CR/VGLUT2mRNA/VGATmRNA
B
CR
E
CR/VGLUT2mRNA
C
VGLUT2mRNA
F
CR/VGATmRNA
D
VGATmRNA
G
VGLUT2mRNA/VGATmRNA

Figure 3: Neurotransmitter phenotypes of the different populations of CR-containing neurons within the SuML.
(A-G) Confocal images of supramammillary (SuM) region obtained from a single optical slice and sequential acquisition of separate wavelength channels, corresponding to the different fluorophores used for simultaneous detection of CR, VGLUT2 mRNA and VGAT mRNA in a coronal section. (A) Image obtained from the merge of the three confocal images corresponding respectively to the labeling of CR (green), VGLUT2 mRNA (blue) and VGAT mRNA (red). Many CR-containing neurons (green) and VGAT/VGLUT mRNAs expressing neurons (purple) were observed in the SuML as well as several neurons expressing VGLUT2 mRNA (blue) only. (B-G) High magnification of the region outline in A, showing that several Among the CR-labelled neurons (B, green, arrows) several co-expressed both VGLUT2 mRNA (C, Blue, arrows) and VGAT mRNA (D, red, arrows) and some express VGLUT2 only. None on these CR-containing neurons expressed VGAT mRNA only. (E) Merge of B and C. (F) Merge of B and D. (G) Merge of C and D. (mt) the mammillary tract. Scale bar: A-G 25µm.

Distribution and proportion of the different populations of CR-containing neurons along the antero-posterior axis of the SuM

All together these results illustrated two populations of neurons within the SuML that innervated the dorsal DG: the first population is composed by neurons that co-expressed VGLUT2 mRNA, VGAT mRNA and CR; the other one is made of neurons that co-express VGAT mRNA and VGLUT2 mRNA but do not contain CR. Finally this SuML region contained also CR-containing neurons that expressed VGLUT2 only but do not innervated the dorsal DG. We went further and examined the distribution of these three populations of SuM neurons along the antero-posterior axis of the SuM. As illustrated in Fig. 4. These different populations were not homogenously distributed within the SuM. CR neurons containing VGLUT2 and VGAT mRNAs (Fig. 4, White labels in B and D) were more numerous at the anterior level (Fig. 4 A, B) than at the posterior level (Fig. 4 C, D) of the SuM. Neurons co-expressing VGLUT2 and VGAT mRNAs but not CR (Fig. 4, Pink labels in B and D) were more numerous at the posterior level than at the anterior level of the SuM region. CR neurons expressing VGLUT2 mRNA only (Fig. 4 blue labels in B and D) were observed mainly at the posterior level of the SuM. Quantitative analysis showed that CR-containing neurons represented 64% (range: 49%-71%) of the entire population of VGLUT2 /VGAT mRNAs-containing neurons. However at the anterior level CR/VGLUT2/VGATmRNAs neurons account for 92 % (range: 72%-100%) of the population of VGLUT2 /VGAT mRNAs-containing neurons whereas it account for 28% at the posterior level (range: 22%-41%).

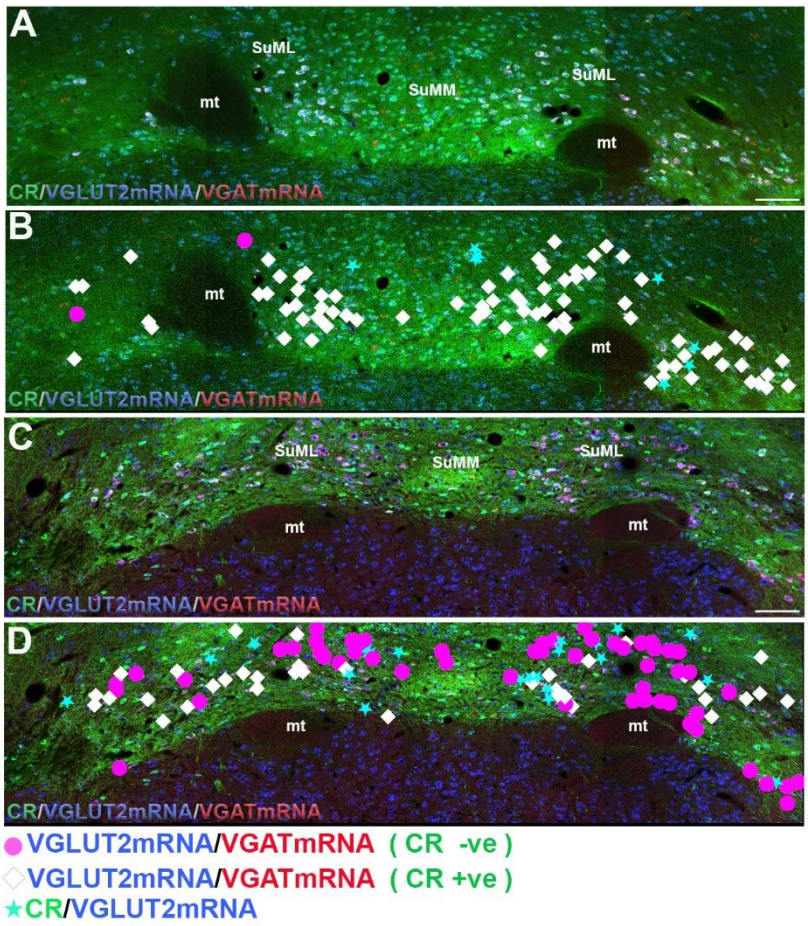

Figure 4: Distribution of calretinin (CR) neurons along the anterio-posterior axis of SuML region. **(**A-D) Images at two different antero (A,C) -posterior (C,D) levels of the SuM obtained by the tile scan of single optical slices and sequential acquisition of separate wavelength channels, corresponding to the different fluorophores used for simultaneous detection of CR, VGLUT2 mRNA and VGAT mRNA in coronal sections. (immunodetection of CR (green) and mRNAs labelling for VGAT(Red) and VGLUT2 (Blue) in coronal sections along the anterio-posterior axis of SuML regions. (B, D) Montage illustrating the distribution of different populations of neurons obtained from the confocal Images illustrating in A and C in which were superposed the analyses performed with the Neurolucida software. (mt) mammillary tract; medial region of the SuM (SuMM); Lateral region of the SuM (SuML) Scale bar: A and C, 200 µm

Neuronal targets of SuML Calretinin-neurons innervating the dorsal DG.

Previous studies performed in the same mouse strain have provided evidence at the anatomica (Billwiller et al., 2019)l and electrophysiological (Pedersen et al., 2017; Hashimotodani et al., 2018; Billwiller et al., 2019) levels that VGAT/VGLUT2-containing neurons innervate both granule cells (GC) and subpopulations of interneurones (IN) mainly corresponding to PARV-IN in the DG. Here we further examined whether the subpopulation of SuML VGLUT2/VGAT neurons containing calretinin targeted also these two populations of DG neurons (GC and PAR-IN) or innervated specifically GC. For this purpose, AAV-5-DIO-EYFP anterograde tracer were

injected bilaterally in the SuML of VGLUT2-cre mice allowing specific EYFP labeling of VGLUT2 neurons and of their axon fibers innervating the dorsal DG. Sections of these VGLUT2-EYFP mice were processed for simultaneous detection of EYFP, CR and PARV (Fig. 5A). In the dorsal DG, EYFP axonal fibers and terminals were mainly located in the supragranular layer of the dorsal and ventral blades of the dentate gyrus (FiG. 5 A, green) but also penetrate deeper in the granule cell layers. CR-containing axon terminals originating from SuML neurons and labeled with EYFP were preferentially located in the supragranular layer of the dorsal and ventral blades of the DG (Fig, 5 A, B, yellow). However, few EYFP-labelled axon terminals containing CR were also present deeper in the granule cell layer (GCL) (Fig 5 B). These EYFP-labelled axon terminals containing CR established putative synaptic contact with either cell bodies and dendrites of putative GCs (Fig. 6) as well as cell bodies (Fig. 5B-E) and dendrites (Fig. 5 F-I) of PARV-containing interneurones.

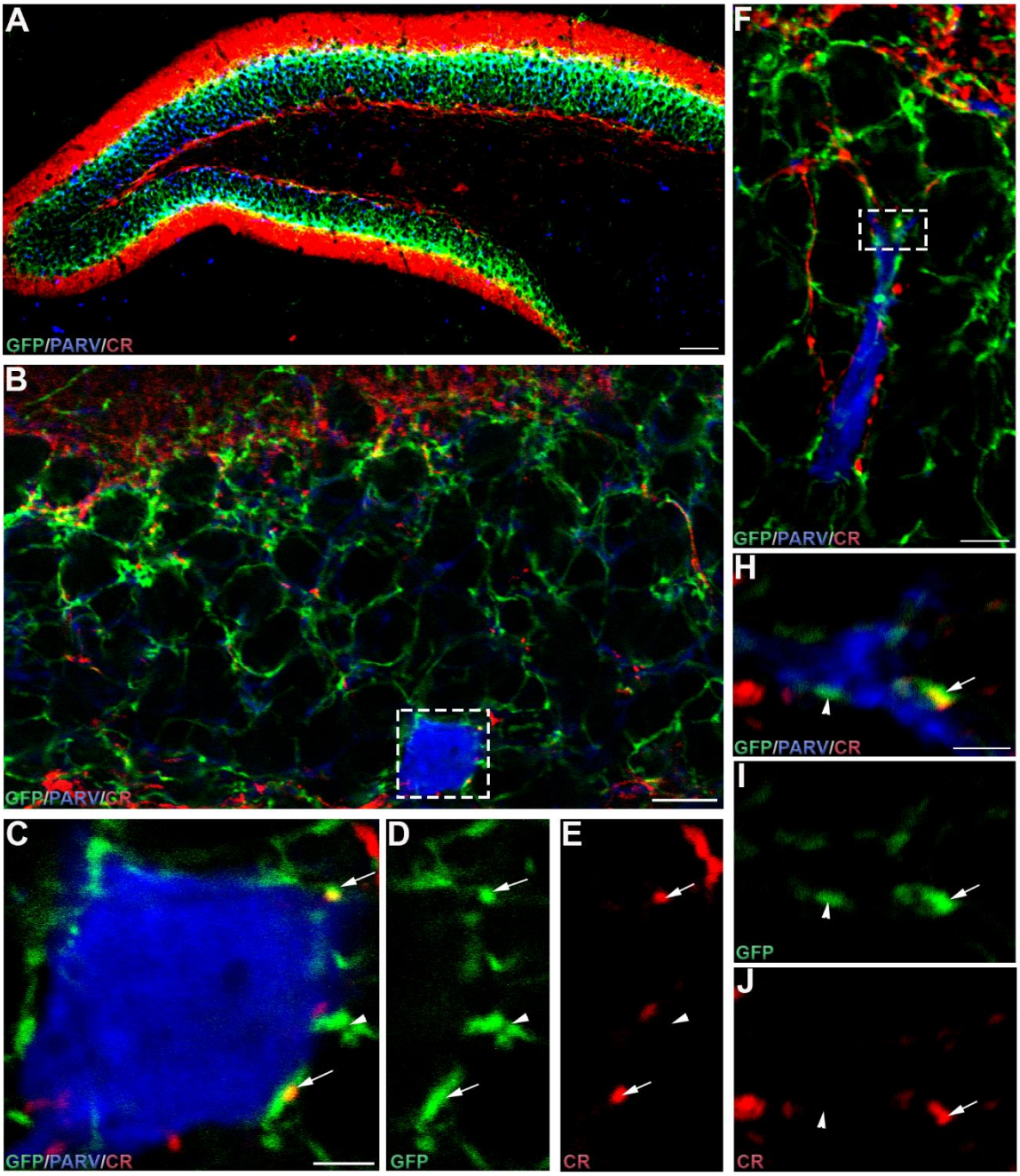

Figure 5: EYFP-labeled axon terminals from SuML containing CR or not innervate Parvalbumin interneuron (Parv) of the dorsal DG.

(A-J) Confocal images for triple immune labelling for CR (red), Parv (blue) and GFP (green) in coronal sections of the dorsal dentate gyrus .(A) Image of dorsal DG showing the distribution of the axon fibers and terminals labeled for GFP and of the CR immnolabeling. Note a high labeling for CR in the inner molecular layer of the DG (red) likely corresponding to CR labeled axon terminals from DG CR-interneurones. A thin band of CR labeled processes is also observed in the surpagranular layer of the DG partially overlapping EYFP-containing terminals. (B-J) Confocal images obtained from a single confocal slice showing many EYFP containing boutons (green) surrounding unlabelled cell bodies of putative GCs (B) as well as the cell body (c, blue)) and dendrite (F, blue) of a PARV- containing interneurones. Some of these EYFP-labeled terminals (D, I green, arrows) surrounding the cell body (C-E) or dendrite (F-I) of the PARV-interneurones contained CR (C, E, F, H, I, arrows) but not all (see arrowheads in C, D, E, H, I, J). (C) High magnification of the region outlined in B. (H) High magnification of the region outlined in F. Merge of I and J. Scale bars: A, 100 µm; B, 20 µm; C -J, 5 µm.

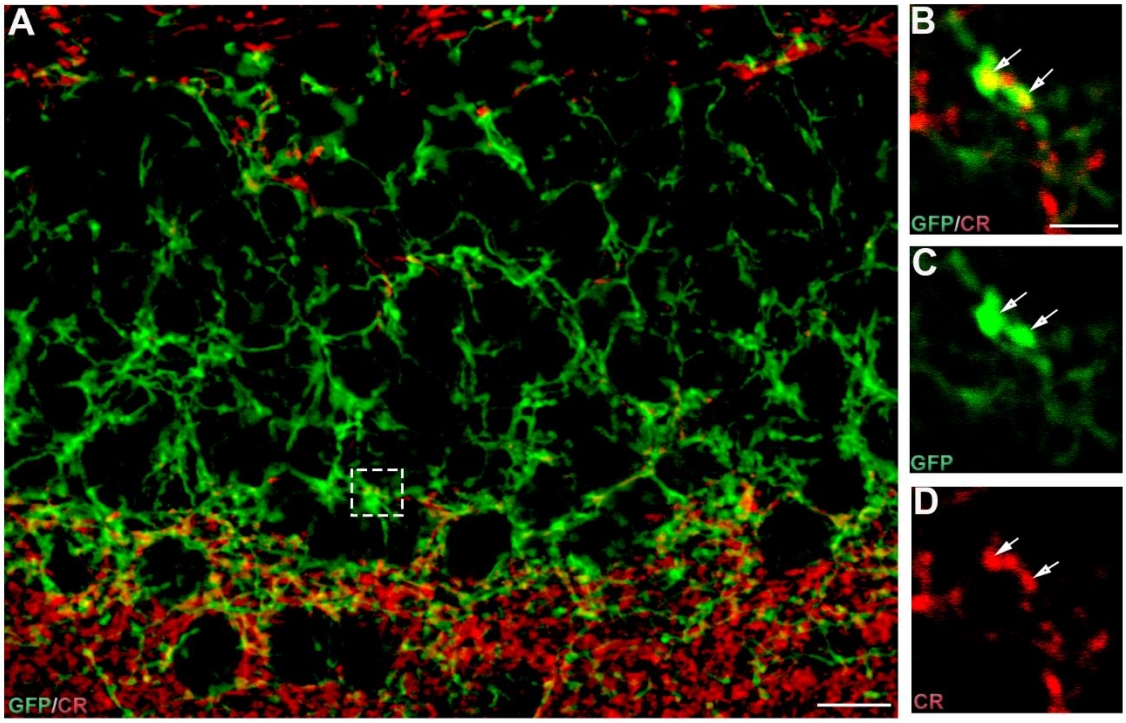

Figure 6: EYFP-labeled axon terminals from SuML containing CR or not innervate Granule cells (GCs) of the dorsal DG..
(A-D) Confocal image of a single optical slice obtained from a coronal section of the DG labelled for CR (red) and EYFP (green). (A) Image of ventral blade of the DG showing the distribution of axonal terminals labelled for GFP (green) located in the supragranular and granule cell layers as well as many axon terminals containing CR (Red) located in the inner molecular and supragranular layers. (B) At higher magnification of the region outlined in A. (C&D) Images of the two different fluorophores obtained by sequential acquisition of separate wavelength channels from the single confocal slice, showing several EYFP labelled boutons (C, green, arrows) containing CR (D, Red, arrows). Scale bars: A, 20 µm; B -D, 5 µm.

Discussion

Two distinct populations of SuML GABA/GLU neurons innervate the dorsal DG

Our results demonstrate heterogeneity of the neurons from the lateral part of the supramammillary nucleus (SuML) that innervate the dorsal dentate gyrus (DG). Indeed whereas we confirm that all these neurons display a dual phenotype for both glutamatergic and GABAergic neurotransmission as described previously in mice (Billwiller et al., 2019) and rat (Esclapez et al., 1999; Soussi et al., 2010). This study reveals two subpopulations of GABA/GLU neurons that differ by their content or not in the calcium binding protein: Calretinin (CR). Several studies in rat have described the SuM origin of the CR-axon terminals in the innermost portion of the dentate molecular layer, also call the supragranular cell layer (Gulyás *et al.*, 1992; Maglóczky *et al.*, 1994; Nitsch & Leranth, 1996b). Several authors have considered, these CR neurons from the SUM innervating the DG as glutamatergic neurons (Maglóczky et al., 1994). Our data establish that these CR-neurons from the SuML represent a subpopulation of GABA/GLU neurons innervating the dorsal DG. Indeed, we show (I) that some retrograde-labeled neurons, located in the SuML or more precisely in the SuM grandicellular region (SuMg, (Pan & McNaughton, 2004a)) after injection of RV in the innermost molecular layer of the DG, contain CR; II) All RV-labeled neurons co-express VGLUT2 and VGLTA mRNAs; III) all RV-labeled neurons containing CR express VGAT mRNA. IV) Among all the CR neurons within the SuML most co-express VGAT and VGLUT2 mRNAs, some express VGLUT2 mRNA only and none of them express VGAT mRNA only. In addition, our results reveal a second subpopulation of GABA/GLU neurons from the SuML innervating the DG that do not contain CR. Indeed we show that not all SuML neurons co-expressing VGAT and VGLUT2 mRNAs and their axon terminals within the supragranular and granule cells layers contain CR. We further demonstrate that these two populations of (GABA/GLU/CR+; GABA/GLU/CR-) neurons account respectively for 64% and 36% of the total GABA/GLU neuron population.

Furthermore, we show that these two subpopulations of GABA/GLU neurons (GABA/GLU/CR+; GABA/GLU/CR-) from the SuML innervating the DG display different distributions within the

antero-posterior level of the SUM. The population of GABA/GLU/CR+ neurons is more numerous in the anterior than posterior level whereas GABA/GLU/CR- neurons predominate at the posterior level. The antero-posterior decreased gradient of GABA/GLU/CR+ neurons apparently does not follow the homogenous distribution of the entire population of CR neurons along the antero-posterior axis of the SuM region reported in rat (Borhegyi and Leranth, 1997). More than a variation between species, this difference certainly reflect the fact that Borhegyi and Leranth (1997) described the distribution the entire population of CR-neurons which included not only those projecting to the DG but also to CA2/CA3a (Borhegyi and Leranth, 1997) and to the septum(Kiss & Szeiffert, 1995; Leranth & Kiss, 1996b) whereas our results concerned only the subpopulation of CR-neurons expressing VGLUT2 and VGAT mRNAs (GABA/GLU/CR+ neurons) that mainly innervate the DG.

We identified also in the SuML, CR-neurons that express VGLUT2 only. These neurons do not innervate the DG since they were not labeled for the RV. Such population of neurons could account for the CR-neurons that innervate the CA2/CA3a pyramidal cells of the hippocampus (Maglóczky et al., 1994) known to be glutamatergic only(Soussi et al., 2010) or the septum (Kiss and Szeiffert, 1995).

Both GABA/GLU/CR+ and GABA/GLU/CR- neuronal populations target DG Granule cells and Parvalbumin (PARV)-interneurones.

The synaptic targets of SuM-DG projections have been well described, showing that the majority of these SuM projections to the DG target the proximal dendrites and somata of granule cells (Maglóczky *et al.*, 1994; Nitsch & Leranth, 1996b; Soussi *et al.*, 2010) but also of some subpopulation of GABAergic interneurones(Nitsch & Leranth, 1996b). Our study confirms these data and further demontrastes that both subpopulations of GABA/GLU/CR+ and GABA/GLU/CR- neurons innervate soma and dendrites of granule cells and PARV-interneurons. However the weight of innervation of each of these two populations, on granule cells and PARV-interneurons still have to be determined.

Speculative functional role of GABA/GLU/CR+ and GABA/GLU/CR- neurons in the control of DG activity.

Despite the fact that these two populations of GABA/GLU/CR+ and GABA/GLU/CR- neurons target both granule cells and PARV-interneurons of the DG, their role in the control of DG activity could differ. Indeed, the physiological properties of these two populations could be different in regard of their content or not in CR. Interestingly, even if electrophysiological recordings in the SuMg (SuML) has been sparse, several studies suggest that this region of SuM, may contain both rhythmic and non-rhythmic cells (Kirk and McNaughton, 1991; Kocsis and Vertes, 1994). Kirk and McNaughton, (1991, 1993) report that some of these SuMg cells discharge rhythmically in phase with hippocampal theta activity. Even if speculative, these rhythmic cells could correspond to the population of GABA/GLU/CR+ neurons that will be responsible for regulation of DG theta activity (for review see (Pan & McNaughton, 2004a)). Whereas the population of GABA/GLU/CR- neurons could correspond to the non-rythmic cells.

Moreover it is known that the SuM as a whole receive afferent from many brain structures including the infralimbic cortex, the dorsal peduncular cortex, DBB, the medial and lateral septal nuclei, the lateral habenula and the medial and lateral preoptic area (Swanson, 1982; Chiba & Murata, 1985; Shibata *et al.*, 1986; Vertes, 1988, 1992; Hayakawa *et al.*, 1993; Thinschmidt, 1993; Risold & Swanson, 1997; Kiss *et al.*, 2002). It is likely that these different brain regions innervate distinct populations of SuM neurons. For example, Leranth et al., 1999 show that the GABAergic neurons located in the border between the lateral septum and the medial septum project specificaly to CR- containing (non-GABAergic) cells in the SuM. Such results suggest that afferent to GABA/GLU/CR+ and GABA/GLU/CR- neurons could be different.

All this information will have to be determine in order to understands the role play by these two populations GABA/GLU/CR+ and GABA/GLU/CR-, knowing that the SuML-DG pathway likely contribute to several functions such as exploration of a novel environment and spatial learning (Wirtshafter et al., 1998; Santín et al., 2003; Ito et al., 2009) as well as REM sleep (Renouard et al., 2015; Billwiller et al., 2019);

References

Billwiller F, Castillo L, Elseedy H, Ivanov A, Scapula J, Ghestem A, Abdelmeguid N, Krook-Magnuson E, Soltesz I, Bernard C, Luppi P-H, Esclapez M. 2019. The Supramammillary – dorsal Dentate Gyrus pathway that display unique GABA and Glutamate co-transmission properties increases theta and gamma powers in the DG during REM sleep.

Borhegyi Z, Leranth C. 1997. Distinct substance P- and calretinin-containing projections from the supramammillary area to the hippocampus in rats; a species difference between rats and monkeys. Exp Brain Res 115:369–374.

Boulland J-L, Jenstad M, Boekel AJ, Wouterlood FG, Edwards RH, Storm-Mathisen J, Chaudhry FA. 2009. Vesicular Glutamate and GABA Transporters Sort to Distinct Sets of Vesicles in a Population of Presynaptic Terminals. Cereb Cortex 19:241–248.

Bras H, Gaytán SP, Portalier P, Zanella S, Pásaro R, Coulon P, Hilaire G. 2008. Prenatal activation of 5-HT2Areceptor induces expression of 5-HT1Breceptor in phrenic motoneurons and alters the organization of their premotor network in newborn mice. Eur J Neurosci 28:1097–1107.

Carnes KM, Fuller TA, Price JL. 1990. Sources of presumptive glutamatergic/aspartatergic afferents to the magnocellular basal forebrain in the rat. J Comp Neurol 302:824–852.

Chiba T, Murata Y. 1985. Afferent and efferent connections of the medial preoptic area in the rat: a WGA-HRP study. Brain Res Bull 14:261–272.

Coulon P, Bras H, Vinay L. 2011. Characterization of last-order premotor interneurons by transneuronal tracing with rabies virus in the neonatal mouse spinal cord. J Comp Neurol 519:3470–3487.

Dent JA, Galvin NJ, Stanfield BB, Cowan WM. 1983. The mode of termination of the hypothalamic projection to the dentate gyrus: an EM autoradiographic study. Brain Res 258:1–10.

Esclapez M, Hirsch JC, Ben-Ari Y, Bernard C. 1999. Newly formed excitatory pathways provide a substrate for hyperexcitability in experimental temporal lobe epilepsy. J Comp Neurol 408:449–460.

Gonzalo-Ruiz A, Alonso A, Sanz JM, Llinás RR. 1992. Afferent projections to the mammillary complex of the rat, with special reference to those from surrounding hypothalamic regions. J Comp Neurol 321:277–299.

Gulyás AI, Miettinen R, Jacobowitz DM, Freund TF. 1992. Calretinin is present in non-pyramidal cells of the rat hippocampus--I. A new type of neuron specifically associated with the mossy fibre system. Neuroscience 48:1–27.

Haglund L, Swanson LW, Köhler C. 1984. The projection of the supramammillary nucleus to the hippocampal formation: An immunohistochemical and anterograde transport study with the lectin PHA-L in the rat. J Comp Neurol 229:171–185.

Hashimotodani Y, Karube F, Yanagawa Y, Fujiyama F, Kano M. 2018. Supramammillary Nucleus Afferents to the Dentate Gyrus Co-release Glutamate and GABA and Potentiate Granule Cell Output. Cell Rep 25:2704-2715.e4.

Hayakawa T, Ito H, Zyo K. 1993. Neuroanatomical study of afferent projections to the supramammillary nucleus of the rat. Anat Embryol (Berl) 188:139–148.

Iseni F, Lafay F, Raux H, Blondel D. 1997. Mapping of monoclonal antibody epitopes of the rabies virus P protein. J Gen Virol 78:119–124.

Ito M, Shirao T, Doya K, Sekino Y. 2009. Three-dimensional distribution of Fos-positive neurons in the supramammillary nucleus of the rat exposed to novel environment. Neurosci Res 64:397–402.

Kirk IJ, McNaughton N. 1991. Supramammillary cell firing and hippocampal rhythmical slow activity. Neuroreport 2:723–725.

Kirk IJ, McNaughton N. 1993. Mapping the differential effects of procaine on frequency and amplitude of reticularly elicited hippocampal rhythmical slow activity. Hippocampus 3:517–525.

Kiss J, Csáki A, Bokor H, Kocsis K, Kocsis B. 2002. Possible glutamatergic/aspartatergic

projections to the supramammillary nucleus and their origins in the rat studied by selective [(3)H]D-aspartate labelling and immunocytochemistry. Neuroscience 111:671–691.
Kiss J, Csáki A, Bokor H, Shanabrough M, Leranth C. 2000. The supramammillo-hippocampal and supramammillo-septal glutamatergic/aspartatergic projections in the rat: a combined [3H]D-aspartate autoradiographic and immunohistochemical study. Neuroscience 97:657–669.
Kiss J, Szeiffert G. 1995. Topographic analysis of connections between the rat septal diagonal band complex and the supramammillary area. In: Fourth IBRO World Congress of Neuroscience, Rapid communications of Oxford Ltd. Vol. 389.
Kocsis B, Vertes RP. 1994. Characterization of neurons of the supramammillary nucleus and mammillary body that discharge rhythmically with the hippocampal theta rhythm in the rat. J Neurosci Off J Soc Neurosci 14:7040–7052.
Kocsis K, Kiss J, Csáki A, Halász B. 2003. Location of putative glutamatergic neurons projecting to the medial preoptic area of the rat hypothalamus. Brain Res Bull 61:459–468.
Leranth C, Carpi D, Buzsaki G, Kiss J. 1999. The entorhino-septo-supramammillary nucleus connection in the rat: morphological basis of a feedback mechanism regulating hippocampal theta rhythm. Neuroscience 88:701–718.
Leranth C, Kiss J. 1996a. A population of supramammillary area calretinin neurons terminating on medial septal area cholinergic and lateral septal area calbindin-containing cells are aspartate/glutamatergic. J Neurosci Off J Soc Neurosci 16:7699–7710.
Leranth C, Kiss J. 1996b. A population of supramammillary area calretinin neurons terminating on medial septal area cholinergic and lateral septal area calbindin-containing cells are aspartate/glutamatergic. J Neurosci Off J Soc Neurosci 16:7699–7710.
Leranth C, Nitsch R. 1994. Morphological evidence that hypothalamic substance P-containing afferents are capable of filtering the signal flow in the monkey hippocampal formation. J Neurosci Off J Soc Neurosci 14:4079–4094.
Maglóczky Z, Acsády L, Freund TF. 1994. Principal cells are the postsynaptic targets of supramammillary afferents in the hippocampus of the rat. Hippocampus 4:322–334.
Nitsch R, Leranth C. 1996. GABAergic neurons in the rat dentate gyrus are innervated by subcortical calretinin-containing afferents. J Comp Neurol 364:425–438.
Pan W-X, McNaughton N. 2004. The supramammillary area: its organization, functions and relationship to the hippocampus. Prog Neurobiol 74:127–166.
Paxinos G, Franklin KBJ. 2004. The Mouse Brain in Stereotaxic Coordinates. Gulf Professional Publishing.
Paxinos G, Watson C. 1998. The Rat Brain in Stereotaxic Coordinates. Academic Press.
Pedersen NP, Ferrari L, Venner A, Wang JL, Abbott SBG, Vujovic N, Arrigoni E, Saper CB, Fuller PM. 2017. Supramammillary glutamate neurons are a key node of the arousal system. Nat Commun [Internet] 8. Available from: https://www.ncbi.nlm.nih.gov/pmc/articles/PMC5680228/
Renouard L, Billwiller F, Ogawa K, Clément O, Camargo N, Abdelkarim M, Gay N, Scoté-Blachon C, Touré R, Libourel P-A, Ravassard P, Salvert D, Peyron C, Claustrat B, Léger L, Salin P, Malleret G, Fort P, Luppi P-H. 2015. The supramammillary nucleus and the claustrum activate the cortex during REM sleep. Sci Adv [Internet] 1. Available from: https://www.ncbi.nlm.nih.gov/pmc/articles/PMC4640625/
Risold PY, Swanson LW. 1997. Connections of the rat lateral septal complex. Brain Res Brain Res Rev 24:115–195.
Santín LJ, Aguirre JA, Rubio S, Begega A, Miranda R, Arias JL. 2003. c-Fos expression in supramammillary and medial mammillary nuclei following spatial reference and working memory tasks. Physiol Behav 78:733–739.
Saper CB. 1984. Organization of cerebral cortical afferent systems in the rat. II. Magnocellular basal nucleus. J Comp Neurol 222:313–342.

Shibata H, Suzuki T, Matsushita M. 1986. Afferent projections to the interpeduncular nucleus in the rat, as studied by retrograde and anterograde transport of wheat germ agglutinin conjugated to horseradish peroxidase. J Comp Neurol 248:272–284.
Soussi R, Zhang N, Tahtakran S, Houser CR, Esclapez M. 2010. Heterogeneity of the supramammillary-hippocampal pathways: evidence for a unique GABAergic neurotransmitter phenotype and regional differences: GABAergic and glutamatergic supramammillary-hippocampal pathways. Eur J Neurosci 32:771–785.
Stanfield BB, Maxwell Cowan W. 1984. An EM autoradiographic study of the hypothalamo-hippocampal projection. Brain Res 309:293–298.
Swanson LW. 1982. The projections of the ventral tegmental area and adjacent regions: a combined fluorescent retrograde tracer and immunofluorescence study in the rat. Brain Res Bull 9:321–353.
Thinschmidt JS. 1993. The supramammillary nucleus: Does it play a role in the mediation of hippocampal theta rhythm?
Vertes RP. 1988. Brainstem afferents to the basal forebrain in the rat. Neuroscience 24:907–935.
Vertes RP. 1992. PHA-L analysis of projections from the supramammillary nucleus in the rat. J Comp Neurol 326:595–622.
Vertes RP. 2015. Major diencephalic inputs to the hippocampus. In: Progress in Brain Research. Vol. 219. Elsevier. p 121–144. Available from: https://linkinghub.elsevier.com/retrieve/pii/S0079612315000424
Vertes RP, McKenna JT. 2000. Collateral projections from the supramammillary nucleus to the medial septum and hippocampus. Synapse 38:281–293.
Wirtshafter D, Stratford TR, Shim I. 1998. Placement in a novel environment induces fos-like immunoreactivity in supramammillary cells projecting to the hippocampus and midbrain. Brain Res 789:331–334.
Wyss JM, Swanson LW, Cowan WM. 1979. Evidence for an input to the molecular layer and the stratum granulosum of the dentate gyrus from the supramammillary region of the hypothalamus. Anat Embryol (Berl) 156:165–176.

THIRD STUDY

Supramammillary lateral- dorsal dentate gyrus pathway modulates seizure dynamics in mouse pilocarpine model of mesial temporal lobe epilepsy.

Abstract

Mesial temporal lobe epilepsies (MTLE) are among the most common clinical forms of drug-resistant partial epilepsies in adults. These epilepsies are characterized by the occurrence of spontaneous recurrent seizures associated with excessive and hypersynchronous discharges of neuronal populations generated by a multi-structural epileptogenic zone involving several regions of the limbic system within the mesial temporal lobe including the hippocampal formation (HF), the entorhinal cortex (EC) and the amygdala. Electroclinical observations as well as studies performed in animal models of MTLE provide evidence that these epilepsies are network diseases in which the emergence of spontaneous seizures requires not only hyperactivity of principal cells within the limbic cortex but also the synchronization of activities between these different limbic structures of the temporal lobe. We hypothesize, that the supramammillary nucleus (SuM) one of the main sub-cortical structures innervating all limbic cortex could play a crucial role in this synchronization and the emergence of seizure according to the emotional and or vigilance state of the patient. Indeed, this hypothalamic nucleus, which provides major projections to the hippocampal formation, plays a key role in the regulation of several hippocampus-dependent activities, including theta rhythms, memory function and emotional behavior, such as stress and anxiety, functions that are known to be altered in MTLE. More recently, it was shown that the projections from neurons of lateral region of the SuM (SuML) that innervate the dorsal dentate gyrus (DG) and display a unique dual GABAergic and Glutamatergic neurotransmission sprout and form additional aberrant connections on DG cells in pilocarpine-treated epileptic rats. In this study we investigate whether the plasticity of these SuML-DG connections in epileptic animals could influence the emergence and strength of seizures. For this purpose, we combined optogenetic manipulation of the SuML-DG pathway in pilocarpine-treated epileptic VGLUT2-Cre mutant mice, expressing Chanelrhodopsine (ChR2, excitatory opsin, VGLUT2-ChR2 mice) or Halorhodopsine (eNpHR3, inhibitory opsin, VGLUT2-HR) within SuML neurons and their axon terminals, with electrophysiological recordings of hippocampal seizures. We first demonstrated, using structural connectivity and neurohistochemical techniques that SuML

neurons formed aberrant connections within an altered dDG in all epileptic VGLUT2-ChR2, VGLUT2-HR or control VGLUT2-EYFP mice as previously described in epileptic rat. We further showed that optogenetic manipulation of this SuML-DG pathway does not modify significantly seizure duration but modulates seizure dynamics as assessed by the variability of their frequency content. Indeed, light activation and inactivation of this pathway respectively increase and decrease the variability of the seizure frequency content power without any beneficial or detrimental effect on the seizures. These results suggest that SuML neurons innervating the dDG could modulate the expression probability of different seizure types. Further studies needed to examine whether such modulation could be instrumental to trigger seizures during specific vigilance states.

Materials and Methods

1. Animals

Knock-in transgenic Vglut2-ires-Cre mice (*Slc17a6*$^{tm2(cre)Lowl}$, FVB background, Jackson Laboratory) were used in all the experiments. The mice were housed in standard cages under a 12h light/dark cycle. All the surgical and experimental procedures that were performed in these animals were according to the European Communities Council Directive of 86/609/EEC and were approved by the University of Aix-Marseille Chancellor's Animal Research Committees.

1.1 *Pilocarpine model.*

In this study, we tried three different protocols in order to reduce the mortality rate of our transgenic mice.

The first protocol (Single dose): Mice (6 to 14 weeks old, n=20) were first injected (i.p.) with a low dose of methyl scopolamine nitrate (1 mg/kg; Sigma, St Louis, MO), 30 min before to receive a single dose of pilocarpine (i.p. 320 to 340 mg/kg; Sigma). With this protocol, we had a very high mortality rate (90%). The mice (n=18) developed very severe generalized seizures and died before to enter in status epilepticus (SE) and two did not develop seizures or SE.

The second protocol (Fractionated): As previously described mice (12-14 weeks old n=20) were injected with methyl scopolamine nitrate 30 min before pilocarpine injection. In this protocol, the animals received a similar final dose of pilocarpine but in a fractionated manner. Each animal was injected every 20 min by a single dose of pilocarpine (100mg/kg) until they developed SE. Each animal received 3 or 4 injections. With this protocol, 80% of the mice developed SE (n=16), 20% (n=4) not. Status Epilepticus was alleviated after 40 min by a single injection of diazepam (i.p.; 10 mg/kg; Roche, Boulogne-Billancourt, France). After the experiment survival mice receive 0.5ml of 0.9%NaCl, 4 hrs after the SE and in the morning. Fifteen mice did not survive after SE. Only one mouse survived for 2 weeks. Therefore, with this protocol we have almost 100% mortality after two weeks.

The third protocol (modified Fractionated): As usual mice were injected with methyl scopolamine nitrate 30 min before pilocarpine injections. In this protocol, pilocarpine was also injected in a fractionated manner but using different concentrations and time intervals between injections to that used in the second protocol. Mice (6-8 weeks old; n=33) were injected (i.p) first with a dose of pilocarpine (100mg/Kg), 20 min later with a second dose (50 mg/kg) and then every 10 min with 50mg/kg until they developed SE. The total number of injection ranges between 3-4. With this protocol 85% of mice (n=28) developed SE, 15% not (n=5). Among the animals that developed SE 75 % died. As described before SE was alleviated after 35 min with diazepam. Then survival animals were injected with saline as mentioned before. Seven animals survive from SE (n= 7).

In this study we used the animals' issue from this third protocol of pilocarpine induced SE and spontaneous limbic seizures. All these mice went for surgery for viral vector injection and optrode implantation (see below) 3 to 4 weeks after the induction of the epilepsy by pilocarpine injection as illustrated in Fig. 16. Indeed, in a pilot study in which the surgery was performed two weeks before performing the pilocarpine injection protocol none of the animals survived to pilocarpine injection.

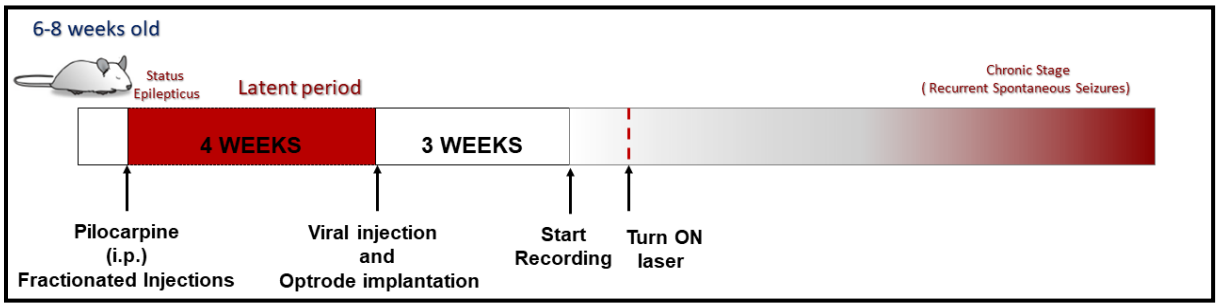

Figure 16: Diagram shows the experimental procedure

The mice were divided into the following experimental groups:

Sham group: 5 animals that did not develop SE.

Epileptic group: 7 animals were divided into 3 groups according to the viral vector injection received.

- Control group. **[AAV5-DIO-EYFP] (n=2)**
- Channelrhodopsin group (excitatory opsin). **[AAV5-DIO-(ChR)-EYFP] (n=3)**
- Halorhodopsin group (inhibitory opsin). **[AAV5-DIO-(HR)-EYFP] (n=2)**

1.1.1 Surgical procedure

All mice (n=12) were anesthetized were anesthetized by an intraperitoneal injection (i.p.) of Ketamin (50mg/kg) / Xylazine (5mg/kg) solution. If necessary, this anesthesia was repeated during the surgery. Animals were then secured in the stereotaxic frame (David Kopf instruments, Tujunga, CA). The body temperature of mice was controlled and maintained at about 37°C during the entire procedure by means of an anal probe and heating blanket respectively. The head was shaved and sanitized with Betanine and 0.9% NaCl. Local anesthesia was performed by infiltration of the scalp with xylocaine (lidocaine hydrochloride 0,5%), and an ophthalmic gel was placed on the eyes to avoid drying. After scalp incision longitudinally and the retraction of muscle attachments, the skull surface was cleaned by saline solution 0.9%. Bregma and lambda coordinates were determined precisely to examine if the skull was correctly positioned. Holes were drilled in the skull at the antero-posterior (AP) and medio-lateral (ML) coordinates (Paxinos & Franklin, 2004) of the SuML and DG. All viral vectors (1µl of AAV5-DIO-EYFP or AAV5-DIO-(ChR)-EYFP or AAV5-DIO-(HR)-EYFP) were pressure injected bilaterally within the SuML at following coordinates (AP = -2.7; LM = + / - 1.25; DV = -4.8) with a Hamilton syringe associated to a micro-pump associated at a rate of 200 nl / minute and using an angle of 11° to avoid the high vascularization at the midline (Fig. 17).

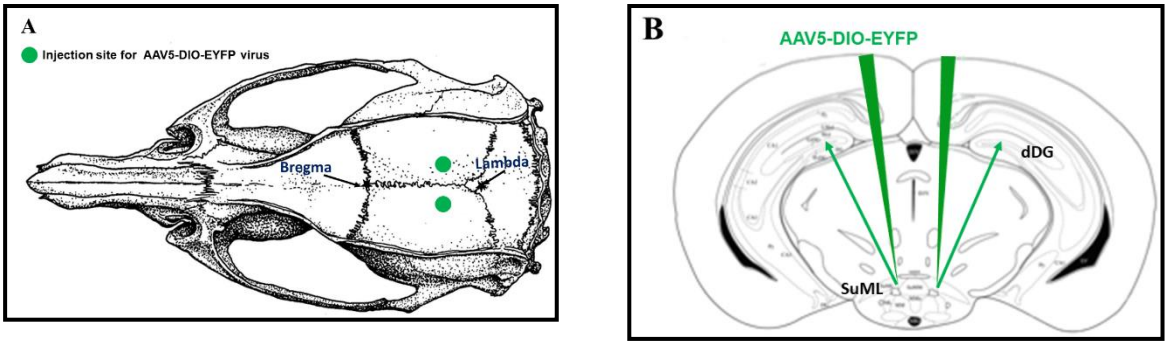

Figure 17: Identification of bregma and lambda locations in mice on stereotaxic apparatus for virus injection. (A) A diagram shows the dorsal surface of the mouse skull at a horizontal plane illustrating the reference points; bregma and lambda and the location of the injection site. **(B)** Diagram of AAV5-EYFP Cre dependent virus injection in SuML bilaterally (Paxinos & Franklin, 2004)**.**

1.1.2 Sham group (n=5)

After injection of the AAV5-DIO-EYFP viral vector, a bipolar electrode (PlasticsOne) Fig.19A was implanted into the DG according to the following coordinates (AP = -2.7; LM = - 1.25; DV = -1.8) and on the other side of the electrode, a screw was implanted to fix the electrode on the head as shown in Fig. 18.

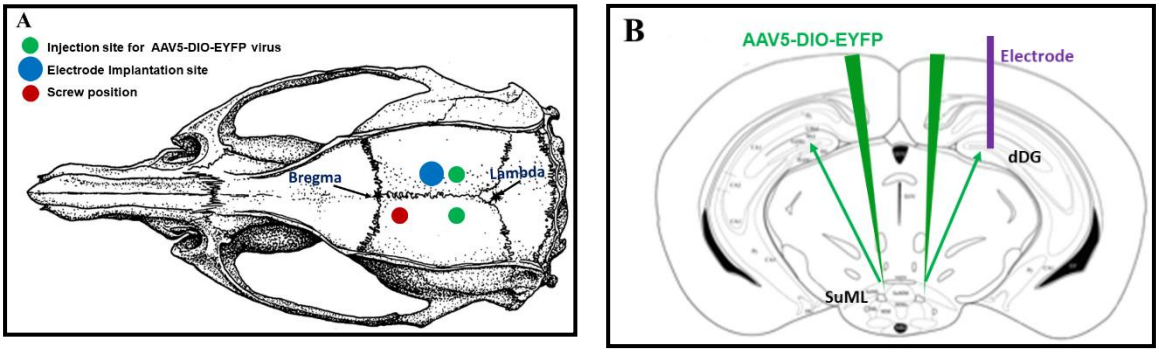

Figure 18: Identification of electrode and virus injection coordinates stereotaxic apparatus for Sham group. (A) A diagram shows the dorsal surface of the mouse skull at a horizontal plane illustrating the reference points; bregma and lambda and the location of the injection site. **(B)** Diagram of AAV5-EYFP Cre dependent virus injection in SuML bilaterally and electrode implantation . (Paxinos & Franklin, 2004)**.**

1.1.3 Epileptic control group (n=2) and Epileptic Channelrhodopsin group (n=3) surgeries

In this group, we need to stimulate, the axon terminals from SuML neurons innervating the

DG and record the DG local field potential (LFP). The optic fiber and the electrode for these groups were implanted together in the DG. Before implantation they were fixed together to form the optrode. It was prepared two days before the surgery.

- **Optrode preparation.**

For this preparation we are using a premade bipolar electrode as shown in Fig. 19A (PlasticsOne) and implantable optical fibers terminated in 1.25-mm diameter ferrules and 5mm length as shown in Fig. 19 B (ThorLabs), Electrode was twisted then bent at 90° to run along the side of the optical fiber. They fixed together by a drop of the glue Fig. 19C.

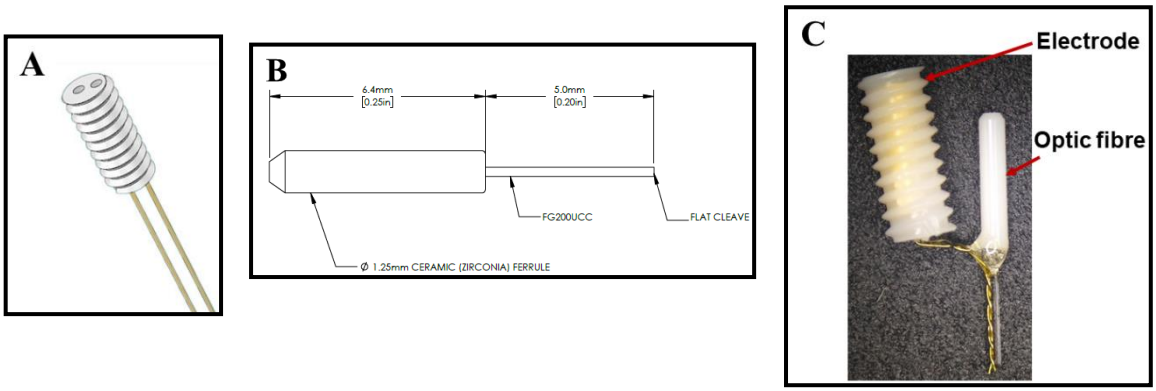

Figure 19: optrode preparation. (A) bipolar electrode (PlasticOne). **(B)** Optic fiber 5 mm (Thorlabs) **(C)** Implantable optrode**.**

- **Optrode implantation.**

After AAV5-DIO-EYFP (Epileptic control mice) or AAV5-DIO-(ChR2)-EYFP (Epileptic *Channelrhodopsin* mice) injection (see above), we implanted the optrode in the dorsal DG of the right hemisphere at the following coordinates (AP = -2.7; LM = - 1.25; DV = -1.8) and a screw on the other side After implantation all the structure were fixed together on the skull by using dental cement (Fig 20). One epileptic control mouse and one epileptic ChR2 mouse died during the surgery

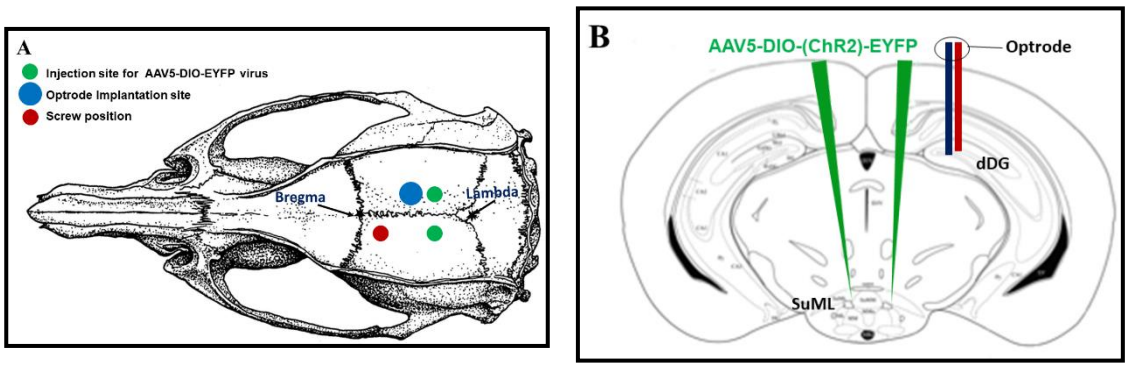

Figure 20: Identification of optrode and virus injection coordinates on stereotaxic apparatus in Epileptic control and ChR mice. (A) A diagram shows the dorsal surface of the mouse skull at a horizontal plane illustrating the reference points; bregma and lambda and the location of virus injection and optrode implantation.**(B)** Diagram of AAV5-DIO-EYFP or AAV5-DIO-(ChR2)-EYFP Cre dependent virus injection in SuML bilaterally (Paxinos & Franklin, 2004)**.**

1.1.4 Halorhodopsin group surgeries. (n=2)

In this group the optic fiber was implanted in the SuML in order to inactivate SUML neurons and the bipolar LFP electrode in the DG.

After AAV5-DIO-(HR)-EYFP injection (see above), the bipolar electrode was implanted in the right DG at the the following coordinates (AP = -2.7; LM = - 1.25; DV = -1.8) and the optic fiber in the SuML at the following coordinates (AP = -2.7; LM = + / - 1.25; DV = -4.8, angle 11°) as illustrate in Fig. 21A and B. One mouse died during the surgery.

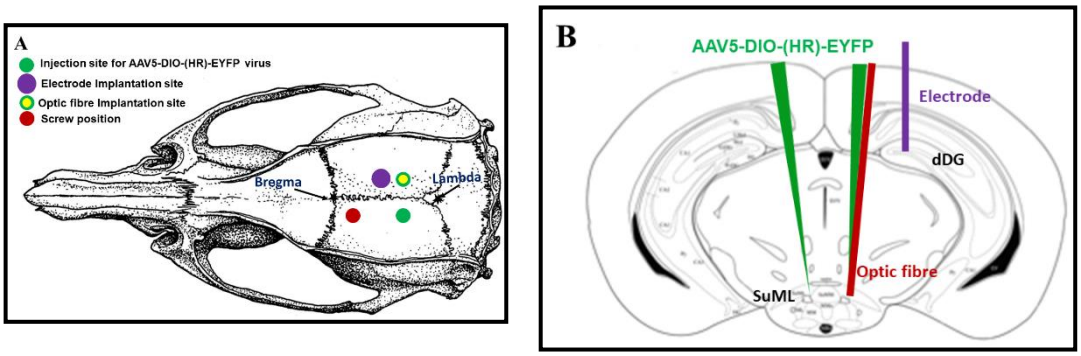

Figure 21: Identification of electrode and virus injection coordinates on stereotaxic apparatus in HR mice. (A) A diagram shows the dorsal surface of the mouse skull at a horizontal plane illustrating the reference points; bregma and lambda and the location of virus injection optic fiber and electrode implantation.**(B)** Diagram of AAV5-DIO-(HR)-EYFP Cre dependent virus injection in SuML bilaterally (Paxinos & Franklin, 2004)**.**

Post- operative recovery.

Animals that survived from surgery **(Sham mice n=5; Epileptic control mouse n=1; Epileptic ChR2 mice n=2; Epileptic HR mouse n=1)** were returned to their cages for three weeks to allow optimal transfection of the opsin or EYFP. After this period of recovery, animals were plugged in the optogenetic apparatus to start the electrical recording and light stimulation.

1.2 Optogenetic recording and stimulation (Closed-loop seizure detection and light delivery).

After the three weeks of recovery period animals were placed in the optogenetic set up (Fig. 22). Under a short-acting inhaled Isoflurane anaesthesia (Aerrane, Baxter; 1 min) mice were connected through an electrical commutator (PlasticOne) to an analogue Brownlee 410 amplifier. The signals were digitized by an NI USB-6221- BNC digitizer (National Instruments) sampled at 2K Hz and analysed in real-time by a PC running a custom MATLAB seizure detection algorithm ((Armstrong *et al.*, 2013a); kindly provided by Dr Soltesz). At the same time, animals were connected to a fiber-coupled diode laser (Shanghai Laser & Optics Century Co., Ltd) of an appropriate wavelength to activate the opsin expression for channelrhodopsin group (blue λ473 nm) and for halorhodopsin group (amber λ589 nm). Optical patch cords (Thorlabs, Doric Lenses) directed the laser light to the mouse through an optical commutator (Doric lenses) and were terminated in a 1.25mm ferrule, which was connected to the implanted optical fiber with a ceramic split sleeve (Precision Fiber Products, Inc.). Continuous video and EEG monitoring were performed for each animal to detect spontaneous recurrent seizures. During the first recording two days, seizures were analyzed in order to characterize parameters that will be used to tune the real-time closed-loop seizure detection software (Armstrong *et al.*, 2013a) to trigger the laser.

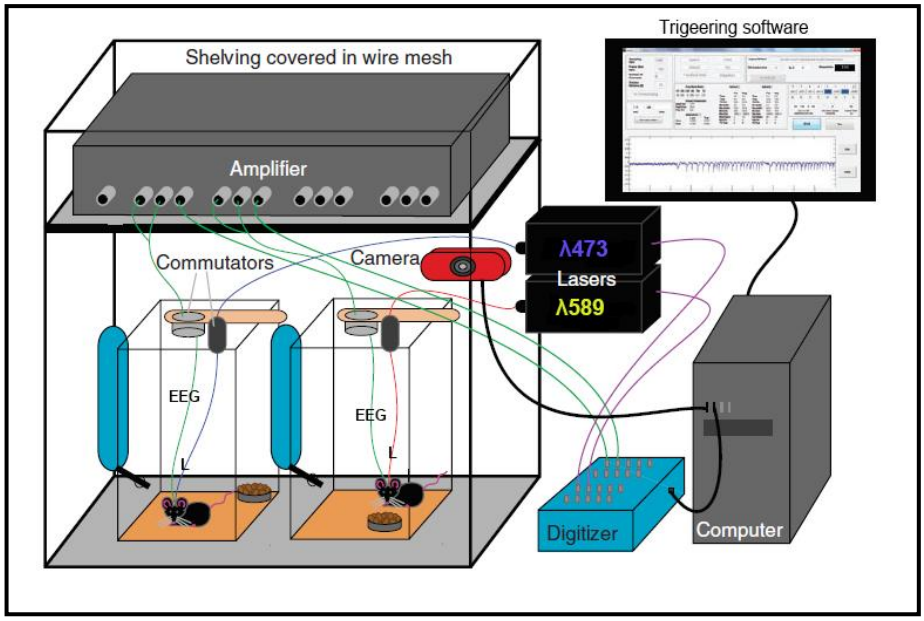

Figure 22: Diagram shows the real-time optogenetics intervention system. (L) red and blue cables for laser stimulation; **(EEG)** green cables for electrical recording; **(λ473)** blue laser; **(λ589)** yellow laser**.** (Armstrong *et al.*, 2013b)**.**

1.2.1 Laser stimulation.

Seizures were detected using custom recording software. The detection was tuned to the specific EEG signature of the seizures in each epileptic animal, using combinations of the spike 1 and 2 features. When the trigger detector met the specified criteria, it is immediately triggered and activated the laser by sending TTL signal (Transistor-Transistor Logic) to the laser. The triggering is adjusted for 50% of cases, meaning that the software does not trigger the laser in 50% of the detected seizures (in a random sequence) in order to have an internal control. Then we adjust the duration of light pulses for each laser:

Blue laser (λ473): (50 ms on, 100 ms off) for 60 s.

Yellow laser (λ589): (2000 ms on, 100 ms off) for 60 s.

1.2.2 Data analysis

For each animal the pattern of distribution of the seizures through out the day and during all recording period (45 to 78 days) was analyzed. In order to estimate the effect of light stimulation on seizure duration, the median seizure duration were calculated for seizures under light stimulation and seizures under no light stimulation for each animal. The duration of the two group of seizure were compared using non-parametric Mann-Whitney two tailed test.

Spectral analysis of the seizure frequency content on pre-whitened LFPs using direct multitaper estimates were performed as previously described by Quilichini et al., 2010). We used a modified version of the multitaper FFT MATLAB package by Mitra and Pesaran (Mitra & Pesaran, 1999) : FFT window size of 2 s, three to five tapers, frequency bins = 0.15 Hz, no overlap between successive windows, time bandwidth = 3. Each seizure was individually detected and thereafter decomposed between 0.1 and 500 Hz. For each animal, the comparison between the frequency contents of seizures of similar duration with or without optogenetic intervention was assessed by using custom-written MATLAB scripts. The standard deviation of the power at each frequency bin was assessed to provide some information regarding the variability of the frequency content of seizures. Behavioral seizures were confirmed by video and EEG analysis. Distribution of seizures for 24hrs for each animal and the number of behavioral and non- behavioral seizures were analyzed for each animal and Comparison between post-detection seizure duration with light and with no light was done with Mann-Whitney two tailed test with GraphPad prism software.

2. Histology

2.1 *Tissue* Preparation

After 2 months of electrophysiological recordings and light stimulation mice were deeply anesthetized with ketamine/ xylazine solution and transcardially perfused with 100 ml of 4% paraformaldehyde (PFA) prepared in 0.12 M sodium phosphate buffer, pH 7.2 - 7.4 (PB). After perfusion, the brains were removed from the skull, post-fixed in the same fixative for 1 h at room temperature (RT) and rinsed in PB cryoprotected in a solution of 20% sucrose in PB overnight at 4°C, quickly frozen on dry ice and sectioned coronally at 40µm with a cryostat. The sections were rinsed in PB, collected sequentially in tubes containing an ethylene glycol-based cryoprotective solution and stored at -20°C until histological process. To determine the general histological characteristics of the tissue along the rostro-caudal axis of the brain every 10 sections was stained with cresyl violet. Selected adjacent sections from each animal were processed for 1) Simultaneous fluorescent in situ hybridization detection of VGLUT2 mRNA and VGAT mRNA within the SuML as previously described in our first and second studies 2) Simultaneous immunohistofluorecent detection of EYFP, VGLUT2 and VGAT within the DG as previously described in our first study. 3) Simultaneous detection of VGLUT1 mRNA and VGAT mRNA within the DG.

2.2 Simultaneous detection of VGLUT1 and VGAT mRNAs with fluorescent In situ hybridization (RNAscope assay).

Selected sections at the level of dorsal DG were first treated with 1% H2O2, rinsed in PB, mounted on SuperFrost Plus slides (Fisher Scientific) and air-dried at room temperature (RT). They were then process for fluorescent RNAscope in situ hybridization (ISH) according to the manufacter's protocol (Advanced Cell Diagnostics). Briefly sections were treated with 100% ethanol and protease III for 30 min at 40°C. They were incubated in a solution containing both RNAscope® Probe - Mm-S1c17a7 (catalog #416631-C2) for detection of VGLUT1 mRNA and Mm-S1c32a1-C3 (catalog #319191-C3) for detection of VGAT mRNA. After hybridization, sections were then processed for visualization using the RNA-scope Multiplex Fluorescent

reagent Kit v2 (Advanced Cell Diagnostics) and the Tyramide Signal Amplification (TSA™) Plus Cyanine 3 and TSA Plus Cyanine 5 systems (Perkin Elmer). All sections were coverslipped with Fluoromount (Electron Microscopy Sciences, Hatfiled, PA, USA).

2.3 Imaging

Sections were analyzed with a Zeiss laser-scanning confocal microscope (LSM 512) (Institute des Neurosciences de la Timone (INT), Aix-Marseille University, France). Images were obtained from a single optical slice or a Z-stacks of optical slices using sequential acquisition of separate wavelength channels to avoid fluorescence cross-talk with objective lenses 10x and 63x (oil immersion lens) and digital zoom 3 at a final definition (2048 pixel X 2048 pixel). Montage were performed using NIH ImageJ and Adobe Photoshop software.

Results.

Behavior and LFP analysis of Epileptic Mice

All mice were recorded five to six weeks after pilocarpine-induced SE for about 8 weeks. All the mice that developed SE after pilocapine injection (fractionated injection, Third protocol) displayed spontaneous seizures, associated to abnormal discharges of neuronal populations recorded by the LFP bipolar electrode in the DG (Fig. 23). No significant differences in the pattern of spontaneous seizures were observed between Epileptic control animal injected with the control viral vector AAV5-EYFP (VGLUT2-EYFP mice), Epileptic mice injected with AAV5-ChR2-EYFP viral vector (VGLUT2-ChR2-EYFP mice) and Epileptic mice injected with AAV5-HR-EYFP viral vector (VGLUT2-HR-EYFP mice). All these animals displayed periods of one to several days with spontaneous seizures that occurred with a frequency of two to eight seizures per day. These periods of seizures were spaced with seizure free periods sometimes lasting more than a week. Most of the seizures occurred during night-time when the animals are mainly active (Fig 24). None of the mice from the Sham group (None SE) displayed spontaneous seizures or abnormal electrical activity.

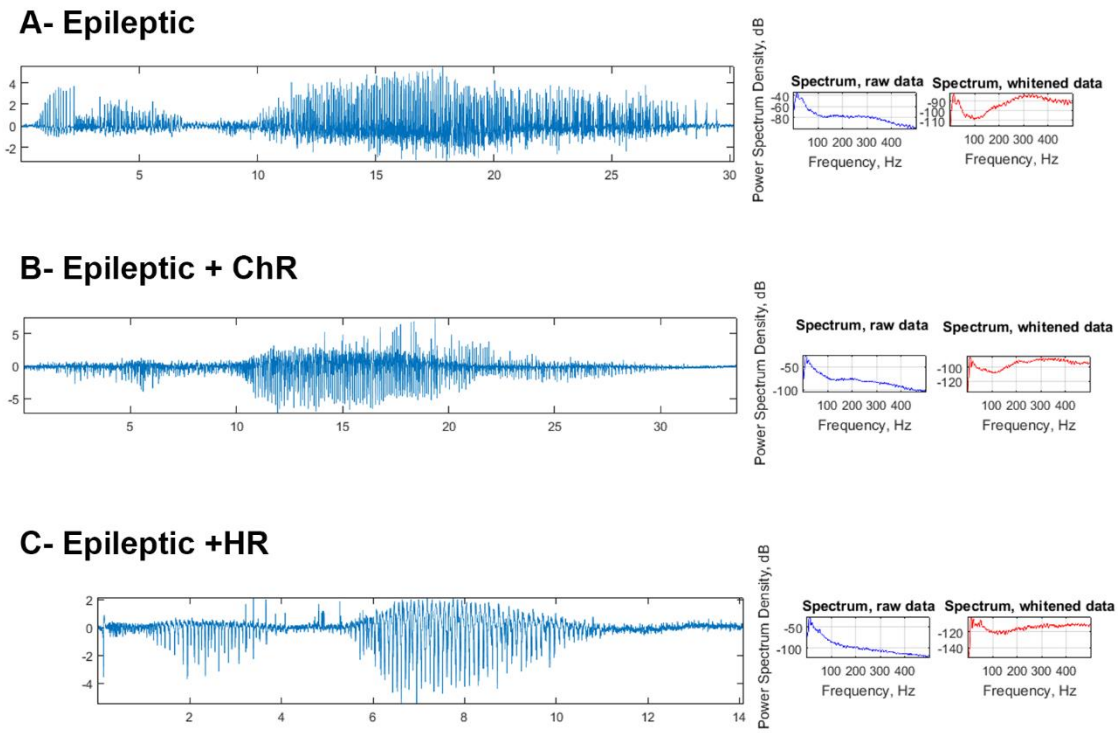

Figure 23: Field potential recording by EEG system for epileptic animals. A- Epileptic VGLUT2 -EYFP mouse, **B-** Epileptic VGLUT2 -ChR-EYFP mouse, **C-** Epileptic VGLUT2 -HR-EYFP mouse.

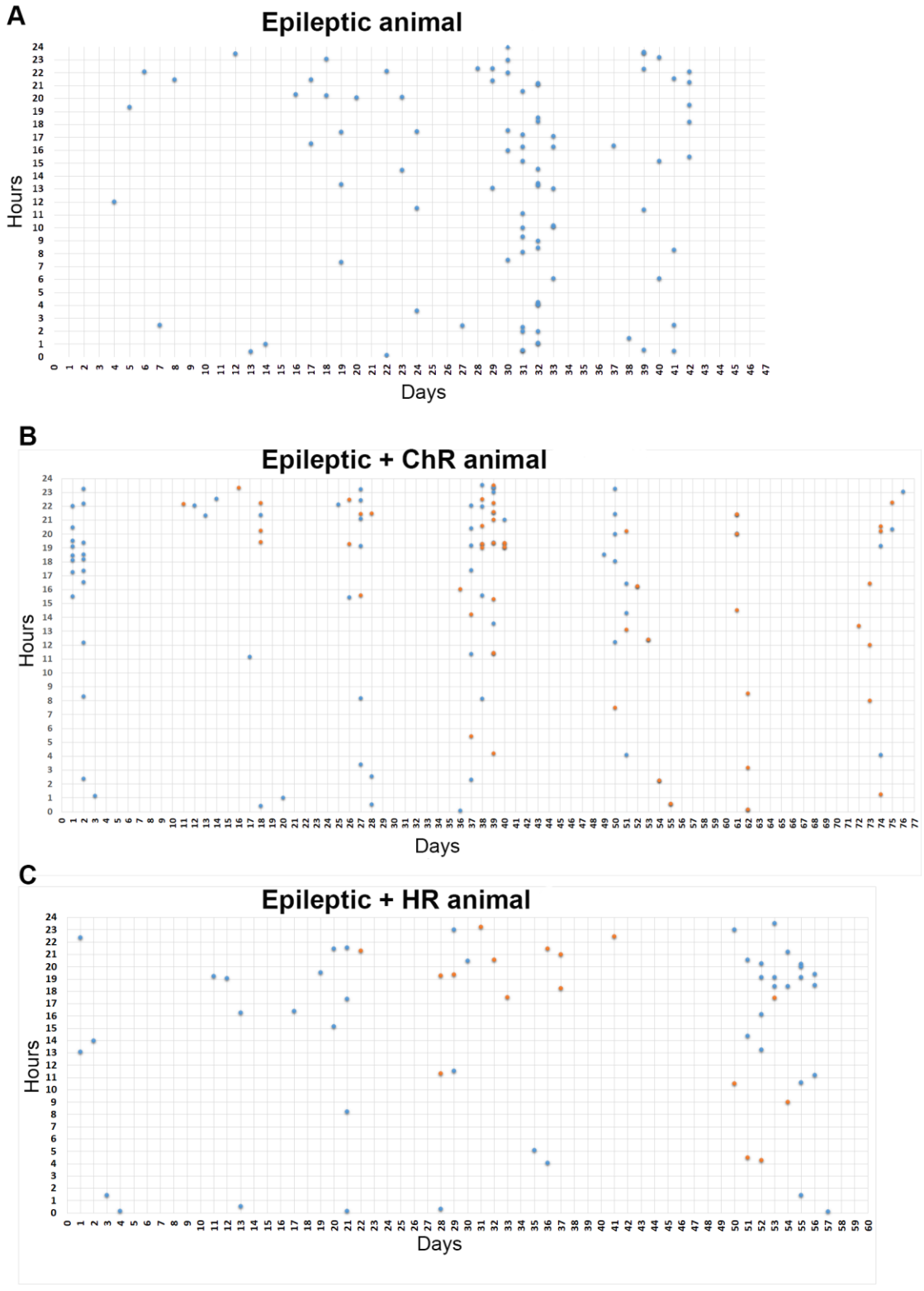

Figure 24: Epileptic seizures time course over 8 weeks. A- Epileptic VGLUT2 -EYFP mouse, **B-** Epileptic VGLUT2 -ChR-EYFP mouse, **C-** Epileptic VGLUT2 -HR-EYFP mouse. **B, C** Laser off (blue dots), laser on (orange dots).

Effect of activation of the SuML-DG pathway on seizure activity.

No significant differences in seizure duration was observed between seizures exposed to light stimulation (blue, 473 nm) and seizures none exposed to light for the two VGLUT2-ChR2-EYFP epileptic mice (median duration, Mouse 1: laser on = 38 ± 8.646 s, laser off = 32 ± 9.177 S.; *p*= 0.1054*;* Mouse 2: laser on = 39 ± 7.550 s, laser off = 32 ± 9.676 S.; *p*= 0.0476*; Mann-Whitney two tailed test)* Fig, 25A,B. In addition, no change in animal behavior and behavioral seizure were observed during light stimulation. The only change we observed in both animals was an increase in the frequency of non-behavioral seizures after 4 weeks of light stimulation (11 weeks after SE) and after 6 weeks of stimulation (13 weeks after SE) an increase of seizure duration for both conditions (laser on and off) without apparent change in seizure behavior.

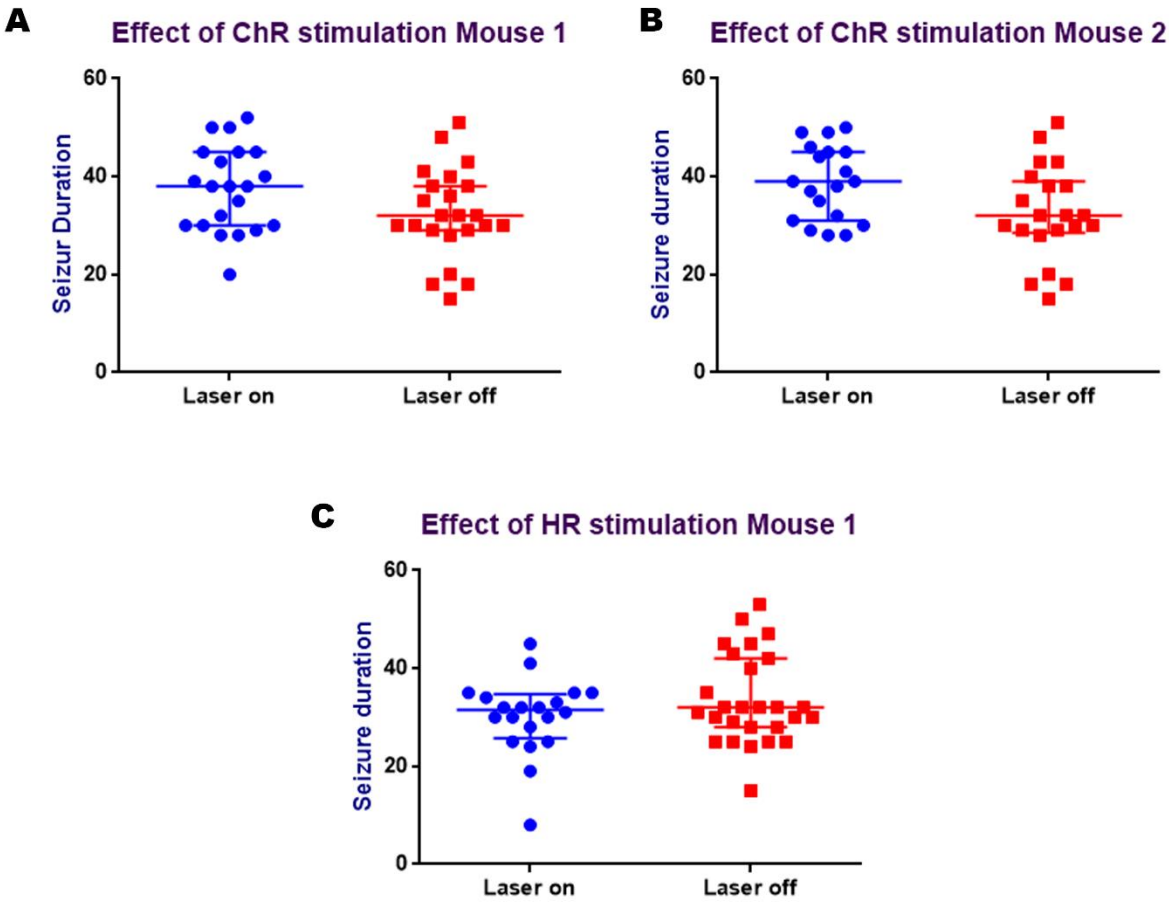

Figure 25: The distributions of seizure around the median number of seizure duration. A and B- epileptic VGLUT2 -ChR-EYFP mouse in which SuM bouton in the DG are activated by ChR ("laser on", blue; " laser off", red); **B-** epileptic VGLUT2 -HR-EYFP mouse in which the cell bodies of the SuM neurons were inhibited by HR ("laser on", blue; " laser off", red).

In order to estimate a potential effect of light stimulation in seizure dynamics, we characterized

the frequency content of all the seizures for each of the two Epileptic VGLUT2-ChR2-EYFP mice. All seizures in both animals, showed a high power in the 10 Hz and 30 Hz frequency bands, as well as in the high frequency domain (200-400 Hz) (Fig. 26).

Activation of axon terminals from SuML neurons did not affect significantly the power of these bands in both. However, the distribution of these power values was changed, the variance showing increased values when the boutons were stimulated (Fig. 26a). Therefore, activation of SuML-DG pathway showed a tendency to increase the variability of seizure dynamics but does not display a beneficial or detrimental effect on the seizures.

Effect of the Inhibition of SuML neurons on seizure activity.

Unilateral light stimulation with amber light (589 nm) of SuML neurons in the Epileptic VGLUT2-HR-EYFP mouse did not affect seizure duration (median duration, laser on = 31 ± 7.791 s, laser off = 32 ± 9.120 S. n = 1 animal; *p*= 0.5592*; Mann-Whitney two tailed test*) Fig, 25C. Animal behavior during seizure was not different when laser was turned on or turned off. However, we noticed that after light delivery condition, many interictal spikes were following the seizures. No non-behavioral seizure was recorded in this animal.

We then performed an analysis of the frequency content of seizures recorded in this Epileptic VGLUT2-HR-EYFP mouse. Light stimulation of the SuML neurons did not modify the power of the 10 Hz, 30 Hz and high frequency (200-400 Hz) bands observed during seizures, as shown in Fig. 26b. However, it decreased strongly the variance of the power values of these bands, suggesting that the seizures dynamics became less variable when SuM neurons are inhibited. Such effect might be caused by a complex network effect, since neurons in this region not only innervate the DG but also other brain regions such as the CA2/CA3a region and the septum.

A- Epileptic+ChR

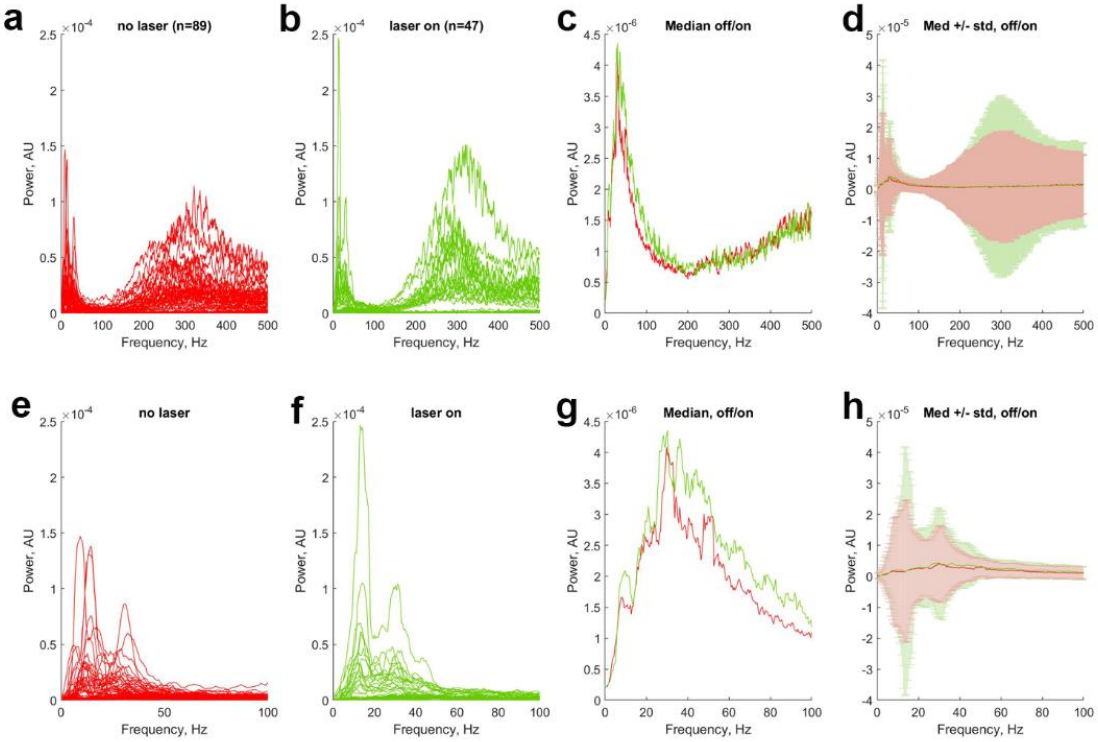

B- Epileptic+HR

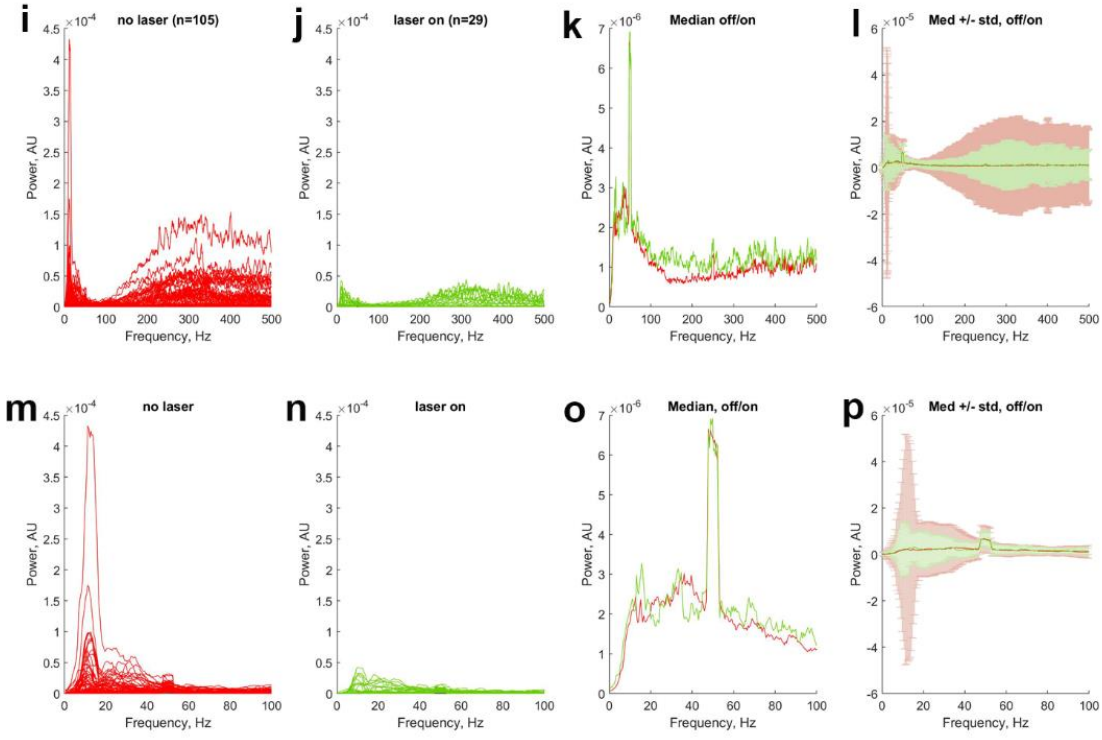

Figure 26: Spectral analysis of the seizure content for both control and optogenetic manipulation of the SuM in. A- one epileptic VGLUT2 -ChR-EYFP mouse in which SuM bouton in the DG are activated by ChR ("laser on", green curves; "no laser", red curves); **B-** one epileptic VGLUT2 -HR-EYFP mouse in which the cell bodies of the SuM neurons were inhibited by HR ("laser on", green curves; "no laser", red curves). **a, b, c, d and l, j, k, l** shows power spectra between 0.1 and 500 Hz, and **e, f, g, h and m, n, o , p** shows the same spectra between 0.1 and 100 Hz in order to visualize the 10 Hz and 30 Hz bands better, which are characteristic bands present during the seizure. **a, b, e, f and l, j, m, n** display the overlay of the power spectra of all the seizures in "no laser" and "laser on" conditions. The **c, g and k, o** shows the median spectra in both conditions. The **d, h and l, p** shows the median spectra ± the standard deviation (std) for each frequency bin. Note the increased std for the ChrR stimulation of the SuM boutons and the decreased std for the HR inhibition of SuM neurons in the 10 Hz, 30 Hz and high frequency bands stated above.

Histological profiles of Sham and Epileptic mice,

Cresyl violet staining was performed in sections of Epileptic control, CHR2 and HR mice as well of Sham mice in order to determine the extent and location of general neuronal loss within the hippocampus following three to four months of pilocarpine –induced spontaneous seizures and light activation of SuML-DG pathway or inhibition of SuM neurons. All Epileptic mice displayed a consistent cell loss in the hilus of the DG (Fig., 27). In sections from Epileptic mice showed less stained neurons in the hilus (Fig., 27 C-H) than that in Sham animals (Fig 27., A-B). This cell loss was particularly striking in the Epileptic control mouse (VGLUT2-EYFP mouse). Although the loss of neurons was clear it was not total and some remaining cell bodies were observed in the hilus. Whereas the Epileptic control mouse showed variable amount of cell los in the CA3 and CA1 hippocampal region (Fig 27 C), the CA1-CA3 pyramidal layers in Epileptic VGLUT2-ChR2 and VGLUT2-HR-mice (Fig 27 E, G) were relatively well preserved. All Epileptic mice displayed changes in the shape of the DG, but no evident cell loss of dentate granule cells was observed. The epileptic control mouse displayed an enlarge granule cell layer resulting from dispersion of these cells particularly evident in the ventral blade (Fig. 27 C, D).

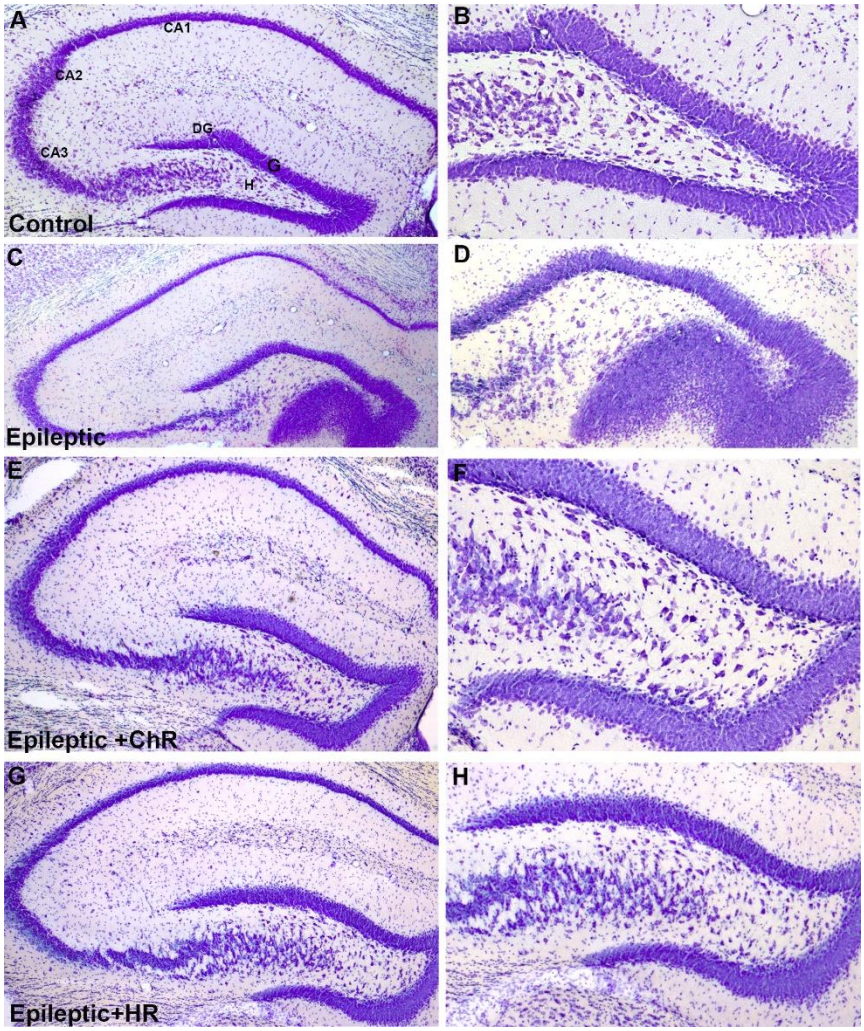

Figure27: Hippocampal changes in pilocarpine induced animals. **A, B-** Control VGLUT2 -EYFP mouse, **C, D-** Epileptic VGLUT2 -EYFP mouse, **E,F-** Epileptic VGLUT2 -ChR-EYFP mouse, **G,H-** Epileptic VGLUT2 -HR-EYFP mouse. **B, D, F, H** -high power magnification of Dorsal DG. **CA1, CA2, CA3: CA1-3** fields of the Ammon Horn; **DG**: dentate gyrus; **G**: layer of granular cells; **H**: hillus

In situ hybridization for detection of VGLUT1-mRNA containing neurons and VGAT mRNA containing interneurones in the DG of Sham and Epileptic mice.

We further characterized the population of neurons responsible of the cell loss observed in the hilus of the DG in epileptic mice. The hilus of the DG contains two main populations of neurons, the mossy cells glutamergic neurons labeled for the vesicular glutamate transporter 1 (VGLUT1) mRNA (Fig. 28, green, arrowheads) and GABAergic interneurons labeled for the vesicular GABA transporter (VGAT) mRNA (Fig 28, red, arrows). Whereas in Sham mice numerous VGLUT1-mRNA containing neurons (arrowheads) and VGAT-containing interneurones (arrows) were present in the hilus of the DG (Fig.28 A), only very few VGAT-mRNA containing interneurons and some VGLUT1 mRNA containing neurons were detected in that of epileptic animals (Fig., 28 B). These data illustrate the major loss of the GABAergic interneurones and at lesser extent of presumed mossy cells in the hilus of the DG in all epileptic mice

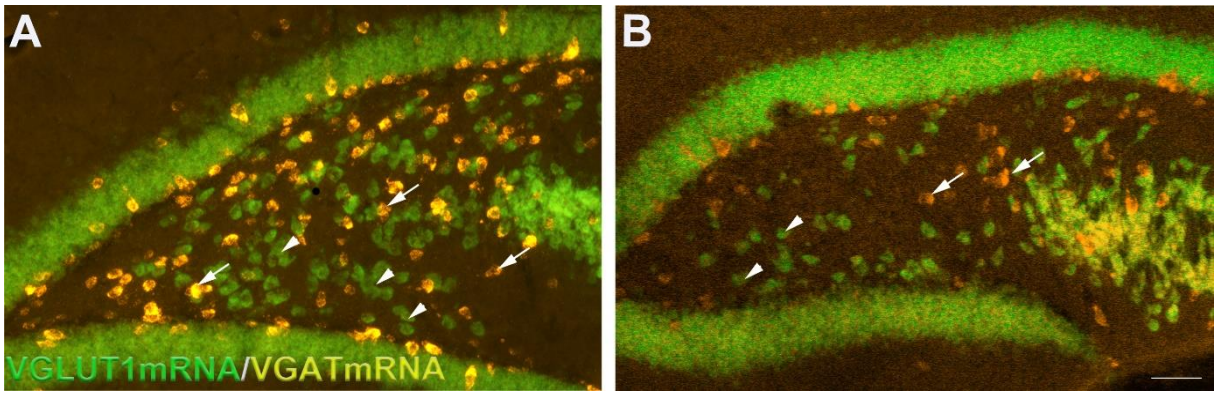

Figure 28: Cell loss in pilocarpine induced mice in Hilus. A- Sham VGLUT2 -EYFP mouse, **B-** Epileptic VGLUT2 -EYFP mouse. VGATmRNA (yellow; arrow) GABAergic interneuron, VGLUT1mRNA (green; head arrow) Glutamergic neurons Scale bar: 100 µm.

In situ hybridization for detection of VGLUT2 / VGAT mRNAs containing neurons in the SuM region of Sham and Epileptic mice.

Our previous studies performed in the same transgenic mouse strain demonstrate that SuM neurons projecting to the dorsal DG co-express markers for GABAergic (VGAT mRNA) and glutamatergic (VGLUT2 mRNA) neurotransmissions. These neurons are located mainly round and above the mammillary tract (mt) within the SuML. Simultaneous detection of VGAT and VGLUT2 mRNAs were performed in this study in order to evaluate possible alteration of these populations of VGAT/VGLUT2 mRNAs containing neurons in epileptic mice. Our results demonstrate the presence of many neuronal cell bodies that co-express mRNA for VGLUT2 and VGAT mRNAs in SuML not only in Sham (non-epileptic) VGLUT2 -EYFP mice (Fig. 29A) but also in all Epileptic mice (Fig 29C and D) including Epileptic control VGLUT2-EYFP (Fig. 29B), Epileptic VGLUT2-ChR2-EYFP (Fig 29 C) and Epileptic VGLUT2-H -EYFP mice (Fig 29 D). Therefore, Epileptic mice did not display, at least at a qualitative level of analysis, major alteration of the population of neurons co-expressing VGAT and VGLUT mRNA within the SuML. In epileptic animals these SuM neurons are present and conserved their dual GABA / GLU neurochemical phenotype.

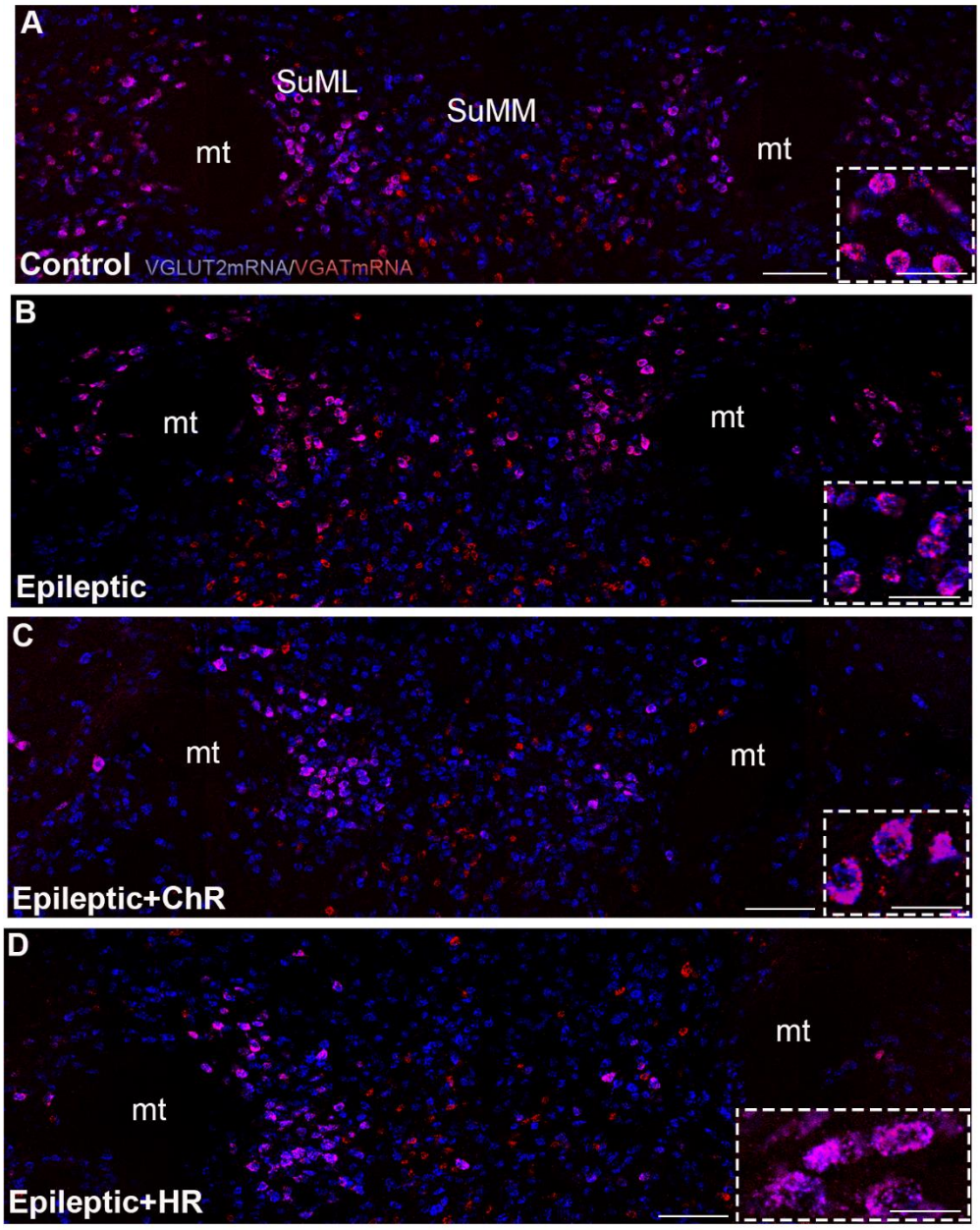

Figure 29: Co-expression of vesicular GABA transporter (VGAT) and glutamate (VGLUT2) mRNA in the supramammilary lateral nucleus (SuML). A- Control VGLUT2 -EYFP mouse, **B-** Epileptic VGLUT2 -EYFP mouse, **C-** Epileptic VGLUT2-ChR-EYFP mouse, **D-** Epileptic VGLUT2 -HR-EYFP mouse. **SuML:** supramammillary lateral region; **SuMM:** supramammillary medial region; **mt:** mammillary tract. Scale bar: A 100 µm; B 150µm; C,D 120µm , Zoom 100µm.

Simultaneous detection of VGLUT2, VGAT and EYFP containing terminals within the dorsal DG of sham and epileptic mice

Numerous axon terminals from SuML neurons labeled for EYFP protein (Fig. 30, green) containing both VGLUT2 (blue) and VGAT (red) proteins where observed within the dorsal DG in Sham (non-epileptic) VGLUT2-EYFP mice (Fig. 30 A-E) as well as in Epileptic mice (Fig. 30F-J). However, there is a clear difference in the distribution of these fibers and axonal terminals from SuML between epileptic and Sham mice. In non-epileptic animals these axonal terminals were restricted to the supragranular (SG) and granule cell layer (G) of DG (Fig. 30 B, D) as described in our previous studies. Whereas epileptic mice (Fig. 30 F-T) displayed an aberrant distribution for these EYPF-containing fibers and terminals compared to the Sham animals. Indeed, in these epileptic mice many labeled fibers giving rise to axon terminals were present not only in the SGL and G but throughout the entire inner molecular layer (IML) (Fig. 30, F, K, P). Many if not all these axon terminals labeled for EYFP contained VGAT and VGLUT2 in sham mice as described in our previous study and in rat (Soussi et al., 2010) as well as in Epileptic control VGLUT2-EYPF (Fig. 30 F-J) and VGLUT2-HR (P-T) mice similar to that described in rat (Soussi et al., 2015). However, in Epileptic VGLUT2-ChR2 mice many of these boutons contained only VGLUT2 (Fig. 30 K-O).

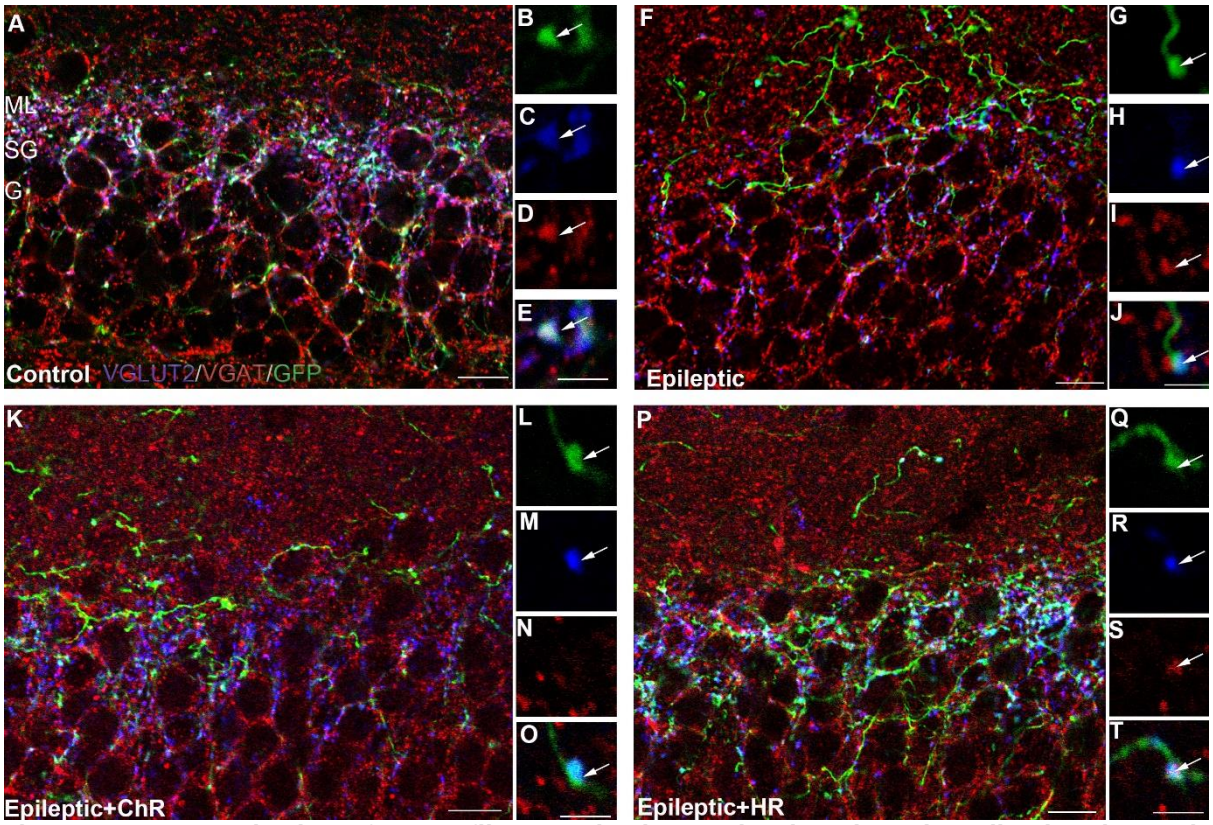

Figure 30: Reorganization of SuML fibers projecting to the dorsal DG in epileptic mice and co-expression of VGLUT2 and VGAT proteins at these projections in epileptic and non-epileptic mice. Confocal images of dorsal DG coronal sections showing the protein expression of VGAT vesicular transporters (red), VGLUT2 (blue) and EYFP protein (green). Epileptic animals show an aberrant distribution characterized by terminals from SuML that completely invade the internal molecular layer (ML) of the dorsal DG (F, K, P) relative to control (A). Numerous axonal pimples from the dorsal DG-innervating SuML neurons, which are labeled with the EYFP fluorescent protein, contain both VGLUT2 (blue) and VGAT (red) proteins in control (non-epileptic) VGLUT2 -EYFP mice. (A, B-E) as in VGLUT2-EYFP /VGLUT2-ChR2-EYFP/ VGLUT2-HR-EYFP epileptic (F-T) mice at the level of the supragranular (SG) and granule (G) layer. Scale bar A, F, K, P 25μm; B-E, G-J, L-O, Q-T 5μm.

Discussion

The main goal of this study was to determine whether SuML neurons that innervate the dorsal DG could modulate seizure activity in the model of chronic limbic seizures induced by pilocarpine in mouse. This study was initiated following Soussi et al. (2015) works showing that axon fibers and terminals originating from SuML neurons innervating the dorsal DG spout and establish aberrant synaptic contact on dentate granule cells in epileptic pilocarpine-treated rat. Such sprouting suggested that the SuML-DG pathway could be instrumental to trigger or modulate seizure activity within the hippocampus.

First our study confirms the general histological pattern of cell loss including GABAergic and at a lesser extent glutamatergic neurons within the hilus of the DG in this model of chronic limbic seizures induced by pilocarpine in transgenic VGLUT2-Cre mice, previously described in Pilocarpine treated mice and rat (see for review Houser 2014). We further establish the axonal spouting of the SUML-DG pathway in these epileptic-treated mice. The axons of SuML neurons invade the entire inner molecular layer of the DG as described in the rat pilocarpine model (Soussi *et al.*, 2015). In addition, we demonstrate at the mRNA and protein levels that most of these neurons within the SuML that project to the DG co-express markers of the glutamatergic (VGLUT2) and GABAergic (VGAT) neurotransmissions in epileptic mice as in naïve mice (Billwiller *et al.*, 2019; Elseedy *et al.*, 2019) or rats (Boulland *et al.*, 2009; Soussi *et al.*, 2010). These VGAT/VGLUT2 neurons in epileptic mice are therefore potentially able to co-release GABA and Glutamate as demonstrated in naïve mice (Pedersen *et al.*, 2017; Hashimotodani *et al.*, 2018; Billwiller *et al.*, 2019). In naïve mice such co-release of GABA and Glutamate induces net excitatory effects on GCs and potentiate GCs firing when temporally associated with perforant path inputs (Hashimotodani *et al.*, 2018). Such co-release will have to be tested in Epileptic VGLUT2-ChR2-EYFP mice. However this group of epileptic mice displays differences with the two other groups of Epileptic animals as well as with sham mice regarding the protein content in VGLUT2 and VGAT in SuML axon terminals innervating the DG. Indeed, in these mice the axon terminals from SuML neurons show an apparent depletion in the VGAT protein

content. Most of these EYFP labeled terminals within the IML contain VGLUT2 and not or very low level of VGAT, in contrast to the SuML boutons in Epileptic control mice or Epileptic VGLUT2-HR mice.

In all cases the SuML-DG pathway through its excitatory effect on GCs could contribute to trigger seizures or to increase seizure activity within a hyperexcitable DG.

Specific activation of SuML-DG pathway or inhibition of SuM neurons does not modify seizure duration but could increases seizure heterogeneity

Our preliminary electrophysiological results show no significant difference in seizure duration following specific activation of the SUML-DG pathway suggesting that this pathway cannot modulate intensity of the seizure. However, our results reveals that when activated during seizures this pathway increases the variability of power in the frequency bands around theta and in the high frequency bands suggesting that this pathway could facilitate expression of different types of seizures. Such hypothesis will have to be tested but interestingly all Epileptic VGLUT2-ChR2 mice seems to display after several weeks of light stimulation an increase of none behavioral seizures. Such increase was not observed in Epileptic control mice or Epileptic VGLUT2-HR mice.

Our results are very preliminary and need a more detailed analysis of the different types of seizures (behavioral versus non-behavioral seizures). In addition, the experimental design needs clearly to be modified. Indeed, in our protocol we have modulated the SuML-DG pathway in only one hemisphere whereas this model of chronic limbic seizure is bilateral. In such bilateral model, spontaneous seizures have equal probability to emerge from one or the other of these hemispheres. Therefore, we could have underestimated the effect of activation of this pathway on seizure duration. Our next animals will have to be implanted with an optrode in each DG.

Inactivation of neurons within the SUML does not modify seizure duration but could decrease the heterogeneity of seizures

Our results show that light inactivation of neurons within the SuML region in epileptic VGLUT2-HR mice, does not modified seizure duration. They indicate that inactivation of these neurons decrease the variability of seizure dynamic reflected by a decreased variability of frequency band power. It suggests that inactivation of these neurons decrease seizure heterogeneity. This effect cannot be relate exclusively to the inactivation of SuML neurons innervating the DG and more likely reflect a network effect. Indeed, despite many neurones within the SuML region correspond to GABA/GLU neurons innervating the DG (Billwiller *et al.*, 2019; Elseedy *et al.*, 2019), the SuML contains other types of VGLUT2-containing cells that have been described in rat to project to others brain structures including the septum or the entorhinal cortex (see for review Pan and McNaughton, 2004). These two structures are also known to innervate the DG. Again this experimental design has to be modified in order to evaluate the effect of the specific inhibition of the SuML-DG pathway. Such approach cannot be performed through light stimulation of HR-expressing axon terminals innervating the DG. Indeed, silencing axon terminal have limited physiological effects as compared to somatic silencing due partly to the ionic composition of the axonal cytosol that differ from the somatodendritic cytosol (Mahn *et al.*, 2016; Wiegert *et al.*, 2017). An approach using retrograde viral vector (such as rAAV or CAV_2) to transfect specifically the SuML-DG with inhibitory or excitatory opsin is developed in the Lab.

Conclusion & Perspectives

The results obtained during my PhD research work contribute to better understand not only the anatomical and physiological properties but also the role of the SuML-DG pathways in physiological condition and in mesial temporal lobe epilepsy. By combining innovative structural connectivity techniques using neurotropic viral vectors (rabies virus, AAV), neurochemical anatomy (immunohistochemistry, in situ hybridization) and imaging (light, electron and confocal microscopy) with optogenetic and electrophysiological recordings performed in transgenic VGLUT2-cre mice:

1) I fully characterize the properties of the SuML-DG projection in the VGLUT2-cre trangenic mouse strain allowing to demonstrate at the anatomical and neurochemical level as well as physiological level the unique properties of the SUML-DG pathways, able to co-release both Glutamate and GABA on DG granule cells (GCs). We provide evidence that this SuML-DG pathway is responsible for the increase of theta power and frequency as well as gamma power and firing of GCs observed in the DG during REM Sleep.

2) I demonstrate the heterogeneity of the population of SuML GABA/GLU neurons innervating the dorsal DG. Among these GABA/GLU neurons 64 %% contain calretinin whereas 36% do not. These two populations are topographically organized, GABA/GLU SuML neurons containing calretinin being more numerous within the rostral part of this nucleus. These two populations of SUML neurons innervating the DG could display different electrophysiological properties and play different roles in the control of DG activity and functions.

3) We confirm in the model of chronic limbic seizures induced by pilocarpine in VGLUT2-cre transgenic mice we developed: the structural plasticity of the SuML-dDG pathway in epileptic animals. We fail to demonstrate a modulator effect of the SUML-DG pathway on seizure intensity (seizure duration). However, our results suggest that the SuM could control seizure dynamic.

After the results obtained in the pilot study conducted in epileptic mice our first goal is to modify the experimental protocol in order to silence and activate specifically this pathway in both DG during seizure or between seizure to better understand its role in control of seizure activity. We will in particular examine whether this pathway could facilitate emergence of seizure during specific vigilance states

References

Abrahams, S., Morris, R.G., Polkey, C.E., Jarosz, J.M., Cox, T.C., Graves, M., & Pickering, A. (1999) Hippocampal involvement in spatial and working memory: a structural MRI analysis of patients with unilateral mesial temporal lobe sclerosis. *Brain Cogn.*, **41**, 39–65.

Amaral, D.G. & Witter, M.P. (1989) The three-dimensional organization of the hippocampal formation: a review of anatomical data. *Neuroscience*, **31**, 571–591.

André, V., Marescaux, C., Nehlig, A., & Fritschy, J.M. (2001) Alterations of hippocampal GAbaergic system contribute to development of spontaneous recurrent seizures in the rat lithium-pilocarpine model of temporal lobe epilepsy. *Hippocampus*, **11**, 452–468.

Aranda, L., Santín, L.J., Begega, A., Aguirre, J.A., & Arias, J.L. (2006) Supramammillary and adjacent nuclei lesions impair spatial working memory and induce anxiolitic-like behavior. *Behav. Brain Res.*, **167**, 156–164.

Armstrong, C., Krook-Magnuson, E., Oijala, M., & Soltesz, I. (2013a) Closed-loop optogenetic intervention in mice. *Nat. Protoc.*, **8**, 1475–1493.

Armstrong, C., Krook-Magnuson, E., Oijala, M., & Soltesz, I. (2013b) Closed-loop optogenetic intervention in mice. *Nat. Protoc.*, **8**, 1475–1493.

Artinian, J., Peret, A., Mircheva, Y., Marti, G., & Crépel, V. (2015) Impaired neuronal operation through aberrant intrinsic plasticity in epilepsy. *Ann. Neurol.*, **77**, 592–606.

Aschauer, D.F., Kreuz, S., & Rumpel, S. (2013) Analysis of Transduction Efficiency, Tropism and Axonal Transport of AAV Serotypes 1, 2, 5, 6, 8 and 9 in the Mouse Brain. *PLOS ONE*, **8**, e76310.

Babb, T.L., Kupfer, W.R., Pretorius, J.K., Crandall, P.H., & Levesque, M.F. (1991) Synaptic reorganization by mossy fibers in human epileptic fascia dentata. *Neuroscience*, **42**, 351–363.

Bannerman, D.M., Yee, B.K., Good, M.A., Heupel, M.J., Iversen, S.D., & Rawlins, J.N. (1999) Double dissociation of function within the hippocampus: a comparison of dorsal, ventral, and complete hippocampal cytotoxic lesions. *Behav. Neurosci.*, **113**, 1170–1188.

Bantel-Schaal, U., Hub, B., & Kartenbeck, J. (2002) Endocytosis of Adeno-Associated Virus Type 5 Leads to Accumulation of Virus Particles in the Golgi Compartment. *J. Virol.*, **76**, 2340–2349.

Bartolomei, F., Wendling, F., Bellanger, J.-J., Régis, J., & Chauvel, P. (2001) Neural networks involving the medial temporal structures in temporal lobe epilepsy. *Clin. Neurophysiol.*, **112**, 1746–1760.

Ben-Ari, Y. & Cossart, R. (2000) Kainate, a double agent that generates seizures: two decades of progress. *Trends Neurosci.*, **23**, 580–587.

Ben-Ari, Y., Crepel, V., & Represa, A. (2008) Seizures beget seizures in temporal lobe epilepsies: the boomerang effects of newly formed aberrant kainatergic synapses. *Epilepsy Curr.*, **8**, 68–72.

Ben-Ari, Y., Tremblay, E., Riche, D., Ghilini, G., & Naquet, R. (1981) Electrographic, clinical and pathological alterations following systemic administration of kainic acid, bicuculline or pentetrazole: metabolic mapping using the deoxyglucose method with special reference to the pathology of epilepsy. *Neuroscience*, **6**, 1361–1391.

Berg, A.T. (2008) Risk of recurrence after a first unprovoked seizure. *Epilepsia*, **49 Suppl 1**, 13–18.

Bettus, G., Wendling, F., Guye, M., Valton, L., Régis, J., Chauvel, P., & Bartolomei, F. (2008) Enhanced EEG functional connectivity in mesial temporal lobe epilepsy. *Epilepsy Res.*, **81**, 58–68.

Beuckmann, C.T., Sinton, C.M., Miyamoto, N., Ino, M., & Yanagisawa, M. (2003) N-type calcium channel alpha1B subunit (Cav2.2) knock-out mice display hyperactivity and vigilance state differences. *J. Neurosci. Off. J. Soc. Neurosci.*, **23**, 6793–6797.

Billwiller, F., Castillo, L., Elseedy, H., Ivanov, A., Scapula, J., Ghestem, A., Abdelmeguid, N., Krook-

Magnuson, E., Soltesz, I., Bernard, C., Luppi, P.-H., & Esclapez, M. (2019) The Supramammillary – dorsal Dentate Gyrus pathway that display unique GABA and Glutamate co-transmission properties increases theta and gamma powers in the DG during REM sleep.

Billwiller, F., Renouard, L., Clement, O., Fort, P., & Luppi, P.-H. (2017) Differential origin of the activation of dorsal and ventral dentate gyrus granule cells during paradoxical (REM) sleep in the rat. *Brain Struct. Funct.*, **222**, 1495–1507.

Blümcke, I., Beck, H., Lie, A.A., & Wiestler, O.D. (1999) Molecular neuropathology of human mesial temporal lobe epilepsy. *Epilepsy Res.*, **36**, 205–223.

Bolte, S. & Cordelières, F.P. (2006) A guided tour into subcellular colocalization analysis in light microscopy. *J. Microsc.*, **224**, 213–232.

Borhegyi, Z. & Leranth, C. (1997) Distinct substance P- and calretinin-containing projections from the supramammillary area to the hippocampus in rats; a species difference between rats and monkeys. *Exp. Brain Res.*, **115**, 369–374.

Bouilleret, V., Ridoux, V., Depaulis, A., Marescaux, C., Nehlig, A., & Le Gal La Salle, G. (1999) Recurrent seizures and hippocampal sclerosis following intrahippocampal kainate injection in adult mice: electroencephalography, histopathology and synaptic reorganization similar to mesial temporal lobe epilepsy. *Neuroscience*, **89**, 717–729.

Boulland, J.-L., Ferhat, L., Solbu, T.T., Ferrand, N., Chaudhry, F.A., Storm-Mathisen, J., & Esclapez, M. (2007) Changes in vesicular transporters for γ-aminobutyric acid and glutamate reveal vulnerability and reorganization of hippocampal neurons following pilocarpine-induced seizures. *J. Comp. Neurol.*, **503**, 466–485.

Boulland, J.-L., Jenstad, M., Boekel, A.J., Wouterlood, F.G., Edwards, R.H., Storm-Mathisen, J., & Chaudhry, F.A. (2009) Vesicular Glutamate and GABA Transporters Sort to Distinct Sets of Vesicles in a Population of Presynaptic Terminals. *Cereb. Cortex*, **19**, 241–248.

Boyce, R., Glasgow, S.D., Williams, S., & Adamantidis, A. (2016) Causal evidence for the role of REM sleep theta rhythm in contextual memory consolidation. *Science*, **352**, 812–816.

Boyden, E.S., Zhang, F., Bamberg, E., Nagel, G., & Deisseroth, K. (2005) Millisecond-timescale, genetically targeted optical control of neural activity. *Nat. Neurosci.*, **8**, 1263–1268.

Bras, H., Gaytán, S.P., Portalier, P., Zanella, S., Pásaro, R., Coulon, P., & Hilaire, G. (2008a) Prenatal activation of 5-HT $_{2A}$ receptor induces expression of 5-HT $_{1B}$ receptor in phrenic motoneurons and alters the organization of their premotor network in newborn mice. *Eur. J. Neurosci.*, **28**, 1097–1107.

Bras, H., Gaytán, S.P., Portalier, P., Zanella, S., Pásaro, R., Coulon, P., & Hilaire, G. (2008b) Prenatal activation of 5-HT2Areceptor induces expression of 5-HT1Breceptor in phrenic motoneurons and alters the organization of their premotor network in newborn mice. *Eur. J. Neurosci.*, **28**, 1097–1107.

Buckmaster, P.S. & Dudek, F.E. (1997) Neuron loss, granule cell axon reorganization, and functional changes in the dentate gyrus of epileptic kainate-treated rats. *J. Comp. Neurol.*, **385**, 385–404.

Buckmaster, P.S., Otero-Corchón, V., Rubinstein, M., & Low, M.J. (2002) Heightened seizure severity in somatostatin knockout mice. *Epilepsy Res.*, **48**, 43–56.

Carnes, K.M., Fuller, T.A., & Price, J.L. (1990) Sources of presumptive glutamatergic/aspartatergic afferents to the magnocellular basal forebrain in the rat. *J. Comp. Neurol.*, **302**, 824–852.

Carre, G.P. & Harley, C.W. (1991) Population spike facilitation in the dentate gyrus following glutamate to the lateral supramammillary nucleus. *Brain Res.*, **568**, 307–310.

Cavalheiro, E.A., Fernandes, M.J., Turski, L., & Naffah-Mazzacoratti, M.G. (1994) Spontaneous recurrent seizures in rats: amino acid and monoamine determination in the hippocampus. *Epilepsia*, **35**, 1–11.

Cavalheiro, E.A., Santos, N.F., & Priel, M.R. (1996) The Pilocarpine Model of Epilepsy in Mice. *Epilepsia*, **37**, 1015–1019.

Cavalheiro, E.A., Silva, D.F., Turski, W.A., Calderazzo-Filho, L.S., Bortolotto, Z.A., & Turski, L. (1987) The susceptibility of rats to pilocarpine-induced seizures is age-dependent. *Brain Res.*, **465**, 43–58.

Cavazos, J.E., Golarai, G., & Sutula, T.P. (1991) Mossy fiber synaptic reorganization induced by kindling: time course of development, progression, and permanence. *J. Neurosci. Off. J. Soc. Neurosci.*, **11**, 2795–2803.
Chauvière, L., Rafrafi, N., Thinus-Blanc, C., Bartolomei, F., Esclapez, M., & Bernard, C. (2009) Early deficits in spatial memory and theta rhythm in experimental temporal lobe epilepsy. *J. Neurosci. Off. J. Soc. Neurosci.*, **29**, 5402–5410.
Chiba, T. & Murata, Y. (1985) Afferent and efferent connections of the medial preoptic area in the rat: a WGA-HRP study. *Brain Res. Bull.*, **14**, 261–272.
Chow, B.Y., Han, X., Dobry, A.S., Qian, X., Chuong, A.S., Li, M., Henninger, M.A., Belfort, G.M., Lin, Y., Monahan, P.E., & Boyden, E.S. (2010) High-performance genetically targetable optical neural silencing by light-driven proton pumps. *Nature*, **463**, 98–102.
Claiborne, B.J., Amaral, D.G., & Cowan, W.M. (1990) Quantitative, three-dimensional analysis of granule cell dendrites in the rat dentate gyrus. *J. Comp. Neurol.*, **302**, 206–219.
Colom, L.V., Castaneda, M.T., Reyna, T., Hernandez, S., & Garrido-Sanabria, E. (2005) Characterization of medial septal glutamatergic neurons and their projection to the hippocampus. *Synap. N. Y. N*, **58**, 151–164.
Cossart, R., Dinocourt, C., Hirsch, J.C., Merchan-Perez, A., De Felipe, J., Ben-Ari, Y., Esclapez, M., & Bernard, C. (2001) Dendritic but not somatic GABAergic inhibition is decreased in experimental epilepsy. *Nat. Neurosci.*, **4**, 52–62.
Coulon, P., Bras, H., & Vinay, L. (2011a) Characterization of last-order premotor interneurons by transneuronal tracing with rabies virus in the neonatal mouse spinal cord. *J. Comp. Neurol.*, **519**, 3470–3487.
Coulon, P., Bras, H., & Vinay, L. (2011b) Characterization of last-order premotor interneurons by transneuronal tracing with rabies virus in the neonatal mouse spinal cord. *J. Comp. Neurol.*, **519**, 3470–3487.
Covolan, L. & Mello, L.E. (2000) Temporal profile of neuronal injury following pilocarpine or kainic acid-induced status epilepticus. *Epilepsy Res.*, **39**, 133–152.
Crépel, V. & Mulle, C. (2015) Physiopathology of kainate receptors in epilepsy. *Curr. Opin. Pharmacol.*, Neurosciences, **20**, 83–88.
Cullinan, W.E., Helmreich, D.L., & Watson, S.J. (1996) Fos expression in forebrain afferents to the hypothalamic paraventricular nucleus following swim stress. *J. Comp. Neurol.*, **368**, 88–99.
de Lanerolle, N.C., Kim, J.H., Robbins, R.J., & Spencer, D.D. (1989) Hippocampal interneuron loss and plasticity in human temporal lobe epilepsy. *Brain Res.*, **495**, 387–395.
Denny, C.A., Kheirbek, M.A., Alba, E.L., Tanaka, K.F., Brachman, R.A., Laughman, K.B., Tomm, N.K., Turi, G.F., Losonczy, A., & Hen, R. (2014) Hippocampal memory traces are differentially modulated by experience, time, and adult neurogenesis. *Neuron*, **83**, 189–201.
Dent, J.A., Galvin, N.J., Stanfield, B.B., & Cowan, W.M. (1983) The mode of termination of the hypothalamic projection to the dentate gyrus: an EM autoradiographic study. *Brain Res.*, **258**, 1–10.
Dinocourt, C., Petanjek, Z., Freund, T.F., Ben-Ari, Y., & Esclapez, M. (2003) Loss of interneurons innervating pyramidal cell dendrites and axon initial segments in the CA1 region of the hippocampus following pilocarpine-induced seizures. *J. Comp. Neurol.*, **459**, 407–425.
Dolleman-Van der Weel, M.J. & Witter, M.P. (2000) Nucleus reuniens thalami innervates gamma aminobutyric acid positive cells in hippocampal field CA1 of the rat. *Neurosci. Lett.*, **278**, 145–148.
Dragunow, M. & Faull, R. (1989) The use of c-fos as a metabolic marker in neuronal pathway tracing. *J. Neurosci. Methods*, **29**, 261–265.
Dubé, C., Boyet, S., Marescaux, C., & Nehlig, A. (2001) Relationship between neuronal loss and interictal glucose metabolism during the chronic phase of the lithium-pilocarpine model of epilepsy in the immature and adult rat. *Exp. Neurol.*, **167**, 227–241.
Dupont, S., Samson, Y., Nguyen-Michel, V.-H., Zavanone, C., Navarro, V., Baulac, M., & Adam, C. (2015) Lateralizing value of semiology in medial temporal lobe epilepsy. *Acta Neurol. Scand.*, **132**, 401–409.

Ekstrand, J.J., Pouliot, W., Scheerlinck, P., & Dudek, F.E. (2011) Lithium pilocarpine-induced status epilepticus in postnatal day 20 rats results in greater neuronal injury in ventral versus dorsal hippocampus. *Neuroscience*, **192**, 699–707.

El-Hassar, L., Milh, M., Wendling, F., Ferrand, N., Esclapez, M., & Bernard, C. (2007) Cell domain-dependent changes in the glutamatergic and GABAergic drives during epileptogenesis in the rat CA1 region. *J. Physiol.*, **578**, 193–211.

Elseedy, H., Scapula, J., Ghestem, A., Bras, H., Abdel Salam, sherine, Abdelmeguid, N., & Esclapez, M. (2019) Two populations of neurons from the lateral supramammillary nucleus innervate the dorsal dentate gyrus: both display a dual glutamatergic and GABAergic neurotransmittion phenotype but differ by their Calretinin content and rostro-caudal distribution.

Engel, J. (1996) Introduction to temporal lobe epilepsy. *Epilepsy Res.*, **26**, 141–150.

Epsztein, J., Represa, A., Jorquera, I., Ben-Ari, Y., & Crépel, V. (2005) Recurrent mossy fibers establish aberrant kainate receptor-operated synapses on granule cells from epileptic rats. *J. Neurosci. Off. J. Soc. Neurosci.*, **25**, 8229–8239.

Esclapez, M., Chang, D.K., & Houser, C.R. (1996) Subpopulations of GABA neurons in the dentate gyrus express high levels of the α1 subunit of the GABAA receptor. *Hippocampus*, **6**, 225–238.

Esclapez, M., Hirsch, J.C., Ben-Ari, Y., & Bernard, C. (1999) Newly formed excitatory pathways provide a substrate for hyperexcitability in experimental temporal lobe epilepsy. *J. Comp. Neurol.*, **408**, 449–460.

Esclapez, M., Hirsch, J.C., Khazipov, R., Ben-Ari, Y., & Bernard, C. (1997) Operative GABAergic inhibition in hippocampal CA1 pyramidal neurons in experimental epilepsy. *Proc. Natl. Acad. Sci.*, **94**, 12151–12156.

Esclapez, M. & Houser, C.R. (1999) Up-regulation of GAD65 and GAD67 in remaining hippocampal GABA neurons in a model of temporal lobe epilepsy. *J. Comp. Neurol.*, **412**, 488–505.

Feldblum, S., Ackermann, R.F., & Tobin, A.J. (1990) Long-term increase of glutamate decarboxylase mRNA in a rat model of temporal lobe epilepsy. *Neuron*, **5**, 361–371.

Ferhat, L., Esclapez, M., Represa, A., Fattoum, A., Shirao, T., & Ben-Ari, Y. (2003) Increased levels of acidic calponin during dendritic spine plasticity after pilocarpine-induced seizures. *Hippocampus*, **13**, 845–858.

Fisher, R.S. (2000) Epilepsy from the Patient's Perspective: Review of Results of a Community-Based Survey. *Epilepsy Behav.*, **1**, S9–S14.

Fisher, R.S., Acevedo, C., Arzimanoglou, A., Bogacz, A., Cross, J.H., Elger, C.E., Engel, J., Forsgren, L., French, J.A., Glynn, M., Hesdorffer, D.C., Lee, B.I., Mathern, G.W., Moshé, S.L., Perucca, E., Scheffer, I.E., Tomson, T., Watanabe, M., & Wiebe, S. (2014) ILAE Official Report: A practical clinical definition of epilepsy. *Epilepsia*, **55**, 475–482.

Fisher, R.S., Cross, J.H., D'Souza, C., French, J.A., Haut, S.R., Higurashi, N., Hirsch, E., Jansen, F.E., Lagae, L., Moshé, S.L., Peltola, J., Roulet Perez, E., Scheffer, I.E., Schulze-Bonhage, A., Somerville, E., Sperling, M., Yacubian, E.M., & Zuberi, S.M. (2017) Instruction manual for the ILAE 2017 operational classification of seizure types. *Epilepsia*, **58**, 531–542.

Fisher, R.S., Cross, J.H., French, J.A., Higurashi, N., Hirsch, E., Jansen, F.E., Lagae, L., Moshé, S.L., Peltola, J., Roulet Perez, E., Scheffer, I.E., & Zuberi, S.M. (2017) Operational classification of seizure types by the International League Against Epilepsy: Position Paper of the ILAE Commission for Classification and Terminology. *Epilepsia*, **58**, 522–530.

Freund, T.F. & Antal, M. (1988) GABA-containing neurons in the septum control inhibitory interneurons in the hippocampus. *Nature*, **336**, 170–173.

Freund, T.F. & Buzsáki, G. (1996) Interneurons of the hippocampus. *Hippocampus*, **6**, 347–470.

Frotscher, M., Seress, L., Schwerdtfeger, W.K., & Buhl, E. (1991) The mossy cells of the fascia dentata: a comparative study of their fine structure and synaptic connections in rodents and primates. *J. Comp. Neurol.*, **312**, 145–163.

Fuhrmann, F., Justus, D., Sosulina, L., Kaneko, H., Beutel, T., Friedrichs, D., Schoch, S., Schwarz, M.K., Fuhrmann, M., & Remy, S. (2015) Locomotion, Theta Oscillations, and the Speed-

Correlated Firing of Hippocampal Neurons Are Controlled by a Medial Septal Glutamatergic Circuit. *Neuron*, **86**, 1253–1264.
Gaykema, R.P., Luiten, P.G., Nyakas, C., & Traber, J. (1990) Cortical projection patterns of the medial septum-diagonal band complex. *J. Comp. Neurol.*, **293**, 103–124.
Gonzalo-Ruiz, A., Alonso, A., Sanz, J.M., & Llinás, R.R. (1992a) A dopaminergic projection to the rat mammillary nuclei demonstrated by retrograde transport of wheat germ agglutinin-horseradish peroxidase and tyrosine hydroxylase immunohistochemistry. *J. Comp. Neurol.*, **321**, 300–311.
Gonzalo-Ruiz, A., Alonso, A., Sanz, J.M., & Llinás, R.R. (1992b) Afferent projections to the mammillary complex of the rat, with special reference to those from surrounding hypothalamic regions. *J. Comp. Neurol.*, **321**, 277–299.
Gonzalo-Ruiz, A., Morte, L., Flecha, J.M., & Sanz, J.M. (1999) Neurotransmitter characteristics of neurons projecting to the supramammillary nucleus of the rat. *Anat. Embryol. (Berl.)*, **200**, 377–392.
Gorter, J.A., van Vliet, E.A., Aronica, E., & Lopes da Silva, F.H. (2001) Progression of spontaneous seizures after status epilepticus is associated with mossy fibre sprouting and extensive bilateral loss of hilar parvalbumin and somatostatin-immunoreactive neurons. *Eur. J. Neurosci.*, **13**, 657–669.
Gradinaru, V., Thompson, K.R., & Deisseroth, K. (2008) eNpHR: a Natronomonas halorhodopsin enhanced for optogenetic applications. *Brain Cell Biol.*, **36**, 129–139.
Gradinaru, V., Zhang, F., Ramakrishnan, C., Mattis, J., Prakash, R., Diester, I., Goshen, I., Thompson, K.R., & Deisseroth, K. (2010) Molecular and Cellular Approaches for Diversifying and Extending Optogenetics. *Cell*, **141**, 154–165.
Greenwood, R.S., Godar, S.E., Reaves, T.A., & Hayward, J.N. (1981) Cholecystokinin in hippocampal pathways. *J. Comp. Neurol.*, **203**, 335–350.
Grove, E.A. (1988) Neural associations of the substantia innominata in the rat: afferent connections. *J. Comp. Neurol.*, **277**, 315–346.
Gulyás, A.I., Miettinen, R., Jacobowitz, D.M., & Freund, T.F. (1992) Calretinin is present in non-pyramidal cells of the rat hippocampus--I. A new type of neuron specifically associated with the mossy fibre system. *Neuroscience*, **48**, 1–27.
Guru, A., Post, R.J., Ho, Y.-Y., & Warden, M.R. (2015) Making Sense of Optogenetics. *Int. J. Neuropsychopharmacol.*, **18**.
Haglund, L., Swanson, L.W., & Köhler, C. (1984a) The projection of the supramammillary nucleus to the hippocampal formation: An immunohistochemical and anterograde transport study with the lectin PHA-L in the rat. *J. Comp. Neurol.*, **229**, 171–185.
Haglund, L., Swanson, L.W., & Köhler, C. (1984b) The projection of the supramammillary nucleus to the hippocampal formation: an immunohistochemical and anterograde transport study with the lectin PHA-L in the rat. *J. Comp. Neurol.*, **229**, 171–185.
Halasy, K., Hajszan, T., Kovács, E.G., Lam, T.-T., & Leranth, C. (2004) Distribution and origin of vesicular glutamate transporter 2-immunoreactive fibers in the rat hippocampus. *Hippocampus*, **14**, 908–918.
Halasy, K., Miettinen, R., Szabat, E., & Freund, T.F. (1992) GABAergic Interneurons are the Major Postsynaptic Targets of Median Raphe Afferents in the Rat Dentate Gyrus. *Eur. J. Neurosci.*, **4**, 144–153.
Han, X. & Boyden, E.S. (2007) Multiple-color optical activation, silencing, and desynchronization of neural activity, with single-spike temporal resolution. *PloS One*, **2**, e299.
Han, X., Chow, B.Y., Zhou, H., Klapoetke, N.C., Chuong, A., Rajimehr, R., Yang, A., Baratta, M.V., Winkle, J., Desimone, R., & Boyden, E.S. (2011) A high-light sensitivity optical neural silencer: development and application to optogenetic control of non-human primate cortex. *Front. Syst. Neurosci.*, **5**, 18.
Hashimotodani, Y., Karube, F., Yanagawa, Y., Fujiyama, F., & Kano, M. (2018) Supramammillary Nucleus Afferents to the Dentate Gyrus Co-release Glutamate and GABA and Potentiate Granule Cell Output. *Cell Rep.*, **25**, 2704-2715.e4.
Hayakawa, T., Ito, H., & Zyo, K. (1993) Neuroanatomical study of afferent projections to the

supramammillary nucleus of the rat. *Anat. Embryol. (Berl.)*, **188**, 139–148.
Helmstaedter, C. & Kurthen, M. (2001) Memory and epilepsy: characteristics, course, and influence of drugs and surgery. *Curr. Opin. Neurol.*, **14**, 211–216.
Hermann, B.P., Seidenberg, M., Schoenfeld, J., & Davies, K. (1997) Neuropsychological characteristics of the syndrome of mesial temporal lobe epilepsy. *Arch. Neurol.*, **54**, 369–376.
Houser, C.R. (1990) Granule cell dispersion in the dentate gyrus of humans with temporal lobe epilepsy. *Brain Res.*, **535**, 195–204.
Houser, C.R. (2007) Interneurons of the dentate gyrus: an overview of cell types, terminal fields and neurochemical identity. *Prog. Brain Res.*, **163**, 217–232.
Houser, C.R. (2014) Do Structural Changes in GABA Neurons Give Rise to the Epileptic State? In Scharfman, H.E. & Buckmaster, P.S. (eds), *Issues in Clinical Epileptology: A View from the Bench*. Springer Netherlands, Dordrecht, pp. 151–160.
Houser, C.R. & Esclapez, M. (1996) Vulnerability and plasticity of the GABA system in the pilocarpine model of spontaneous recurrent seizures. *Epilepsy Res.*, **26**, 207–218.
Houser, C.R. & Esclapez, M. (2003) Downregulation of the alpha5 subunit of the GABA(A) receptor in the pilocarpine model of temporal lobe epilepsy. *Hippocampus*, **13**, 633–645.
Houser, C.R., Miyashiro, J.E., Swartz, B.E., Walsh, G.O., Rich, J.R., & Delgado-Escueta, a V (1990) Altered patterns of dynorphin immunoreactivity suggest mossy fiber reorganization in human hippocampal epilepsy. *J. Neurosci. Off. J. Soc. Neurosci.*, **10**, 267–282.
Iseni, F., Lafay, F., Raux, H., & Blondel, D. (1997) Mapping of monoclonal antibody epitopes of the rabies virus P protein. *J. Gen. Virol.*, **78**, 119–124.
Ishizuka, N. (2001) Laminar organization of the pyramidal cell layer of the subiculum in the rat. *J. Comp. Neurol.*, **435**, 89–110.
Ito, M., Shirao, T., Doya, K., & Sekino, Y. (2009) Three-dimensional distribution of Fos-positive neurons in the supramammillary nucleus of the rat exposed to novel environment. *Neurosci. Res.*, **64**, 397–402.
Jarero-Basulto, J., Gasca-Martínez, Y., Rivera-Cervantes, M., Ureña-Guerrero, M., Feria-Velasco, A., & Beas-Zarate, C. (2018) Interactions Between Epilepsy and Plasticity. *Pharmaceuticals*, **11**, 17.
Jiao, Y. & Nadler, J.V. (2007) Stereological analysis of GluR2-immunoreactive hilar neurons in the pilocarpine model of temporal lobe epilepsy. *Exp. Neurol.*, **205**, 569–582.
Kahane, P. & Bartolomei, F. (2010) Temporal lobe epilepsy and hippocampal sclerosis: lessons from depth EEG recordings. *Epilepsia*, **51 Suppl 1**, 59–62.
Kahane, P. & Landré, E. (2008) [The epileptogenic zone]. *Neurochirurgie.*, **54**, 265–271.
Kheirbek, M.A., Drew, L.J., Burghardt, N.S., Costantini, D.O., Tannenholz, L., Ahmari, S.E., Zeng, H., Fenton, A.A., & Hen, R. (2013) Differential control of learning and anxiety along the dorsoventral axis of the dentate gyrus. *Neuron*, **77**, 955–968.
Kirk, I.J. & McNaughton, N. (1991) Supramammillary cell firing and hippocampal rhythmical slow activity. *Neuroreport*, **2**, 723–725.
Kirk, I.J. & McNaughton, N. (1993) Mapping the differential effects of procaine on frequency and amplitude of reticularly elicited hippocampal rhythmical slow activity. *Hippocampus*, **3**, 517–525.
Kiss, J., Csáki, A., Bokor, H., Kocsis, K., & Kocsis, B. (2002) Possible glutamatergic/aspartatergic projections to the supramammillary nucleus and their origins in the rat studied by selective [(3)H]D-aspartate labelling and immunocytochemistry. *Neuroscience*, **111**, 671–691.
Kiss, J., Csáki, A., Bokor, H., Shanabrough, M., & Leranth, C. (2000) The supramammillo-hippocampal and supramammillo-septal glutamatergic/aspartatergic projections in the rat: a combined [3H]D-aspartate autoradiographic and immunohistochemical study. *Neuroscience*, **97**, 657–669.
Kiss, J. & Szeiffert, G. (1995) Topographic analysis of connections between the rat septal diagonal band complex and the supramammillary area. In *Fourth IBRO World Congress of Neuroscience, Rapid Communications of Oxford Ltd*.

Kiyama, H., Shiosaka, S., Takami, K., Tateishi, K., Hashimura, E., Hamaoka, T., & Tohyama, M. (1984) CCK pathway from supramammillary region to the nucleus anterior ventralis thalami of the young rats. *Peptides*, **5**, 889–893.
Kiyama, H., Shiosaka, S., Tateishi, K., Hashimura, E., Hamaoka, T., & Tohyama, M. (1984) Cholecystokinin-8-like immunoreactive neuron pathway from the supramammillary region to the ventral tegmental nucleus of Gudden of the rat. *Brain Res.*, **304**, 397–400.
Kiyohara, T., Miyata, S., Nakamura, T., Shido, O., Nakashima, T., & Shibata, M. (1995) Differences in Fos expression in the rat brains between cold and warm ambient exposures. *Brain Res. Bull.*, **38**, 193–201.
Kobayashi, M. & Buckmaster, P.S. (2003) Reduced inhibition of dentate granule cells in a model of temporal lobe epilepsy. *J. Neurosci. Off. J. Soc. Neurosci.*, **23**, 2440–2452.
Kocsis, B. & Kaminski, M. (2006) Dynamic changes in the direction of the theta rhythmic drive between supramammillary nucleus and the septohippocampal system. *Hippocampus*, **16**, 531–540.
Kocsis, B. & Vertes, R.P. (1994) Characterization of neurons of the supramammillary nucleus and mammillary body that discharge rhythmically with the hippocampal theta rhythm in the rat. *J. Neurosci. Off. J. Soc. Neurosci.*, **14**, 7040–7052.
Kocsis, K., Kiss, J., Csáki, A., & Halász, B. (2003) Location of putative glutamatergic neurons projecting to the medial preoptic area of the rat hypothalamus. *Brain Res. Bull.*, **61**, 459–468.
Köhler, C., Swanson, L.W., Haglund, L., & J-Yen, W. (1985) The cytoarchitecture, histochemistry and projections of the tuberomammillary nucleus in the rat. *Neuroscience*, **16**, 85–110.
Kosaka, T., Katsumaru, H., Hama, K., Wu, J.Y., & Heizmann, C.W. (1987) GABAergic neurons containing the Ca2+-binding protein parvalbumin in the rat hippocampus and dentate gyrus. *Brain Res.*, **419**, 119–130.
Lanteaume, L., Bartolomei, F., & Bastien-Toniazzo, M. (2009) How do cognition, emotion, and epileptogenesis meet? A study of emotional cognitive bias in temporal lobe epilepsy. *Epilepsy Behav. EB*, **15**, 218–224.
Lantos, T.A., Görcs, T.J., & Palkovits, M. (1995) Immunohistochemical mapping of neuropeptides in the premamillary region of the hypothalamus in rats. *Brain Res. Brain Res. Rev.*, **20**, 209–249.
Lehmann, T.N., Gabriel, S., Eilers, A., Njunting, M., Kovacs, R., Schulze, K., Lanksch, W.R., & Heinemann, U. (2001) Fluorescent tracer in pilocarpine-treated rats shows widespread aberrant hippocampal neuronal connectivity. *Eur. J. Neurosci.*, **14**, 83–95.
Leite, J.P., Bortolotto, Z.A., & Cavalheiro, E.A. (1990) Spontaneous recurrent seizures in rats: An experimental model of partial epilepsy. *Neurosci. Biobehav. Rev.*, **14**, 511–517.
Leranth, C., Carpi, D., Buzsaki, G., & Kiss, J. (1999) The entorhino-septo-supramammillary nucleus connection in the rat: morphological basis of a feedback mechanism regulating hippocampal theta rhythm. *Neuroscience*, **88**, 701–718.
Leranth, C. & Hajszan, T. (2007) Extrinsic afferent systems to the dentate gyrus. *Prog. Brain Res.*, **163**, 63–84.
Leranth, C. & Kiss, J. (1996a) A population of supramammillary area calretinin neurons terminating on medial septal area cholinergic and lateral septal area calbindin-containing cells are aspartate/glutamatergic. *J. Neurosci. Off. J. Soc. Neurosci.*, **16**, 7699–7710.
Leranth, C. & Kiss, J. (1996b) A population of supramammillary area calretinin neurons terminating on medial septal area cholinergic and lateral septal area calbindin-containing cells are aspartate/glutamatergic. *J. Neurosci. Off. J. Soc. Neurosci.*, **16**, 7699–7710.
Leranth, C. & Nitsch, R. (1994) Morphological evidence that hypothalamic substance P-containing afferents are capable of filtering the signal flow in the monkey hippocampal formation. *J. Neurosci. Off. J. Soc. Neurosci.*, **14**, 4079–4094.
Liu, Z., Nagao, T., Desjardins, G.C., Gloor, P., & Avoli, M. (1994) Quantitative evaluation of neuronal loss in the dorsal hippocampus in rats with long-term pilocarpine seizures.

Epilepsy Res., **17**, 237–247.
Long, L., Xiao, B., Feng, L., Yi, F., Li, G., Li, S., Mutasem, M.A., Chen, S., Bi, F., & Li, Y. (2011) Selective loss and axonal sprouting of GABAergic interneurons in the sclerotic hippocampus induced by LiCl-pilocarpine. *Int. J. Neurosci.*, **121**, 69–85.
Lowenstein, D., Thomas, M., Smith, D., & McIntosh, T. (1992) Selective vulnerability of dentate hilar neurons following traumatic brain injury: a potential mechanistic link between head trauma and disorders of the hippocampus. *J. Neurosci.*, **12**, 4846–4853.
Lübke, J., Deller, T., & Frotscher, M. (1997) Septal innervation of mossy cells in the hilus of the rat dentate gyrus: an anterograde tracing and intracellular labeling study. *Exp. Brain Res.*, **114**, 423–432.
Luo, A.H., Tahsili-Fahadan, P., Wise, R.A., Lupica, C.R., & Aston-Jones, G. (2011) Linking context with reward: a functional circuit from hippocampal CA3 to ventral tegmental area. *Science*, **333**, 353–357.
Maglóczky, Z., Acsády, L., & Freund, T.F. (1994) Principal cells are the postsynaptic targets of supramammillary afferents in the hippocampus of the rat. *Hippocampus*, **4**, 322–334.
Mahn, M., Prigge, M., Ron, S., Levy, R., & Yizhar, O. (2016) Biophysical constraints of optogenetic inhibition at presynaptic terminals. *Nat. Neurosci.*, **19**, 554–556.
Maillard, L., Vignal, J.-P., Gavaret, M., Guye, M., Biraben, A., McGonigal, A., Chauvel, P., & Bartolomei, F. (2004) Semiologic and electrophysiologic correlations in temporal lobe seizure subtypes. *Epilepsia*, **45**, 1590–1599.
Maquet, P., Laureys, S., Peigneux, P., Fuchs, S., Petiau, C., Phillips, C., Aerts, J., Del Fiore, G., Degueldre, C., Meulemans, T., Luxen, A., Franck, G., Van Der Linden, M., Smith, C., & Cleeremans, A. (2000) Experience-dependent changes in cerebral activation during human REM sleep. *Nat. Neurosci.*, **3**, 831–836.
Marcelin, B., Chauvière, L., Becker, A., Migliore, M., Esclapez, M., & Bernard, C. (2009) h channel-dependent deficit of theta oscillation resonance and phase shift in temporal lobe epilepsy. *Neurobiol. Dis.*, **33**, 436–447.
Margerison, J.H. & Corsellis, J.A. (1966) Epilepsy and the temporal lobes. A clinical, electroencephalographic and neuropathological study of the brain in epilepsy, with particular reference to the temporal lobes. *Brain J. Neurol.*, **89**, 499–530.
Mathern, G.W., Babb, T.L., Pretorius, J.K., & Leite, J.P. (1995) Reactive synaptogenesis and neuron densities for neuropeptide Y, somatostatin, and glutamate decarboxylase immunoreactivity in the epileptogenic human fascia dentata. *J. Neurosci. Off. J. Soc. Neurosci.*, **15**, 3990–4004.
McCown, T.J. (2011) Adeno-Associated Virus (AAV) Vectors in the CNS. *Curr. Gene Ther.*, **11**, 181–188.
Mello, L.E., Cavalheiro, E.A., Tan, A.M., Kupfer, W.R., Pretorius, J.K., Babb, T.L., & Finch, D.M. (1993) Circuit mechanisms of seizures in the pilocarpine model of chronic epilepsy: cell loss and mossy fiber sprouting. *Epilepsia*, **34**, 985–995.
Mitra, P.P. & Pesaran, B. (1999) Analysis of dynamic brain imaging data. *Biophys. J.*, **76**, 691–708.
Mizumori, S., McNaughton, B., Barnes, C., & Fox, K. (1989) Preserved spatial coding in hippocampal CA1 pyramidal cells during reversible suppression of CA3c output: evidence for pattern completion in hippocampus. *J. Neurosci.*, **9**, 3915–3928.
Moser, M.B. & Moser, E.I. (1998) Functional differentiation in the hippocampus. *Hippocampus*, **8**, 608–619.
Nadler, J.V., Perry, B.W., Gentry, C., & Cotman, C.W. (1980) Degeneration of hippocampal CA3 pyramidal cells induced by intraventricular kainic acid. *J. Comp. Neurol.*, **192**, 333–359.
Nagel, G., Brauner, M., Liewald, J.F., Adeishvili, N., Bamberg, E., & Gottschalk, A. (2005) Light activation of channelrhodopsin-2 in excitable cells of Caenorhabditis elegans triggers rapid behavioral responses. *Curr. Biol. CB*, **15**, 2279–2284.
Nagel, G., Szellas, T., Huhn, W., Kateriya, S., Adeishvili, N., Berthold, P., Ollig, D., Hegemann, P., & Bamberg, E. (2003) Channelrhodopsin-2, a directly light-gated cation-selective membrane channel. *Proc. Natl. Acad. Sci.*, **100**, 13940–13945.
Nakanishi, K., Saito, H., & Abe, K. (2001) The supramammillary nucleus contributes to

associative EPSP-spike potentiation in the rat dentate gyrus in vivo. *Eur. J. Neurosci.*, **13**, 793–800.
Nitsch, R. & Leranth, C. (1996a) GABAergic neurons in the rat dentate gyrus are innervated by subcortical calretinin-containing afferents. *J. Comp. Neurol.*, **364**, 425–438.
Nitsch, R. & Leranth, C. (1996b) GABAergic neurons in the rat dentate gyrus are innervated by subcortical calretinin-containing afferents. *J. Comp. Neurol.*, **364**, 425–438.
Nyakas, C., Luiten, P.G., Spencer, D.G., & Traber, J. (1987) Detailed projection patterns of septal and diagonal band efferents to the hippocampus in the rat with emphasis on innervation of CA1 and dentate gyrus. *Brain Res. Bull.*, **18**, 533–545.
Obenaus, A., Esclapez, M., & Houser, C.R. (1993) Loss of glutamate decarboxylase mRNA-containing neurons in the rat dentate gyrus following pilocarpine-induced seizures. *J. Neurosci. Off. J. Soc. Neurosci.*, **13**, 4470–4485.
Okazaki, M.M., Evenson, D.A., & Nadler, J.V. (1995) Hippocampal mossy fiber sprouting and synapse formation after status epilepticus in rats: visualization after retrograde transport of biocytin. *J. Comp. Neurol.*, **352**, 515–534.
Okazaki, M.M. & Nadler, J.V. (2001) Glutamate receptor involvement in dentate granule cell epileptiform activity evoked by mossy fiber stimulation. *Brain Res.*, **915**, 58–69.
Ouedraogo, D.W., Lenck-Santini, P.-P., Marti, G., Robbe, D., Crépel, V., & Epsztein, J. (2016) Abnormal UP/DOWN Membrane Potential Dynamics Coupled with the Neocortical Slow Oscillation in Dentate Granule Cells during the Latent Phase of Temporal Lobe Epilepsy. *eNeuro*, **3**.
Pan, W.X. & McNaughton, N. (1997) The medial supramammillary nucleus, spatial learning and the frequency of hippocampal theta activity. *Brain Res.*, **764**, 101–108.
Pan, W.-X. & McNaughton, N. (2002) The role of the medial supramammillary nucleus in the control of hippocampal theta activity and behaviour in rats. *Eur. J. Neurosci.*, **16**, 1797–1809.
Pan, W.-X. & McNaughton, N. (2004a) The supramammillary area: its organization, functions and relationship to the hippocampus. *Prog. Neurobiol.*, **74**, 127–166.
Pan, W.-X. & McNaughton, N. (2004b) The supramammillary area: its organization, functions and relationship to the hippocampus. *Prog. Neurobiol.*, **74**, 127–166.
Pan, W.-X. & McNaughton, N. (2004c) The supramammillary area: its organization, functions and relationship to the hippocampus. *Prog. Neurobiol.*, **74**, 127–166.
Panula, P., Pirvola, U., Auvinen, S., & Airaksinen, M.S. (1989) Histamine-immunoreactive nerve fibers in the rat brain. *Neuroscience*, **28**, 585–610.
Parent, J.M. (2007) Adult neurogenesis in the intact and epileptic dentate gyrus. *Prog. Brain Res.*, **163**, 529–540.
Parent, J.M., Elliott, R.C., Pleasure, S.J., Barbaro, N.M., & Lowenstein, D.H. (2006) Aberrant seizure-induced neurogenesis in experimental temporal lobe epilepsy. *Ann. Neurol.*, **59**, 81–91.
Parent, J.M., Yu, T.W., Leibowitz, R.T., Geschwind, D.H., Sloviter, R.S., & Lowenstein, D.H. (1997) Dentate granule cell neurogenesis is increased by seizures and contributes to aberrant network reorganization in the adult rat hippocampus. *J. Neurosci. Off. J. Soc. Neurosci.*, **17**, 3727–3738.
Parmentier, R., Ohtsu, H., Djebbara-Hannas, Z., Valatx, J.-L., Watanabe, T., & Lin, J.-S. (2002) Anatomical, physiological, and pharmacological characteristics of histidine decarboxylase knock-out mice: evidence for the role of brain histamine in behavioral and sleep-wake control. *J. Neurosci. Off. J. Soc. Neurosci.*, **22**, 7695–7711.
Pasquier, D.A. & Reinoso-Suarez, F. (1976) Direct projections from hypothalamus to hippocampus in the rat demonstrated by retrograde transport of horseradish peroxidase. *Brain Res.*, **108**, 165–169.
Pasquier, D.A. & Reinoso-Suarez, F. (1978) The topographic organization of hypothalamic and brain stem projections to the hippocampus. *Brain Res. Bull.*, **3**, 373–389.
Paxinos, G. & Franklin, K.B.J. (2004) *The Mouse Brain in Stereotaxic Coordinates*. Gulf Professional Publishing.

Paxinos, G. & Watson, C. (1998) *The Rat Brain in Stereotaxic Coordinates*. Academic Press.
Pedersen, N.P., Ferrari, L., Venner, A., Wang, J.L., Abbott, S.B.G., Vujovic, N., Arrigoni, E., Saper, C.B., & Fuller, P.M. (2017) Supramammillary glutamate neurons are a key node of the arousal system. *Nat. Commun.*, **8**.
Peng, Z., Zhang, N., Wei, W., Huang, C.S., Cetina, Y., Otis, T.S., & Houser, C.R. (2013) A Reorganized GABAergic Circuit in a Model of Epilepsy: Evidence from Optogenetic Labeling and Stimulation of Somatostatin Interneurons. *J. Neurosci.*, **33**, 14392–14405.
Peret, A., Christie, L.A., Ouedraogo, D.W., Gorlewicz, A., Epsztein, J., Mulle, C., & Crépel, V. (2014) Contribution of Aberrant GluK2-Containing Kainate Receptors to Chronic Seizures in Temporal Lobe Epilepsy. *Cell Rep.*, **8**, 347–354.
Perez, Y., Morin, F., Beaulieu, C., & Lacaille, J.C. (1996) Axonal sprouting of CA1 pyramidal cells in hyperexcitable hippocampal slices of kainate-treated rats. *Eur. J. Neurosci.*, **8**, 736–748.
Pierce, J.P., McCloskey, D.P., & Scharfman, H.E. (2011) Morphometry of Hilar Ectopic Granule Cells in the Rat. *J. Comp. Neurol.*, **519**, 1196–1218.
Pitkänen, A., Pikkarainen, M., Nurminen, N., & Ylinen, A. (2000) Reciprocal connections between the amygdala and the hippocampal formation, perirhinal cortex, and postrhinal cortex in rat. A review. *Ann. N. Y. Acad. Sci.*, **911**, 369–391.
Quilichini, P., Sirota, A., & Buzsáki, G. (2010) Intrinsic Circuit Organization and Theta–Gamma Oscillation Dynamics in the Entorhinal Cortex of the Rat. *J. Neurosci.*, **30**, 11128–11142.
Raimondo, J.V., Kay, L., Ellender, T.J., & Akerman, C.J. (2012) Optogenetic silencing strategies differ in their effects on inhibitory synaptic transmission. *Nat. Neurosci.*, **15**, 1102–1104.
Ravassard, P., Hamieh, A.M., Joseph, M.A., Fraize, N., Libourel, P.-A., Lebarillier, L., Arthaud, S., Meissirel, C., Touret, M., Malleret, G., & Salin, P.-A. (2016) REM Sleep-Dependent Bidirectional Regulation of Hippocampal-Based Emotional Memory and LTP. *Cereb. Cortex N. Y. N 1991*, **26**, 1488–1500.
Renouard, L., Billwiller, F., Ogawa, K., Clément, O., Camargo, N., Abdelkarim, M., Gay, N., Scoté-Blachon, C., Touré, R., Libourel, P.-A., Ravassard, P., Salvert, D., Peyron, C., Claustrat, B., Léger, L., Salin, P., Malleret, G., Fort, P., & Luppi, P.-H. (2015) The supramammillary nucleus and the claustrum activate the cortex during REM sleep. *Sci. Adv.*, **1**.
Represa, A., Jorquera, I., Salle, G. le gal la, & Ben-Ari, Y. (1993) Epilepsy induced collateral sprouting of hippocampal mossy fibers: Does it induce the development of ectopic synapses with granule cell dendrites? *Hippocampus*, **3**, 257–268.
Ribak, C.E., Shapiro, L.A., Yan, X.-X., Dashtipour, K., Nadler, J.V., Obenaus, A., Spigelman, I., & Buckmaster, P.S. (2012) Seizure-induced formation of basal dendrites on granule cells of the rodent dentate gyrus. In Noebels, J.L., Avoli, M., Rogawski, M.A., Olsen, R.W., & Delgado-Escueta, A.V. (eds), *Jasper's Basic Mechanisms of the Epilepsies*, 4th edn. National Center for Biotechnology Information (US), Bethesda (MD).
Richmond, M.A., Yee, B.K., Pouzet, B., Veenman, L., Rawlins, J.N., Feldon, J., & Bannerman, D.M. (1999) Dissociating context and space within the hippocampus: effects of complete, dorsal, and ventral excitotoxic hippocampal lesions on conditioned freezing and spatial learning. *Behav. Neurosci.*, **113**, 1189–1203.
Risold, P.Y. & Swanson, L.W. (1997) Connections of the rat lateral septal complex. *Brain Res. Brain Res. Rev.*, **24**, 115–195.
Santín, L.J., Aguirre, J.A., Rubio, S., Begega, A., Miranda, R., & Arias, J.L. (2003) c-Fos expression in supramammillary and medial mammillary nuclei following spatial reference and working memory tasks. *Physiol. Behav.*, **78**, 733–739.
Saper, C.B. (1984) Organization of cerebral cortical afferent systems in the rat. II. Magnocellular basal nucleus. *J. Comp. Neurol.*, **222**, 313–342.
Schmidt, B., Marrone, D.F., & Markus, E.J. (2012) Disambiguating the similar: the dentate gyrus and pattern separation. *Behav. Brain Res.*, **226**, 56–65.
Schwarzer, C., Williamson, J.M., Lothman, E.W., Vezzani, A., & Sperk, G. (1995) Somatostatin, neuropeptide Y, neurokinin B and cholecystokinin immunoreactivity in two chronic models of temporal lobe epilepsy. *Neuroscience*, **69**, 831–845.
Scorza, F.A., Arida, R.M., Naffah-Mazzacoratti, M. da G., Scerni, D.A., Calderazzo, L., & Cavalheiro,

E.A. (2009) The pilocarpine model of epilepsy: what have we learned? *An. Acad. Bras. Ciênc.*, **81**, 345–365.
Segal, M. (1979) A potent inhibitory monosynaptic hypothalamo-hippocampal connection. *Brain Res.*, **162**, 137–141.
Segal, M. & Landis, S. (1974) Afferents to the hippocampus of the rat studied with the method of retrograde transport of horseradish peroxidase. *Brain Res.*, **78**, 1–15.
Shahidi, S., Motamedi, F., Bakeshloo, S.A., & Taleghani, B.K. (2004) The effect of reversible inactivation of the supramammillary nucleus on passive avoidance learning in rats. *Behav. Brain Res.*, **152**, 81–87.
Shahidi, S., Motamedi, F., & Naghdi, N. (2004) Effect of reversible inactivation of the supramammillary nucleus on spatial learning and memory in rats. *Brain Res.*, **1026**, 267–274.
Shapiro, L.A., Figueroa-Aragon, S., & Ribak, C.E. (2007) Newly generated granule cells show rapid neuroplastic changes in the adult rat dentate gyrus during the first five days following pilocarpine-induced seizures. *Eur. J. Neurosci.*, **26**, 583–592.
Shepard, P.D., Mihailoff, G.A., & German, D.C. (1988) Anatomical and electrophysiological characterization of presumed dopamine-containing neurons within the supramammillary region of the rat. *Brain Res. Bull.*, **20**, 307–314.
Shibata, H., Suzuki, T., & Matsushita, M. (1986) Afferent projections to the interpeduncular nucleus in the rat, as studied by retrograde and anterograde transport of wheat germ agglutinin conjugated to horseradish peroxidase. *J. Comp. Neurol.*, **248**, 272–284.
Sik, A., Penttonen, M., & Buzsáki, G. (1997) Interneurons in the hippocampal dentate gyrus: an in vivo intracellular study. *Eur. J. Neurosci.*, **9**, 573–588.
Silveira, M.C., Sandner, G., & Graeff, F.G. (1993) Induction of Fos immunoreactivity in the brain by exposure to the elevated plus-maze. *Behav. Brain Res.*, **56**, 115–118.
Sloviter, R.S. (1987) Decreased hippocampal inhibition and a selective loss of interneurons in experimental epilepsy. *Science*, **235**, 73–76.
Sloviter, R.S., Zappone, C.A., Harvey, B.D., Bumanglag, A.V., Bender, R.A., & Frotscher, M. (2003) "Dormant basket cell" hypothesis revisited: relative vulnerabilities of dentate gyrus mossy cells and inhibitory interneurons after hippocampal status epilepticus in the rat. *J. Comp. Neurol.*, **459**, 44–76.
Soussi, R., Boulland, J.-L., Bassot, E., Bras, H., Coulon, P., Chaudhry, F.A., Storm-Mathisen, J., Ferhat, L., & Esclapez, M. (2015) Reorganization of supramammillary–hippocampal pathways in the rat pilocarpine model of temporal lobe epilepsy: evidence for axon terminal sprouting. *Brain Struct. Funct.*, **220**, 2449–2468.
Soussi, R., Zhang, N., Tahtakran, S., Houser, C.R., & Esclapez, M. (2010) Heterogeneity of the supramammillary-hippocampal pathways: evidence for a unique GABAergic neurotransmitter phenotype and regional differences: GABAergic and glutamatergic supramammillary-hippocampal pathways. *Eur. J. Neurosci.*, **32**, 771–785.
Stanfield, B.B. & Maxwell Cowan, W. (1984) An EM autoradiographic study of the hypothalamo-hippocampal projection. *Brain Res.*, **309**, 293–298.
Sutula, T., Cascino, G., Cavazos, J., Parada, I., & Ramirez, L. (1989) Mossy fiber synaptic reorganization in the epileptic human temporal lobe. *Ann. Neurol.*, **26**, 321–330.
Suzuki, F., Heinrich, C., Boehrer, A., Mitsuya, K., Kurokawa, K., Matsuda, M., & Depaulis, A. (2005) Glutamate receptor antagonists and benzodiazepine inhibit the progression of granule cell dispersion in a mouse model of mesial temporal lobe epilepsy. *Epilepsia*, **46**, 193–202.
Swanson, C.J. & Kalivas, P.W. (2000) Regulation of locomotor activity by metabotropic glutamate receptors in the nucleus accumbens and ventral tegmental area. *J. Pharmacol. Exp. Ther.*, **292**, 406–414.
Swanson, L.W. (1982) The projections of the ventral tegmental area and adjacent regions: a combined fluorescent retrograde tracer and immunofluorescence study in the rat. *Brain Res. Bull.*, **9**, 321–353.
Swanson, L.W. & Cowan, W.M. (1977) An autoradiographic study of the organization of the

efferent connections of the hippocampal formation in the rat. *J. Comp. Neurol.*, **172**, 49–84.
Talairach, J. & Bancaud, J. (1966) Lesion, "irritative" zone and epileptogenic focus. *Confin. Neurol.*, **27**, 91–94.
Tamamaki, N. (1997) Organization of the entorhinal projection to the rat dentate gyrus revealed by Dil anterograde labeling. *Exp. Brain Res.*, **116**, 250–258.
Tauck, D.L. & Nadler, J.V. (1985) Evidence of functional mossy fiber sprouting in hippocampal formation of kainic acid-treated rats. *J. Neurosci. Off. J. Soc. Neurosci.*, **5**, 1016–1022.
Thinschmidt, J.S. (1993) The supramammillary nucleus: Does it play a role in the mediation of hippocampal theta rhythm?
Thom, M. (2004) Recent advances in the neuropathology of focal lesions in epilepsy. *Expert Rev. Neurother.*, **4**, 973–984.
Thomas, C.E., Storm, T.A., Huang, Z., & Kay, M.A. (2004) Rapid Uncoating of Vector Genomes Is the Key to Efficient Liver Transduction with Pseudotyped Adeno-Associated Virus Vectors. *J. Virol.*, **78**, 3110–3122.
Tsunematsu, T., Kilduff, T.S., Boyden, E.S., Takahashi, S., Tominaga, M., & Yamanaka, A. (2011) Acute optogenetic silencing of orexin/hypocretin neurons induces slow-wave sleep in mice. *J. Neurosci. Off. J. Soc. Neurosci.*, **31**, 10529–10539.
Turski, L., Cavalheiro, E.A., Sieklucka-Dziuba, M., Ikonomidou-Turski, C., Czuczwar, S.J., & Turski, W.A. (1986) Seizures produced by pilocarpine: Neuropathological sequelae and activity of glutamate decarboxylase in the rat forebrain. *Brain Res.*, **398**, 37–48.
Turski, L., Ikonomidou, C., Turski, W.A., Bortolotto, Z.A., & Cavalheiro, E.A. (1989) Review: cholinergic mechanisms and epileptogenesis. The seizures induced by pilocarpine: a novel experimental model of intractable epilepsy. *Synap. N. Y. N*, **3**, 154–171.
Turski, W., Cavalheiro, E., Turski, L., & Kleinrok, Z. (1983) Intrahippocampal bethanechol in rats: Behavioural, electroencephalographic and neuropathological correlates. *Behav. Brain Res.*, **7**, 361–370.
Turski, W.A., Cavalheiro, E.A., Bortolotto, Z.A., Mello, L.M., Schwarz, M., & Turski, L. (1984) Seizures produced by pilocarpine in mice: A behavioral, electroencephalographic and morphological analysis. *Brain Res.*, **321**, 237–253.
Turski, W.A., Cavalheiro, E.A., Schwarz, M., Czuczwar, S.J., Kleinrok, Z., & Turski, L. (1983) Limbic seizures produced by pilocarpine in rats: Behavioural, electroencephalographic and neuropathological study. *Behav. Brain Res.*, **9**, 315–335.
Ugolini, G. (2010) Advances in viral transneuronal tracing. *J. Neurosci. Methods*, **194**, 2–20.
Vann, S.D., Brown, M.W., & Aggleton, J.P. (2000) Fos expression in the rostral thalamic nuclei and associated cortical regions in response to different spatial memory tests. *Neuroscience*, **101**, 983–991.
Vertes, R.P. (1988) Brainstem afferents to the basal forebrain in the rat. *Neuroscience*, **24**, 907–935.
Vertes, R.P. (1992) PHA-L analysis of projections from the supramammillary nucleus in the rat. *J. Comp. Neurol.*, **326**, 595–622.
Vertes, R.P. (2015) Major diencephalic inputs to the hippocampus. In *Progress in Brain Research*. Elsevier, pp. 121–144.
Vertes, R.P., Fortin, W.J., & Crane, A.M. (1999) Projections of the median raphe nucleus in the rat. *J. Comp. Neurol.*, **407**, 555–582.
Vertes, R.P. & Kocsis, B. (1997) Brainstem-diencephalo-septohippocampal systems controlling the theta rhythm of the hippocampus. *Neuroscience*, **81**, 893–926.
Vertes, R.P. & McKenna, J.T. (2000) Collateral projections from the supramammillary nucleus to the medial septum and hippocampus. *Synapse*, **38**, 281–293.
Vyazovskiy, V.V., Kopp, C., Bösch, G., & Tobler, I. (2005) The GABAA receptor agonist THIP alters the EEG in waking and sleep of mice. *Neuropharmacology*, **48**, 617–626.
Wiegert, J.S., Mahn, M., Prigge, M., Printz, Y., & Yizhar, O. (2017) Silencing Neurons: Tools, Applications, and Experimental Constraints. *Neuron*, **95**, 504–529.
Wieser, H.-G. & ILAE Commission on Neurosurgery of Epilepsy (2004) ILAE Commission Report.

Mesial temporal lobe epilepsy with hippocampal sclerosis. *Epilepsia*, **45**, 695–714.
Wirtshafter, D., Stratford, T.R., & Shim, I. (1998) Placement in a novel environment induces fos-like immunoreactivity in supramammillary cells projecting to the hippocampus and midbrain. *Brain Res.*, **789**, 331–334.
Witter, M.P. & Amaral, D.G. (2004) Hippocampal Formation. *Rat Nerv. Syst.*, 635–704.
Wu, Z., Asokan, A., & Samulski, R.J. (2006) Adeno-associated virus serotypes: vector toolkit for human gene therapy. *Mol. Ther. J. Am. Soc. Gene Ther.*, **14**, 316–327.
Wyss, J.M., Swanson, L.W., & Cowan, W.M. (1979a) A study of subcortical afferents to the hippocampal formation in the rat. *Neuroscience*, **4**, 463–476.
Wyss, J.M., Swanson, L.W., & Cowan, W.M. (1979b) Evidence for an input to the molecular layer and the stratum granulosum of the dentate gyrus from the supramammillary region of the hypothalamus. *Anat. Embryol. (Berl.)*, **156**, 165–176.
Yoshida, K. & Oka, H. (1995) Topographical projections from the medial septum-diagonal band complex to the hippocampus: a retrograde tracing study with multiple fluorescent dyes in rats. *Neurosci. Res.*, **21**, 199–209.
Zeitlin, S.B., Bradburn, D.O., & Lawson-Kerr, K. (1995) Selective processing of epilepsy-related cues in patients with high fear of seizures. *J. Epilepsy*, **8**, 16–22.
Zhang, F., Aravanis, A.M., Adamantidis, A., de Lecea, L., & Deisseroth, K. (2007) Circuit-breakers: optical technologies for probing neural signals and systems. *Nat. Rev. Neurosci.*, **8**, 577–581.
Zhang, F., Gradinaru, V., Adamantidis, A.R., Durand, R., Airan, R.D., de Lecea, L., & Deisseroth, K. (2010) Optogenetic interrogation of neural circuits: technology for probing mammalian brain structures. *Nat. Protoc.*, **5**, 439–456.
Zhang, N. & Houser, C.R. (1999) Ultrastructural localization of dynorphin in the dentate gyrus in human temporal lobe epilepsy: a study of reorganized mossy fiber synapses. *J. Comp. Neurol.*, **405**, 472–490.
Zhao, S., Cunha, C., Zhang, F., Liu, Q., Gloss, B., Deisseroth, K., Augustine, G.J., & Feng, G. (2008) Improved expression of halorhodopsin for light-induced silencing of neuronal activity. *Brain Cell Biol.*, **36**, 141–154.
Zhu, P., Narita, Y., Bundschuh, S.T., Fajardo, O., Zhang Schärer, Y.-P., Chattopadhyaya, B., Arn Bouldoires, E., Stepien, A.E., Deisseroth, K., Arber, S., Sprengel, R., Rijli, F.M., & Friedrich, R.W. (2009) Optogenetic dissection of neuronal circuits in zebrafish using viral gene transfer and the Tet system. *Front. Neural Circuits*, **3**.